UNIVERSITÉ PARIS DESCARTES

École doctorale Hématologie - Oncogenèse - Biothérapies (ED 561)

Laboratoire INSERM UMR 970

Développement et évaluation de nouveaux outils d'analyse géométrique 3D pour la prévention et le traitement des maladies aortiques

Par Damian CRAIEM

Thèse de Doctorat de Science
Specialité : Pathologie Cardio-Vasculaire

Dirigée par le Professeur Alain SIMON
et codirigée par le Docteur Jean-Marc ALSAC

Présentée et soutenue publiquement le 13 Octobre 2016

Devant un jury composé de :

Alain SIMON (PU-PH)	Directeur de thèse
Jean-Marc ALSAC (MCU-PH)	Co-directeur de thèse
Nadjia KACHENOURA (PhD)	Rapporteur
Hicham KOBEITER (PU-PH)	Rapporteur
Bernard LEVY (PU-PH)	Examinateur
Elie MOUSSEAUX (PU-PH)	Examinateur

« Deviens ce que tu es »
Πίνδαρος(518-438 av. J.-C.)

Résumé

Les nouvelles technologies d'imagerie basées sur la tomodensitométrie en coupe permettent l'évaluation de très haute qualité de la structure 3D de l'aorte thoracique. La reconstruction virtuelle et les modèles géométriques de l'aorte sont indispensables à l'exploitation des images dont le temps de traitement manuel reste cependant considérable et les outils numériques insuffisants ou inadaptés pour mesurer correctement sa morphologie.

L'aorte n'est pas un simple tube de conduction du sang mais un organe de régulation de la pulsatilité des ondes de pression provoquées par l'éjection cardiaque. Ses désordres biomécaniques peuvent accélérer la formation de calcifications dans sa paroi et entrainer des risques de graves complications, comme les anévrismes et les dissections. La réparation aortique basée sur l'implantation d'endoprothèses est en pleine évolution et requiert des renseignements morphologiques précis pour en améliorer le taux de succès.

Notre objectif a été d'étudier la géométrie tridimensionnelle de l'aorte en développant des algorithmes appropriés. Une plateforme informatique a été conçue et testée pour étudier trois pathologies de l'aorte : l'athérosclérose calcifiée, l'anévrisme et la dissection. L'hypothèse du travail a été que la géométrie spécifique des artères de chaque individu joue un rôle complémentaire à celui des facteurs de risque traditionnels dans le développement de ces pathologies. Notre premier travail a montré que trois facteurs résument 80% de la variabilité géométrique de l'aorte thoracique : le volume aortique, le déroulement et la symétrie de l'arche aortique, avec des taux de variabilité respectifs de 46%, 22% et 12%.

Dans deux travaux suivants, nous avons montré que les calcifications de l'aorte thoracique se concentrent principalement dans la crosse et dans le segment descendant proximal, et que cette distribution était associée à la morphologie de l'aorte indépendamment de l'âge, du sexe, de la surface corporelle et des facteurs de risque traditionnels. Le quatrième travail a montré que le score de dépôt calcique dans toute l'aorte thoracique incluant la crosse était plus étroitement associé aux complications non-cardiaques, vasculaires périphériques et cérébrales, que le score traditionnel de calcium coronaire. Il faut noter que la crosse aortique n'est pas visualisée dans les études de routine de calcium coronaire sans injection.

Le cinquième travail décrit un modèle déformable capable de segmenter la lumière aortique dans un contexte pathologique. Il a été appliqué pour étudier de façon automatisée la taille d'un anévrisme abdominal avant et après la pose d'une endoprothèse. Dans le dernier travail, la méthode précédente a été adaptée pour étudier la géométrie aortique des patients atteints de dissection comparativement à un groupe témoin de patients qui en étaient indemnes. Trois variables géométriques ont été identifiées dans le modèle de prédiction du risque de dissection : le diamètre de la crosse, la longueur de l'aorte thoracique et l'âge.

En conclusion, nos résultats montrent que les maladies aortiques sont étroitement associées à la géométrie de l'aorte indépendamment des facteurs de risque traditionnels. Les algorithmes que nous avons développés ouvrent la voie à l'automatisation et à une réduction de la variabilité des mesures.

Mots clefs : Aorte, tomodensitométrie, traitement numérique d'images, calcification artérielle, anévrisme aortique, dissection aortique.

Abstract

Title : Development and evaluation of new 3D geometric analysis tools to prevent and treat aortic diseases.

New imaging technologies, including those associated with multislice computed tomography, allow to evaluate the structure of the thoracic aorta in 3D with an impressive resolution. Aortic virtual reconstruction and geometric modeling are essential for imaging evaluation because manual measurements are time-consuming, and the available tools still need to be adapted to complex aortic morphologies.

The aorta is more than a simple tubular conduit vessel for blood. It also regulates the pulsatile pressure waves that are injected into the arterial system by the left ventricle. The biomechanical disorders produced by these waves can accelerate the formation of calcium deposits within the arterial wall. Furthermore, they are thought to be responsible for severe aortic complications, including aneurysms and dissections. Endovascular aortic repair is a modern technique based on the implantation of an endograft to restore the normal blood flow. Precise morphological measurements are required to improve this technique, for both surgery planning and patient follow up.

Our objective was to develop original algorithms to study the aortic geometry in 3D. A computing platform was designed and tested to analyze three main aortic pathologies : calcified atherosclerosis, aneurysms and dissections. The hypothesis of our study was that the individual arterial geometry of a subject plays a complementary role in the development of vascular pathologies beyond traditional risk factors.

Our first work revealed that 80% of the total geometric variability in the thoracic aorta might be explained using 3 factors : the aortic volume, the aortic arc unfolding and its asymmetry. Variability percentages accounted for 46%, 22% and 12%, respectively.

The next 2 works, showed that calcifications in the thoracic aorta were concentrated in the aortic arch and in the proximal descending segment. This spatial distribution was associated with aortic morphology, independently of age, sex, body surface area and traditional risk factors. Our fourth article revealed that calcium deposits in the entire thoracic aorta (including the aortic arch) was associated with non-cardiac events, beyond the standard coronary artery calcium score. It is noteworthy that the aortic arch region is systematically excluded from standard scans.

Our fifth manuscript described a novel deformable model applied to the aortic segmentation under pathological contexts. It was used to estimate the size and shape of abdominal aneurysms before and after endograft implantation. In the last work, this method was adapted to study the geometry of the thoracic aorta of patients with an aortic dissection with respect to a control group. Three anatomic variables were identified for the risk prediction model : the aortic arch diameter, the thoracic aortic length and the age of the patient.

In conclusion, our results show that aortic diseases are closely associated with aortic geometry, independently from traditional risk factors. The developed algorithms improved the automation of measurements and reduced the variability of the estimations.

Keywords : Aorta, computed tomography, digital image processing, arterial calcification, aortic aneurysm, aortic dissection

Table des matières

Remerciements

Au Professeur Alain Simon
Pour m'avoir ouvert les portes de votre service et m'avoir sans cesse encouragé et conseillé dans la réalisation d'un tel projet. L'amitié se construit avec persévérance dans les bons et mauvais moments. Veuillez trouver ici l'expression de ma profonde reconnaissance, de mon admiration et de mon amitié.
Au Docteur Jean-Marc Alsac
Pour avoir inspiré, guidé et soutenu avec force ce projet qui ne cesse de se projeter dans le temps. Merci de m'avoir fait bénéficier de votre expertise au bloc opératoire. Avec le témoignage de ma reconnaissance et de mon amitié.
Au Professeur Elie Mousseaux
Pour votre aide et votre soutient tout au long de ce travail. Veuillez trouver ici l'expression de ma profonde gratitude.
Au Professeur Bernard Levy
Pour vos conseils et vos premiers mots qui m'ont encouragés dans la réalisation d'un tel défi. C'est un honneur et un plaisir pour moi de vous compter parmi les membres du jury.
Au Docteur Nadjia Kachenoura
Pour m'avoir permis d'initier un nouveau chemin de recherche en collaboration ensemble qui a déjà démarré avec les meilleurs expectatives. Veuillez trouver ici l'expression de ma profonde admiration et gratitude.
Au docteur Salma El-Batti
Pour avoir suivi avec sollicitude l'évolution de notre recherche avec patience, intérêt et passion. Avec le témoignage de ma reconnaissance et de mon amitié.
Au Professeur Hisham Kobeiter
Pour avoir eu la gentillesse de juger avec attention ce travail. Soyez assuré de ma profonde gratitude.

A l'ensemble des membres du CMPCV.
Au service de Radiologie et Chirurgie Cardiovasculaire de l'HEGP.
A l'INSERM et particulièrement à la Docteur Chantal Boulanger.
A l'Université Favaloro et à toute l'équipe de la Faculté d'Ingénierie.
A ma famille, à Gustavo et à mes amis.

Abréviations

2D	Bidimensionnelle/deux dimensions
3D	Tridimensionnelle/trois dimensions
AAA	Anévrisme de l'aorte abdominale
AAT	Anévrisme de l'aorte thoracique
AIT	Accident ischémique transitoire
AOMI	Artériopathie oblitérante des membres inférieurs
AVC	Accident vasculaire cérébral
CAC	Calcium artérielle coronaire
CAT	Calcium artérielle thoracique
DATB	Dissection de l'aorte thoracique type B
ECG	Electrocardiogramme
IRM	Imagerie par résonance magnétique
MSCT	*Multi-Slice computed tomography*
TDM	Tomodensitométrie

Table des figures

Publications

Articles originaux de l'auteur correspondant au travail présenté dans la thèse :

Article #1 : Casciaro ME, **Craiem D**, Chironi G, Graf S, Macron L, Mousseaux E, Simon A, Armentano RL. Identifying the principal modes of variation in human thoracic aorta morphology. J Thorac Imaging 2014 Jul ;29(4) :224-32.

Article #2 : **Craiem D**, Chironi G, Casciaro ME, Graf S, Simon A. Calcifications of the thoracic aorta on extended non-contrast-enhanced cardiac CT. PLoS One 2014 Oct 10 ;9(10) :e109584.

Article #3 : **Craiem D**, Chironi G, Casciaro ME, Sirieix ME, Mousseaux E, Simon A. Association of thoracic aorta calcium and non cardiac vascular events in cardiac disease-free individuals. Atherosclerosis 2016 Feb ;245 :22-7.

Article #4 : **Craiem D**, Alsac JM, Casciaro ME, El Batti S, Mousseaux E, Sirieix ME, Simon A. Association between thoracic aorta calcium and thoracic aorta geometry in a cohort of asymptomatic participants at increased cardiovascular risk. Rev Esp Cardiol (Engl Ed) 2016 May. pii : S1885-5857(16)30008-1.

Article #5 : Casciaro ME, El-Batti S, Chironi G, Simon A, Mousseaux E, Armentano RL, Alsac JM, **Craiem D**. Deformable surface model for the evaluation of abdominal aortic aneurysms treated with an endovascular sealing system. Ann Biomed Eng. 2016 May ;44(5) :1381-91.

Article #6 : **Craiem D**, El-Batti S, Casciaro ME, Mousseaux E, Sirieix M-E, Simon A, Alsac JM. Age-related changes of thoracic aorta geometry used to predict the risk for acute type B dissection. (Soumis)

Articles préliminaires :

Craiem D, Chironi G, Redheuil A, Casciaro M, Mousseaux E, Simon A, Armentano RL. Aging impact on thoracic aorta 3D morphometry in intermediate-risk subjects : looking beyond coronary arteries with non-contrast cardiac CT. Ann Biomed Eng. 2012 May ;40(5) : 1028-38.

Craiem D, Chironi G, Casciaro ME, Redheuil A, Mousseaux E, Simon A. Three-dimensional evaluation of thoracic aorta enlargement and unfolding in hypertensive men using non-contrast computed tomography. J Hum Hypertens. 2013 Aug ;27(8) :504-9.

Chapitre 1

Introduction

1.1 Introduction générale

La médecine moderne produit un ensemble de données qui ne cesse d'augmenter chaque année. En particulier les différentes techniques modernes d'imagerie médicale accumulent des énormes volumes de données. Ainsi, l'utilisation du scanner multibarrettes et de la résonance magnétique nucléaire pour le diagnostic et le traitement des maladies cardiovasculaires peut produire des milliers d'images en quelques minutes. Face à cet impressionnant potentiel technologique, les outils de visualisation et les systèmes informatiques capables de faire des mesures spécifiques et puissantes adaptées aux véritables enjeux des médecins restent insuffisantes. Le verdict est incontestable : une large majorité de l'information stockée dans les images reste inutilisée.

Une solution à cette problématique est de concevoir des nouveaux outils informatiques pour aider la démarche médicale. L'interaction avec les logiciels doit être facilitée avec des algorithmes de visualisation adaptés au diagnostic et au traitement médical. Ces algorithmes doivent être ensuite testés et finalement validés. Le travail multidisciplinaire, qui rapproche les médecins et les radiologues des ingénieurs biomédicaux capables de développer ces outils informatiques, reste essentiel pour assurer les objectifs des uns et des autres. *Les résultats de cette thèse montrent justement la puissance de cette collaboration interdisciplinaire dans la conception, la mise au point et l'utilisation d'une plateforme informatique capable de quantifier l'anatomie tridimensionnelle de l'aorte en présence des trois maladies aortiques principales.*

Les deux techniques d'imagerie 3D plus utilisées sont la tomodensitométrie (TDM) mesurée avec le scanner multibarrettes (nommé en anglais *Multi-Slice Computer Tomography* ou MSCT) et l'imagerie par résonance magnétique (IRM). Brièvement, le scanner reconstruit un volume 3D de la densité des tissus par les projections de rayon X dans des différentes orientations. Le temps d'acquisition se réduit systématiquement chaque année avec l'innovation des machines. Aujourd'hui, par exemple, un volume du cœur humain avec des voxels d'une taille <0.5 mm peut être acquis en 100 ms. L'IRM se sert des champs magnétiques statiques et variables pour générer des volumes 3D. L'évolution vers des champs magnétiques plus puissants et plus de résolution est inéluctable. Même si la résolution est parfois inférieure au scanner, le contraste entre les tissus mous est supérieur. Cette technique a deux autres avantages : elle permet une analyse fonctionnelle, au niveau par exemple des

flux 4D (3D + temps) sur des plans obliques ou de connectivité de neurones (tractographie), le tout sans aucune radiation ionisante. Pourtant, en termes de coût opérationnel et temps d'acquisition, l'IRM et moins performante que le scanner. *Ce dernier reste privilégié pour la visualisation structurelle de l'aorte, et sera utilisé dans les six travaux présentés dans cette thèse.*

L'aorte peut être atteinte de trois maladies structurelles principales : l'athérosclérose, l'anévrisme et la dissection. Dans le premier cas, les plaques aortiques calcifiées qui s'accumulent dans la paroi aortique peuvent être facilement repérées avec un scanner sans injection. La détection des calcifications chez des patients en prévention primaire peut améliorer la prédiction des maladies cardiovasculaires, indépendamment des facteurs de risque traditionnels. Une quantification infra-clinique de ces calcifications constitue un outil diagnostique puissant pour la médecine préventive cardiovasculaire, en particulier chez les patients asymptomatiques à risque intermédiaire. Pourtant, la quantification des calcifications se fait dans les parties ascendantes et descendantes de l'aorte thoracique, car ces deux régions sont visibles également sur le scanner cardiaque utilisé pour la mesure du calcium artérielle coronaire (CAC). Le score de CAC est un prédicteur indépendant de mortalité cardiovasculaire mais la valeur ajoutée du calcium aortique à cette prédiction du risque reste à déterminer. L'absence de mesures du calcium dans la crosse de l'aorte, une région proche des artères supra-aortique et qui reste inexplorée dans les séquences classiques du scan cardiaque, représente une limitation méthodologique importante pour évaluer la performance pronostique du calcium aortique. Nous nous sommes donc particulièrement intéressés à l'étude simultanée de la distribution des calcifications dans cette région de l'arche aortique et de la géométrie aortique. La formation des plaques est fortement liée à la morphologie des artères, qui intervient également dans les profils de vitesse. Pour cette raison, nous estimons que la géométrie de l'aorte est un facteur déterminant pour expliquer cette distribution. Le fait de rajouter pour la première fois une partie "invisible" de l'aorte aux mesures de calcifications coronaires et aortiques, nous a donné la possibilité d'étudier la valeur prédictive du calcium aortique associée aux événements non-cardiaques. Actuellement, il n'y a pas d'outil informatique capable de quantifier simultanément, d'une façon rapide et fiable, la géométrie de l'aorte thoracique et ses calcifications. *Même si le score d'Agatston existant pour quantifier les calcifications coronaires peut être appliqué à l'aorte thoracique, la partie curvilinéaire de l'arche nécessite un algorithme spécifique pour saisir sa morphologie. Une étude comme celle-ci chez un grand nombre de patients peut contribuer aussi à déterminer statistiquement la variabilité dans la morphologie de l'aorte thoracique pour mieux comprendre les valeurs normales.*

L'anévrisme et la dissection sont deux maladies aortiques dégénératives graves. Dans le premier cas, la paroi artérielle se dilate localement d'une façon pathologique, augmentant le risque de rupture. Dans le deuxième cas, une déchirure dans la paroi de l'aorte ouvre une porte d'entrée pour la circulation et provoque la création d'un faux chenal parallèle au chenal principal. La circulation par ce faux chenal peut déclencher des thromboses et compromettre la structure de l'aorte et des artères en aval. L'issue de ces maladies sans traitement est généralement fatale. La TDM joue un rôle capital dans le diagnostic de la maladie, l'évaluation du risque et la planification et le suivi des éventuelles interventions. Des prothèses endovasculaires sont utilisées pour exclure la zone anévrismale ou fermer la porte d'entrée des dissections. Ces traitements endovasculaires constituent des alternatives de plus

en plus acceptées pour minimiser le risque opératoire. D'autres traitements médicaux et chirurgicaux sont également disponibles. Cependant, dans toutes ces stratégies, visualiser la morphologie de l'aorte d'une façon quantitative, répétable et précise est un défi considérable. Notamment, en termes de temps si des mesures 3D comme des longueurs ou des volumes sont demandées. Concernant les algorithmes, ils doivent être capables de prendre en compte des géométries pathologiques extrêmement complexes, comme celles d'un vrai chenal qui s'écrase en présence d'un thrombus ou d'un anévrisme abdominale qui compromet les artères rénales et/ou iliaques. *La conception et la mise au point de ces algorithmes, testés sur des cas réels en présence de dissections et anévrismes, constituent les derniers défis de cette thèse.*

1.2 Maladies aortiques. Organisation de l'introduction.

Les principales pathologies de l'aorte sont l'anévrisme, la dissection, l'hématome intra mural, l'ulcère pénétrant athéroscléreux, le faux-anévrisme et la lésion traumatique, pouvant entrainer une rupture aortique, et les affections inflammatoires, athéroscléreuses, dystrophiques génétiques (par ex. syndrome de Marfan) et les anomalies congénitales comme la coarctation de l'aorte. Cette liste s'ajoute à la liste des maladies artérielles coronaires et périphériques.

Comme les autres maladies artérielles, celles de l'aorte peuvent se développer de façon silencieuse (au cours d'une période infra-clinique) ou avoir une présentation aiguë. Le taux de mortalité globale liée aux anévrismes et dissections aortiques a augmenté de 2.48 par 100 000 habitants à 2.78 entre 1990 et 2010 [95]. Au contraire, la prévalence et l'incidence de l'anévrisme de l'aorte abdominale (AAA) ont diminué au cours de la même période. Le taux augmente avec l'âge et les hommes sont plus atteints que les femmes [95].

Les dernières recommandations de la Société Européenne de Cardiologie sur le diagnostic et traitement des maladies aortiques ont été publiées en 2014 et seront utilisées comme référence dans notre travail [34]. Deux registres internationaux, l'IRAD (*International Registry of Aortic Dissection* [48] et le GERAADA (*German Registry for Acute Aortic Dissection Type A*) [93], les recommandations des sociétés américaines [50], des conférences de consensus [37, 106] et le rapport sur l'évaluation des endoprothèse de la HAS (Haute Autorité de Santé) française [88] seront consultés.

L'introduction s'organisera de la manière suivante. L'anatomie de l'aorte normale sera d'abord présentée. Nous préciserons ensuite les techniques d'imagerie utilisées pour évaluer l'aorte ainsi que les traitements disponibles. En termes d'imagerie, nous nous focaliserons sur la TDM qui est l'outil par excellence actuellement utilisé pour visualiser l'aorte. Les effets du vieillissement sur la structure et la fonction de l'aorte seront ensuite abordés. À ce sujet, d'importants résultats préliminaires à ce travail ont été publiés par notre équipe entre 2012 et 2013 [25, 26]. En particulier, la méthodologie pour calculer la morphologie 3D de l'aorte à partir des images du scanner sera expliquée. Notre travail se concentrera sur trois pathologies aortiques : i) les affections athéroscléreuses, notamment l'athérome calcifié, ii) l'anévrisme de l'aorte abdominale (AAA) et iii) la dissection de l'aorte thoracique de type B (DATB) selon la classification de Stanford. Dans toutes les sections de l'introduction, les détails concernant ces trois pathologies seront privilégiés. L'introduction finira avec la formulation des objectifs et l'hypothèse de travail.

1.3 Anatomie de l'aorte non-pathologique

Issue du ventricule gauche, l'aorte donne naissance à l'ensemble du réseau artériel qui transporte le sang oxygéné vers les organes et les tissus. Pendant une vie moyenne, l'aorte conduit 200 millions de litres de sang. L'aorte est séparée par le diaphragme en deux portions : l'aorte thoracique et l'aorte abdominale. L'aorte thoracique est constituée de trois segments : ascendante, crosse aortique et descendante (Figure 1.1). L'aorte abdominale se ramifie en deux artères de plus petits calibres : les artères iliaques qui se dirigent vers les deux membres inférieurs. La paroi artérielle est composée de 3 couches concentriques : l'intima, la media et l'adventice [41]. L'endothélium vasculaire repose sur une couche interne de l'intima en contact avec le sang. La media est plus épaisse et se caractérise par la présence de fibres d'élastine et collagène, ainsi que de cellules musculaires lisses vasculaires. L'adventice est la couche externe qui contient du collagène, des vasa vasorum et des fibres nerveuses du système lymphatique.

L'aorte est considérée principalement comme une artère de conduction mais sa fonction d'amortisseur est essentielle pour réguler la pulsatilité des ondes de pression et le débit provoquée par l'éjection cardiaque. Cette fonction est associée directement à l'élasticité de l'aorte, qui fonctionne comme un réservoir pendant la phase diastolique, assurant parallèlement une perfusion coronaire suffisante [21]. Le segment ascendant et la crosse aortique concentrent 60% de l'élasticité totale du réseau systémique. L'aorte joue également un rôle important dans la régulation de la résistance vasculaire systémique et sur la fréquence cardiaque, par le biais de récepteurs (sensibles aux changements de pression) localisés dans l'aorte ascendante et dans la crosse aortique [41]. Ainsi, une augmentation de la pression artérielle, provoque une baisse de la fréquence cardiaque et de la résistance systémique et inversement.

Les diamètres d'une aorte saine chez un adulte ne dépassent pas en général 40 mm. Le rétrécissement de l'aorte entre le segment ascendant et descendant peut être de l'ordre de 25%, et atteindre jusqu'à 50% pour l'aorte abdominale distale. La taille est influencée par l'âge, le sexe, la surface corporelle (taille et poids) et la pression artérielle [62, 75, 87, 90, 117]. L'expansion progressive du diamètre de l'aorte avec l'âge est de 0.9 mm chez l'homme et 0.7 mm chez la femme, par décennie [115]. Le diamètre de l'aorte descendante progresse plus rapidement que celui de l'ascendante : les taux d'élargissement sont de 3% et de 1% par an, respectivement [33]. L'élargissement de l'aorte est probablement lié à plusieurs facteurs : i) augmentation de la rigidité artérielle, ii) fatigue mécanique accélérée associée au vieillissement, iii) pression artérielle et iv) modification structurelle de la paroi aortique (rapport élastine/collagène). Il est important de connaitre la taille normale de l'aorte. Plusieurs décisions thérapeutiques dépendent de cette estimation. Chaque mesure de l'aorte est sujette à l'erreur. Les valeurs doivent être comparées avec précaution en considérant : i) la résolution des images et la modalité d'acquisition, ii) l'inclusion/exclusion de la paroi artérielle, iii) l'angulation des artères et des plans de mesure, iv) la variabilité intra-inter observateur. Les valeurs typiques de la taille de l'aorte indexées par sexe et surface corporelle sont présentées dans le Tableau 1.1.

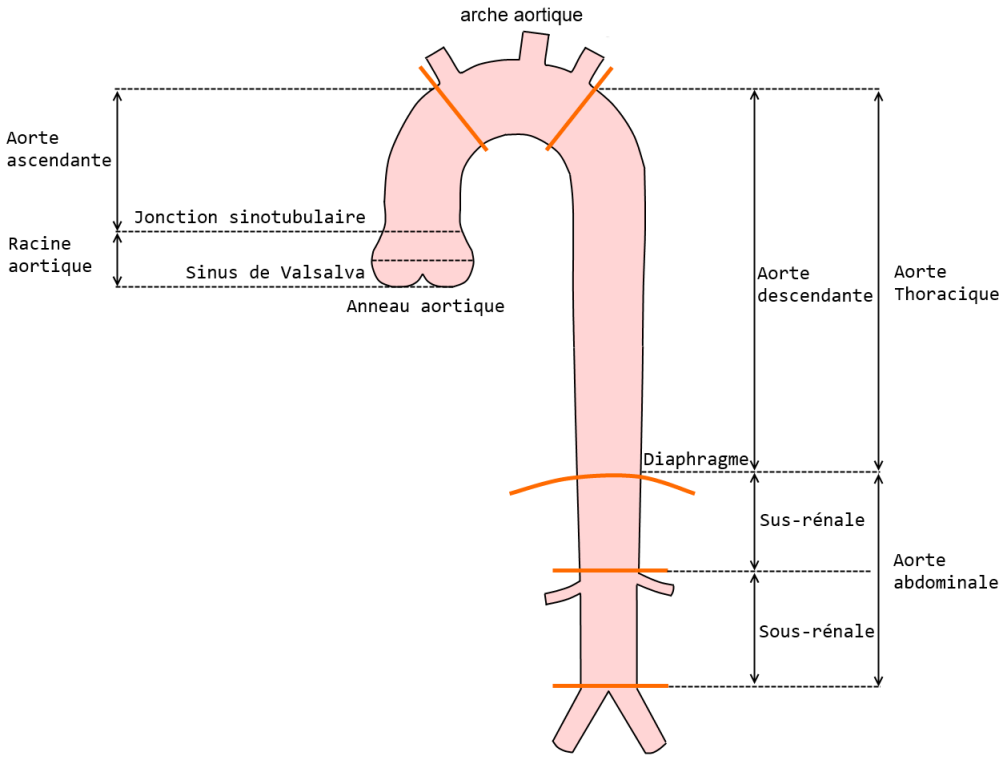

FIGURE 1.1 – Anatomie de l'aorte et ses différents segments

1.4 Evaluation de l'aorte : modalités d'imagerie

Cliniquement, les maladies aortiques progressent généralement de façon silencieuse, mais quelques symptômes peuvent se manifester comme des douleurs abdominales ou thoraciques à migration dorsale, une toux ou des douleurs à la déglutition et d'autres symptômes associés aux accidents vasculaires cérébraux (AVC). L'examen physique doit comporter une palpation/auscultation de l'abdomen à la recherche de pulsations artérielles majorées. Les examens biologiques doivent inclure le bilan des facteurs de risque cardiovasculaires traditionnels.

L'examen de l'aorte par imagerie reste l'évaluation de référence. L'aorte a une morphologie complexe qui est parfois difficile à saisir en 2D. Même les mesures unidimensionnelles (par ex. un diamètre) exigent un positionnement perpendiculaire à l'axe du flux. A ces limitations majeures s'ajoutent la résolution de l'image, la variation du cycle cardiaque, l'effet du mouvement, la détermination précise des bordures et la reproductibilité des méthodes par plusieurs observateurs. Il faut noter aussi que l'aorte n'a pas une section strictement circulaire, et que cette forme tubulaire peut encore se déformer en cas de maladie. Cela rend difficile sa description par un simple diamètre localisé. Plus largement, la standardisation des mesures de la morphologie aortique reste un sujet de discussion systématique dans les conférences internationales spécialisées. *Dans notre travail, ces considérations seront appli-*

TABLE 1.1 – Mesure du diamètre aortique par échographie transœsophagienne chez les adultes [35].

Segment	Sexe	Diamètres (cm)
Anneau aortique	H	2.6±0.3
	F	2.3±0.2
Sinus de Valsalva	H	3.4±0.3
	F	3.0±0.3
Racine aortique		<3.7
Aorte ascendante proximale	H	2.9±0.3
	F	2.6±0.3
Aorte ascendante		<3.7
Aorte descendante		<3.2
Paroi aortique		<0.4

quées à la conception d'algorithmes de segmentation et de mesure sophistiqués et adaptés à ces exigences.

Idéalement, la mesure de la surface de section de l'aorte doit se faire dans un plan orthogonal à sa ligne centrale. Comme le parcours de cette ligne est tortueux, ce plan diffère en générale des coupes courantes (sagittales, frontales ou transversales). Une méthode de reconstruction multi-planaire d'une coupe orthogonale en 3D est donc recommandée [55]. Si cette reconstruction n'est pas disponible, le diamètre s'estime avec l'axe court de l'ellipse. Cette approximation se complique d'avantage si l'artère est pathologique, dilatée ou tortueuse. En plus, il existe toujours des controverses autour de l'inclusion ou non de la paroi dans la mesure de la taille de l'aorte [33].

Les méthodes d'imagerie disponibles pour visualiser l'aorte sont : i) la radiographie du thorax, ii) l'échographie (quatre variantes : échographie transœsophagienne, transthoracique, abdominale et intravasculaire), iii) la TDM (ou tomographie par scanner), iv) la tomographie par émission de positrons, v) l'imagerie par résonance magnétique (IRM) et vi) l'aortographie (angiographie). La modalité préférée pour la détection des calcifications et l'évaluation des anévrismes et/ou des dissections est la TDM multi-barrettes [91]. Dans notre travail, nous avons travaillé avec un scanner de 64 barrettes. Trois des avantages du scanner sont la vitesse d'acquisition et de traitement d'images, l'obtention d'un volume 3D de l'aorte complète avec une haute résolution spatiale et sa disponibilité dans les centres hospitaliers [44]. Une acquisition non-injectée permet de repérer facilement les calcifications dans les artères coronaires, ainsi que dans l'aorte. Une acquisition injectée permet la détection et la localisation des segments disséqués, la présence d'athéromes, de thrombus,

d'ulcères et d'extension de la maladie dans les différentes branches collatérales. Cette modalité est généralement synchronisée avec l'ECG pour éviter les artefacts dus au mouvement, en particulier pour visualiser l'aorte ascendante. Actuellement, la planification des traitements par endoprothèse se fait préférentiellement à l'aide du scanner, du fait de sa précision et de sa fiabilité. Le scanner a deux limitations principales : l'exposition aux radiations ionisantes (en particulier pour les enfants et les femmes) et le produit de contraste iodé qui peut provoquer des allergies. Les doses d'irradiation au cours d'une séquence non-injectée et injectée sont inférieures à 3 mSv et 15 mSv respectivement. Les fabricants promettent une diminution considérable de cette dose pour la nouvelle génération de machines. L'IRM reste une modalité attractive, notamment du fait de sa résolution temporelle. Elle permet ainsi la mesure des profils de vitesses et même de la distensibilité de l'aorte. La large résolution spatiale du scanner assure une évaluation précise de la structure de l'aorte tandis que la résolution temporelle de l'IRM ouvre la voie d'une quantification complémentaire de sa fonction. Pourtant, le coût et la vitesse d'acquisition de l'IRM dans les applications cardiologiques sont moins performants que le scanner.

1.5 Traitements existants

Les traitements disponibles pour les maladies aortiques sont : i) médicamenteux, ii) endovasculaires et iii) chirurgicaux.

Le traitement médicamenteux a pour objectif la diminution de la tension de cisaillement sur la paroi aortique malade. Une réduction de la pression artérielle et de la contractilité cardiaque est envisagée. Les comorbidités des patients ayant une maladie aortique sont : les maladies coronaires et rénales, le diabète, l'hypertension et la dyslipidémie, entre autres. Les stratégies de prévention doivent être concordantes. Fumer produit un effet de dilatation sur l'aorte et doit être déconseillé [16]. Les efforts physiques doivent être évités et l'activité physique limitée. En présence d'une dissection, les bêtabloquants peuvent réduire la fréquence cardiaque et aider à maintenir une pression systolique entre 100-120 mmHg. A long terme, la pression doit être contrôlée dans des niveaux de 140/90 mmHg avec l'utilisation d'antihypertenseurs [34]. Quelques études observationnelles ont montré un effet bénéfique des statines sur les anévrismes, mais des essais cliniques sont toujours en cours [51].

Il existe actuellement deux traitements endovasculaires possibles. Le premier pour réparer l'aorte thoracique et le deuxième pour l'aorte abdominale. Suite à une dissection (ou anévrisme thoracique), la technique endovasculaire a pour objectif l'exclusion du faux chenal (ou de l'anévrisme) de la circulation par l'implantation d'une endoprothèse auto-expansible couverte, ce qui préviendra ainsi la dilatation de l'aorte et sa rupture. En particulier, chez les patients ayant une dissection de l'aorte thoracique descendante, l'endoprothèse est posée en regard de la porte d'entrée pour obturer la circulation du faux chenal. La dépressurisation du faux chenal réduit son volume et augmente celui du vrai chenal. Dans le cas où le positionnement de l'endoprothèse (pour des raisons d'ancrage) obture l'origine d'une artère supra aortique (par ex. sous-clavière), une chirurgie de revascularisation peut être réalisée par voie cervicale (traitement hybride). Les détails de ces procédures sont disponibles dans la littérature [45]. Une exclusion incomplète de la lésion aortique peut mener à des fuites qui nécessitent un traitement complémentaire. Il existe cinq types d'endofuite : au niveau de l'ancrage de l'endoprothèse (type I), liées à une perfusion par des branches collatérales

(type II, les plus fréquentes), liées à une déconnection des modules de l'endoprothèse elle-même (type III), à sa porosités (type IV), ou en rapport avec une cause non détectée par l'imagerie (type V). Des complications neurologiques, comme une paraplégie ou un AVC, ont été constatées avec une prévalence de 1.5% et 3%, respectivement en cas de traitement des dissections aortiques. Les dissections de type B (classification Stanford) qui s'étendent à l'aorte ascendante de façon rétrograde correspondent à 1.3% des patients [32]. La technique qui concerne la pose d'endoprothèses abdominales a ses propres spécificités. Par exemple, la longueur et l'angulation du collet proximal (partie saine de l'aorte au-dessus de l'anévrisme où les parois sont parallèles) doivent être systématiquement évaluées pour assurer une fixation et une étanchéité correctes. Les calcifications de la paroi et le thrombus à l'intérieur de l'anévrisme jouent aussi un rôle important. Les différents modèles d'endoprothèses commercialisés en France ont chacun leurs propres caractéristiques techniques et seront abordés ultérieurement (section 1.9, page 25). Les complications qui nécessitent une chirurgie ouverte intéressent 0.6% des patients. L'incidence d'infection de l'endoprothèse est <1%. Les endofuites type I et III peuvent demander une chirurgie de correction, tandis que celles de type II peuvent se tarir spontanément dans 50% des cas.

Le traitement chirurgical des dissections/anévrismes par l'implantation d'une prothèse chirurgicale cherche à restaurer les dimensions originales de l'aorte pour prévenir sa rupture. Une chirurgie ouverte est pratiquée plus fréquemment quand l'aorte ascendante et/ou la crosse aortique sont concernées. La procédure est lourde, avec arrêt circulatoire en hypothermie, circulation extracorporelle et perfusion cérébrale. Quand seule l'aorte descendante est touchée, la technique endovasculaire offre une alternative nettement moins invasive. Pour traiter les anévrismes abdominaux, la chirurgie conventionnelle (par voie ouverte ou laparotomie) supprime la zone anévrismale et restaure la continuité artérielle en utilisant aussi une prothèse. Il s'agit également d'une chirurgie lourde induisant une durée d'hospitalisation prolongée.

1.6 Vieillissement de l'aorte

Les dimensions de l'aorte sont directement liées à l'âge et à la surface corporelle [117]. Généralement l'estimation de la taille aortique est simplifiée avec une mesure de diamètre. Cependant, des effets d'allongement et même de déroulement avec l'âge ont été rapportés [82, 103]. La dilatation de l'aorte proximale est expliquée par le principe de fatigue matérielle, liée à la fracture des fibres d'élastine causée par l'extension cyclique de l'éjection cardiaque. L'augmentation de la rigidité artérielle est considérée comme une conséquence de cette dilatation. Comme nous allons expliquer dans un premier travail préliminaire de cette thèse [26], la dilatation de l'aorte thoracique avec l'âge n'est pas homogène dans tous ses segments. Le segment ascendant est particulièrement intéressant en raison d'un possible effet de remodelage compensatoire qui limite l'augmentation de la pression systolique [23,82,87,115]. Selon nos propres études, et en conformité avec la littérature, le diamètre moyen, la longueur et le volume de l'aorte thoracique chez les individus normotendus augmentent de 4%, 5% et 14% par décennie, respectivement [26]. En dix ans, nous avons trouvé que le diamètre moyen et la longueur augmentent de 0.1 cm et de 1.2 cm, respectivement. Si nos mesures ont été faites avec des images de scanner sans injection, elles restent cohérentes avec d'autres méthodes comme l'échographie ou l'IRM [30, 86, 103, 117]. Le déroulement de

la crosse aortique est fortement lié au vieillissement [26,86]. En fait, nous avons montré dans un modèle de régression linéaire multivarié, ajusté à la surface corporelle, que l'âge et la largeur de l'arche expliquent 65% de la variabilité de la taille aortique. Finalement, dans un deuxième travail préliminaire, nous expliquerons comment l'hypertension artérielle accélère ces déformations [25].

1.7 Lésions athérosclérotiques

Les deux lésions athéroscléreuses les plus fréquentes sont l'athérothrombose pouvant se compliquer d'embolies, et la calcification.

Définition d'une lésion d'athérothrombose emboligène

Un processus athéroscléreux conduit à l'accumulation de lipides dans l'interface intima-media de l'aorte. Une inflammation secondaire, la déposition d'un tissu fibreux et une érosion de la surface avec l'apparition d'un thrombus peuvent provoquer des embolies thrombotiques ou athéroscléreuses. Une embolie thrombotique est généralement large et peut obstruer la lumière vasculaire des artères de moyen calibre, provoquer un AVC, une ischémie transitoire, un infarctus rénal et une thromboembolie périphérique. Une embolie athéroscléreuse peut bloquer les artères de petit calibre et provoquer un syndrome des orteils bleus.

Epidémiologie

Les facteurs de risque des plaques athéroscléreuses dans l'aorte sont l'âge, le sexe, l'hypertension, le diabète, l'hypercholestérolémie, la sédentarité et le tabac. Dans une étude Framingham réalisée par IRM, des plaques aortiques ont été détectées chez 46% des individus normotendus, avec une prévalence supérieure chez les femmes. La charge athéroscléreuse augmente avec l'hypertension et les maladies cardiovasculaires. Le risque d'AVC et d'évènements périphériques est également associé à la présence de lésions aortiques [1].

Les interventions peuvent entrainer des événements emboliques. L'athérosclérose dans l'aorte ascendante implique un risque majoré d'AVC après une chirurgie cardiaque [112].

Diagnostique et traitement

L'athérome aortique se détecte avec plusieurs techniques d'imagerie, parmi lesquelles l'échographie, la tomographie et l'IRM restent privilégiées. En particulier, le scanner offre la possibilité de localiser les calcifications tandis que l'IRM peut donner plus de détails sur les plaques non-calcifiées et la fonction artérielle.

Pour prévenir le risque thromboembolique, les traitements antiplaquettaires et anticoagulants ont été proposés mais les études comparatives sont rares. L'utilisation des statines et leurs effets nécessitent des études randomisées plus larges qui ne sont pas disponibles à ce stade. La prévention des AVC par une intervention chirurgicale n'est pas recommandée.

Calcium artérielle thoracique (CAT)

La calcification vasculaire peut se produire sur deux sites de paroi artérielle : l'intima et la media. La calcification intimale se présente dans un contexte d'athérosclérose associé à des cellules lipidiques, macrophages et musculaires lisses, tandis que la calcification médiale peut exister d'une façon indépendante et être associé à de l'élastine et à des cellules musculaires lisses vasculaires [85]. Les calcifications aortiques sont corrélées aux événements cardiovasculaires [58]. La localisation et l'extension des calcifications dans le réseau artériel, et en particulier dans l'aorte thoracique, donnent une information essentielle pour prédire la mortalité cardiovasculaire et non-cardiovasculaire [7]. Le CAT peut être détecté et quantifié avec des images de scanner sans injection, et la méthode du score Agatston utilisée pour mesurer le calcium artérielle coronaire (CAC) [4]. L'hypertension artérielle et la rigidité de l'aorte sont aussi des variables significativement liées aux calcifications aortiques [6, 59].

L'évaluation et quantification du CAT seront abordées ultérieurement dans l'un des travaux de cette thèse. Les questions posées seront principalement i) quelle est la distribution des calcifications dans les différents segments de l'aorte thoracique ?, ii) comment la géométrie de l'aorte influence la présence et l'extension du CAT ?, et iii) quelle est la valeur prédictive du CAT par rapport au CAC ?

1.8 Dissection de l'aorte

Définition

Une dissection aortique est définie par la rupture de la couche mediale provoquée par un saignement dans la paroi artérielle qui a pour résultat la séparation des couches pariétales et la formation de deux chenaux (vrai et faux) avec ou sans communication. Dans la plupart des cas, une déchirure intimale initie la dissection et ouvre la voie d'une porte d'entrée dans la media. Une rupture de l'aorte s'en suit si la lésion atteint l'adventice. Une deuxième déchirure peut se produire, pour ouvrir une voie de sortie ou de réentrée dans la vraie lumière aortique. Le faux chenal peut être ou non circulant. Dans ce dernier cas, un flux ralenti est observé dans le faux chenal par rapport au vrai chenal. Les dissections peuvent être rétrogrades ou antérogrades. Dans la classification Stanford, le type A regroupe les dissections s'étendant à l'aorte ascendante et le type B concerne les dissections limitées à l'aorte descendante (Figure 1.2). Notre travail se concentre sur les dissections type B ou le traitement par endoprothèse peut actuellement être proposé.

Epidémiologie

L'incidence d'une dissection aortique est estimée à 6 per 100.000 personnes par an [52]. Un tiers des dissections se produisent dans l'aorte thoracique descendante [64]. L'incidence est plus importante chez l'homme et augmente avec l'âge. Le facteur de risque le plus fréquent est l'hypertension (70%), généralement non-contrôlée. Dans le registre IRAD [48], la médiane d'âge de survenue est de 63 ans.

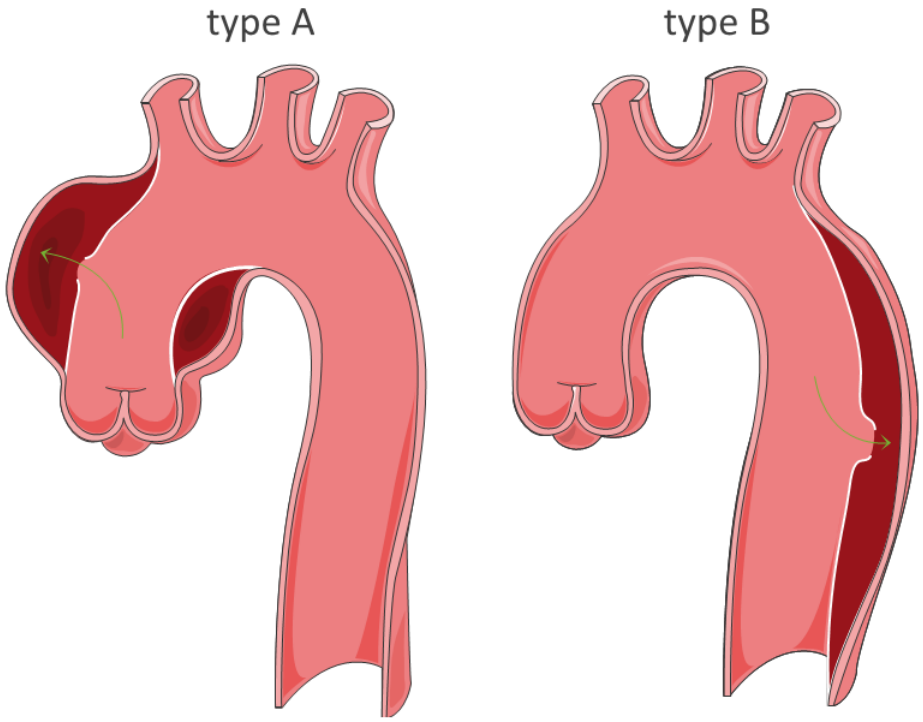

FIGURE 1.2 – Classification Stanford des dissections de l'aorte thoracique (Servier medical images).

Présentation et complications

La présentation la plus fréquente d'une dissection est une douleur thoracique ou abdominale aiguë. La douleur est décrite comme migratrice, en direction de la progression de la dissection. Les manifestations cliniques sont insidieuses (douleur abdominale non spécifique) et rendent difficile le diagnostic précoce. Une absence de douleur est même rapportée dans 40% des cas. Les dissections aortiques de type A peuvent se compliquer d'une ischémie myocardique ou infarctus, d'une insuffisance de la valve aortique, d'une rupture dans le péricarde, déclenchant une tamponnade et une défaillance cardiaque. La progression de la dissection peut compromettre la perfusion d'autres branches collatérales de l'aorte. La dissection d'autres artères peut entrainer une ischémie localisée et affecter les structures et organes adjacents. En pratique, les complications les plus graves sont celles concernant le cœur et n'arrivent que si la dissection concerne l'aorte ascendante (type A). D'autres complications neurologiques, pulmonaires, viscérales et périphériques sont envisageables. Les problèmes de perfusion peuvent être intermittents à cause du mouvement du *flap* (paroi qui sépare le vrai et le faux chenal). Sur le plan biologique, la présence de D-dimères élevés augmente la suspicion de dissection [89]. D'autres biomarqueurs sensibles aux lésions de la paroi artérielle sont en train d'être testés [104].

Technique d'imagerie

Le diagnostic radiologique doit permettre une évaluation intégrale de l'aorte, mesurer sa taille et sa forme ainsi que l'extension de la dissection, la localisation des portes d'entrées (et les éventuelles réentrées), le comportement du flap et les répercussions sur les organes et structures adjacentes. La discrimination entre le vrai et le faux chenal est indispensable. En générale, le faux chenal a un débit inférieur (qui s'il se ralenti entraine l'apparition de la thrombose) et un diamètre supérieur par rapport au vrai chenal. L'utilisation du scanner est une technique rapide, disponible dans tous les hôpitaux, avec une sensibilité >95% et une spécificité >96% [99]. Sur une séquence non-injectée, les calcifications aortiques dans l'intima et/ou dans la media (et celles qui sont restées sur le flap) sont visibles. Pourtant, les séquences injectées et synchronisées (angio-scanner) sont capitales pour décrire la morphologie de l'aorte et les chenaux, évaluer la progression de la dissection et analyser les conséquences de la dissection sur les branches distales. En pratique, avec cette unique séquence, les embolies pulmonaires, les pathologies coronaires et les dissections peuvent être écartées chez les patients ayant une douleur thoracique. Avec une résolution spatiale <0.5 mm dans les coupes axiales et <1 mm dans les coupes longitudinales, le scanner de 64 barrettes multiplie les possibilités pour les ingénieurs de développer des algorithmes et des outils de mesures volumétriques. La visualisation de l'aorte avec une coupe transverse native, peut facilement être améliorée par une reconstruction multiplanaire dans n'importe quel plan oblique en 3D (Figure 1.3).

Traitement

Dans les dissections du type A, la chirurgie ouverte reste le traitement de choix. La mortalité dans les 48hs atteint 50% sans traitement. La chirurgie réduit la mortalité de 90% à 30% dans le premier mois [84]. Malgré les avancées techniques chirurgicales, la mortalité périopératoire (25%) et les complications neurologiques (18%) restent élevées [111].

Dans le cas d'une DATB non-compliquée (absence de déficit de perfusion ou de signes de progression), le patient peut être stabilisé par un traitement médical pour contrôler la douleur, la fréquence cardiaque et la pression artérielle. Actuellement, le traitement endovasculaire est plus accessible et commence à être fréquemment utilisé, surtout chez les patients présentant une DATB compliquée (douleur persistante, hypertension non-contrôlée malgré le traitement médical, déficit de perfusion, dilatation de l'aorte et signes de rupture). La technique consiste en la pose d'une endoprothèse en regard de la porte d'entrée pour exclure le faux chenal de la circulation et contribuer à sa thrombose. La diminution de la pression de ce dernier et la restauration du flux dans le vrai chenal permettent ainsi de reperfuser les artères viscérales et les membres inférieurs. La thrombose du faux chenal prévient une évolution vers l'anévrisme et une éventuelle rupture. Le choix entre le traitement médical et la pose d'une endoprothèse chez les patients présentant une DATB non-compliquée reste un sujet d'actualité [96]. Le rapport INSTEAD (*Investigation of Stent Grafts in Patients with Type B Aortic Dissection*) à 2 ans de suivi, a montré que le traitement endoluminal est efficace mais la survie des patients n'était pas supérieure à ceux traités médicalement [80]. Les évidences d'une différence en faveur du traitement par endoprothèse se manifestent à 5 ans, avec une diminution de la mortalité liée à la maladie aortique et à sa progression [79]. Les résultats du registre IRAD sont similaires, même chez les patients présentant une DATB

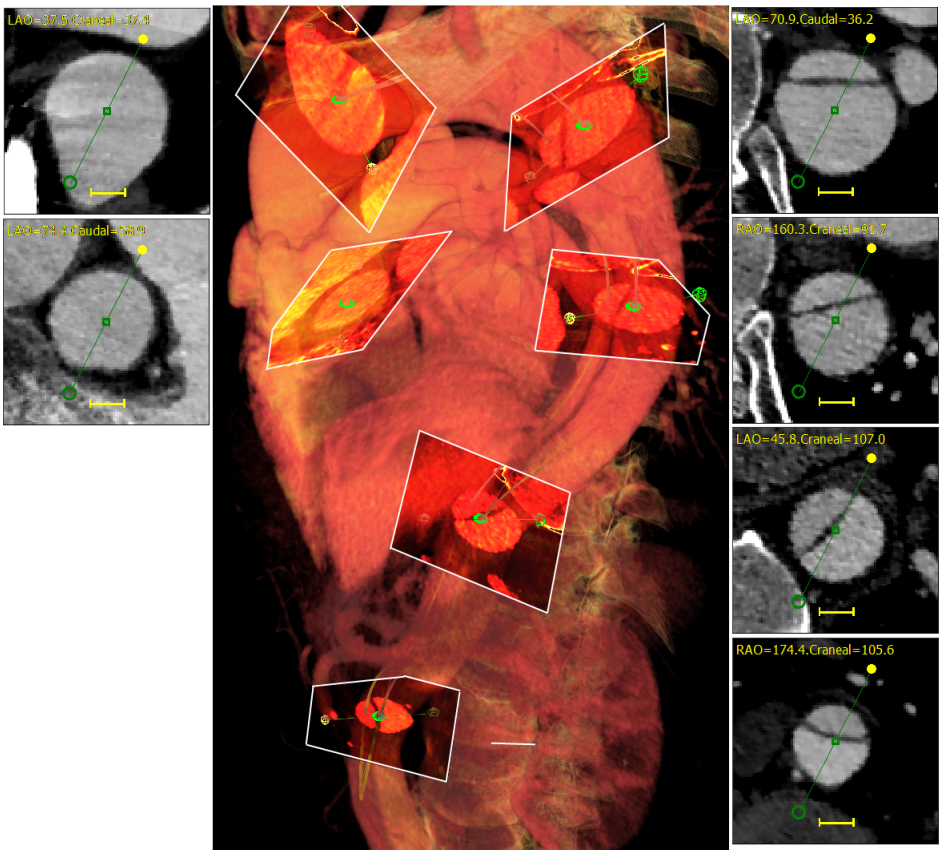

FIGURE 1.3 – Image transversale d'une dissection de type B. Reconstruction multiplanaire oblique.

compliquée [38].

Le traitement chirurgical ouvert d'une DATB est finalement réservé aux patients chez qui l'accès endovasculaire est compromis, où ceux chez qui la zone d'ancrage d'une endoprothèse est trop courte pour pouvoir réaliser l'étanchéité de la porte d'entrée de la dissection. L'objectif de la chirurgie ouverte est le remplacement de l'aorte descendante par une prothèse pour diriger le flux dans le vrai chenal. Le chirurgie est lourde avec une mortalité intra-hospitalière de 25-50% [69]. Parmi les complications figurent l'insuffisance rénale (19%), l'AVC (9%), l'ischémie médullaire (7%) et l'ischémie mésentérique (5%). De façon générale, elle a été largement remplacée aujourd'hui par les techniques endovasculaires, et a quasiment disparu de l'algorithme thérapeutique dans les centres expérimentés.

Les outils informatiques actuels permettent une évaluation précise de la géométrie de l'aorte, la localisation et l'extension de la dissection. Pourtant, la segmentation manuelle de l'aorte avec la présence d'un vrai et un faux chenal reste un défi de taille. Les questions posées dans notre travail sont 3 : i) Est-ce possible de créer un algorithme capable de segmenter les chenaux d'une façon qui soit cliniquement acceptable en termes de temps et précision ? ii) Quelles sont les variables géométriques qui différencient une aorte saine

d'une aorte disséquée ? iii) Peut-on prédire le risque de dissection à partir d'un modèle statistique basé sur ces variables morphologiques ?

1.9 Anévrismes de l'aorte

L'anévrisme de l'aorte est une pathologie de la paroi artérielle responsable d'une dilatation permanente et localisée de la lumière. Elle résulte d'une altération des fibres élastiques et elle concerne l'aorte thoracique et/ou l'aorte abdominale. Il y a une tendance à séparer les anévrismes par région en fonction des spécialistes qui s'en occupent. Pourtant, cette séparation est en quelque sorte artificielle pour 2 raisons : premièrement, parce que les anévrismes se présentent assez souvent en tandem [22,53], ou étendus à d'autres artères comme les iliaques [29] ; deuxièmement, car les patients ayant un anévrisme aortique partagent les facteurs de risque traditionnels (tabagisme, hypertension) des individus à haut risque cardiovasculaire. En fait, après une réparation aortique, les patients restent à haut risque d'autres évènements cardiovasculaires.

La répartition des anévrismes de l'aorte thoracique (AAT) dans la portion ascendante, crosse et descendante est estimée à 51%, 11% et 38%, respectivement. La dilatation progressive de l'artère suit la loi de Laplace et peut évoluer vers la rupture. Environ la moitié des anévrismes de l'aorte abdominale (AAA) est d'origine athéroscléreuse due à un remodelage de la paroi aortique. Ce processus conduit à un épaississement de l'intima qui prend un aspect calcifié et présente une quantité élevée d'acides gras extracellulaires. D'autres origines peuvent concerner les défauts de certains composants protéiques de la matrice extracellulaire (par ex. syndrome de Marfan), l'évolution à partir d'une dissection, un traumatisme ou une pathologie inflammatoire.

Les AAA peuvent entrainer des perturbations hémodynamiques entrainant la formation d'un thrombus intra-luminale, la compression de structures adjacentes et une éventuelle rupture de la paroi artérielle. Suite à une dilatation, le profil de vitesse à l'intérieur de l'anévrisme devient turbulent. La stagnation du sang et la formation du thrombus peuvent occasionner des occlusions et des embolies dans la vascularisation des membres inférieurs. Si l'expansion de l'aorte comprime la veine cave inférieure, des œdèmes des membres inférieurs peuvent apparaitre. Au-delà d'une certaine taille, l'anévrisme peut se rompre. La rupture se traduit cliniquement par une douleur abdominale intense associée à un état de choc hémorragique et nécessite une prise en charge en urgence. Dans le cas contraire, le décès survient de façon inéluctable.

Dans notre travail, nous étudierons les effets de la pose d'une endoprothèse de nouvelle génération pour traiter les AAA. Leurs caractéristiques seront détaillées par la suite.

Définition, prévalence et facteurs de risque des AAA

On parle d'AAA quand le diamètre infra-rénal est $\geq$30 mm ou lorsque le diamètre atteint une valeur supérieure à 50% de la valeur normale. Cette dernière définition est plus compliquée lorsque la transition entre la zone saine et la zone pathologique de l'aorte n'est pas évidente. L'étiologie de la maladie est dégénérative, bien qu'elle soit généralement associée à la maladie athéroscléreuse. La présence d'un AAA est associée à l'âge, au sexe

masculin, aux antécédents familiaux d'AAA et aux antécédents d'athérosclérose et d'hypertension. La prévalence des anévrismes abdominaux est estimée entre 2 et 6 % chez les sujets de plus de 65 ans [3,105]. Les AAA présentent une expansion infra-clinique de l'aorte d'entre 1 et 6 mm par an. Cette variabilité dépend de nombreux facteurs, le tabagisme étant reconnu comme l'un des principaux. L'épidémiologie des AAA est en pleine évolution, avec une baisse de son incidence, cohérente avec la réduction du tabagisme [105]. Le taux d'expansion d'un AAA chez les fumeurs atteint 0.35 mm par an, presque le double que chez les non-ou-anciens fumeurs. Le dépistage systématique par échographie est en discussion dans plusieurs pays [3, 101].

Présentation et complications

L'AAA est une maladie silencieuse avant la rupture et sa découverte est en général fortuite dans le cadre d'une exploration échographique ou suite à une palpation abdominale. La compression d'un organe adjacent peut aussi provoquer des symptômes. La rupture de l'anévrisme est la principale cause de mortalité liée à cette pathologie. Son risque de rupture est proportionnel à sa taille.

Technique d'imagerie

L'échographie est un outil sans risque et à bas coût pour le dépistage et la surveillance des AAA. Pourtant, actuellement la tomographie et l'IRM sont considérées comme des méthodes plus fiables pour les évaluations pré/post opératoires. L'avantage du scanner est sa capacité à visualiser les calcifications. L'IRM reste attractive à cause de l'absence de radiation ionisante et de contraste iodé, même si certaines contre-indications comme les implants métalliques peuvent la limiter.

Pour évaluer un anévrisme il faut se positionner perpendiculairement à la ligne centrale de l'aorte et mesurer le diamètre transversal maximal. D'autres mesures préopératoires sont recommandées, comme la longueur de l'anévrisme et du collet sous-rénal d'aorte saine, le diamètre aortique au niveau des artères rénales, l'angulation des artères iliaques, la tortuosité et la présence de thrombus.

Traitement

Le diamètre maximal ne doit pas être la seule mesure à considérer pour indiquer l'opération d'un anévrisme ou pour continuer à le surveiller. Pourtant, une valeur entre 30-49 mm (ou même 30-54 mm) est souvent évoquée pour décrire un anévrisme de petite taille. Les bénéfices en terme de survie à long terme entre la chirurgie et la surveillance des AAA de petite taille sont similaires [11, 20]. Ça ne veut pas dire que les patients doivent être surveillés de façon passive car ces individus sont à haut risque cardiovasculaire. Par exemple, une étude montre qu'avec un AAA > 30 mm le risque de mortalité par infarctus à 10 ans est de 38% contre 2% seulement par rupture de l'anévrisme [39]. Le traitement médical chez ces patients doit prévenir les événements cardiovasculaires, éviter une progression de la lésion et les préparer pour une éventuelle intervention. Une surveillance par échographie avec des intervalles de 3, 2 et 1 an pour des diamètres de 30-39 mm, 40-44 mm et 45-54 mm sont recommandés, respectivement [15]. Pour réduire la taille des AAA ou limiter leur

expansion, de multiples traitements médicaux (bétabloquants, statines, aspirine, inhibiteurs de l'enzyme de conversion) ont été évalués avec des résultats parfois contradictoires [34]. La dernière recommandation de la Société Européenne de Cardiologie pour les patients hypertendus et avec un AAA est le traitement par bétabloquants [74].

Si le diamètre de l'AAA augmente au-dessus de 55 mm ou le taux de croissance est >10 mm/an ou la lésion devient symptomatique, une réparation de l'aorte par endoprothèse ou par chirurgie conventionnelle à cœur ouvert est recommandée. La maladie coronarienne est présente chez 2/3 des patients ayant un AAA et reste la principale cause de mortalité après la chirurgie. Dans des meta-analyses d'essais cliniques randomisés [27, 102], les périodes de suivi ont été fixées à court (30 jours), moyen (2 ans) et long (>3 ans) terme. Les résultats montrent que la mortalité à court terme est 66% inférieure avec le traitement par endoprothèse. Pourtant, ce bénéfice disparait graduellement avec le temps et le taux de interventions secondaires dévient supérieur en comparaison avec la chirurgie conventionnelle. Pour résumer, le traitement par endoprothèse (chez les patients ayant une anatomie appropriée) réduit de 66% la mortalité péri-opératoire, un bénéfice qui s'érode au cours du suivi à long terme, avec un coût de reintervention supérieur. Pour les patients qui ne sont pas éligibles à l'endoprothèse, la chirurgie ouverte reste le traitement de choix.

La technique endovasculaires et les modèles d'endoprothèses

La technique consiste à exclure l'anévrisme de la circulation sanguine à l'aide d'une endoprothèse auto-expansible introduite par les artères fémorales. L'endoprothèse est un stent couvert. Cette technique permet une réduction de la durée opératoire, de la durée de séjour hospitalier et des complications. Il existe des critères morphologiques précis à respecter, comprenant la longueur du collet, l'angulation formée par l'anévrisme, et la présence de calcifications ou de thrombus sur la paroi du collet. La voie endovasculaire n'est pas dénuée pour autant de complications. La complication la plus fréquente est la survenue d'endofuite. D'autres complications peuvent être une migration de la prothèse, une thrombose des artères iliaques, une claudication fessière suite à la couverture des artères hypogastriques ou encore une détérioration de la fonction rénale suite à une obstruction des artères rénales.

Les détails sur l'abord et la technique de pose d'une endoprothèse sont disponibles dans une excellente revue en ligne [2]. Brièvement, l'abord des artères fémorales se fait par une petite incision. Au bloc opératoire, sous anesthésie générale ou locale, et sous contrôle radiologique, un cathéter d'angiographie est inséré pour permettre la visualisation de l'aorte et assurer le positionnement correct du dispositif. Les modèles d'endoprothèses comprennent celles composées d'une ou 2 pièces (plus des extensions) pour assurer l'irrigation des deux iliaques. En fonction du système de déploiement, une dilatation peut être réalisée en fin de procédure à l'aide d'un cathéter à ballonnet, en particulier au niveau du collet proximal et des jambages iliaques, ceci afin de renforcer l'étanchéité du dispositif. Un contrôle angiographique est réalisé en fin de procédure. Une anatomie complexe est caractérisée par l'absence de collet et/ou par des lésions occlusives des artères viscérales. Les patients ne pouvant pas être traités par endoprothèses bifurquées classiques, peuvent être traités par des endoprothèses de type fenêtrées sur mesure. Pour les anatomies simples, en France il existe cinq fournisseurs d'endoprothèses remboursées : *Cook, Endologix, Medtronic, Gore et Vascutek* (voire Figure 1.4). Les photos et les descriptions de chaque modèle d'endoprothèse

peuvent se trouver ici [12].

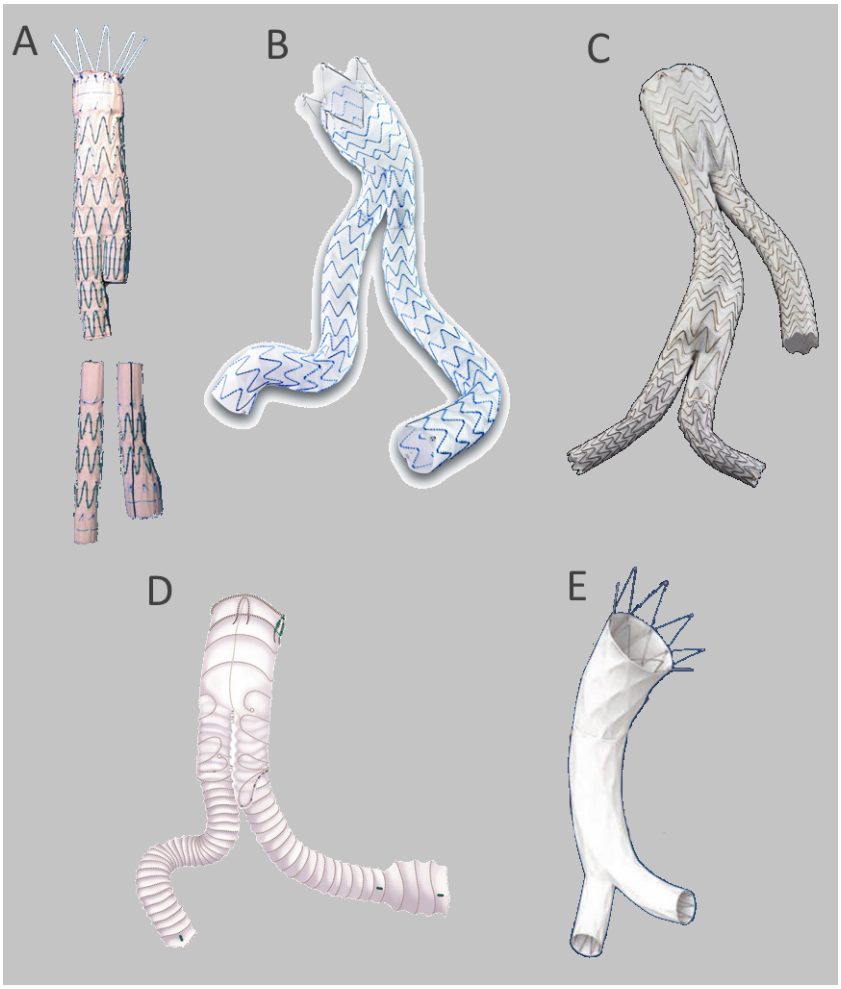

FIGURE 1.4 – Modèles d'endoprothèse : A. Zenith (Cook), B. Endurant II (Medtronic), C. Ecluder (Gore), D. Anaconda (Vascutek), E. Powerlink/AFX (Endologix)

— Zenith^{TM}(*Cook*) est l'endoprothèse la plus utilisée en France. Elle est composée d'un corps principal associé à deux jambages. Le stent est en nitinol avec une couverture en Dacron. L'étanchéité est obtenue par une fixation supra-rénale avec crochets. Le largage du dispositif est réalisé par deux fils de sécurité en nitinol. Ce système possède une extrémité très souple utile pour les artères iliaques tortueuses.
— Endurant II^{TM}(*Medtronic*) est l'endoprothèse la plus utilisée en Europe. Elle est composée de polyester tissé, avec un stent en nitinol. Elle utilise des marqueurs de nouveaux types. La fixation est supra-rénale avec crochets, la partie couverte venant se positionner au ras des artères rénales. L'endoprothèse n'est pas repositionnable lors de sa pose.
— Excluder^{TM}(*Gore*) est une endoprothèse composée de ePTFE renforcé par du PEF

(polyéthylène fluoré). La prothèse est soutenue par une armature en nitinol posée sur la surface externe du ePTFE. Le système se compose du tronc principal et du jambage homolatéral en un seul bloc, auquel est ajouté ensuite le jambage controlatéral et (si nécessaire) des extensions aortiques et iliaques. L'étanchéité est infra-rénale et la fixation à la paroi est assurée par sept paires de crochets. Le système de pose permet de repositionner l'endoprothèse déployée au cours de l'intervention.

— L'Anaconda^{TM}(*Vascutek*) est un système trimodulaire, c'est-à-dire comportant initialement le corps principal de l'endoprothèse associé à ses deux jambages iliaques. La partie proximale de la prothèse est en forme de selle (ou bouche d'Anaconda), les faces antérieure et postérieure se positionnant un peu plus en hauteur que les faces latérales. Ceci permet d'anticiper une augmentation du diamètre du collet proximal. La fixation de l'endoprothèse ne peut se faire que sous les artères rénales et elle fait intervenir un mécanisme passif (deux anneaux) et actif (crochets). Un système de capture magnétique du guide controlatéral est censé faciliter le cathétérisme de l'accès fémoral controlatéral. Le stent proximal est raccordé au système de libération par des fils qui permettent de replier temporairement le dispositif après son déploiement et de le repositionner avant la libération finale.

— Powerlink/AFX^{TM}(*Endologix*) propose une fixation anatomique. L'endoprothèse se fixe sur la zone de bifurcation donnant naissance aux deux artères iliaques. Ainsi, le corps principal de la prothèse est forcément bifurqué. La zone de fixation est donc différente de la zone où se fait l'étanchéité. Ce type de dispositif permet d'être efficace sur des bifurcations aortiques plus étroites. Le stent se compose d'un seul fil d'un alliage de chrome et de cobalt et recouvert de PTFE, uniquement suturé aux extrémités.

Les technologies associées aux endoprothèses ne cessent d'évoluer et sont en plein essor. L'endoprothèse Nellix^{TM}(*Endologix*) a proposé récemment une approche innovante : remplir l'anévrisme d'un polymère se durcissant in situ. Deux stents couverts non déployés (un pour chaque iliaque) sont insérés dans l'anévrisme. Autour des stents, deux sacs de polyuréthane sont remplis d'un polymère. La quantité de polymère à injecter est déterminée avec un critère de pression intra-luminale défini par le fabricant. L'objectif de cette technologie est de minimiser le risque d'endofuites et de migration du dispositif à long terme.

Dans notre cinquième travail, l'étude de la géométrie de l'aorte abdominale avant et après la pose d'une endoprothèse Nellix^{TM}sera abordé. Les 3 questions posées seront : i) Peut-on estimer la quantité de polymère à injecter avec une segmentation volumique de l'anévrisme par scanner ? ii) La quantité de polymère injecté avec le critère de la pression proposé par le fabricant peut-elle produire une expansion de l'anévrisme ? iii) Quelles sont les zones des anévrismes les plus affectées par cette expansion ?

1.10 Résultats préliminaires sur la géométrie de l'aorte thoracique

Notre équipe de recherche s'est intéressée à la géométrie de l'aorte thoracique avant le début de cette thèse. Les résultats de ces travaux ont permis de mettre au point l'approche théorique et méthodologique qui est à la base de notre travail actuel. Deux articles ont été

publiés dans ce contexte [25, 26] et ils sont disponibles dans l'Annexe. Le premier article décrit la méthodologie de séparation numérique de l'aorte pour l'isoler des structures environnantes (segmentation en termes de traitement d'images), les mesures automatisées de la géométrie aortique et l'étude de l'influence de l'âge. Le deuxième article utilise la même méthodologie pour effectuer une étude élargie d'une population de patients hypertendus.

1.10.1 Travail préliminaire #1 : Influence du vieillissement

« Aging impact on thoracic aorta 3D morphometry in intermediate-risk subjects : looking beyond coronary arteries with non-contrast cardiac CT »

Ce travail a été publié dans le journal *Annals of Biomedical Engineering* en 2012 sous la référence :

Craiem D, Chironi G, Redheuil A, Casciaro M, Mousseaux E, Simon A, Armentano RL. Aging impact on thoracic aorta 3D morphometry in intermediate-risk subjects : looking beyond coronary arteries with non-contrast cardiac CT. Ann Biomed Eng. 2012 May ;40(5) : 1028-38.

La quantification du CAC a été incluse dans les guidelines pour améliorer la prédiction des maladies cardiovasculaires [46]. Un score calcique est calculé à partir de la taille et la densité des calcifications coronaires détectées sur les images cardiaques sans contraste du scanner [4]. Ce score a montré une valeur prédictive ajoutée à celles des facteurs de risque traditionnels pour prédire les maladies cardiovasculaires. En conséquence, le nombre de patients examinés par scanner dans les centres de prévention est en constante augmentation. Curieusement, les calcifications de l'aorte thoracique ont été moins explorées, même si une grande partie de l'aorte thoracique descendante est visualisée dans la fenêtre d'acquisition standard d'un scan cardiaque. Les deux objectifs de ce premier travail ont été i) développer une méthodologie pour quantifier la géométrie de l'aorte thoracique en profitant des études du CAC et ii) d'évaluer le rôle du vieillissement sur cette morphologie. Les trois résultats principaux ont été les suivants :

- Les études du CAC peuvent être utilisées pour regarder au-delà des artères coronaires et saisir ainsi la géométrie de l'aorte thoracique dans ses trois segments.
- En élargissant la fenêtre d'acquisition, pour inclure l'arche aortique, un algorithme a permis d'automatiser les mesures 3D de longueur, diamètre moyen et volume de l'aorte thoracique avec un coefficient de variation inter-opérateur inférieur à 4%. D'autres mesures de forme comme le rayon de courbure, la largeur, la hauteur et la tortuosité de l'arche aortique ont été également possibles.
- Dans une population de 200 hommes normo-tendus, l'effet du vieillissement produit une dilatation de 1.3 mm, un élargissement de 1.2 cm et une augmentation du volume de 21 cm^3 par décennie. La crosse aortique change de forme aussi : l'aorte se déroule avec une vitesse de 7 mm en largeur par rapport à 3 mm en hauteur chaque 10 ans, avec une diminution concomitante de la tortuosité de 4% dans cette période. Toutes les valeurs ont été ajustées à la surface corporelle.

Ce travail a été le premier à quantifier la géométrie de l'aorte thoracique en 3D à partir

des images sans contraste au scanner. La méthode automatisée est rapide et reproductible. Elle a deux limitations. L'algorithme prévoit une section artérielle circulaire. Pour l'obtenir dans la région curvilinéaire (crosse aortique), une reconstruction des plans obliques a été calculée. Pourtant, cette méthode ne peut pas être appliques dans des cas pathologique comme les anévrismes ou les dissections. Une deuxième limitation méthodologique est liée à l'élargissement de la fenêtre d'acquisition de l'ordre de 10-15% qui implique une radiation supplémentaire pour les patients. La dose effective de radiation pour ces 200 patients a été 1.23±0.14 mSv (0.96-2.1 mSv) et correspond aux valeurs typiques d'une étude de CAC.

Les algorithmes développés dans la méthodologie de cet article seront décrits en détail dans la section des résultats du premier travail consacrée à l'étude de la variabilité géométrique (Section 2.2, page 32).

1.10.2 Travail préliminaire 2 : Influence de l'hypertension

« Three-dimensional evaluation of thoracic aorta enlargement and unfolding in hypertensive men using non-contrast computed tomography »

Ce travail a été publié dans le journal *Journal of Human Hypertension* en 2013 sous la référence :

Craiem D, Chironi G, Casciaro ME, Redheuil A, Mousseaux E, Simon A. Three-dimensional evaluation of thoracic aorta enlargement and unfolding in hypertensive men using non-contrast computed tomography. J Hum Hypertens. 2013 Aug ;27(8) :504-9.

L'hypertension artérielle a été identifiée comme un facteur déterminant de la taille de l'aorte [5, 23, 113]. Cependant, la taille de l'aorte est souvent estimée à partir d'un diamètre et non de sa morphologie globale. L'objectif de ce travail a été de déterminer l'impact de l'hypertension sur la morphologie 3D de l'aorte thoracique. Deux cent patients normotendus et 200 patients hypertendus ont été recrutés. Les trois résultats principaux ont été :

- Un élargissement global de l'aorte thoracique a été observé chez les patients hypertendus par rapport aux normotendus, indépendamment de l'âge. Les valeurs de diamètre et de volume ont été en moyen 5% et 20% supérieurs, respectivement chez les hypertendus. Le déroulement de la crosse aortique s'accélère avec l'hypertension.
- La dilatation et le déroulement de l'aorte thoracique provoqués par l'hypertension sont équivalents à un vieillissement artériel de 5 à 8 ans.
- L'analyse de l'influence de la pression diastolique et systolique sur les variables anatomiques de l'aorte montre que la largeur de l'arche aortique est très sensible à la pression systolique, augmentant de 12% pour chaque augmentation de 10mmHg, indépendamment de l'âge et du traitement antihypertenseur.

Ce travail a été le premier à réaliser une exploration exhaustive de la géométrie 3D de l'aorte thoracique chez un grand nombre de patients avec des images de scanner sans injection. Il a pu quantifier l'impact de l'hypertension en terme d'années équivalentes de vieillissement. L'aorte d'un patient hypertendu a en moyen entre 5 et 8 ans de plus qu'un individu normotendu. La relation entre la dilatation de l'aorte ascendante et la pression systolique reste controversée. Des associations positive ou négative entre ces deux variables ont

été publiés [5,56,61,68,77,113]. La notion classique propose une séquence de réalimentation positive entre âge et taille : fragmentation élastique, allongement aortique, augmentation de la rigidité, accélération de la vitesse de propagation de l'onde de pouls et augmentation de la pression systolique comme conséquence. A l'inverse, un mécanisme de compensation peur être envisagé : la dilatation provoquerait une restriction à l'augmentation de la pression systolique par un changement d'impédance caractéristique. Nos résultats montrent une relation positive entre la pression systolique et le diamètre de l'aorte, mais cette relation est moins importante dans le segment ascendant qu'au niveau de l'arche ou de la descendante. C'est la pression diastolique qui semble déterminer cet élargissement. Cependant, des nouvelles études prospectives sont nécessaires pour confirmer ces observations.

1.11 Hypothèse et objectifs de la thèse

L'objectif de ce travail est de déterminer l'influence de la géométrie de l'aorte sur les principales maladies qui l'affectent. Pour cela, des outils informatiques innovants de traitement numérique d'images ont été développés pour obtenir, au-delà des estimations traditionnelles de diamètre et de surface sectionnelle, des mesures tridimensionnelles de la morphologie de l'aorte (saine et malade) utiles pour améliorer la prévention et le traitement des maladies aortiques.

L'hypothèse de la recherche est que la géométrie spécifique des artères de chaque individu joue un rôle additionnel à celui des facteurs de risque traditionnels dans la survenue et le traitement des maladies aortiques.

Une première partie du travail concerne l'étude de la variabilité de la morphologie de l'aorte thoracique chez un grand nombre de sujets en prévention primaire. Un premier module du logiciel a été conçu pour quantifier cette morphologie 3D à partir des images de scanner non-injectés. Le protocole d'acquisition des images a été légèrement modifié pour assurer que toute l'aorte thoracique soit visible, en particulier l'arche aortique.

Dans une deuxième partie du travail, le module du logiciel a été adapté pour ajouter aux mesures géométriques, une quantification des calcifications aortiques, qui sont considérées comme un marqueur d'athérosclérose. La méthode d'Agatston, utilisée pour mesurer le score de CAC a ainsi été appliquée à l'aorte thoracique d'une façon automatisée afin de calculer un score de CAT. Avec cet outil, nous avons étudié simultanément la relation entre la géométrie de l'aorte et ce score calcique chez des patients en prévention primaire. Trois objectifs ont été fixés : i) identifier les régions de l'aorte ou se trouvent les calcifications, ii) mettre en relation cette distribution spatiale avec les variables anatomiques qui décrivent la morphologie aortique, et iii) étudier la valeur prédictive de ces mesures par rapport aux facteurs de risque traditionnels et au CAC, notamment en ce qui concerne les événements extra-coronaires.

Dans une troisième partie, les algorithmes de segmentation de l'aorte saine (appliquées aux images sans contraste) ont été adaptés pour tenir compte des déformations de l'aorte pathologique. L'outil de visualisation a été doté d'un module 3D plus puissant pour aider l'opérateur à faire les mesures sur des images avec contraste. Un algorithme de segmentation plus complexe, basé sur la théorie des modèles déformables, a été programmé et d'abord

testé pour quantifier la morphologie de l'aorte abdominale en présence d'un anévrisme et pour évaluer la performance d'une nouvelle génération d'endoprothèses. Ensuite, nous nous sommes fixés l'objectif d'étudier la morphologie de l'aorte thoracique avec cette méthode et de prédire le risque de dissection à partir des variables anatomiques calculées.

Ainsi, le but du travail de doctorat a été la conception d'une plateforme informatique qui permette l'analyse d'images tridimensionnelles de l'aorte thoracique et abdominale à partir du scanner. La plateforme sera utilisée chez les patients en prévention primaire et secondaire permettant :

1. Une étude de la variabilité géométrique de la aorte thoracique.
2. La détection et quantification des calcifications aortiques.
3. L'analyse morphologique des anévrismes abdominales.
4. La prédiction du risque de dissections de l'aorte thoracique descendante.

1.12 Organisation du manuscrit

Dans le chapitre 2, les résultats des cinq articles publiés et d'un manuscrit soumis seront présentés. Un résumé en français des objectifs, la méthodologie, les résultats et la conclusion précédera la copie de chaque un des articles originaux en anglais. Le chapitre 3 sera consacré à la discussion générale des travaux, les perspectives et les conclusions.

Chapitre 2

Résultats

2.1 Résumé du chapitre

Cette thèse comporte 6 articles. L'Article #1 présente la méthodologie pour segmenter l'aorte thoracique saine à partir d'images de scanner non injecté. L'étude montrera comment résumer statistiquement la variabilité de cette géométrie en faisant une analyse en composantes principales. Les Articles #2, #3 et #4 seront consacrés à l'étude des calcifications dans l'aorte thoracique, et plus spécifiquement dans la crosse aortique. La crosse aortique est une région qui échappe généralement à l'exploration par scanner cardiaque conventionnel. La méthodologie pour calculer un score calcique, analyser la distribution spatiale et interpréter la valeur prédictive de ce score seront les sujets principaux de ces articles. L'Article #5 présente une nouvelle méthodologie de segmentation de l'aorte adaptée à la présence d'un anévrisme. Cette méthodologie sera appliquée à l'étude d'une nouvelle génération d'endoprothèses pour traiter les anévrismes abdominaux. Enfin, l'Article #6 montre comment segmenter le vrai et le faux chenal en présence d'une dissection aortique pour identifier les variables anatomiques qui pourraient la prédire. Les objectifs, la méthodologie et les résultats principaux de chaque article seront présentés, suivis des travaux originaux publiés en anglais.

2.2 Article #1

« Identifying the Principal Modes of Variation in Human Thoracic Aorta Morphology »

Ce travail a été publié dans le journal *Journal of Thoracique Imaging* en 2014 sous la référence :

Casciaro ME, **Craiem D**, Chironi G, Graf S, Macron L, Mousseaux E, Simon A, Armentano RL. Identifying the principal modes of variation in human thoracic aorta morphology. J Thorac Imaging 2014 Jul ;29(4) :224-32.

2.2.1 Introduction et objectifs

La détection précoce de la maladie cardiovasculaire infra-clinique nécessite de nouveaux outils diagnostiques d'imagerie. La quantification du CAC par TDM en est un exemple. A partir des images d'un scanner cardiaque à faible dose de radiation et sans contraste, un score calcique qui mesure la taille et la densité des calcifications coronaires peut être calculé [4]. Ce score a une valeur prédictive additionnelle à celle des facteurs de risque traditionnels [46]. Pourtant, dans cette exploration de routine des artères coronaires, il y d'autres informations extra-coronaires qui peuvent être exploitées. Récemment, nous avons montré qu'en élargissant la fenêtre d'acquisition pour inclure la crosse aortique dans le champ du scanner cardiaque, la géométrie de l'aorte thoracique pouvait être quantifiée en 3D [26]. Dans un échantillon de 400 patients asymptomatiques à risque intermédiaire, nous avons trouvé une relation positive de la taille et du déroulement de l'aorte thoracique avec l'âge, qui s'accélère avec l'hypertension [25]. L'analyse minutieuse de ces données a mis en évidence une variabilité morphologique qui n'avait pas été quantifiée auparavant.

L'intérêt des méthodes de quantification de la morphologie aortique ne se limite pas à étudier l'influence du vieillissement ou de l'hypertension sur l'anatomie. La détection précoce d'une déformation pathologique de l'aorte peut aider au diagnostic d'anévrismes et d'autres maladies aortiques [33]. Les efforts pour synthétiser et chiffrer la variabilité géométrique de l'aorte peuvent améliorer la conception de nouvelles endoprothèses qui soient mieux adaptées aux morphologies aortiques [17]. Finalement, la géométrie aortique joue un rôle central dans la détermination des profils de vitesse, des débits, et des forces de cisaillement qui interviennent dans la formation des plaques d'athérome [73]. Des modèles 3D de l'aorte, représentatifs d'une large population, pourraient ainsi être utiles aux études de la dynamique des fluides.

L'objectif de cette étude a été l'identification des modes principaux de variation dans la géométrie de l'aorte thoracique chez un grand nombre de patients. Une analyse en composantes principales a été menée avec des variables anatomiques représentatives pour trouver les facteurs déterminants de la variabilité morphologique de l'aorte. Un atlas d'aorte et de ses modes de variation a pu ainsi être construit et mis en ligne à disposition d'autres chercheurs.

2.2.2 Méthodes

Un algorithme de segmentation de l'aorte, permettant de l'isoler des structures environnantes, a été appliqué pour étudier une population de 500 patients asymptomatiques du centre de Médecine Préventive Cardiovasculaire de l'Hôpital Européen Georges Pompidou. La description détaillée de l'algorithme peut être consultée dans l'article préliminaire disponible dans l'annexe [26]. Brièvement, à partir des images non-injectées de scanner cardiaque (initialement prévu pour la mesure du score CAC et modifié pour explorer aussi la crosse aortique) une procédure d'extraction de la ligne centrale de l'aorte sur une centaine de points et d'estimation des diamètres respectifs a été mise au point à l'aide d'une plateforme informatique. La Figure 1 de l'Article #1 décrit schématiquement cette procédure. Dans une première étape, l'utilisateur marque le point CA dans l'aorte ascendante et le point CD dans la descendante, au niveau de la bifurcation de l'artère pulmonaire (Figure 1A de l'article). Ensuite, et à partir de CD, un algorithme automatique inscrit et recentre un cercle de rayon

maximal à l'intérieur de la lumière artérielle. Cette action est répétée séquentiellement pour toutes les coupes axiales en direction du diaphragme, en utilisant comme centre de départ celui de la coupe précédente (Figure 1B de l'article). L'aorte descendante est ainsi segmentée à partir des images axiales. Pour la partie curvilinéaire, une reconstruction multiplanaire de plans obliques en pas de 2° est calculée à partir de l'angle 0° (point CD), en passant par 180° (point CA) et jusqu'au 240° (Figure 1C). Dans ces plans obliques, la section de l'aorte devient presque circulaire, permettant l'application successive de l'algorithme. L'union des centres des cercles constitue une ligne centrale préliminaire qui est ensuite lissée. L'algorithme qui inscrit les cercles dans la lumière artérielle est une nouvelle fois appliqué mais en calculant des nouveaux plans orthogonaux à cette ligne centrale lissée. Le diamètre et la position spatiale des cercles à chaque point de la ligne centrale sont ensuite utilisés pour calculer 12 variables anatomiques qui décrivent la morphologie aortique (Figure 2 de l'article). Parmi ces variables on peut trouver le diamètre moyen, la longueur, le volume, la largeur et la hauteur de l'arche aortique, la symétrie, la tortuosité et les angles d'inclinaison et transversale, entre autres.

Une analyse en composantes principales a été utilisée sur l'échantillon de 12 variables anatomiques chez 500 patients pour identifier les facteurs déterminants. Toutes les variables ont été normalisées par soustraction de la moyenne et division par la déviation standard (DS). Les 3 facteurs prédominants, qui concentrent 80% de la variation, ont été identifiés. Un atlas des aortes moyennes et de leurs variations ($\pm$2.DS) a été construit pour visualiser et interpréter géométriquement ces 3 facteurs. Finalement, les coefficients de corrélation de chaque variable anatomique avec ces 3 facteurs ont été calculés pour toute la population, ainsi que dans de sous-groupes séparés par les médianes d'âge, de surface corporelle et du score de risque Framingham à 10 ans [46]. Dans la représentation graphique de ces coefficients de corrélation, les valeurs >0.4 ont été marquées pour aider à l'interprétation des variables anatomiques associées à chaque facteur.

2.2.3 Résultats principaux

Dans le Tableau 1 de l'article se trouvent les caractéristiques cliniques de la population. La plupart des patients avaient au moins un facteur de risque cardiovasculaire. Le score de Framingham à dix ans était de 11$\pm$6 %. Les femmes, représentant 19% de la population, étaient plus âgées ($p<0.001$) et avaient une surface corporelle inferieure ($p<0.001$) par rapport aux hommes. Le pourcentage des patients avec un traitement antihypertenseur et hypocholestérolémique était de 92% et 68%, respectivement. Les 12 variables géométriques qui décrivent l'aorte thoracique sont présentées dans la Table 2 de l'article. Le diamètre, la longueur et le volume aortique étaient en moyenne de 2.9 cm, 28.0 cm et 157 cm^3, respectivement. La largeur et la hauteur de l'arche aortique ont été estimées à 7.8 cm et 4.7 cm, respectivement, avec une asymétrie biaisée vers l'aorte descendante proximale. La taille de l'aorte chez les femmes était plus petite que chez les hommes. Pourtant, en termes de forme, on n'a pas trouvé des différences significatives.

Les trois facteurs principaux dans l'analyse en composantes principales ont représenté 46%, 22% et 12% de la variance totale. Autrement, 80% de la variabilité morphologique de l'aorte pouvait s'expliquer avec seulement 3 facteurs. Les Figures 4 et 6 de l'article montrent que ces trois facteurs s'associent à trois déformations de l'aorte. Pour le facteur 1,

c'est la taille qui change proportionnellement dans tous les segments. Le facteur 2 répond à un rétrécissement de la largeur et une augmentation de la hauteur, qui s'associent au déroulement de l'arche aortique. En observant les modifications liées au facteur 3, une sorte d'asymétrie est perceptible, dans laquelle l'aorte ascendante se rétrécit et l'aorte descendante proximale s'élargit.

Finalement, en séparant la population par médiane d'âge (58 ans), surface corporelle (2.0 m^2) et risque de Framingham (9.4%), les variations morphologiques de l'aorte ne semblaient pas être sensiblement modifiées.

2.2.4 Conclusion

Dans cette étude nous avons analysé la variabilité anatomique de l'aorte thoracique chez 500 patients asymptomatiques à partir d'images non-injectées de scanner cardiaque. En regardant la dispersion des variables anatomiques qui décrivent la morphologie de l'aorte (Tableau 2), les variations restent modérées, de l'ordre de 10%. Le coefficient de variation interquartile est de 6% pour le diamètre et la longueur, 16% pour le volume et 14% pour la tortuosité.

L'analyse en composantes principales, appliquée à des variables anatomiques pertinentes pour décrire la morphologie de l'aorte, a montré que cette variation peut s'expliquer avec 3 facteurs qui synthétisent 80% de la variance totale. L'interprétation anatomique de ces facteurs a déterminé 3 contributions de variabilité dominantes : i) la taille du vaisseau, ii) le déroulement de l'arche, et iii) son asymétrie. Le facteur taille avec 46% domine les variances et concerne un changement homogène de diamètre, longueur et volume. Il peut être perçu comme un index d'échelle. Avec 22%, le facteur déroulement se caractérise par un changement différencié de largeur et de hauteur de l'arche aortique, concomitant avec une modification de la tortuosité et de l'angle d'inclinaison de l'arche aortique. Cette caractéristique peut être associée aux formes anatomiques de l'arche aortique dans les catégories *romanesque, gotique et cubique* [40]. Les pourcentages trouvés par Frydrychowicz chez 62 patients non-pathologiques ont été 71%, 18% et 11%, respectivement. Dans une comparaison qualitative avec notre étude, et en variant le deuxième facteur en 3 catégories, on trouve des pourcentages similaires à 68%, 17% et 14%. Pour le dernier facteur lié à l'asymétrie, les déformations s'observent dans les vecteurs obliques (45° et 135°) qui annoncent une crosse aortique asymétrique. Il ne représente que 12% de la variabilité totale.

Globalement, la variabilité dans la morphologie de l'aorte thoracique n'a pas été influencée par l'âge, la surface corporelle et le risque de Framingham. Il faut analyser ce résultat avec précaution. Par exemple, l'âge est un déterminant essentiel de la forme de l'aorte mais, d'après nos résultats, il n'intervient pas dans la dispersion des variables anatomiques. En d'autres termes, la variabilité des valeurs anatomiques chez nos patients de plus de 58 ans est similaire à la variabilité chez les patients de moins de 58 ans. Avec le même raisonnement, l'analyse des paramètres de taille et de forme pour les hommes et les femmes (Tableau 2 de l'article) montre que le sexe n'est pas une source de variabilité importante.

Les valeurs numériques qui sont à la base du catalogue d'aortes moyennes et de ses modes principaux de variation (Figure 4 de l'article) sont disponibles en ligne (`http://links.lww.com/JTI/A51`). Les données incluent la ligne centrale en 3D, les vecteurs normaux et les diamètres pour chaque facteur et ses variations. Les chercheurs intéressés par la simulation

des flux et à la conception d'endoprothèses pourront ainsi profiter de ces valeurs anatomiques réelles mises à leur disposition.

Dans ce premier travail nous avons montré comment extraire une information extra-coronaire concernant la géométrie aortique à partir des images de scanner cardiaque sans contraste qui était originalement prévues pour une mesure de CAC. L'algorithme numérique de segmentation a permis d'effectuer les mesures en moins de 5 minutes par patient. Les coefficients de variation intra- et inter-observateur ont été inférieurs à 4% et 6%, respectivement [26]. La procédure a été adaptée pour mesurer les 3 segments de l'aorte thoracique, notamment dans les régions tubulaires ou l'algorithme se montre performant. En présence d'une pathologie sévère, une autre approche sera nécessaire comme nous allons proposer ultérieurement. Avec les outils développés pour quantifier la géométrie aortique en 3D et les notions des valeurs normales pour la taille et la forme de l'aorte non-pathologique, nous avançons vers l'étude simultanée du calcium aortique et de sa valeur prédictive.

Identifying the Principal Modes of Variation in Human Thoracic Aorta Morphology

Mariano E. Casciaro, Eng,† Damian Craiem, PhD,*†‡§ Gilles Chironi, MD,‡§ Sebastian Graf, PhD,*† Laurent Macron, MD,§‖ Elie Mousseaux, MD,§‖ Alain Simon, MD,‡§ and Ricardo L. Armentano, PhD**

Purpose: Diagnosis and management of thoracic aorta (TA) disease demand the assessment of accurate quantitative information of the aortic anatomy. We investigated the principal modes of variation in aortic 3-dimensional geometry paying particular attention to the curvilinear portion.

Materials and Methods: Images were obtained from extended noncontrast multislice computed tomography scans, originally intended for coronary calcium assessment. The ascending, arch, and descending aortas of 500 asymptomatic patients (57 ± 9 y, 81% male) were segmented using a semiautomated algorithm that sequentially inscribed circles inside the vessel cross-section. Axial planes were used for the descending aorta, whereas oblique reconstructions through a toroid path were required for the arch. Vessel centerline coordinates and the corresponding diameter values were obtained. Twelve size and shape geometric parameters were calculated to perform a principal component analysis.

Results: Statistics revealed that the geometric variability of the TA was successfully explained using 3 factors that account for $\sim$80% of total variability. Averaged aortas were reconstructed varying each factor in 5 intervals. Analyzing the parameter loadings for each principal component, the dominant contributors were interpreted as vessel size (46%), arch unfolding (22%), and arch symmetry (12%). Variables such as age, body size, and risk factors did not substantially modify the correlation coefficients, although some particular differences were observed with sex.

Conclusions: We conclude that vessel size, arch unfolding, and symmetry form the basis for characterizing the variability of TA morphology. The numerical data provided in this study as supplementary material can be exploited to accurately reconstruct the curvilinear shape of normal TAs.

Key Words: principal component analysis, noncontrast multislice computed tomography, 3-dimensional arterial modeling, aortic arch

(*J Thorac Imaging* 2014;29:224–232)

From the *Facultad de Ingeniería, Ciencias Exactas y Naturales (FICEN), Universidad Favaloro; †Consejo Nacional de Investigaciones Científicas y Técnicas (CONICET), Buenos Aires, Argentina; ‡Centre de Médecine Préventive Cardiovasculaire; ‖Département de Radiologie Cardiovasculaire, Hôpital Européen Georges Pompidou; and §APHP, Paris Descartes University, INSERM U970, Paris, France.

The authors declare no conflicts of interest.

Reprints: Damian Craiem, PhD, Facultad de Ingeniería, Ciencias Exactas y Naturales (FICEN), Universidad Favaloro, Solis 453, CP 1078, Ciudad de Buenos Aires, Argentina (e-mails: dcraiem@favaloro.edu.ar).

Supplemental Digital Content is available for this article. Direct URL citations appear in the printed text and are provided in the HTML and PDF versions of this article on the journal's Website, www.thoracicimaging.com.

Early detection of cardiovascular diseases in a subclinical stage has strengthened efforts to find new noninvasive diagnostic tools. Within several available approaches for risk stratification in asymptomatic adults, multislice computed tomography (MSCT) imaging for coronary calcium assessment was recently recommended in persons at intermediate-risk and even low 10-year-risk levels.[1] The coronary artery calcium (CAC) test exploits the high contrast between calcium and soft tissue and estimates the total amount of calcium within the coronary arteries in a single score at a low radiation dose (typical values are < 2 mSv). Routine CAC tests provide new possibilities to assess extracoronary information. For instance, calcifications are not restricted to coronary arteries, and they can also be found all along the thoracic aorta (TA).[2] Consequently, our group has recently explored the whole TA in a large cohort of patients, extending the scanning field of view (FOV) to include the top of the aortic arch. All this extracoronary information was utilized to build a 3-dimensional (3D) geometric model of the TA and to analyze the effects of aging on the vessel morphology, as described in prior work.[3] Within this process, in which geometric features of the TA curvilinear portion were intensely investigated, we remarked a rich interpatient variability in TA morphology that deserved further attention.[4]

The assessment of TA size is usually used for an early diagnosis of aneurysms or other TA diseases.[5] Furthermore, recent statistics on the incidence and management of TA disease were reported, and the importance of early recognition and diagnosis by modern imaging modalities such as MSCT was enhanced.[6] The combination of MSCT and 3D reconstruction algorithms is essential for endovascular stent design and placement.[7] In a procedure known as endovascular repair of TA, the use of stents originally designed with the shape of the abdominal aorta might limit their success.[8] In particular, these devices often fail to properly adapt to the tortuous shape of the aortic arch and other segments of the TA, inducing changes in blood flow, thrombosis, and/or direct injury to the endothelium.[8,9] There are no commercially available stent grafts for aortic aneurysms of the ascending, root, and arch locations, although investigational designs that include fenestrations to accommodate the branch supra-aortic arteries are being evaluated.[10,11] Further efforts are needed to assess accurate morphologic information of the human TA.[12] Ideally, an anatomic database containing statistical models should be created to explain the natural TA geometric variability using a set of meaningful parameters.

In another context, aortic geometry has proven to be a determinant in primary and secondary blood flow patterns, such as vortex and helix blood flow, verified in numerical

simulations[13] and in vivo.[14] This influence is strongly related to plaque formation in TA, together with the recognized influence of flow-induced shear-stress on atherogenesis.[15,16] Novel quantitative reports, including detailed TA geometric features in 3D for a large cohort of patients, are then indispensable for both the development of innovative stent grafts and the understanding of blood flow patterns.

The aim of this paper was to study the 3D TA morphology in a large cohort of patients and to identify the principal modes of geometric variation. Meaningful geometric variables were selected to perform a principal component analysis (PCA). PCA often requires the placement of landmark points along boundaries to analyze shape variability; however, hybrid parameters can be envisaged as well.[17] In our approach, a set of meaningful size and shape parameters were extracted from TA segmentation and then included into a statistical factor analysis to assess TA geometric variability. The principal factors that explained aortic geometric variations were identified and anatomically interpreted. Animations of the morphologic change associated with each factor and the numerical information to reconstruct the averaged vessels are provided as supplementary material (Videos F1, F2, and F3, Supplemental Digital Contents 1, 2, and 3, http://links.lww.com/JTI/A48, http://links.lww.com/JTI/A49, http://links.lww.com/JTI/A50).

MATERIALS AND METHODS

In the following section, the segmentation algorithm to isolate the TA from noncontrast MSCT images is summarized. Further details can be found in Craiem et al.[3] The subsequent Population Description and Data Acquisition section includes the population description, image acquisition details, and the statistical analysis.

Semiautomatic Segmentation Algorithm

The segmentation process starts when the user places seed points within the ascending and descending aorta at the level of the pulmonary artery, named CA and CD, respectively (Fig. 1A). Using these points, an automatic adaptive circle-fitting algorithm will extract the central skeleton and the circular cross-section of the vessel. The steps of the algorithm that inscribes a circle inside the vessel cross-section area are:

- A median filter within a 10×10 cm region of interest for noise removal.
- A morphologic opening filter using a circular structuring element of radius $r = 1$ cm to separate the aorta from surrounding tissues.
- A binarization isodata algorithm.
- An iterative growth algorithm in which a circle located in the seed expands until it touches the limits of the aorta. Contact with this limit generates the displacement of the center of the circle in the opposite direction to the point of contact, and growth is resumed. The algorithm ends when the biggest circle inscribed inside the vessel cross-section is found.

The result of this algorithm is a point of coordinates (x_i, y_i, z_i) corresponding to the center of the circle and a radius r_i determining the area of the circumference that approximates the cross-section of the aorta in that position (Figs. 1B, C). This algorithm is sequentially applied over the axial CT slices for the descending portion of the aorta below the seed point CD (Fig. 1B) and over oblique planes reconstructed in steps of 2-degree angles by trilinear interpolation following a semitoroidal path joining the CA and CD points, until a maximum angle of 240 degrees is obtained or the coronary sinus is found (Fig. 1C). In both cases, the center point of the circle found at the end of the algorithm is used as a seed point for the next slice or reconstructed plane. The algorithm assumes the aorta as a variable radius cylinder deformed in space along a curve corresponding to its central skeleton. This simplification would ensure that the cross-section of the aorta, perpendicular to its central skeleton is always circular. As the curvilinear portion of the aorta does not necessarily follow a strict toroidal shape[14,18] and the descending aorta might not be perfectly vertical, a postprocessing correction is performed. Accordingly, orthogonal planes to the central skeleton obtained from the previous step are reconstructed, and the circle-fitting algorithm is rerun to find the final aortic diameters for each centerline point. In this correction stage, the new reconstructed planes are perpendicular to the true aortic skeleton thus ensuring a more adequate assessment of the vessel diameter.

The resulting TA model has 2 elements: (i) an ordered set of points for the central skeleton following the aortic path; and (ii) a circular cross-section for each point of the skeleton. This model allows the measurement of geometric and shape parameters of the aorta and can be easily adapted to mesh the aortic surface to perform volumetric or surface calculations.

From the central skeleton of the aorta, a linear regression plane passing through the midpoint between CA and CD (called point "o") is calculated using the orthogonal vectors v1 and v2 shown in Figure 2A. Combining the model with this plane of regression, the following 12 geometric size and shape parameters were measured:

- Mean TA arch diameter (D), including the whole curvilinear portion from CA to CD.
- Total TA length (L) and volume (V).
- Radius of curvature (R) calculated as the inverse of the TA arch curvature from CA to CD.
- Vessel tortuosity (T) calculated as the arc-chord ratio between points CA and CD minus 1.
- Aortic arch width corresponding to the distance between CD and CA (Fig. 2A) and aortic arch height corresponding to the distance between point "o" and point C_{90} (Fig. 2A).
- Distance from center point "o" to 45-degree (C_{45}) and 135-degree (C_{135}) vectors (Fig. 2A).
- Arch symmetry calculated as the difference between C_{135} and C_{45} vectors measured in centimeters.
- The inclination angle α between the plane of regression and the line connecting point "o" with C_{90}. It is an indicator of the arch top inclination (Fig. 2B).
- The transversal angle β between the projection of the lines connecting C_{90} with points CA and CD, over the axial plane (perpendicular to the regression plane). It is an indicator of the inclination of the ascending and descending portions (Fig. 2C).

Population Description and Data Acquisition

We modeled the aorta of 500 asymptomatic patients from the Centre de Médecine Préventive Cardiovasculaire unit of the Georges Pompidou Hospital (Paris, France) studied between September 2009 and October 2010. Subjects were hospitalized in an ongoing cardiovascular risk

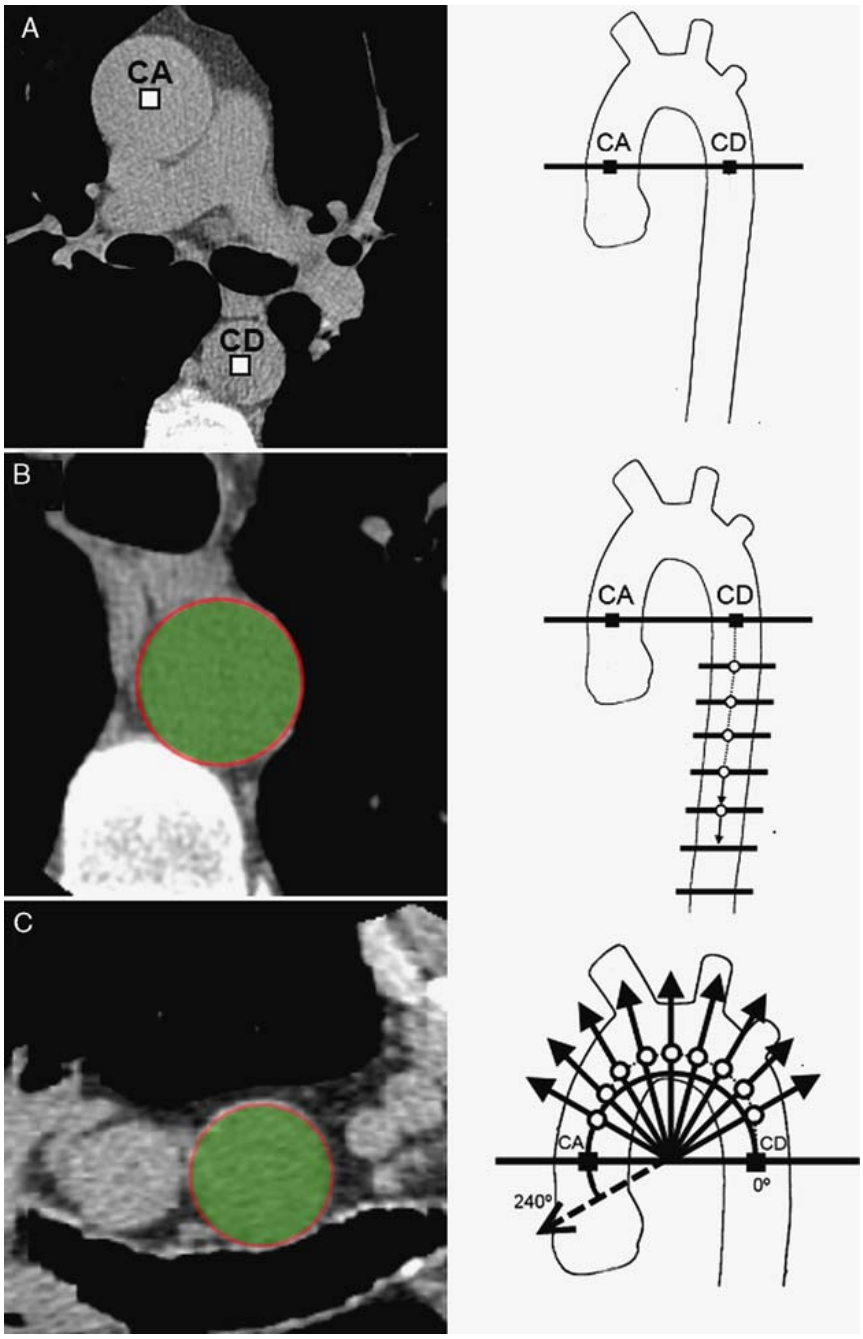

FIGURE 1. A, Axial tomographic slice at the level of pulmonary artery where aortic ascending (CA) and descending (CD) seed points are placed by the user. B, Descending aorta is automatically segmented with an algorithm that finds the inscribed circles (green) inside vessel cross-section in sequential axial slices. C, The same algorithm is applied in reconstructed oblique planes that follow a toroid path to segment the aortic curvilinear portion. full color online

screening program on the basis of cardiovascular risk stratification including Framingham risk score (FRS) calculation,[19] subclinical atherosclerosis imaging,[20] and CAC scoring by thoracic noncontrast CT. Subjects were consecutively selected from the hospital database provided they had undergone complete TA imaging during the CAC measurement. Hypertension was defined by a resting brachial blood pressure of 140 and/or 90 mm Hg or above and/or by the presence of antihypertensive medication. Hypercholesterolemia was defined by a fasting low-density lipoprotein (LDL) cholesterol level of >3.3 mmol/L or by the presence of LDL-lowering drug treatment. Blood glucose was measured after overnight fast, and diabetes was defined by a fasting blood glucose level of 7 mmol/L or above or by the presence of antidiabetic medication. Past or current smokers were defined as subjects who smoke or had smoked at least 1 cigarette per day, every day or someday. All subjects were free of any history or symptom of cardiovascular disease. This retrospective study was authorized by the Commission Nationale de l'informatique et des Libertés and in accordance with the Declaration of Helsinki. Images were obtained in a single breath-hold (craniocaudal direction from above the aortic arch to the diaphragm) using an MSCT scanner (64-slice Light-speed

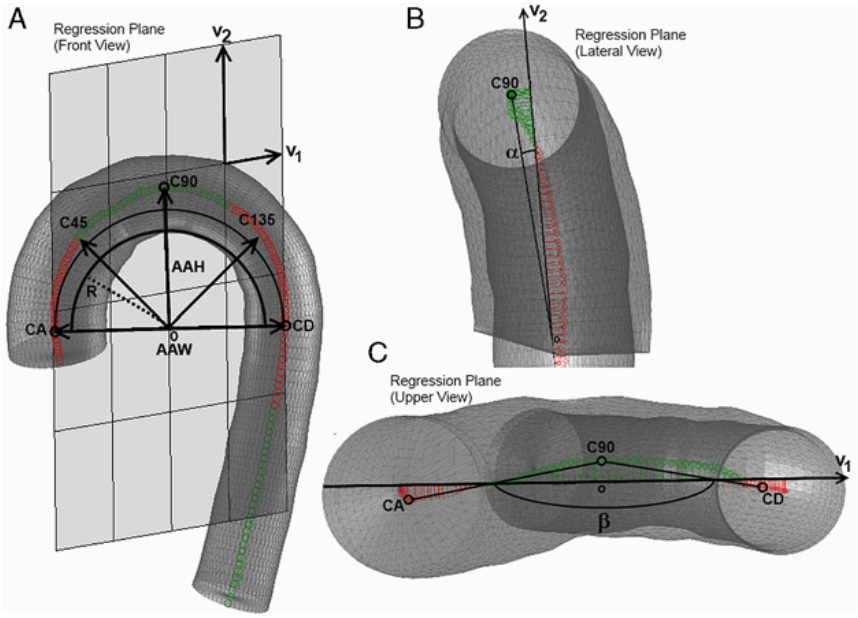

FIGURE 2. A, Aortic mesh and regression plane defined by vectors $\vec{v}_1$ and $\vec{v}_2$. Twelve geometric parameters are calculated to describe the aortic geometry as listed in the Materials and methods section. B, Lateral view of aortic mesh, where the inclination angle α is defined. C, Upper view of aortic mesh, where the transversal angle β is defined. Green and red points indicate TA centerline in front and behind the regression plane, respectively. AAH indicates aortic arch height; AAW, aortic arch width.

VCT; GE Health Care, Milwaukee, WI) with a slice thickness of 2.5 mm, *xy*-resolution of 0.47 mm/pixel, 120 kV, tube current 250 mA, 250 ms exposure, a 2350 mm FOV, and electrocardiogram-triggering at 60% of the RR interval (middiastole).

Statistical Analysis

Baseline characteristics of men and women were compared using a χ^2 statistic for dichotomous variables and analysis of variance for continuous variables. Size and shape parameters were expressed by median and interquartile values (25th and 75th percentile) and compared using a Wilcoxon nonparametric test. Statistical analyses were performed with JMP (SAS, NC) software, and significance was set at $P < 0.05$.

A PCA was performed using a data vector combining the 12 shape and size parameters of each patient.[21] Before the analysis, all variables were normalized by subtracting the mean value and dividing the result by its SD.

The 3 main factors were identified in a PCA scree plot to show the amount of total variance explained by each principal component. Aortic morphology variation, as a function of principal components variation, was studied by plotting an average aorta for patients whose *i*-th principal component F_i fell inside 1 of the following 5 intervals:

$$F_i < -\sqrt{\lambda_i}; -\sqrt{\lambda_i} < F_i < -\frac{\sqrt{\lambda_i}}{2}; -\frac{\sqrt{\lambda_i}}{2} <$$

$$F_i < \frac{\sqrt{\lambda_i}}{2}; \frac{\sqrt{\lambda_i}}{2} < F_i < \sqrt{\lambda_i}; \sqrt{\lambda_i} < F_i, \qquad (1)$$

where λ_i represents the *i*-th eigenvalue of the covariance matrix. For visualization and interpretation purposes, an average aorta was calculated for each interval. This was performed by matching all the corresponding vessels in a unique regression plane and aligning them around the midpoint between CA and CD (point "o"). For every centerline position, an average centerline and diameter value is obtained for all the aligned aortas. The numerical values of the averaged aortic models for the 5 intervals and animations including smooth transitions along these intervals are provided as supplementary material (Videos F1, F2, and F3, Supplemental Digital Contents 1, 2, and 3, http://links.lww.com/JTI/A48, http://links.lww.com/JTI/A49, http://links.lww.com/JTI/A50).

For the first 3 significant eigenvalues ($\lambda_i > 1$) of the covariance matrix, the corresponding eigenvectors were calculated. Using these vectors and the corresponding eigenvalues, the correlation coefficient (r) between the geometric parameters and the principal components were calculated and represented in a parallel plot. Parameters with $r > 0.6$ were considered to be strongly associated with that factor, whereas parameters with $0.4 < r < 0.6$ were considered as mildly associated. Finally, and to further understand the source of TA geometric variability, correlation coefficients were also calculated in 6 subgroups obtained after splitting the whole population in half, separated by median values of (i) age, (ii) FRS, and (iii) body surface area (BSA). The maximum and minimum correlation values in each geometric parameter after division by age, FRS, or BSA were indicated in the parallel plot, together with an individual curve for women in order to visualize the effect of sex.

RESULTS

Population characteristics are detailed in Table 1. Age ranged from 32 to 83 years. Most of the patients had at least 1 risk factor, and the 10-year FRS range was 1% to 32%. Women, representing 19% of the population, were older ($P < 0.001$) and had lower BSA ($P < 0.001$) and lower 10-year FRS ($P < 0.001$) compared with men. The prevalence of traditional risk factors was similar between groups. The percentage of patients receiving treatment for hypertension and hypercholesterolemia was 92% and 68%, respectively. The geometric parameters selected to describe

TABLE 1. Clinical Characteristics of the Study Population

Patients Characteristics	Total	Men	Women
No. subjects [n (%)]	500 (100)	405 (81)	95 (19)
Age (y)	57 ± 9	56 ± 9	61 ± 7*
BSA (m^2)	1.95 ± 0.21	2.0 ± 0.2	1.7 ± 0.2*
10-y Framingham risk (%)	11 ± 6	12 ± 6	5 ± 3*
Hypertension [n (%)]	245 (49)	201 (50)	44 (46)
Hypercholesterolemia [n (%)]	400 (80)	322 (80)	78 (82)
Diabetes [n (%)]	45 (9)	39 (10)	6 (6)
Past or current smoking [n (%)]	279 (56)	235 (58)	44 (46)

Data are mean ± SD or n (%).
*$P < 0.001$ (t test with respect to men).

TA morphology are listed in Table 2. The average TA height and width of the curvilinear portion were 4.7 and 7.8 cm, respectively. The radius of curvature was 3.5 cm. In fact, the curvilinear shape was not strictly symmetrical: the vector C_{135} was slightly longer than vector C_{45}, evidencing a differential deformation in the distal section of the arch, near the proximal descending portion. Vessel centerlines were not completely coplanar with their regression planes (Fig. 2A), as evidenced by mean inclination and transversal angles of 8 and 152 degrees, respectively. Globally, values were in agreement with previous reports.[3,22] In the female population, all size parameters (diameter, length, volume, arch width and height, and C_{45} and C_{135} vectors) were significantly lower ($P < 0.001$) than those in men, whereas shape parameters (tortuosity, arch symmetry, inclination, and transversal angles) did not differ. In addition, the radius of curvature was lower in women than in men ($P < 0.01$).

TABLE 2. TA Morphology

Size and Shape Parameters	Median Q1-Q3 (CQV%) Total	Men	Women
Mean diameter (cm)	2.9 2.8-3.1 (6)	2.9 2.8-3.1 (6)	2.8** 2.7-2.9 (4)
Length (cm)	28.0 26.4-30.0 (6)	28.3 26.5-30.3 (7)	26.9** 25.5-28.3 (6)
Volume (cm^3)	157 132-182 (16)	156 136-187 (16)	137** 119-152 (12)
Radius of curvature (cm)	3.5 3.2-3.9 (9)	3.6 3.3-3.9 (9)	3.4* 3.2-3.7 (8)
Tortuosity	0.81 0.71-0.94 (14)	0.83 0.70-0.93 (14)	0.82 0.72-1.02 (18)
Aortic arch width (cm)	7.8 7.1-8.5 (9)	7.9 7.3-8.6 (8)	7.0** 6.6-7.8 (9)
Aortic arch height (cm)	4.7 4.2-5.1 (9)	4.8 4.3-5.1 (9)	4.3** 4.0-4.6 (8)
C_{45} vector (cm)	4.2 3.9-4.6 (8)	4.3 4.0-4.6 (8)	3.9** 3.6-4.2 (8)
C_{135} vector (cm)	4.4 4.0-4.9 (10)	4.5 4.1-5.0 (10)	4.2** 3.9-4.6 (8)
Arch symmetry ($C_{135}-C_{45}$) (cm)	0.2 −0.1 to 0.6 (160)	0.2 −0.2 to 0.6 (170)	0.3 0.0-0.6 (98)
Arch inclination angle α (deg.)	8 6-10 (23)	8 6-10 (21)	8 5-9 (29)
Transversal angle β (deg.)	152 145-161 (5)	152 145-160 (5)	152 146-162 (5)

N = 500 patients.
Data are median and interquartiles Q1 − Q3 (25th and 75th percentiles).
*$P < 0.01$, **$P < 0.001$ (Wilcoxon test with respect to men).
CQV% indicates coefficient of quartile variation calculated as $(Q3-Q1)/(Q1+Q3)\times 100$.

The scree plot (Fig. 3) shows 3 principal factors representing 46%, 22%, and 12% of the total variance with corresponding eigenvalues of 5.5, 2.7, and 1.5, respectively. The remaining eigenvalues were <1. In other words, 80% of the variability in TA morphology inherent in the measured geometric parameters was explained with these 3 factors.

For the whole population, the aortic shape as a function of variation in the 3 principal factors (within the intervals of Eq. 1) is plotted in Figure 4 for the coronal plane. At first sight, factor 1 can be associated with a proportional size change (scale factor), factor 2 with an unfolding effect that can also be observed in the sagittal plane (Fig. 5), and factor 3 with a modification of the vessel symmetry. Animations are available as a supplementary material to better understand these variations (Videos F1, F2, and F3, Supplemental Digital Contents 1, 2, and 3, http://links.lww.com/JTI/A48, http://links.lww.com/JTI/A49, http://links.lww.com/JTI/A50). Further, centerline coordinates, normal vectors, and diameters for each reconstruction in Figure 4 are provided in an attached spreadsheet (Supplementary Table Average Aortas, Supplemental Digital Content 4, http://links.lww.com/JTI/A51).

The correlation of each geometric parameter with the 3 principal components can be observed in Figure 6. The parameters inside the dark gray band (strong correlation values, $|r| > 0.6$) and the light gray band (mild correlation, $0.6 > |r| > 0.4$) were analyzed for each factor. Factor 1 is dominated by a consistent increase of the principal size parameters (scale effect). In factor 2, arch width and height show an opposite behavior, and whereas arch tortuosity and inclination angle α increase, the transversal angle β decreases (unfolding effect). In factor 3, we observe that the inclination angle is reduced, and, whereas vector C_{45} shortens, the difference with vector C_{135} ($\Delta C = C_{135}-C_{45}$) grows (symmetry effect). To analyze whether the modes of variation were influenced by age, BSA, and 10-year FRS, the population was split into groups on the basis of median values that gave results of 58 years, 2.0 m^2, and 9.4%, respectively. The overall trend of the correlation values was similar in these subgroups with respect to the whole population (Fig. 6, where dashed lines represent the maximum and minimum correlation values found among all subgroups). Correlation coefficients for women were analyzed separately for each factor (dotted lines in Fig. 6). Curves followed the global trend, although some discrepancies in shape unfolding and symmetry factors (2 and 3) were observed (arrows in Fig. 6 indicate values that entered or left both significant correlation bands).

DISCUSSION

In this study, the anatomic variability of the human TA was analyzed in a cohort comprising 500 asymptomatic patients using extended noncontrast MSCT coronary scans that included the top of the aortic arch. PCA, applied to meaningful geometric parameters selected to describe the vessel tridimensional morphology, revealed that TA geometric variation can be successfully explained using 3 key factors that account for ~80% of the total variability

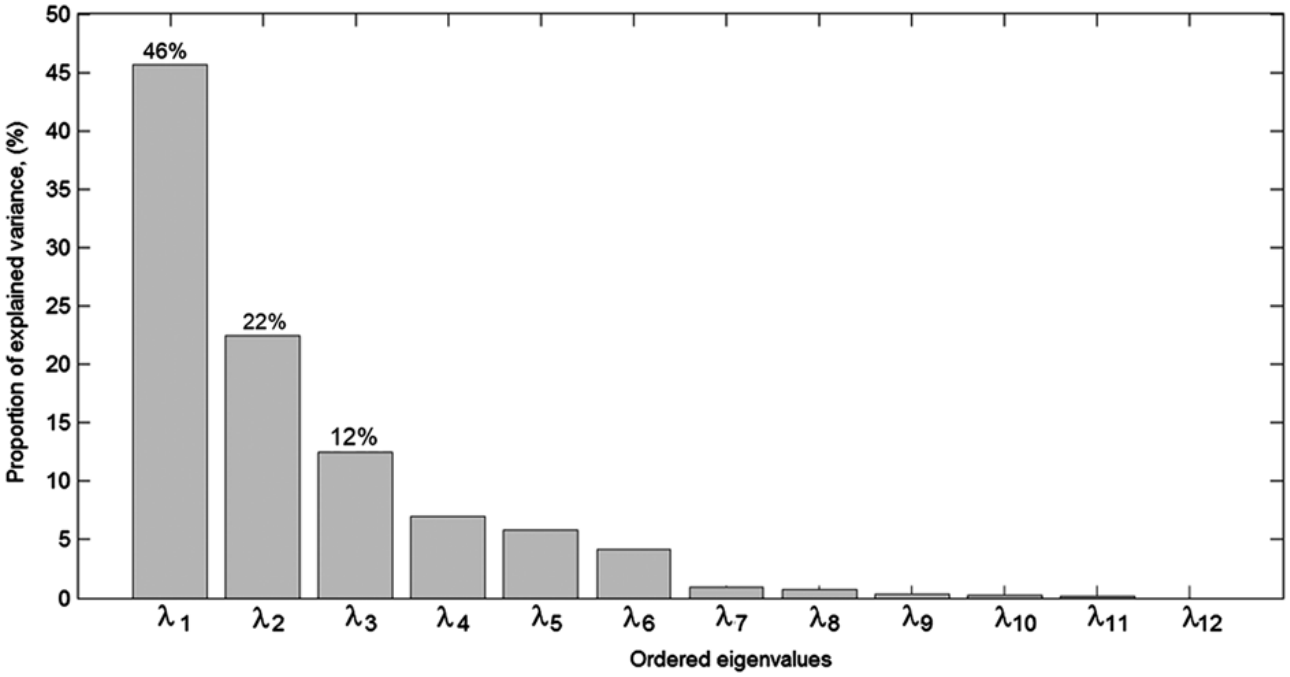

FIGURE 3. Scree plot representing the percentage of total variation for each eigenvalue of the covariance matrix, sorted in descending order. The first 3 factors account for 46%, 22%, and 12% of total variability, respectively.

expressed by these parameters. After analyzing the factor correlations and mean aortic shapes, each mode of variation showed a simple anatomic interpretation. The following dominant contributors resulted: (i) vessel size, (ii) arch unfolding, and (iii) arch symmetry, stating the basis for characterizing the variability of TA morphology. A spreadsheet with numerical data of averaged aortas, including centerline coordinates, normal vectors, and the corresponding diameter values are provided as supplementary material (Supplementary Table Average Aortas, Supplemental Digital Content 4, http://links.lww.com/JTI/A51). This quantitative information catalogues the aortic geometric variability of midlevel-risk patients and can be exploited by researchers interested in aortic blood flow simulations and stent-graft design.

The PCA in this study was applied to geometric parameters selected to describe TA size and shape characteristics (Fig. 2). A similar approach was successfully used to catalogue the geometry of the human coronary arteries.[16] Briefly, instead of estimating the vessel centerline coordinates to examine the statistics of the positions of the points in a classical point distribution model,[23] the variation of 12 anatomic variables that defined the vessel geometry were studied. Actually, the set of parameters was

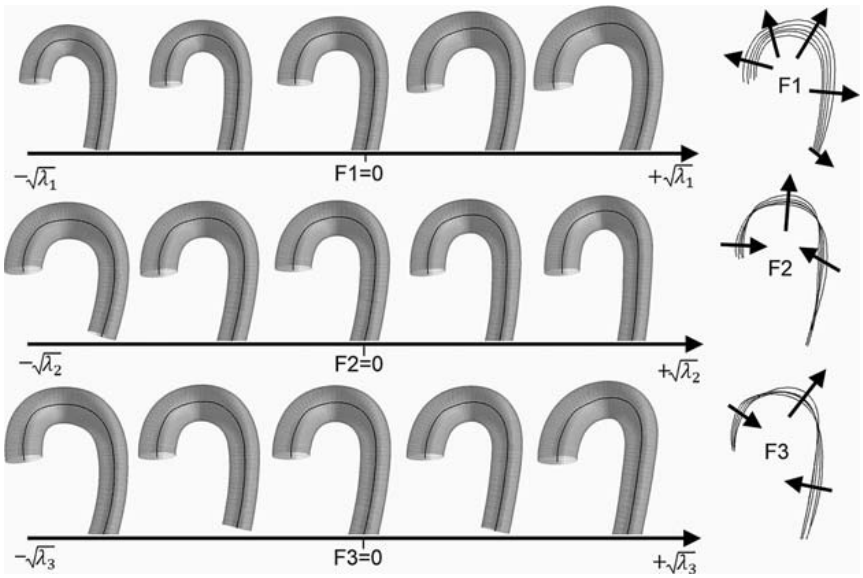

FIGURE 4. Averaged aortic shapes grouped in 5 intervals for positive and negative changes of each factor (Eq. 1). On the right, sketches of the observed effects produced by the increase of each factor over the aortic centerline are shown with arrows.

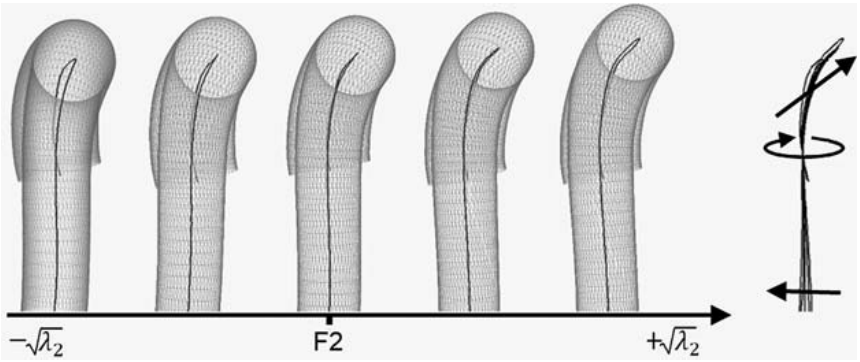

FIGURE 5. Lateral view of averaged aortic shapes for factor 2 (F_2). Positive and negative changes of F_2 are shown in 5 intervals. On the right, a sketch of the twisting effects produced by F_2 on aortic centerline.

not arbitrarily chosen. Recent reports on the aging influence on aortic diameter, length, arch width and height, radius of curvature, and tortuosity were determinant to define it.[22,24] Clinically, all these measures are easily interpreted by a radiologist. Further, our approach did not require any manual scaling/aligning process that could interfere with the variability assessment.[23] Vessels were segmented in 3D from noncontrast MSCT images, and all geometric parameters were measured from skeleton coordinates and their corresponding cross-section diameters using an aortic model. For each patient, inclination and transversal angles were referenced to their own regression plane to avoid aligning ambiguities (Fig. 2). Aortas were aligned using these planes and vectors connecting points CA and CD (Figs. 4, 5) only for visualization purposes and to better understand the different anatomic variations associated with each factor. Essentially, we proposed to explain the anatomic nature of geometric variability identifying those features with high loadings in the factor analysis and interpreting the variations.

The analysis of the geometric parameters exhibited a global moderate dispersion that did not exceed 23% (Table 2), showing that aortas conform to a singular morphology even for a heterogenous group of subjects. Variability of arch symmetry was particularly high due to negative values in the vector differences. In a sex comparison, aortas of women were proportionally smaller compared with those of men, although shape deformation parameters and dispersion values were similar (Table 2). To better summarize these variations by a smaller number of independent factors, a PCA was performed revealing 3 principal factors (scree plot in Fig. 3).

The first factor (F_1) was strongly associated with aortic size parameters: TA volume, length, mean diameter, arch width and height, and C_{45} and C_{135} vectors (top panel of Fig. 6, measures inside shaded region). As seen in Figure 4 and Video F1 (Supplemental Digital Content 1, http://links.lww.com/JTI/A48), all size parameters increase homogenously with F_1 (in the same direction). We can call F_1 a "scale factor" because of its overall relation to vessel size and because it is independent from shape parameters. In other words, 46% of total geometric variability in human TA can be attributed to a proportional size change. The correlation coefficients for women (dotted line in Fig. 6) followed the overall population curves, indicating that even with smaller vessels their mode of variation was similar.

The second factor (F_2) was positively associated with arch tortuosity, arch height, and inclination angle but negatively with arch width and transversal angle (Fig. 6). As seen in Figure 4 and Video F2 (Supplemental Digital Content 2, http://links.lww.com/JTI/A49), the increase of F_2 results in tall and narrow aortas that tend to bend in the sagittal plane. See how the inclination and transversal angles diminish for smaller values of F_2 in the lateral view of Figure 5. The inverse relation between aortic arch width and height in Figure 6 suggests that F_2 describes an anatomic variation associated with an uncoiling deformation of the aortic arch that simultaneously increases the vessel tortuosity. Consequently, we designated F_2 as an "unfolding factor," accounting for 22% of total variability. Aortic unfolding was shown as the consequence of a complex mechanism of aortic dilation and lengthening with aging, accelerated by hypertension.[22,25–27] In other reports, aortas were classified into 3 characteristic shapes related to arch morphology: circular or "romanesque," "gothic," and cubic or "crenel."[14,18] In 62 patients without TA disease, Frydrychowicz et al[14] found 11% of cubic, 71% circular, and 18% gothic arcs. A qualitative comparison of the average shapes found in this study using PCA suggests that the cubic form resembles the aortas with a low value of F_2 ($F_2 < \mu_2 - \sqrt{\lambda_2}$), aortas become circular for intermediate values (between $\mu_2 - \sqrt{\lambda_2}$ and $\mu_2 + \sqrt{\lambda_2}$), and tend to a Gothic shape for high values of this factor ($F_2 > \mu_2 + \sqrt{\lambda_2}$). Patients found in each of these intervals correspond to approximately 14%, 68%, and 17%, respectively, showing a similar proportion to that found in Frydrychowicz et al.[14] It should be noticed that these shapes emerged from mean aortas after PCA, without performing an explicit search for these particular geometries, suggesting that these shapes are also inherently related to the parameters studied in this work. Finally, a particular twisting over the regression plane can be observed in the lateral plane of Figure 5 as the aortic arch flattens. This effect is coherent with a decreased helicity or even a change in helix direction reported in older subjects.[14] Helical flow plays an important role in LDL transport and is thought to compensate the adverse effects of aortic curvature by protecting the arterial wall from atherogenic effects.[13] The morphologic variability described by F_2 seems to anatomically influence the aortic velocity profiles, arterial blood pressure,[28] and aortic stiffness[18,29] and could be a valid starting point to analyze helical flow patterns. In women, a similar unfolding behavior was observed, whereas it also involved a proximal descending

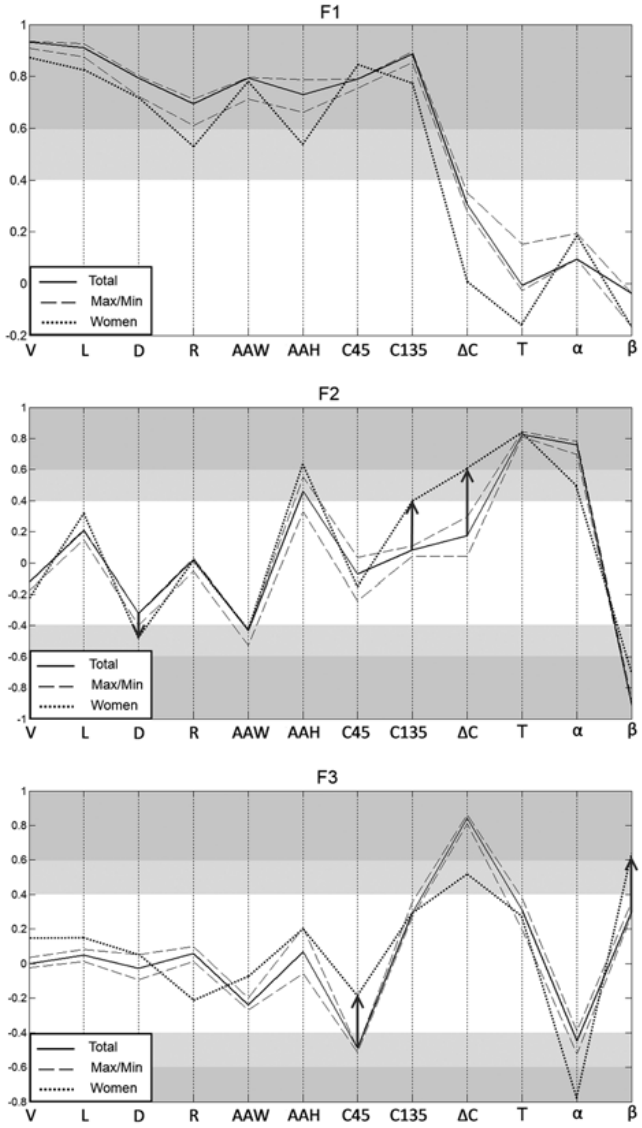

FIGURE 6. Coefficients of correlation (r) of each aortic geometric parameter in PCA for the 3 principal factors. Dark gray bands indicate strong correlations ($|r|>0.6$), and light gray bands indicate mild correlation ($0.6>|r|>0.4$). α and β indicate inclination and transversal angles; AAW and AAH, aortic arch width and height; C_{45} and C_{135}, arch vector distances, D, diameter; R, radius of curvature; L, length; T, tortuosity; V, volume. See Figure 2 for the definition of geometric parameters. Solid lines represent the r values obtained in the PCA of the entire population. Dashed lines represent the maximum and minimum r values found when the population was divided by medians of age, BSA, or FRS. Correlation values for women are shown with a dotted line, and arrows were included where r values differed from the entire population, entering or leaving the gray bands.

aorta deformation (C_{135}) that increased the correlation with the symmetric indicator ΔC (arrows in Fig. 6). This might indicate a specific asymmetric unfolding in women that deserves further attention in future works.

The third factor (F_3), which accounted for 12% of total variability, was dominated by this symmetrical parameter ΔC, defined as the difference between C_{45} and C_{135} vectors. When F_3 grows, ΔC increases and C_{45} decreases (bottom panel of Fig. 6). This particular effect, which pushes the ascending portion toward the center while pulling the proximal descending segment, can be perceived from the sketch in the bottom right corner of Figure 4 and Video F3 (Supplemental Digital Content 3, http://links.lww.com/JTI/A50). Accordingly, F_3 was designated as the "symmetry factor," representing the skew deformation of the aortic arch. In women, we observed that these deformations were slightly attenuated with a more pronounced influence of the transversal and inclination angles (Fig. 6). A numerical simulation as in Liu et al[13] is being designed to provide new insights on the specific role of F_3 on aortic flow and velocity profiles.

In the present study, the role of age, BSA, and FRS on TA morphology variability was also assessed. Maximum and minimum correlation coefficients can be observed with dashed lines in Figure 6. Globally, all relevant parameters presented a negligible deviation. This should not lead to the misinterpretation that TA mean geometric parameters are independent from aging, body size, or the patient risk profile. The fact that the correlation coefficients between these parameters and the 3 main factors remained stable indicates that there exist a natural variability of TA geometry that is not modified by age, BSA, or FRS. Although a "standard aortic arch" does not really exist[4] due to the complex 3D structure of the aorta, the anatomic variability can still be quantified using the proposed method.

Some limitations of the present study need to be addressed. Inherent to the nature of noncontrast MSCT images, only external diameters were measured during a static phase of the cardiac cycle. The assessment of arterial wall thickness and time dependencies would require other techniques such as enhanced CT or magnetic resonance imaging.[22] We decided to exploit coronary calcium scans, extending the FOV by 15% to cover the top of the aortic arch. Radiation exposure for the patient always remained <2 mSv. Regarding the segmentation algorithm, the proposed model required some manual interventions with an estimated intraobserver coefficient of variation of $<4\%$.[3] The circular shape assumption was efficient to extract the vessel centerline and to estimate a diameter, even in the presence of calcified lesions and supra-aortic branches. The inclusion of data regarding the configuration of these branches would have been beneficial but would have also required additional user interventions. Regarding the anatomic landmarks, the aortic root was excluded, and the ascending aorta was defined starting at the ostium of left coronary artery. As the aortic annulus has an oval shape,[30] the circular assumption in the current model should be revised to include it in the proximal ascending portion. Distally, a cross-sectional circularity was actually observed in our population. It is noteworthy that diameter measures are still widely informed using traditional methods (eg, angiography). Moreover, using a circle rather than an arbitrary contour shape was effective for the reconstruction of average vessels, as circles lying in an equivalent centerline position were straightforwardly compared between subjects and needed no angular alignment. Still, other methods recently reported using a level set framework could be explored to improve the cross-sectional shape assessment and to reduce reading variability.[31] Substantially more men than women were included in this study because of a bias in subjects referred to cardiovascular tests by general practitioners to our hospital. Finally, only midlevel-risk patients with no abnormal aortas were selected for this study. Modifications in the segmentation algorithm should be introduced in future studies to assess the morphology variation in diseased aortas.

In conclusion, noncontrast MSCT scans allowed the reconstruction, modeling, and meshing of the entire TA, offering new valuable extracoronary information with respect to the original goal of calcium score assessment. A PCA carried out on aortic morphology showed that vessel size, arch unfolding, and arch symmetry are the principal modes of anatomic variation, accounting for 46%, 22%, and 12% of total variability, respectively. Age, body size, and risk factors did not modify this distribution. The morphometric information reported in this study is aimed at constructing a quantitative catalog of average TAs in midlevel-risk patients.

REFERENCES

1. Greenland P, Alpert JS, Beller GA, et al. 2010 ACCF/AHA Guideline for assessment of cardiovascular risk in asymptomatic adults: a report of the American College of Cardiology Foundation/American Heart Association Task Force on practice guidelines developed in collaboration with the American Society of Echocardiography, American Society of Nuclear Cardiology, Society of Atherosclerosis Imaging and Prevention, Society for Cardiovascular Angiography and Interventions, Society of Cardiovascular Computed Tomography, and Society for Cardiovascular Magnetic Resonance. *J Am Coll Cardiol*. 2010;56:e50–e103.
2. Wong ND, Gransar H, Shaw L, et al. Thoracic aortic calcium versus coronary artery calcium for the prediction of coronary heart disease and cardiovascular disease events. *JACC Cardiovasc Imaging*. 2009;2:319–326.
3. Craiem D, Chironi G, Redheuil A, et al. Aging impact on thoracic aorta 3D morphometry in intermediate-risk subjects: looking beyond coronary arteries with non-contrast cardiac CT. *Ann Biomed Eng*. 2012;40:1028–1038.
4. Demertzis S, Hurni S, Stalder M, et al. Aortic arch morphometry in living humans. *J Anat*. 2010;217:588–596.
5. Elefteriades JA, Farkas EA. Thoracic aortic aneurysm clinically pertinent controversies and uncertainties. *J Am Coll Cardiol*. 2010;55:841–857.
6. Hiratzka LF, Bakris GL, Beckman JA, et al. 2010 ACCF/AHA/AATS/ACR/ASA/SCA/SCAI/SIR/STS/SVM Guidelines for the diagnosis and management of patients with thoracic aortic disease. A report of the American College of Cardiology Foundation/American Heart Association Task Force on Practice Guidelines, American Association for Thoracic Surgery, American College of Radiology, American Stroke Association, Society of Cardiovascular Anesthesiologists, Society for Cardiovascular Angiography and Interventions, Society of Interventional Radiology, Society of Thoracic Surgeons, and Society for Vascular Medicine. *J Am Coll Cardiol*. 2010;55:e27–e129.
7. Rousseau H, Chabbert V, Maracher MA, et al. The importance of imaging assessment before endovascular repair of thoracic aorta. *Eur J Vasc Endovasc Surg*. 2009;38:408–421.
8. Worz S, von Tengg-Kobligk H, Henninger V, et al. 3-D quantification of the aortic arch morphology in 3-D CTA data for endovascular aortic repair. *IEEE Trans Biomed Eng*. 2010;57:2359–2368.
9. Gyongyosi M, Yang P, Khorsand A, et al. Longitudinal straightening effect of stents is an additional predictor for major adverse cardiac events. Austrian Wiktor Stent Study Group and European Paragon Stent Investigators. *J Am Coll Cardiol*. 2000;35:1580–1589.
10. Brozzi NA, Roselli EE. Endovascular therapy for thoracic aortic aneurysms: state of the art in 2012. *Curr Treat Options Cardiovasc Med*. 2012;14:149–163.
11. Monahan TS, Schneider DB. Fenestrated and branched stent grafts for repair of complex aortic aneurysms. *Semin Vasc Surg*. 2009;22:132–139.
12. Ueda T, Fleischmann D, Rubin GD, et al. Imaging of the thoracic aorta before and after stent-graft repair of aneurysms and dissections. *Semin Thorac Cardiovasc Surg*. 2008;20:348–357.
13. Liu X, Pu F, Fan Y, et al. A numerical study on the flow of blood and the transport of LDL in the human aorta: the physiological significance of the helical flow in the aortic arch. *Am J Physiol Heart Circ Physiol*. 2009;297:H163–H170.
14. Frydrychowicz A, Berger A, Munoz Del Rio A, et al. Interdependencies of aortic arch secondary flow patterns, geometry, and age analysed by 4-dimensional phase contrast magnetic resonance imaging at 3 Tesla. *Eur Radiol*. 2012;22:1122–1130.
15. Malek AM, Alper SL, Izumo S. Hemodynamic shear stress and its role in atherosclerosis. *JAMA*. 1999;282:2035–2042.
16. Zhu H, Ding Z, Piana RN, et al. Cataloguing the geometry of the human coronary arteries: a potential tool for predicting risk of coronary artery disease. *Int J Cardiol*. 2009;135:43–52.
17. Bryan R, Mohan PS, Hopkins A, et al. Statistical modelling of the whole human femur incorporating geometric and material properties. *Med Eng Phys*. 2010;32:57–65.
18. Ou P, Celermajer DS, Mousseaux E, et al. Vascular remodeling after "successful" repair of coarctation: impact of aortic arch geometry. *J Am Coll Cardiol*. 2007;49:883–890.
19. Greenland P, Alpert JS, Beller GA, et al. 2010 ACCF/AHA guideline for assessment of cardiovascular risk in asymptomatic adults: a report of the American College of Cardiology Foundation/American Heart Association Task Force on Practice Guidelines. *Circulation*. 2010;122:e584–e636.
20. Chironi G, Orobinskaia L, Megnien JL, et al. Early thoracic aorta enlargement in asymptomatic individuals at risk for cardiovascular disease: determinant factors and clinical implication. *J Hypertens*. 2010;28:2134–2138.
21. Hotelling H. Analysis of a complex of statistical variables into principal components. *J Educ Psychol*. 1933;24:417–441.
22. Redheuil A, Yu WC, Mousseaux E, et al. Age-related changes in aortic arch geometry: relationship with proximal aortic function and left ventricular mass and remodeling. *J Am Coll Cardiol*. 2011;58:1262–1270.
23. Cootes TF, Taylor CJ, Cooper DH, et al. Active shape models—their training and application. *Comput Vis Image Underst*. 1995;61:38–59.
24. Craiem D, Casciaro ME, Graf S, et al. Effects of aging on thoracic aorta size and shape: a non-contrast CT study. Engineering in Medicine and Biology Society (EMBC), 2012 Annual International Conference of the IEEE, San Diego, USA. August 28, San Diego, USA. August 28, 2012:4986–4989.
25. Craiem D, Chironi G, Casciaro ME, et al. Three-dimensional evaluation of thoracic aorta enlargement and unfolding in hypertensive men using non-contrast computed tomography. *J Hum Hypertens*. 2013;27:504–509.
26. O'Rourke M, Farnsworth A, O'Rourke J. Aortic dimensions and stiffness in normal adults. *JACC Cardiovasc Imaging*. 2008;1:749–751.
27. Sugawara J, Hayashi K, Yokoi T, et al. Age-associated elongation of the ascending aorta in adults. *JACC Cardiovasc Imaging*. 2008;1:739–748.
28. Ou P, Bonnet D, Auriacombe L, et al. Late systemic hypertension and aortic arch geometry after successful repair of coarctation of the aorta. *Eur Heart J*. 2004;25:1853–1859.
29. Ou P, Celermajer DS, Raisky O, et al. Angular (Gothic) aortic arch leads to enhanced systolic wave reflection, central aortic stiffness, and increased left ventricular mass late after aortic coarctation repair: evaluation with magnetic resonance flow mapping. *J Thorac Cardiovasc Surg*. 2008;135:62–68.
30. Tops LF, Wood DA, Delgado V, et al. Noninvasive evaluation of the aortic root with multislice computed tomography implications for transcatheter aortic valve replacement. *JACC Cardiovasc Imaging*. 2008;1:321–330.
31. Kurugol S, San Jose Estepar R, Ross J, et al. Aorta segmentation with a 3D level set approach and quantification of aortic calcifications in non-contrast chest CT. Engineering in Medicine and Biology Society (EMBC), 2012 Annual International Conference of the IEEE, San Diego, USA. August 28, 2012:2343–2346.

2.3 Articles #2, #3 et #4

« Calcifications of the thoracic aorta on extended non-contrast-enhanced cardiac CT. »

« Association of thoracic aorta calcium and non cardiac vascular events in cardiac disease-free individuals. »

« Association between thoracic aorta calcium and thoracic aorta geometry in a cohort of asymptomatic participants at increased cardiovascular risk. »

Ces travaux ont été publiés dans le journal *Plos One* en 2014, *Atherosclerosis* en 2015 et *Revista española de Cardiología* en 2016, sous les références :

Craiem D, Chironi G, Casciaro ME, Graf S, Simon A. Calcifications of the thoracic aorta on extended non-contrast-enhanced cardiac CT. PLoS One 2014 Oct 10 ;9(10) :e109584.

Craiem D, Chironi G, Casciaro ME, Sirieix ME, Mousseaux E, Simon A. Association of thoracic aorta calcium and non cardiac vascular events in cardiac disease-free individuals. Atherosclerosis 2016 Feb ;245 :22-7.

Craiem D, Alsac JM, Casciaro ME, El Batti S, Mousseaux E, Sirieix ME, Simon A. Association between thoracic aorta calcium and thoracic aorta geometry in a cohort of asymptomatic participants at increased cardiovascular risk. Rev Esp Cardiol (Engl Ed) 2016 May. pii : S1885-5857(16)30008-1.

2.3.1 Introduction et objectifs

Le score d'Agatston, calculé par TDM sans injection, est utilisé pour quantifier la présence et l'extension des calcifications coronaires. Ce score de calcium artérielle coronaire (CAC) est un prédicteur indépendant de mortalité cardiovasculaire, au-delà des facteurs de risque traditionnels [18]. Aujourd'hui, cet index infra-clinique est utilisé couramment en prévention primaire et le nombre d'images de scanner s'accumulent sans que pourtant d'autres informations extra-coronaires soient exploitées. Entre autre, comme une partie de l'aorte thoracique ascendante et descendante est visible sur le même scan que celui du scanner coronaire, l'estimation d'un score de calcium de l'aorte thoracique (CAT) est envisageable. Même si le score de CAT est considéré comme un facteur de risque à long terme d'ACV ischémique récurrent [8] et peut être mesuré en même temps que le CAC [118], sa valeur pronostique reste à établir. Il faut noter que les études qui analysent le score de CAT excluent la crosse aortique pour des raisons méthodologiques. Pourtant, cette région est la plus vulnérable à la maladie athéroscléreuse et est proche des artères supra-aortiques.

Nous avons menés l'étude des calcifications aortiques dans 3 travaux avec des objectifs spécifiques. Dans l'Article #2, notre étude a cherché à déterminer la distribution de calcifications aortiques chez un grand nombre de patients asymptomatiques en prévention primaire (N≈1000). La méthode automatisée pour repérer les lésions calcifiées sur l'aorte thoracique et pour les quantifier a été publiée. Une analyse sur le profil de risque des patients

qui auraient échappés la détection standard du CAT (sans l'exploration de la crosse aortique) a été faite. Dans l'Article #3, analysant des patients de prévention secondaire qui ont bénéficié d'un scanner sans injection et ont eu un accident vasculaire non-cardiaque, nous avons cherché à déterminer la valeur prédictive du CAT par rapport au CAC, notamment en explorant la crosse aortique. Sur la base des multiples associations rapportées entre l'athérosclérose et la géométrie des vaisseaux [43, 72, 120] dans l'Article #4 , nous avons cherché à comprendre quelle est la relation entre la morphologie aortique et la distribution des calcifications. À notre connaissance, c'est la première fois qu'une étude de cette ampleur sur la relation calcium-géométrie de l'aorte thoracique entière a été réalisée.

2.3.2 Méthodes

Dans l'Article #2, la plateforme informatique développée dans le travail précèdent a été améliorée en ajoutant un module de quantification des calcifications pour aider l'opérateur à les repérer rapidement, à les associer au segment de l'aorte le plus proche et à calculer le score du CAT. La méthode d'Agatston propose une quantification des calcifications basée sur la taille et la densité maximale de chaque lésion [4]. Les calcifications apparaissent comme des taches blanches sur chaque coupe du scan sans injection comme montre la Figure 2 de l'Article #4 sur les trois segments de l'aorte thoracique. Le score calcique se calcule en sommant le score Agatston de chaque lésion. Les échelles classiques utilisées pour analyser le score de CAC sont 0 (pas de calcification), 1-100, 101-400 et >400. Dans le cas du score de CAT, un consensus reste à établir du fait de controverses [57]. En principe, une valeur de dépôt calcique plus élevée est attendue à cause d'une extension plus importante des calcifications à la surface de l'aorte que dans les artères coronaire. Pourtant, comme la crosse aortique reste souvent hors de la fenêtre d'acquisition, la valeur complète du CAT est rarement calculée. Des rapports qui utilisent des déciles ou même de normalisations par la surface corporelle peuvent être trouvés [118]. Dans notre étude, l'aorte thoracique a été séparée en 5 segments comme montre la Figure 1C de l'Article #2. Les segments 1 et 5, visibles dans un scan cardiaque standard, correspondent à l'aorte ascendante et descendante distale. Les segments 2, 3 et 4 comprennent la crosse aortique et ont été visualisés dans le protocole élargi proposé pour inclure l'arche aortique. Trois histogrammes et des interquartiles ont été calculés pour : i) le CAC, ii) le CAT standard (segments 1 et 5), iii) le CAT total. Pour analyser la possibilité de reclasser les individus ayant un CAT>0, et qui auraient pu échapper à la détection classique, la population de 970 patients a été séparée en 3 groupes. Groupe 1 : sans calcifications (CAC=0 et CAT=0). Groupe 2 : patients détectés avec la méthode standard (CAC>0 ou CAT standard>0). Group 3 : détectés exclusivement avec la nouvelle méthode (CAC=0 et CAT standard=0 mais CAT total >0). Une analyse de variance a été calculée sur les facteurs de risque des 3 groupes.

Dans l'Article #3, les scores de CAC et CAT ont été calculés chez 1000 patients consécutifs, dont 30 avaient présenté des événements non-cardiaques (AVC, AIT, AOMI). Toutes les calcifications coronaires et aortiques ont été quantifiées dans 4 scores : i) le score de CAC classique, ii) le score du CAT total (nommé *total TAC* dans l'article en anglais), iii) le score du CAT standard (nommé *partial TAC*), et iv) le score de CAT crosse-aortique (nommé *aortic arch TAC*). La relation entre chaque score avec les événements non-cardiaques a été estimée avec des régressions logistiques multivariées. Les 4 modèles de régression ont été

ajustés à l'âge, le sexe, le cholestérol total, la pression artérielle systolique et le traitement antihypertenseur et/ou avec statines. Le rapport des risques (*odds ratio* en anglais) d'avoir un événement non-cardiaque a été calculé pour chaque cofacteur avec les intervalles de confiance respectifs. Des valeurs log-transformées du score de CAT ont été utilisées dans le calcul des histogrammes et les modèles logistiques.

Une analyse détaillée sur la relation entre la morphologie de l'aorte thoracique et le score de CAT a été faite dans l'Article #4. Neuf cent soixante dix patients asymptomatiques en prévention primaire ont été évalués. Quatorze variables anatomiques ont été calculées pour chaque individu à partir du logiciel de segmentation des images sans injection du scanner. Le score de CAT des segments ascendant, crosse et descendant a été analysé séparément. Les patients ont été séparés par niveau de CAT en 4 groupes avec un modèle non-paramétrique calculé avec les percentiles 50 et 90 du score de TAC (P50 et P90) et l'âge. Les groupes par niveau croissant de CAT ont été : CAT=0, CAT>0 et CAT<P50, CAT>P50 et CAT<P90, CAT>P90. Une analyse de variance ajustée à l'âge, le sexe, la surface corporelle, l'hypertension et l'hypercholestérolémie, a permis la comparaison des variables anatomiques entre les 4 groupes. La relation entre la présence/absence de calcifications dans chaque groupe et les variables anatomiques a été estimée avec des régressions logistiques multivariées. Le rapport des cotes des probabilités d'avoir des calcifications a été calculé pour les groupes 2, 3 et 4, par l'augmentation d'une déviation standard de chaque variable géométrique et normalisée avec le groupe 1 sans lésions. La même méthodologie a été appliquée pour estimer la probabilité d'avoir des calcifications dans chacun des 3 segments de l'aorte par rapport aux 14 variables anatomiques.

2.3.3 Résultats principaux

Au total, 970 patients asymptomatiques (77% d'hommes) ont été étudiés dans l'Article #2 (voir Tableau 1 de l'article). L'arche aortique et l'aorte descendante proximale, deux régions invisibles dans une TDM de routine sans contraste, ont concentré 60% des 11000 calcifications repérées dans la population examinée (Figure 3A de l'article). En normalisant la quantité de lésions par cm, l'arche aortique a été le segment plus densément atteint (Figure 3B de l'article). La présence des calcifications dans l'aorte thoracique a été corrélée à l'âge, avec une prévalence de 89% chez les individus de plus de 64 ans (Figure 4 de l'article). Avec le champ élargi modifié pour regarder la crosse aortique, la prévalence de CAT a doublé, en passant de 31% à 64%. Cela veut dire que 52% des patients auraient échappé à la détection des calcifications avec la méthode standard (Figure 2B). Dans l'analyse de variance, 3 groupes d'individus ont été comparés : ceux libres de calcifications (22%), ceux avec des calcifications détectables sur un scan standard (67%) et ceux repérés seulement avec un scan élargi (11%). Nous avons observé une proportion supérieure de femmes dans ce dernier groupe à reclassifier, avec un profil de risque similaire au premier groupe.

Les 30 individus avec une histoire d'événements non-cardiaques étudiés dans l'Article #3 (12 AVC, 5 AIT et 13 AOMI) ont eu un score de CAT (total et standard) supérieur au reste de la cohorte, avec un score de CAC similaire. Le rapport des risques d'avoir un événement non-cardiaque, par augmentation d'une déviation standard du score log-transformé, a été significatif pour le CAT total (1.56 [1.12-2.24], $p<0.01$) et pas pour le CAC (1.13 [0.86-1.50]). Cette tendance s'est maintenue quand les scores sont entrés individuellement ou ensemble

dans le modèle logistique.

Dans l'analyse calcium-géométrie de l'Article #4, nous avons trouvé que les aortes plus calcifiées étaient celles les plus grandes, les plus déroulées, les plus tortueuses et les moins rétrécies (*less tapered* en anglais). Plusieurs variables anatomiques ont été associées au score de CAT. Pourtant, le score de CAT n'a pas été corrélé aux dimensions de l'aorte ascendante. Au contraire, la dilatation de l'aorte descendante a eu une association significative : le risque d'être au-dessus du percentile 90 dans le niveau du CAT a été 3.62 [2.30-5.91] fois plus important par chaque augmentation de 2.5 mm du diamètre descendant ($p<0.001$).

2.3.4 Conclusion

Les résultats principaux de notre étude des calcifications aortiques concernent la distribution spatiale des lésions, sa relation avec les variables anatomiques et l'association du score de CAT avec les événements non-cardiaques.

La plateforme informatique développée a permis de quantifier chaque calcification et de les localiser dans le segment aortique le plus proche. La distribution des lésions par cm a été hétérogène. Les régions les plus touchées ont été l'arche aortique, suivi par l'aorte descendante proximale et distale. L'aorte ascendante a été la région la moins touchée. Ce constat est important car la partie curvilinéaire de l'aorte thoracique n'est pas explorée avec un scan cardiaque standard. Parmi les individus qui auraient échappé à toute détection de calcium (coronaire ou thoracique) avec le scan standard, se trouvent les femmes d'âge moyen à risque cardiovasculaire modéré. Cette information suggère qu'elles pourraient être les principales bénéficiaires d'une reclassification avec un scan élargi.

Dans le scanner cardiaque utilisé pour mesurer le calcium coronaire, la détection du CAT est étudiée marginalement. Pourtant, des études prospectives ont montré sa valeur prédictive des événements cardiaques et non-cardiaques [19, 49, 57, 63, 118, 119]. Les études ont montré une relation entre le score de CAT et l'âge, l'hypertension, l'hypercholestérolémie, le diabète et le tabac [63, 107]. Une association avec le score de CAC (indépendante des facteurs de risque) a été également démontrée, suggérant un processus athérosclérotique commun dans les deux sites. Cependant, la relation entre le score de CAT et les événements cardiaques reste controversée : i) dans l'étude *Eisner* il n'y a pas eu de relation avec les maladies coronaires et cardiovasculaires [118], ii) des relations modestes mais significatives ont été trouvées avec les maladies coronaires dans les études *Mesa* et *Heinz Nixdorf Recall* [19, 63], iii) une association forte avec l'ACV a été trouvée dans cette dernière étude et avec des événements cardiovasculaires et des événements non-cardiaques dans l'étude *Nelson* [57]. D' Autres travaux montrent que la prédiction avec le score du CAT de la maladie coronaire est supérieure pour les femmes par rapport aux hommes [119], meilleure pour les événements non-cardiaques que pour les événements cardiovasculaires [49, 57, 63], inférieure par rapport au score de CAC pour prédire les maladies coronaires et cardiovasculaires en général [63,118] et plus performante que le score de CAC dans la prédiction des événements non-cardiaques et l'ACV [49,57]. Enfin, les études *Eisner* et *MESA* ont conclu que le score de CAT n'apportait aucune valeur ajoutée au score de Framingham complémentaire à celle du CAC [118, 119], à l'exception des femmes, pour prédire les événements coronaires [19].

Néanmoins, toutes ces études ont des limites qui peuvent nuire à leurs résultats. Dans la plupart, la région balayée par le scanner cardiaque standard n'a pas visualisé la crosse

de l'aorte. Nous remarquons l'étude Nelson, est la seule à mesurer le calcium dans l'aorte thoracique entière, et a trouvé comme nous une forte corrélation avec les événements vasculaires non-cardiaques [57]. Ces résultats montrent que la mesure partielle du score de CAT, excluant les dépôts de calcium dans l'arche aortique, affaiblit la performance du score de CAT dans la prédiction des maladies cardiovasculaires.

Par ailleurs, le CAT n'est pas un synonyme d'athérosclérose. Les dépôts de calcium dans l'aorte peuvent se trouver dans l'intima et/ou dans la media, avec différentes implications pronostiques [85]. Malheureusement, le scanner non-injecté n'est pas capable à ce stade de séparer ces deux phénomènes. Récemment, une étude a repéré les calcifications qui sont restées dans la paroi externe du faux chenal chez des patients ayant une dissection aortique, et suggérait que le calcium détecté par le scanner dans l'aorte thoracique est plutôt localisé dans la media [28]. En outre, le score de CAT a été associé à une diminution accélérée de distensibilité aortique, indépendamment d'autres facteurs [6]. Pourtant, comme nous avons montré dans l'Article #4, la taille de l'aorte descendante a été la plus sensible à la présence des calcifications aortiques. Cela veut dire qu'un mécanisme compensatoire de dilatation aortique peut aussi être envisagé, sachant que le processus d'athérosclérose commence précocement dans l'aorte descendante [47]. En plus, la distribution hétérogène des calcifications dans l'aorte thoracique, qui épargne le segment ascendant où le flux hélicoïdal est puissant, indique que les profils de vitesse associés à la géométrie et à la formation de plaques jouent aussi un rôle important. Probablement, si le score de CAC est plutôt associé à l'athérosclérose, le score du CAT doit être pensé comme un indicateur plus large qui intègre aussi les mécanismes liés à l'artériosclérose. Nous allons revenir sur ce sujet dans la discussion générale du chapitre 3.

OPEN ACCESS Freely available online

PLOS ONE

Calcifications of the Thoracic Aorta on Extended Non-Contrast-Enhanced Cardiac CT

Damian Craiem[1,2]*, Gilles Chironi[2], Mariano E. Casciaro[1], Sebastian Graf[1], Alain Simon[2]

1 Favaloro University. Facultad de Ingeniería, Ciencias Exactas y Naturales, CONICET, Buenos Aires, Argentina, **2** APHP, Hôpital Européen Georges Pompidou, INSERM U970, Université Paris-Descartes, Paris, France

Abstract

Background: The presence of calcified atherosclerosis in different vascular beds has been associated with a higher risk of mortality. Thoracic aorta calcium (TAC) can be assessed from computed tomography (CT) scans, originally aimed at coronary artery calcium (CAC) assessment. CAC screening improves cardiovascular risk prediction, beyond standard risk assessment, whereas TAC performance remains controversial. However, the curvilinear portion of the thoracic aorta (TA), that includes the aortic arch, is systematically excluded from TAC analysis. We investigated the prevalence and spatial distribution of TAC all along the TA, to see how those segments that remain invisible in standard TA evaluation were affected.

Methods and Results: A total of 970 patients (77% men) underwent extended non-contrast cardiac CT scans including the aortic arch. An automated algorithm was designed to extract the vessel centerline and to estimate the vessel diameter in perpendicular planes. Then, calcifications were quantified using the Agatston score and associated with the corresponding thoracic aorta segment. The aortic arch and the proximal descending aorta, "invisible" in routine CAC screening, appeared as two vulnerable sites concentrating 60% of almost 11000 calcifications. The aortic arch was the most affected segment per cm length. Using the extended measurement method, TAC prevalence doubled from 31% to 64%, meaning that 52% of patients would escape detection with a standard scan. In a stratified analysis for CAC and/or TAC assessment, 111 subjects (46% women) were exclusively identified with the enlarged scan.

Conclusions: Calcium screening in the TA revealed that the aortic arch and the proximal descending aorta, hidden in standard TA evaluations, concentrated most of the calcifications. Middle-aged women were more prone to have calcifications in those hidden portions and became candidates for reclassification.

Citation: Craiem D, Chironi G, Casciaro ME, Graf S, Simon A (2014) Calcifications of the Thoracic Aorta on Extended Non-Contrast-Enhanced Cardiac CT. PLoS ONE 9(10): e109584. doi:10.1371/journal.pone.0109584

Editor: Jeroen Hendrikse, University Medical Center (UMC) Utrecht, Netherlands

Received May 29, 2014; **Accepted** September 2, 2014; **Published** October 10, 2014

Data Availability: The authors confirm that all data underlying the findings are fully available without restriction. All relevant data are available from Figshare under the following link: http://dx.doi.org/10.6084/m9.figshare.1164360.

Funding: This work was supported by Consejo Nacional de Investigaciones Científicas y Técnicas (www.conicet.gov.ar), Grant PIP number 11220090100734. The funder had no role in study design, data collection and analysis, decision to publish, or preparation of the manuscript.

Competing Interests: The authors have declared that no competing interests exist.

* Email: dcraiem@favaloro.edu.ar

Introduction

Calcified atherosclerosis has been associated with a higher risk of mortality but the strength of this relation depends on the affected vascular beds [1]. In particular, thoracic aorta calcium (TAC) has been related to all-cause mortality, independently of conventional cardiovascular risk factors and the presence of coronary artery calcium (CAC) [2]. TAC is less frequently performed than CAC and its ability to further refine clinical event prediction is still controversial [3,4]. A recent report states that CAC but not TAC measurements improve cardiovascular risk prediction beyond standard risk assessment [5]. Other reports indicate that TAC is a better predictor of future coronary events than CAC only in women [6] or when analyzing non-cardiac events [7]. Unfortunately, as the TAC score is commonly calculated on the same CT coronary scan of CAC studies, only the ascending and descending aortic portions are partially visible and the aortic arch is systematically excluded. Eventually, this lack of consistency to determine the exact parts of the TA included in TAC screening may have limited prior assessments for the prognostic value of TAC. The curvilinear portion of the aorta has a complex geometry that demands advanced segmentation algorithms to properly investigate its morphology [8,9]. An extended scan length might improve not only the detection of lesions associated with the risk of ischemic stroke, but also the early recognition of aneurysms [10,11]. In this study, we investigated the differences in TAC assessment using an extended CT scan that included the aortic arch, with respect to a standard heart scan. In particular, patients that would escape calcium detection with a standard measurement method were stratified and analyzed separately as candidates for reclassification.

Methods

Study Subjects

Individuals were initially referred to our cardiovascular prevention unit by occupational health physicians or general interns for in-depth stratification of coronary risk. In the present study we

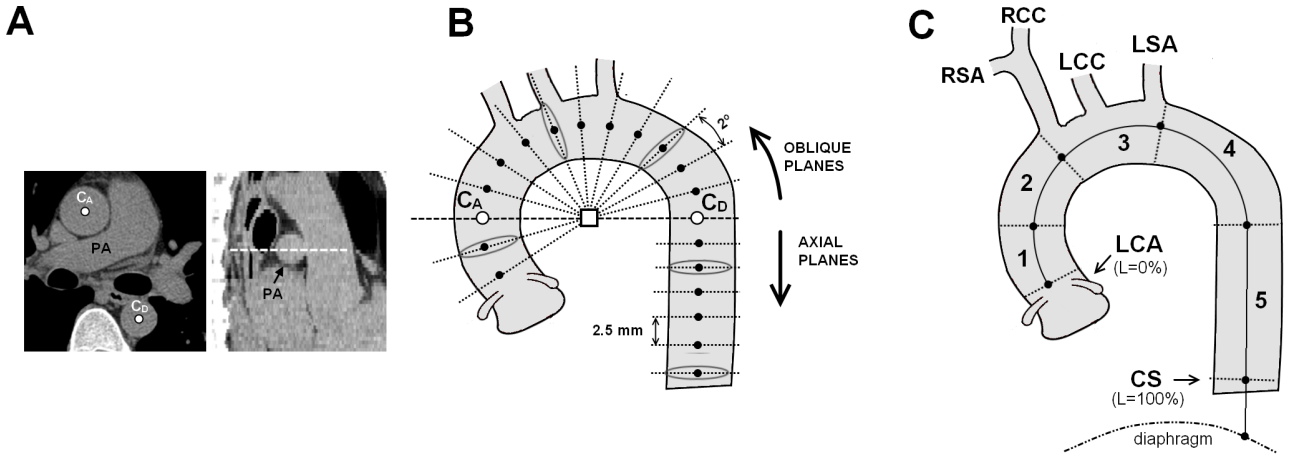

Figure 1. Thoracic aorta segmentation. A. The user selected 2 seed points in the center of ascending (C_A) and descending (C_D) aorta at the level of the pulmonary artery bifurcation. **B**. The algorithm sequentially inscribed circles inside the vessel cross-section using axial planes below C_D and oblique planes above for the curvilinear portion. **C**. The vessel was divided into 5 segments using anatomical landmarks. LCA: left coronary artery. RSA: Right subclavian artery. RCC and LCC: right and left carotid arteries. LSA: left subclavian artery. CS: coronary sinus.
doi:10.1371/journal.pone.0109584.g001

included all patients over 2 years from September 2009 who had undergone extended (including the aortic arch) non-contrast cardiac computed tomography (CT) for CAC and aortic aneurisms screening during their hospitalization. For this study, only primary prevention patients without symptoms were included. Weight and height were measured for calculation of body mass index. Brachial blood pressure (BP) was determined as the mean of 3 measurements by sphygmomanometer procedure in the supine position after a 10 minute rest. Hypertension was defined by BP of 140/90 mmHg or above, or use of anti-hypertensive medication. Total and HDL (high-density lipoprotein) blood cholesterol and triglyceride were measured in the supine position after 14 hours fasting and LDL (low-density lipoprotein) was calculated with the Friedewald formula or, if not applicable, directly measured. Hypercholesterolemia was defined by fasting LDL cholesterol above 3.3 mmol/l or by presence of LDL-lowering drug treatment. Blood glucose was measured after an overnight fast and diabetes was defined by fasting blood glucose of 7 mmol/l or above, or by presence of antidiabetic medication.

The retrospective analysis of personal health data of study subjects had the authorization of the CNIL (*Commission nationale de l'informatique et des libertés*) and was in accordance with the Helsinki declaration. Patient information was anonymized and de-identified prior to analysis.

Image acquisition

Aortic images were obtained with non-contrast cardiac 64-slice MSCT (Light-speed VCT; GE Health care, Milwaukee, Wisconsin, USA) during an extended scan length acquisition. Images were acquired with prospective-ECG gating at 60% of R-R interval in the cranio-caudal direction from the top of the aortic arch to the level of the diaphragm. Measurements were taken with 2.5 mm axial slices, 120 kVp, 250-mA tube current, 250-ms exposure time, and average 250-mm field of view. Scans were analyzed by custom-designed software that estimated the thoracic aorta (TA) geometry in 3D and quantified the TA calcifications. The effective radiation dose was assessed in a group of 200 patients and was 1.23±0.14 mSv (range 0.96–2.1 mSv) [8].

Semiautomatic segmentation algorithm

Details of the complete segmentation process to separate the TA from surrounding tissues and to analyze its 3D geometry were recently reported [8,12]. For each patient, the custom software isolated the thoracic aorta, assessed its geometry in 3D and

Table 1. Population description. Continuous variables are expressed as mean±SD.

Characteristics	
Number of subjects, n	970
Male gender, n (%)	754 (77)
Age, yrs	57±9
Body mass index, kg.m^{-2}	26.4±4.2
Hypertension, n (%)	476 (49)
Hypercholesterolemia, n (%)	796 (82)
Current or past smokers, n (%)	524 (54)
Diabetes, n (%)	83 (9)
10-years Framingham risk score, %	10±6

doi:10.1371/journal.pone.0109584.t001

Table 2. Presence and extent of coronary artery and thoracic aorta calcifications. Presence/absence of calcium and Agatston scores are reported.

Calcifications	
Extended TAC >0, n (%)	618 (64)
Extended TAC score, median [25–75 percentile]	39 [0–333]
Standard TAC >0, n (%)	296 (31)
Standard TAC score, median [25–75 percentile]	0 [0–5]
CAC >0, n (%)	598 (62)
CAC score, median [25–75 percentile]	16 [0–148]
CAC >0 and extended TAC >0, n (%)	457 (47)
CAC =0 and extended TAC =0, n (%)	211 (22)

Standard TAC was calculated only including segments 1 and 5. Extended TAC included all 5 segments as in Figure 1C.
doi:10.1371/journal.pone.0109584.t002

quantified the calcifications. Briefly, the user started with a manual selection of two seed points in the axial slices at the central level of the pulmonary artery (see C_A and C_D in Figure 1A). Then, an automatic algorithm extracted the central skeleton and estimated the vessel diameter, dynamically expanding and centering circles to inscribe them inside the vessel cross-section area [8]. This circle-fitting algorithm was sequentially applied over the axial CT slices for the descending portion of the aorta and over oblique planes for the curvilinear part (Figure 1B). These planes were reconstructed in steps of 2° angles by trilinear interpolation following a semitoroidal path until an angle of 240°. In both cases, the center point of the circle found at the end of the algorithm was used as a seed point for the next slice or reconstructed plane. As the curvilinear portion of the aorta did not necessarily follow a strict toroidal shape and the descending aorta was not perfectly vertical, a post-processing correction was performed to ensure that reconstructed planes remained perpendicular to the true aortic centerline. The result of this process in each patient was a list of $\approx$150 centerline points with the corresponding diameters that approximated the cross section of the aorta in each position.

To finish the TA geometry assessment, the user indicated 4 anatomic landmarks: Left main coronary artery (LMCA), Right and left subclavian arteries (RSA and LSA) and the coronary sinus (CS). The aorta was then divided in 5 segments as shown in Figure 1C. The whole automated process was reported to take less than 1 min per patient, with maximum intra- and inter-observer coefficient of variation values of 0.4% for TA diameter and 4.4% for TA volume [8].

Calcification assessment

Lesions were quantified with a semi-automatic algorithm using the Agatston score method [13]. For each axial image, the algorithm highlighted in red all candidate lesions. Then, the user went over every axial plane and clicked on the red lesions to validate them and turn them green. At this point, the Agatston score was automatically calculated for each green lesion that was then orthogonally projected over the vessel centerline curve and associated with the corresponding segment (from 1 to 5). Finally, the lesions scores were accumulated for each segment. Global and segmental scores were reported for each subject.

Candidates for reclassification

Patients with calcifications that would escape detection with a standard scan (either CAC or TAC), were designated as candidates for reclassification. For such stratified analysis, the population was divided into 3 groups. Group 1: patients free of calcifications (CAC = 0 and TAC = 0). Group 2: patients detected with the standard method (CAC>0 or standard TAC>0). Group 3: patients detected exclusively with the extended measurement method (CAC = 0 and standard TAC = 0 and extended TAC>0). The characteristics of each group were analyzed separately. Ten-year Framingham risk score (10-years FRS, % probability of CHD event in the next 10 years) was estimated with the Framingham risk model by entering age, total cholesterol, high-density lipoprotein (HDL) cholesterol, and systolic blood pressure as continuous variables and sex, diabetes, and current smoking as categorical variables (presence or absence) [14]. Comparisons for age and FRS between the 3 groups were made with ANOVA and Tukey's HSD post hoc test. We used chi-square test for categorical data and post hoc tests were performed pair-wise with a Bonferroni correction for multiple comparisons (e.g. 3). A value of $p<0.05$ was considered significant.

Results

Table 1 shows the baseline characteristics of the study population (n = 970). Presence and extent of CAC, standard assessed TAC and extended TAC are reported in Table 2. Standard TAC was calculated only including lesions in segments 1 and 5, whereas extended TAC included all 5 segments. Overall, 62% and 64% of subjects had detectable CAC and TAC, respectively. TAC prevalence would drop to 31% using a standard scan. Almost half of the patients had both CAC and TAC whereas 22% did not have any detectable calcium.

TAC prevalence was heterogeneous across the aortic segments as shown in Fig 2A. Calcifications appeared in 4%-to-12% of subjects in the ascending portions, increased to 42% in the arch and attained a peak of 55% in the proximal descending segment. Distally, TAC was detected in 31% of subjects. The impact of exploring segments 2, 3 and 4 in the extended method with respect to a standard TA scan is shown in Figure 2B. Of 64% of subjects that had TAC, 33% were detected exclusively with the extended method. Only 2% of subjects had TAC in segments 1 and/or 5 and not in segments 2, 3 or 4. Both methods would identify the other 29% of subjects with calcifications. The inspection of segments 2, 3 and 4 would ensure the detection of 97% of patients with aortic calcifications.

The distribution of calcifications across the aortic segments is shown in Figure 3A. We quantified 10831 calcifications in 618 subjects. Most of the lesions were found in the proximal descending portion (n = 3824 lesions, 35%), followed by descend-

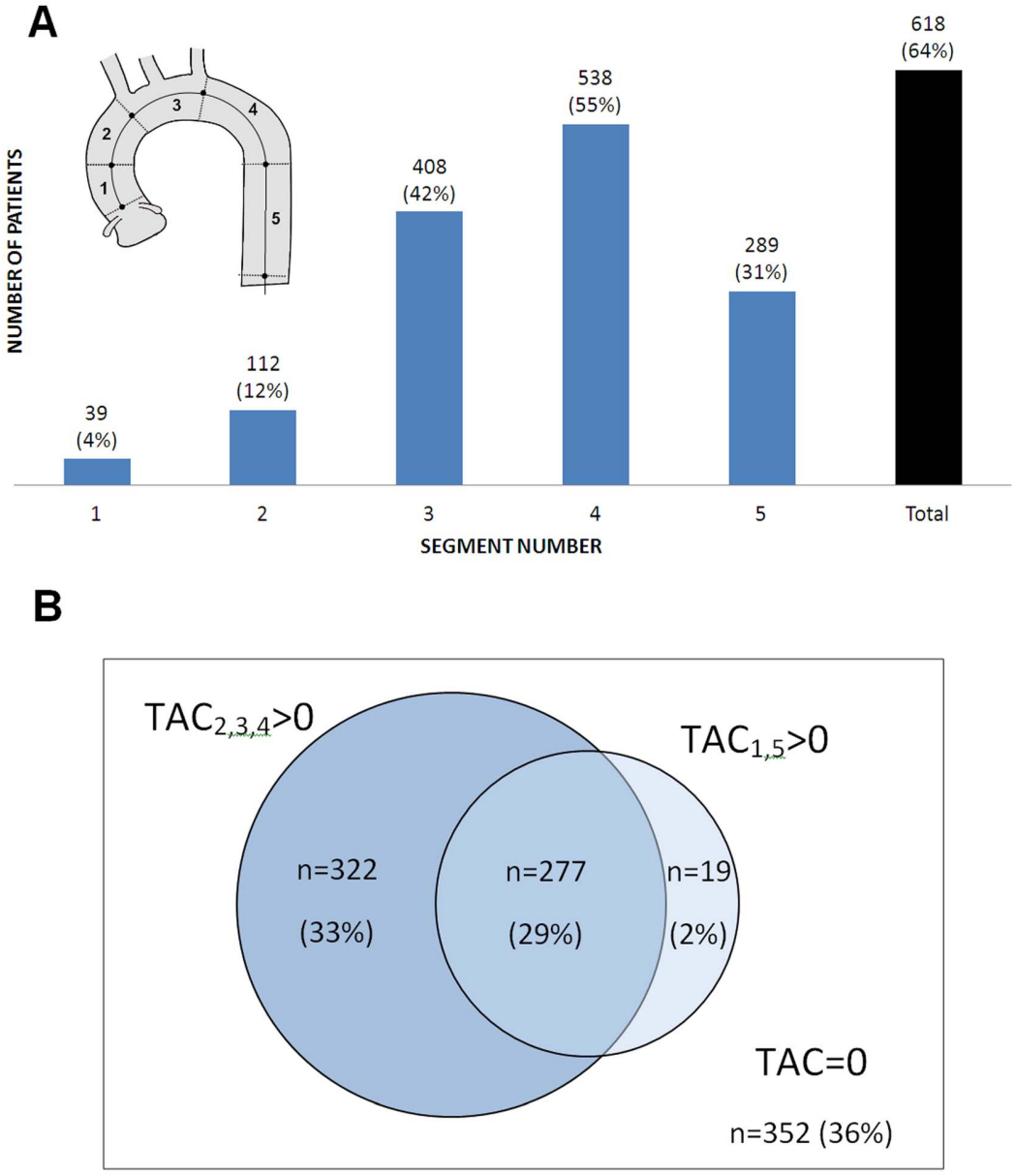

Figure 2. Calcified thoracic aorta segments in the whole population (n = 970). A. Number and proportion of patients with TAC score>0 by aortic segments. **B**. Number and percentage of patients with calcifications assessed with the standard method that explored segments 1 and 5 ($TAC_{1,5}$>0) and the extended method that included the aortic arch ($TAC_{2,3,4}$>0).
doi:10.1371/journal.pone.0109584.g002

ing aorta (n = 3421, 32%) and the aortic arch (n = 2803, 26%). Only 7% of the total number of calcifications was found in the ascending aorta (segments 1 and 2). When the number of calcifications was expressed by unit of segment length, the aortic arch appeared as the most diseased with 934 calcifications per cm (Fig 3B).

The prevalence of TAC by age tertiles for the 5 segments is shown in Figure 4. Globally, we found a 38% of prevalence for the 1st tertile of age, 65% for the 2nd and 89% for the 3rd tertile. The proximal descending aorta was affected in 85% of subjects above the 3rd tertile of age.

Reclassification candidates

To discover whether reclassification of subjects that escaped detection by the standard method is possible, participants were divided into 3 groups according to the presence of calcium in the coronary arteries and/or in the TA. Overall, 22% of subjects were free of any calcium (Group 1), 67% had either CAC and/or TAC detectable with a standard scan (Group 2) and 11% were exclusively found with the extended measurement method (Group 3). Characteristics of each group are shown in Table 3. Age and 10-years FRS were significantly different between groups ($p < 0.001$, ANOVA). A higher proportion of women was observed in Group 3 compared to the other groups ($p<0.05$). Risk scores did not differ between Groups 1 and 3.

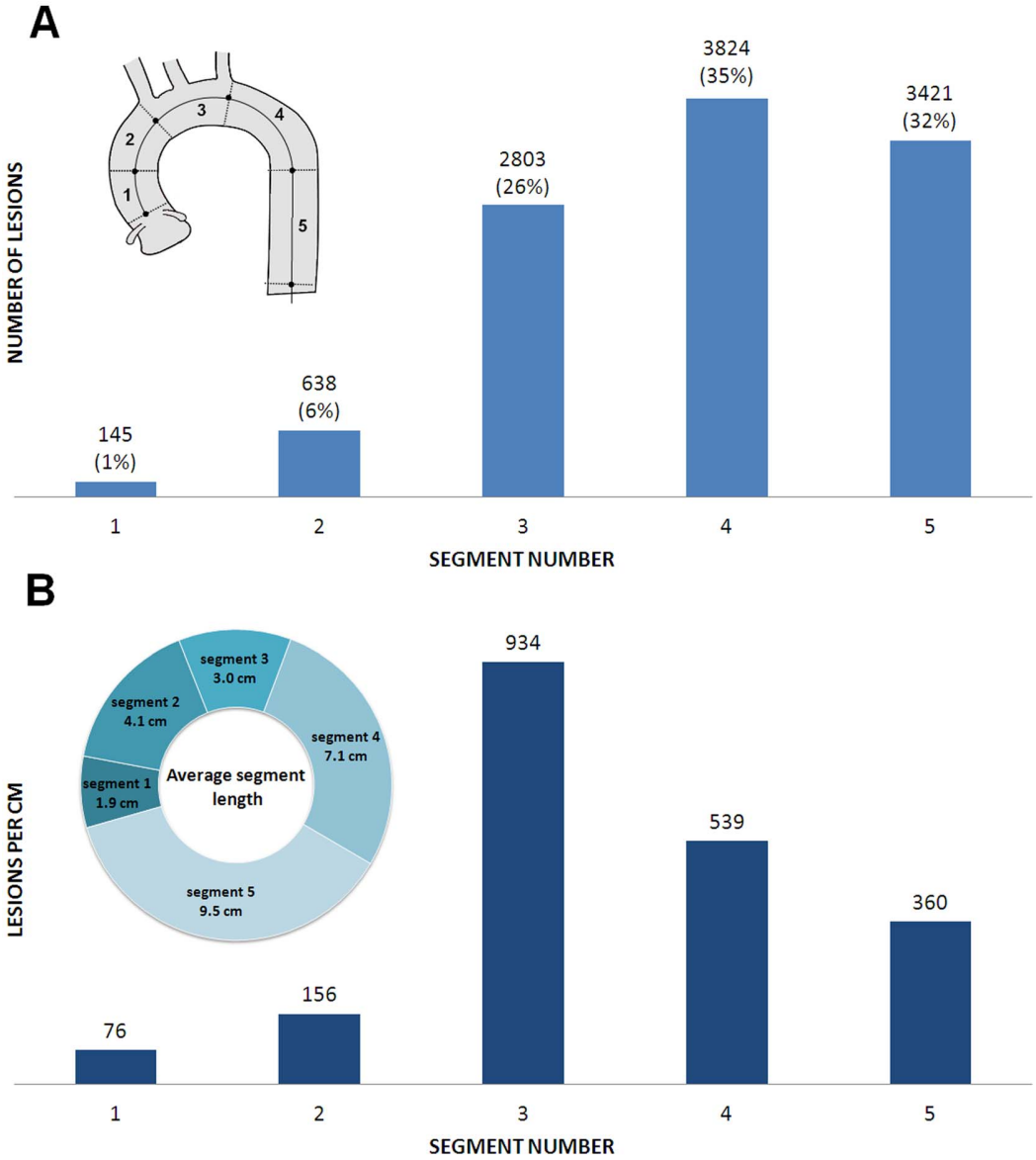

Figure 3. Spatial distribution of 10831 calcifications found in 618 patients across thoracic aorta segments. A. Number of calcifications by segment and % of total number of calcifications. **B**. Number of calcifications by average segment length in cm.
doi:10.1371/journal.pone.0109584.g003

Discussion

In this study we show that calcified lesions in the TA of asymptomatic patients occurred at two preferential sites that remain "invisible" in routine CAC screening: the aortic arch and the proximal descending aorta. These hidden regions were explored by extending the scan length of a standard coronary scan to cover the aortic arch. Using the enlarged scan, TAC prevalence doubled from 31% to 64%. After accurately reading 970 heart scans, 60% of the almost 11000 calcifications were identified in the upper segments, the aortic arch being the most densely affected sector per cm length. To our knowledge, this is the first geometrical TA study that has additionally calculated the TAC Agatston score, including the aortic arch, in a cohort of almost 1000 asymptomatic patients.

The detection of coronary and aortic calcification in our population was 62% and 64%, respectively. In other reports that did not include the aortic arch, these percentages averaged 47%-to-56% and 22%-to-31%, respectively [2,3,6,15,16]. Certainly, the extension of the scan length increased the TAC prevalence detected. In fact, if we only consider segments 1 and 5, our values did not differ from others. Reports where all aortic segments were measured are scarce. Jacobs et al. measured the whole TA in a sub-cohort of 958 asymptomatic subjects (from a population of 7557 heavy smokers) and found a prevalence of CAC and TAC above 60%, closer to our values [7]. It is to note that the proportions of men, hypertensive and hypercholesterolemic patients were also comparable with our study. Allison et al. studied 4544 patients that underwent a whole body CT scanning and found a 55% and 37% of prevalence for CAC and TAC, respectively [1]. Probably, TAC prevalence detected was lower

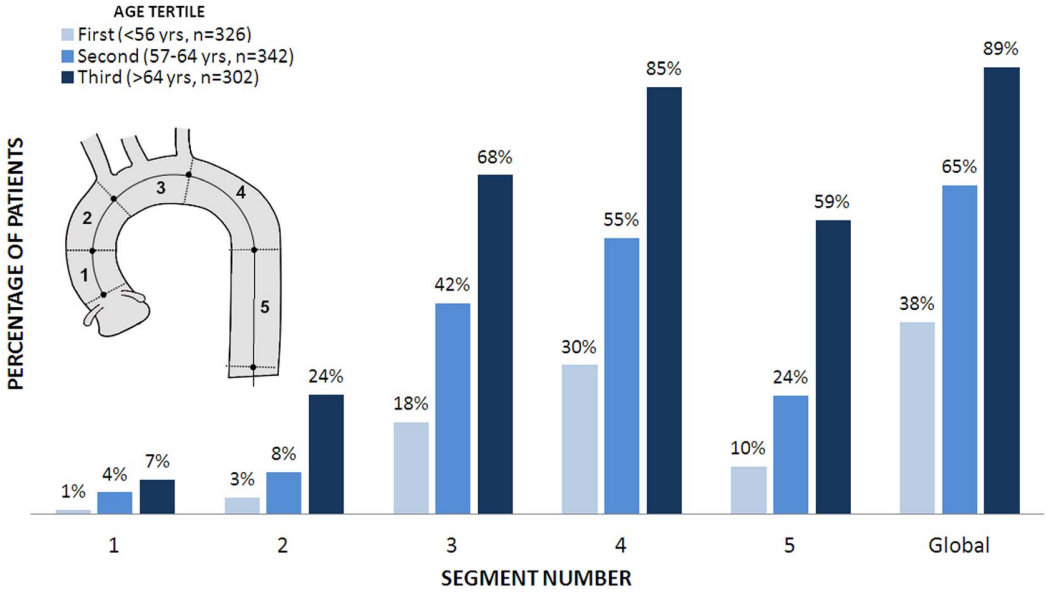

Figure 4. Proportion of patients with calcifications across thoracic aorta segments separated by age tertiles.
doi:10.1371/journal.pone.0109584.g004

than in our study due to a higher participation of women and a healthier cohort. Direct comparisons with other studies should be made with caution, because small differences associated with the population risk profile might introduce substantial bias in prevalence values [17].

Essentially, the main finding of our work is that about half of patients with no visible TAC on a standard coronary scan were detected with the extended method. To search for patients that could be reclassified, we performed a stratified analysis in three groups, including coronary and/or thoracic calcifications and comparing both methods. We found 11% of subjects that would escape any calcium detection with a standard scan (Group 3). It is noteworthy that globally, 33% of subjects would be considered free of calcium using the standard TA evaluation, instead of the true 22% reported for Group 1. Candidates for reclassification in Group 3 were 5 years older than patients with no calcium and 4 years younger than those detected with the standard method. We also observed a higher proportion of women in this group (46% vs ≈20% in the other 2 groups) and a risk profile closer to subjects free of calcium. This information suggests that middle-aged women at increased cardiovascular risk could benefit most from an extended scan for TAC detection and they would have a better chance to be reclassified.

The spatial distribution of calcifications through the aortic segments in our study was far from homogeneous. It revealed a high prevalence in the descending aorta and showed a predilection for the aortic arch when normalized per segment length. Calcifications were distributed as follows: 9% for the ascending segment, 25% for the arch and 66% for the descending aorta. Only a few previous studies analyzed the complete aorta and they globally identified the aortic arch as a vulnerable place for calcifications. Takasu et al. divided the TA into 6 segments and

Table 3. Stratified analysis to identify candidate patients for reclassification.

Characteristics	GROUP 1 (no calcium)	GROUP 2 (standard method)	GROUP 3 (reclassification candidates)	P value
Number of subjects, n (%)	211 (22)	648 (67)	111 (11)	
Male gender, n (%)	167 (79)	527 (81)	60 (54)*$^{+}$	<0.001
Age, yrs	50±8	59±8*	55±8*$^{+}$	<0.001
Hypertension, n (%)	80 (38)	354 (55)*	42 (38)$^{+}$	<0.001
Hypercholesterolemia, n (%)	146 (69)	561 (87)*	89 (80)	<0.001
Diabetes, n (%)	19 (9)	54 (8)	10 (9)	NS
Current or past smokers, n (%)	104 (49)	371 (57)*	49 (44)$^{+}$	<0.05
10-years Framingham risk score, %	8±5	11±6*	8±5^{+}	<0.001

Group 1: CAC = 0 and extended TAC = 0 (free of calcium). Group 2: CAC>0 or standard TAC>0. Group 3: CAC = 0 and standard TAC = 0 and extended TAC>0.
CAC = Coronary artery calcium. Standard TAC was calculated only including segments 1 and 5. Extended TAC included all 5 segments (see Figure 1C).
*p<0.05 with respect to Group1.
$^{+}$p<0.05 with respect to Group 2.
Patients were separated into subjects free of calcium (Group 1), those assessed with traditionally measured method (Group 2) and candidates for reclassifications that were exclusively assesed with the proposed extended method (Group 3).
doi:10.1371/journal.pone.0109584.t003

found calcifications predominantly in the aortic arch [18]. In another large Japanese cohort aimed at screening lung cancer, the frequency of calcification for the ascending was 3%, attained a peak of 20% at the aortic arch and dropped to 10% for the descending [19]. For the same three segments using transesophageal electrocardiography in a general population, Agmon et al. found percentages of 8%, 31% and 45%, respectively [20]. Possible explanations for this heterogeneous distribution remain somehow speculative and include disturbed flow and wall shear stress conditions [21,22], small geometrical ondulations in the vecinity of ductus arteriosius scar and intercostal branches [23] and LDL concentration and transportation dynamics [24,25].

A strong association between TAC and age was observed in the aortic arch and the descending aorta. A global prevalence of almost 90% was found for age>64years, being again the aortic arch and the descending aorta the most affected sites. The exponential increment of TAC prevalence with age, that even surpasses CAC after the age of 70 years, was reported before [1,4]. Our global prevalence for older subjects seems higher with respect to other reports [15,26], probably due to the extension of the scan length.

With respect to effective radiation doses, there is a wide disparity in reported values for a single coronary calcium screening, although there is a general agreement on average values. Kim *et al.* reported median and mean values of 2.3 and 3.1 mSv (range 0.8–10.5), respectively [27]. The AHA Science Advisory reported representative values of 3 mSv (range 1–12 mSv) [28]. Recent recommendations suggest the average value to remain in the range of 1.0–1.5 mSv and should not exceed 3.0 mSv [29]. Our dose values did not exceed 2.1 mSv, remaining below average thresholds reported values using the same scanner model [27].

This study has some limitations that need to be addressed. The cross-sectional design of our study did not allow assessment of time-dependent and causal relationships between parameters. Recent evidence regarding the lack of TAC screening to improve cardiovascular risk prediction beyond Framingham Risk Score and CAC screening are based on standard TA evaluation [5]. The incorporation of "hidden" aortic regions has shown that it may be worth discussing how lack of consistency in field of measurement settings may have limited the prognostic value of TAC in previous prospective studies. There are two different mechanisms of vascular calcification: intimal (atherosclerotic) and medial (arteriosclerotic) [30]. Whereas CAC is mostly intimal, TAC is thought to better represent a generalized atherosclerosis process [4,7]. The differentiation of the aortic wall from the lumen would need enhanced CT protocols that are not recommended for our patients [31]. Aortic valve calcium was not measured in this study because the vessel segmentation method was limited to tubular cross-sections starting at the left main coronary artery [8]. Our patients were mostly men due to a recruitment bias. Finally, TA geometry was accurately estimated in 3D but size and shape variables were not associated with TAC distribution. The association between aortic morphology, calcifications and traditional risk factors (i.e. hypertension) should be addressed in future investigations.

In conclusion, calcium screening in the TA revealed that the aortic arch and the proximal descending aorta, hidden in standard TA evaluations, concentrated most of the calcifications, being the arch the most densely affected segment per cm length. In our population of asymptomatic subjects at increased cardiovascular risk, TAC prevalence doubled from 31% to 64% using the extended scan method. Middle-aged women were more prone to have calcifications in those hidden portions and became candidates for reclassification. Our results should encourage prospective studies to investigate whether extended TAC assessment improves cardiovascular risk prediction beyond standard methods.

Acknowledgments

We would like to thank doctors Alban Redheuil and Elie Mousseaux for their valuable contributions.

Author Contributions

Conceived and designed the experiments: DC MEC GC SG AS. Performed the experiments: DC GC AS. Analyzed the data: DC MEC GC AS. Contributed reagents/materials/analysis tools: DC MEC GC SG AS. Wrote the paper: DC MEC GC AS. Designed the software: DC MEC SG.

References

1. Allison MA, Hsi S, Wassel CL, Morgan C, Ix JH, et al. (2012) Calcified Atherosclerosis in Different Vascular Beds and the Risk of Mortality. Arteriosclerosis, Thrombosis, and Vascular Biology 32: 140–146.
2. Santos RD, Rumberger JA, Budoff MJ, Shaw LJ, Orakzai SH, et al. (2010) Thoracic aorta calcification detected by electron beam tomography predicts all-cause mortality. Atherosclerosis 209: 131–135.
3. Wong ND, Gransar H, Shaw L, Polk D, Moon JH, et al. (2009) Thoracic aortic calcium versus coronary artery calcium for the prediction of coronary heart disease and cardiovascular disease events. JACC Cardiovasc Imaging 2: 319–326.
4. Kalsch H, Lehmann N, Mohlenkamp S, Hammer C, Mahabadi AA, et al. (2013) Prevalence of thoracic aortic calcification and its relationship to cardiovascular risk factors and coronary calcification in an unselected population-based cohort: the Heinz Nixdorf Recall Study. Int J Cardiovasc Imaging 29: 207–216.
5. Yeboah J, Carr JJ, Terry JG, Ding J, Zeb I, et al. (2013) Computed tomography-derived cardiovascular risk markers, incident cardiovascular events, and all-cause mortality in nondiabetics: the Multi-Ethnic Study of Atherosclerosis. Eur J Prev Cardiol.
6. Budoff MJ, Nasir K, Katz R, Takasu J, Carr JJ, et al. (2011) Thoracic aortic calcification and coronary heart disease events: the multi-ethnic study of atherosclerosis (MESA). Atherosclerosis 215: 196–202.
7. Jacobs PC, Prokop M, van der Graaf Y, Gondrie MJ, Janssen KJ, et al. (2010) Comparing coronary artery calcium and thoracic aorta calcium for prediction of all-cause mortality and cardiovascular events on low-dose non-gated computed tomography in a high-risk population of heavy smokers. Atherosclerosis 209: 455–462.
8. Craiem D, Chironi G, Redheuil A, Casciaro M, Mousseaux E, et al. (2012) Aging Impact on Thoracic Aorta 3D Morphometry in Intermediate-Risk Subjects: Looking Beyond Coronary Arteries with Non-Contrast Cardiac CT. Ann Biomed Eng 40: 1028–1038.
9. Demertzis S, Hurni S, Stalder M, Gahl B, Herrmann G, et al. (2010) Aortic arch morphometry in living humans. J Anat 217: 588–596.
10. Cohen A, Tzourio C, Bertrand B, Chauvel C, Bousser MG, et al. (1997) Aortic plaque morphology and vascular events: a follow-up study in patients with ischemic stroke. FAPS Investigators. French Study of Aortic Plaques in Stroke. Circulation 96: 3838–3841.
11. Hartnell GG (2001) Imaging of aortic aneurysms and dissection: CT and MRI. J Thorac Imaging 16: 35–46.
12. Craiem D, Chironi G, Casciaro ME, Redheuil A, Mousseaux E, et al. (2013) Three-dimensional evaluation of thoracic aorta enlargement and unfolding in hypertensive men using non-contrast computed tomography. J Hum Hypertens 27: 504–509.
13. Agatston AS, Janowitz WR, Hildner FJ, Zusmer NR, Viamonte M, Jr., et al. (1990) Quantification of coronary artery calcium using ultrafast computed tomography. J Am Coll Cardiol 15: 827–832.
14. Wilson PW, D'Agostino RB, Levy D, Belanger AM, Silbershatz H, et al. (1998) Prediction of coronary heart disease using risk factor categories. Circulation 97: 1837–1847.
15. Nasir K, Roguin A, Sarwar A, Rumberger JA, Blumenthal RS (2007) Gender differences in coronary arteries and thoracic aorta calcification. Arterioscler Thromb Vasc Biol 27: 1220–1222.
16. Rivera JJ, Nasir K, Katz R, Takasu J, Allison M, et al. (2009) Relationship of thoracic aortic calcium to coronary calcium and its progression (from the Multi-Ethnic Study of Atherosclerosis [MESA]). Am J Cardiol 103: 1562–1567.

17. Erbel R, Delaney JAC, Lehmann N, McClelland RL, Möhlenkamp S, et al. (2008) Signs of subclinical coronary atherosclerosis in relation to risk factor distribution in the Multi-Ethnic Study of Atherosclerosis (MESA) and the Heinz Nixdorf Recall Study (HNR). European Heart Journal 29: 2782–2791.
18. Takasu J, Takanashi K, Naito S, Onishi M, Miyazaki A, et al. (1992) Evaluation of morphological changes of the atherosclerotic aorta by enhanced computed tomography. Atherosclerosis 97: 107–121.
19. Itani Y, Watanabe S, Masuda Y (2004) Aortic Calcification Detected in a Mass Chest Screening Program Using a Mobile Helical Computed Tomography Unit Relationship to Risk Factors and Coronary Artery Disease. Circulation Journal 68: 538–541.
20. Agmon Y, Khandheria BK, Meissner I, Schwartz GL, Petterson TM, et al. (2000) Independent Association of High Blood Pressure and Aortic Atherosclerosis: A Population-Based Study. Circulation 102: 2087–2093.
21. Shahcheraghi N, Dwyer HA, Cheer AY, Barakat AI, Rutaganira T (2002) Unsteady and three-dimensional simulation of blood flow in the human aortic arch. J Biomech Eng 124: 378–387.
22. Suo J, Ferrara DE, Sorescu D, Guldberg RE, Taylor WR, et al. (2007) Hemodynamic shear stresses in mouse aortas: implications for atherogenesis. Arterioscler Thromb Vasc Biol 27: 346–351.
23. Vincent PE, Plata AM, Hunt AA, Weinberg PD, Sherwin SJ (2011) Blood flow in the rabbit aortic arch and descending thoracic aorta. J R Soc Interface 8: 1708–1719.
24. Giddens DP, Zarins CK, Glagov S (1993) The role of fluid mechanics in the localization and detection of atherosclerosis. J Biomech Eng 115: 588–594.
25. Liu X, Pu F, Fan Y, Deng X, Li D, et al. (2009) A numerical study on the flow of blood and the transport of LDL in the human aorta: the physiological significance of the helical flow in the aortic arch. Am J Physiol Heart Circ Physiol 297: H163–170.
26. Wong ND, Sciammarella M, Arad Y, Miranda-Peats R, Polk D, et al. (2003) Relation of thoracic aortic and aortic valve calcium to coronary artery calcium and risk assessment. Am J Cardiol 92: 951–955.
27. Kim KP, Einstein AJ, Berrington de Gonzalez A (2009) Coronary artery calcification screening: estimated radiation dose and cancer risk. Arch Intern Med 169: 1188–1194.
28. Gerber TC, Carr JJ, Arai AE, Dixon RL, Ferrari VA, et al. (2009) Ionizing radiation in cardiac imaging: a science advisory from the American Heart Association Committee on Cardiac Imaging of the Council on Clinical Cardiology and Committee on Cardiovascular Imaging and Intervention of the Council on Cardiovascular Radiology and Intervention. Circulation 119: 1056–1065.
29. Voros S, Rivera JJ, Berman DS, Blankstein R, Budoff MJ, et al. (2011) Guideline for minimizing radiation exposure during acquisition of coronary artery calcium scans with the use of multidetector computed tomography: a report by the Society for Atherosclerosis Imaging and Prevention Tomographic Imaging and Prevention Councils in collaboration with the Society of Cardiovascular Computed Tomography. J Cardiovasc Comput Tomogr 5: 75–83.
30. Zhu D, Mackenzie NC, Farquharson C, Macrae VE (2012) Mechanisms and clinical consequences of vascular calcification. Front Endocrinol (Lausanne) 3: 95.
31. de Jong PA, Hellings WE, Takx RA, Isgum I, van Herwaarden JA, et al. (2014) Computed tomography of aortic wall calcifications in aortic dissection patients. PLoS One 9: e102036.

Atherosclerosis 245 (2016) 22–27

Contents lists available at ScienceDirect

Atherosclerosis

journal homepage: www.elsevier.com/locate/atherosclerosis

Association of thoracic aorta calcium and non cardiac vascular events in cardiac disease-free individuals☆

Damian Craiem [a, c], Dr Gilles Chironi [a, *], Mariano E. Casciaro [c], Marie-Emmanuelle Sirieix [a], Elie Mousseaux [b], Alain Simon [a]

[a] APHP, Hôpital Européen Georges Pompidou, Centre de Médecine Préventive Cardiovasculaire, INSERM U970, Université Paris-Descartes, Paris, France
[b] Département de Radiologie, INSERM U970, Université Paris-Descartes, Paris, France
[c] Favaloro University, Facultad de Ingeniería, Ciencias Exactas y Naturales, CONICET, Buenos Aires, Argentina

ARTICLE INFO

Article history:
Received 12 November 2014
Received in revised form
1 October 2015
Accepted 26 November 2015
Available online 30 November 2015

Keywords:
Cardiovascular risk
Cerebrovascular disease
Coronary artery calcium
Vascular calcification
Peripheral vascular disease

ABSTRACT

Objective: Thoracic aorta calcium (TAC) is measurable on the same computed tomography (CT) scan as coronary artery calcium (CAC) but has still unclear clinical value. We assessed TAC and CAC relations with non-cardiac vascular events history in a cohort of subjects at risk for cardiovascular disease.
Methods: We analyzed retrospectively 1000 consecutive subjects having undergone CAC detection by non-contrast multi-slice CT with measurement field longer than usual in order to measure total TAC including aortic arch calcium. We also determined partial TAC restricted to ascending and descending thoracic aorta sites by removing arch calcium from total TAC. Calcium deposits were measured with a custom made software using Agatston score.
Results: Compared with the rest of the cohort, the 30 subjects with non-cardiac vascular event history had higher median values [95% CI] of total TAC (282 [28–1809] *vs* 39 [0–333], $p < 0.01$) and partial TAC (4 [0–284] *vs* 0 [0–5], $p < 0.01$) but no different value of CAC (73 [0–284] *vs* 16 [0–148]). Odds ratio [95% CI] of having non-cardiac vascular event per 1-SD increase in log-transformed calcium value was significant for total TAC but not for CAC, if total TAC and CAC were entered separately (1.56 [1.12–2.24], $p < 0.01$ and 1.13 [0.86–1.50], respectively) or together (1.57 [1.10–2.32], $p < 0.01$ and 0.98 [0.73–1.32], respectively) in the logistic adjusted model.
Conclusion: TAC assessment simultaneous with CAC detection provides complementary information on the extra coronary component of cardiovascular risk beyond CAC's coronary risk prediction. Further studies are required to prospectively confirm this result.

1. Introduction

The detection of coronary artery calcium (CAC) by new generation low-dose non-contrast computed tomography (CT) has become a recognized and robust strategy to improve coronary risk stratification [1–3]. Indeed, it is well established that CAC predicts future coronary events beyond traditional risk factors prediction [4–8]. Interestingly, the CT that measures CAC can simultaneously quantify thoracic aorta calcium (TAC) on the same scan [9]. However, the clinical relevance and complementarity of TAC detection as regards CAC prognostic information have to be clarified. Some studies suggest that TAC detection does not provide incremental information beyond CAC prediction [4,10]. Conversely, other studies suggest that TAC may relate to, or predict non-cardiac vascular events better than CAC [11–13], especially when calcium deposit is assessed in the aortic arch [14]. This latter result merits attention because the CT assessment of TAC concomitantly with CAC detection uses traditionally a field of measurement that does not visualize aortic arch [15,16] so raising the question whether the lack of assessment of aortic arch calcium may attenuate the prognostic performance of TAC.

To address these issues, we performed a retrospective analysis of a cohort of 1000 consecutive subjects at risk for cardiovascular disease, having undergone a non-contrast multi-slice computed tomography (MSCT) scan in the framework of routine care. The

☆ All authors take responsibility for all aspects of the reliability and freedom from bias of the data presented and their discussed interpretation.

* Corresponding author. Centre de Médecine Préventive Cardiovasculaire, Hôpital Européen Georges Pompidou, 20 rue Leblanc, 75908 Paris, France.
E-mail address: gilles.chironi@aphp.fr (D.G. Chironi).

http://dx.doi.org/10.1016/j.atherosclerosis.2015.11.030
0021-9150/

length of the CT field of measurement was more extended than usual in order to include the aortic arch in view of detecting early aortic dilatation [17,18] in the entire thoracic aorta. This complete thoracic aortic scan allowed detecting and quantifying total TAC including aortic arch calcium. To analyze the incremental information of aortic arch calcium, we also calculated partial TAC, defined as excluding the arch from aorta calcium measurement [4,16]. Our main objective was to assess and compare the relations of total TAC, partial TAC, and CAC with history of non-cardiac vascular event. We also evaluated the association of total TAC with non-cardiac vascular events compared to partial TAC.

2. Methods

2.1. Subjects

Participants were recruited as part of a cardiovascular risk stratification program between 2010 and 2012. They were consecutively included in our study if they had undergone a non-contrast MSCT scan in view of a double screening: (i) estimation of calcified coronary atherosclerosis burden and (ii) detection of early aortic dilatation in all thoracic aortal sites including ascending aorta, arch and descending aorta. Such scan allowed measuring total TAC, i.e. the amount of calcium deposit in the entire thoracic aorta. Exploration was performed during a one-day hospitalization and was accompanied by concomitant measurements of traditional risk factors according to a procedure previously described in detail [19]. The presence or the absence of history of non-cardiac vascular disease, including cerebrovascular and peripheral vascular events, was documented in each subject from their clinical examination and medical records. The exclusion criteria were history of coronary heart disease in whom CAC detection is not recommended [20] and cardiac arrhythmia because this condition is incompatible with optimal CT-gating image acquisition. Finally, this retrospective study allowed us to analyze 1000 consecutive subjects.

The retrospective analysis of personal health data of study subjects had the authorization of the French CNIL (Commission Nationale de l'Informatique et des Libertés) and was in accordance with the Helsinki declaration. Patient's information was anonymized and de-identified prior to analysis.

2.2. Image acquisition

Cardiac and aortic images were obtained with non-contrast cardiac 64-slice MSCT (light-sped VCT; GE Health care, Milwaukee, Wisconsin, USA) during an extended scan length acquisition, as previously described [21]. Briefly, images were acquired with prospective-ECG gating at 60% of R–R interval in the cranio-caudal direction from the top of the aortic arch to the level of the diaphragm. Measurements were taken with 2.5 mm axial slices, 120 KVp, 250-mA current, 250-ms exposure time, and average 250-mm field of view. The effective radiation dose assessed in a previous group of 200 subjects was 1.23 ± 0.14 mSv (range 0.92–2.1 mSv) [18].

Global amount of CAC and TAC deposits were measured using the Agatston score method [22], implemented in a custom made software previously described [21]. Total TAC was assessed from the apex of the heart until the top of the aortic arch, so including the entire thoracic aorta with the exception of the sinotubular junction (Fig. 1). Partial TAC restricted to ascending and descending thoracic aorta sites was calculated by removing aortic arch calcium amount from total TAC measurement (Fig. 1).

2.3. Statistical analysis

Normally distributed continuous variables were described by means (standard deviation), categorical variables were described as frequencies (percentages) and skewed variables were described by median [interquartiles]. CAC, total TAC, and partial TAC were expressed as raw values and log-transformed values (Log (raw value + 1)). The differences in study parameters were analyzed by presence or absence of history of non-cardiac vascular events using chi-square tests for categorical variables, student t-tests for variables with normal distribution, and non-parametric Man–Whitney test for parameters with skewed distribution. The association of history of non-cardiac vascular events with CAC, total TAC and partial TAC taken separately were examined with three logistic regressions adjusted for age, gender, total cholesterol, systolic blood pressure, and statin and anti-hypertensive treatments. The odds ratio (OR) of having history of non-cardiac vascular events was determined per 1-SD increase in log-transformed CAC, total TAC and partial TAC. Such SD increase was calculated from nonzero values of total TAC, partial TAC or CAC. The associations of non-cardiac vascular events with CAC and total TAC taken together were determined with a logistic regression adjusted for age, gender, total cholesterol, systolic blood pressure, statin and anti-hypertensive treatments and the OR of having non cardiac vascular event was calculated for each parameter entered in the logistic model, using 1-SD increase for each quantitative parameters. All analyses were performed with JMP 8 software (SAS institute, Cary, NC).

3. Results

Clinical characteristics of the study population are shown in Table 1. Half had hypertension (45% with anti-hypertensive treatment), 82% had hypercholesterolemia (53% with statin treatment), 20% were current smokers and 8% had diabetes. Thirty subjects (3% of the cohort) had documented history of non-cardiac vascular events including 17 patients with cerebrovascular event (12 with stroke and 5 with transient ischemic attack) and 13 patients with peripheral vascular disease.

Raw and log-transformed values of total TAC, partial TAC, aortic arch TAC and CAC are shown in Table 1. Medians [interquartile] were 41 [0–242], 0 [0–6], 34 [0–290] and 17 [0–149], respectively. The distributions of log-transformed total TAC, partial TAC and CAC are shown in Fig. 2. Distributions of nonzero values of log-transformed total TAC and CAC were approximately normal but the frequency of total TAC and CAC equal to zero were high, 36% and 28% respectively. The distribution of nonzero values of log-transformed partial TAC had a non-normal shape that reflects a truncated phenomenon due to the lack of aortic arch calcium measurement resulting in a very high frequency of zero partial TAC (69%). Additionally, Fig. 2 shows that the number of patients with total TAC, partial TAC and CAC above 100 were 402 (40%), 141 (14%) and 301 (30%), respectively. Thus, the number of participants detected as having aortic calcium was 50% lesser if the measures excluded aortic arch, resulting in a lack of sensitivity for partial TAC, as compared with total TAC assessment.

The comparison of subjects with and without history of non-cardiac vascular event showed that age and gender did not differ (Table 1). Comparison of traditional risk factors showed that hypertension, anti-hypertensive and statin treatment were more frequent ($p < 0.05$, $p < 0.01$, $p < 0.05$), lifelong smoking dose was greater ($p < 0.001$) and total cholesterol was lower ($p < 0.01$) in the group with history of non-cardiac vascular events than in the group without (Table 1). Lastly, total TAC, partial TAC and aortic arch TAC were higher in subjects with history of non-cardiac vascular events

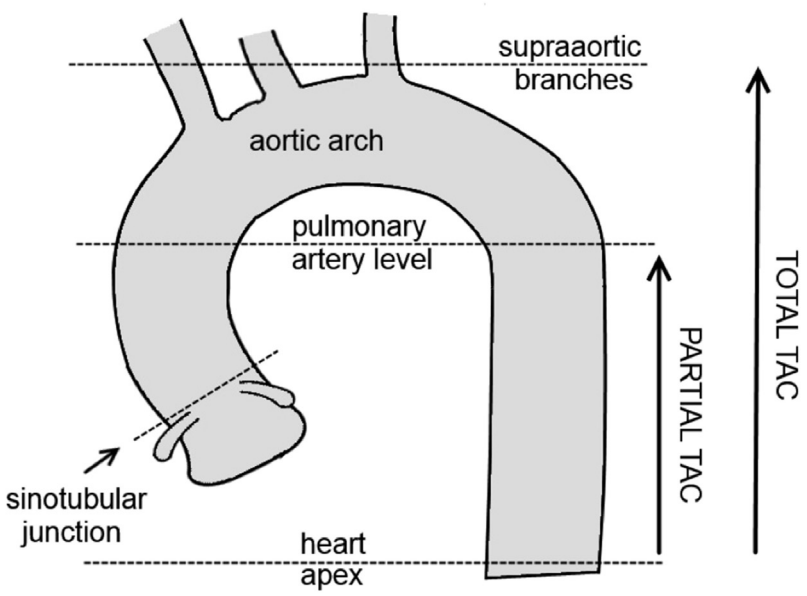

Fig. 1. Definition of total and partial thoracic aorta calcium (TAC).

Table 1
Clinical characteristics of the study population.

Parameter	All patients (n = 1000)	History of non-cardiac vascular events		p value (1 *vs* 2)
		Absence (1) (n = 970)	Presence (2) (n = 30)	
Age, years	57 ± 9	57 ± 9	59 ± 10	NS
Male gender, n (%)	776 (78)	754 (78)	22 (73)	NS
Body mass index, kg/m^2	26 ± 4	26 ± 4	26 ± 4	NS
Hypertension, n (%)	497 (50)	476 (49)	21 (70)	<0.05
Anti-hypertensive treatment, n (%)	446 (45)	425 (44)	21 (70)	<0.01
Systolic pressure, mmHg	124 ± 13	124 ± 13	127 ± 14	NS
Diastolic pressure, mmHg	73 ± 9	73 ± 9	75 ± 10	NS
Hypercholesterolemia, n (%)	823 (82)	796 (82)	27 (90)	NS
Statin treatment, n (%)	527 (53)	506 (52)	21 (70)	<0.05
Total cholesterol, mmol/l	5.19 ± 1.17	5.21 ± 1–17	4.62 ± 1.15	<0.01
Current smoker, n (%)	204 (20)	198 (20)	6 (20)	NS
Lifelong smoking dose, pack yrs	10 [0–25]†	10 [0–25]	30 [15–40]	<0.001
Blood glucose, mmol/l	5.55 ± 1.04	5.55 ± 1.05	5.42 ± 0.66	NS
Diabetes, n (%)	84 (8)	83 (9)	1 (3)	NS
Type of non-cardiac vascular events				
– *Cerebrovascular disease, n*	17	0	17	
– *Peripheral vascular disease, n*	13	0	13	
Total TAC value				
– *Raw*	41 [0–342]	39 [0–333]	282 [28–1809]	<0.01
– *Log-transformed*	3.33 ± 2.91	3.28 ± 2.89	5.05 ± 2.91	<0.001
Partial TAC value				
– *Raw*	0 [0–6]	0 [0–5]	4 [0–284]	<0.01
– *Log-transformed*	1.33 ± 2.30	1.28 ± 2.26	2.84 ± 3.09	<0.001
Aortic arch TAC value				
– *Raw*	34 [0–290]	33 [0–269]	253 [20–1242]	<0.01
– *Log-transformed*	3.16 ± 2.83	3.11 ± 2.82	4.77 ± 2.91	<0.001
CAC value				
– *Raw*	17 [0–149]	16 [0–148]	73 [0–284]	NS
– *Log-transformed*	2.79 ± 2.57	2.77 ± 2.56	3.57 ± 2.67	NS

Values are number of subjects, n (%) or mean ± SD with range or median [interquartile range].
CAC, coronary artery calcium; NS, non-significant; TAC, thoracic aorta calcium.

than in those without ($p < 0.01$ for raw values and $p < 0.001$ for log-transformed values) but CAC did not differ between both groups (Table 1).

Table 2 shows that the adjusted OR of having a history of non-cardiac vascular events per 1-SD increase in log-transformed calcium value was significant and similar for total TAC (OR [95%

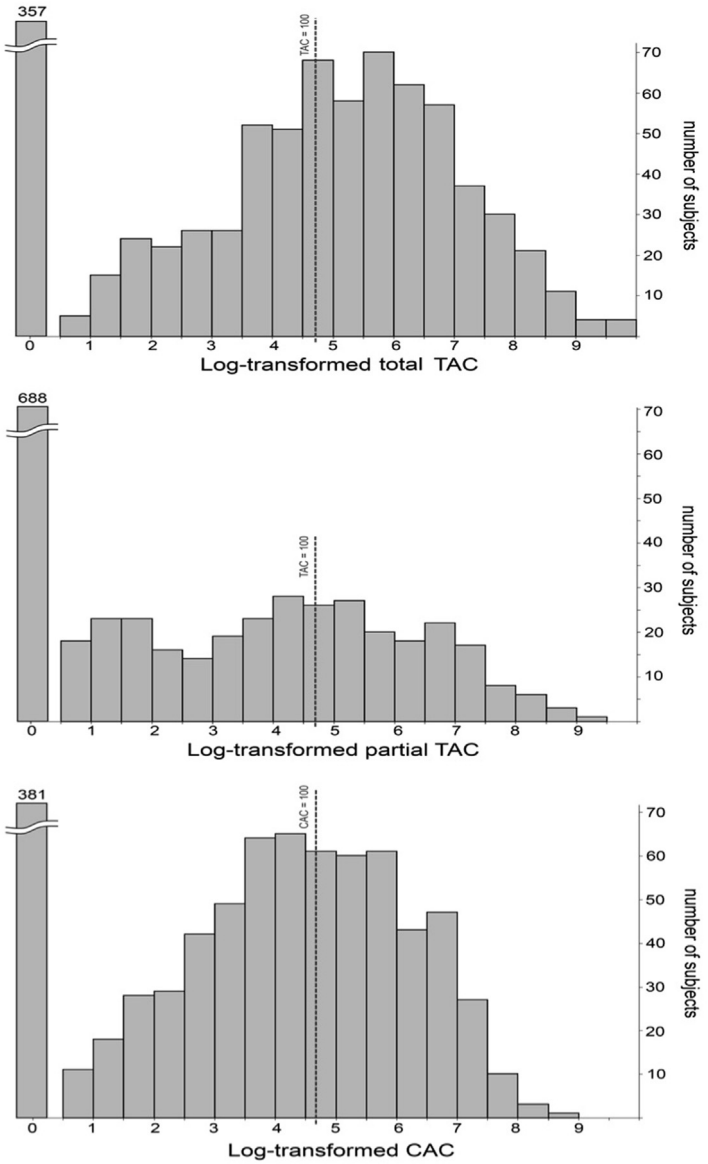

TAC, thoracic aorta calcium; CAC, coronary artery calcium. The raw score threshold of 100 is indicated with a dotted line.

Fig. 2. Distribution of log-transformed total TAC, partial TAC and CAC in the overall study population.

Table 2
Separate logistic regressions of the presence of non-cardiac vascular events on log-transformed calcium values.

Log-transformed parameter	OR	95% CI
Total TAC	1.56†	1.12–2.24
Partial TAC	1.58†	1.12–2.25
Aortic arch TAC	1.47*	1.08–2.06
CAC	1.13	0.86–1.50

Each logistic regression was adjusted for age, gender, total cholesterol, systolic blood pressure, anti-hypertensive and statin treatment. 1-SD increments for log-transformed total TAC, partial TAC, aortic arch TAC and CAC were 1.89, 1.13, 1.79 and 1.71, respectively.
†, $p < 0.01$; *, $p < 0.05$; CAC, coronary artery calcium; CI, confidence interval; SD, standard deviation; TAC, thoracic aorta calcium.

CI] = 1.56 [1.12–2.24], $p < 0.01$), partial TAC (1.58 [1.12–2.25], $p < 0.01$), aortic arch TAC (1.47 [1.08–2.06], $p < 0.05$) but not for CAC (1.13 [0.86–1.50]).

Fig. 3 shows the OR of having history of non-cardiac vascular events by 1-SD increase in each parameter when entering total TAC and CAC together in the logistic regression as well as risk factors. Of all covariates, OR were significant only for total TAC (1.57 [1.10–2.32], $p < 0.01$) and negatively for cholesterol (0.62 [0.40–0.97], $p < 0.05$).

4. Discussion

Our study used an original MSCT-based method that allows determining the amount of calcium in the entire thoracic aorta including aortic arch, concomitantly with the CAC detection

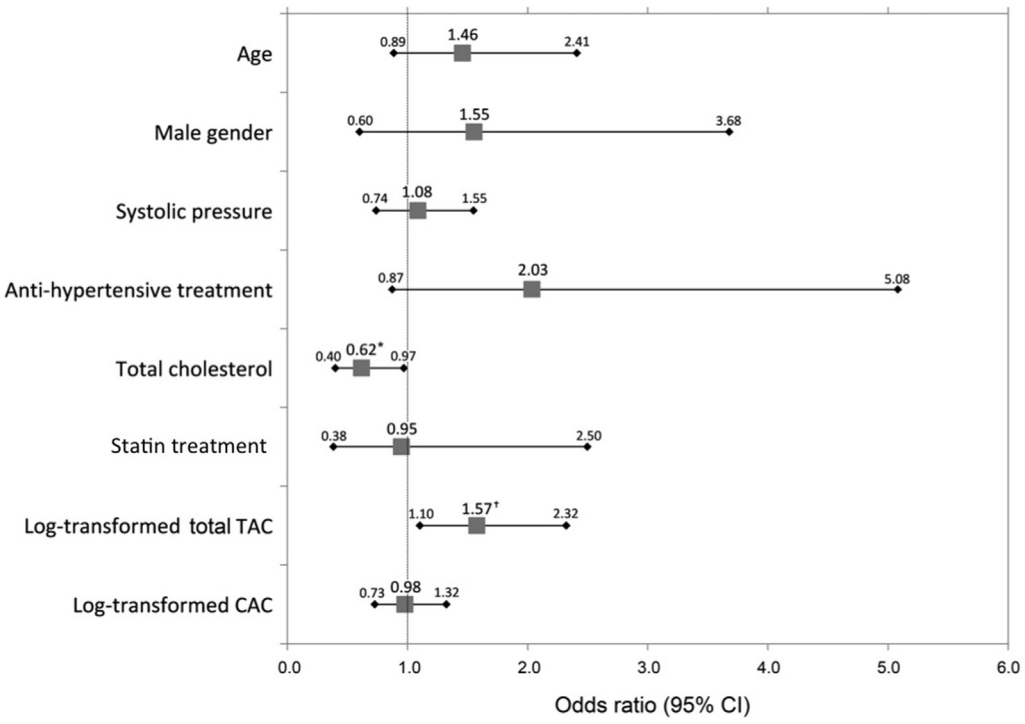

Odds ratios of having non-cardiac vascular events calculated from a logistic regression that included both total TAC and CAC and adjusted for age, gender, total cholesterol, systolic blood pressure and anti-hypertensive and statin medication. Odds ratios were calculated per 1 standard deviation increase of age (9.2 years), systolic pressure (13.5 mmHg), total cholesterol (1.17 mmol/l) and log-transformed TAC and CAC (1.89 and 1.71, respectively).
†, p<0.01; *, p<0.05; CAC, coronary artery calcium; CI, confidence interval; TAC, thoracic aorta calcium.

Fig. 3. Independent association of total TAC with history of non-cardiac vascular events.

procedure.

A first result is the strong association of total TAC with history of non-cardiac vascular event, independently of age, gender and coexisting cardiovascular risk factors. A noteworthy exception to the lack of relation of total TAC with traditional risk factors is provided by total cholesterol found independently and negatively associated with non-cardiac event history. This latter finding likely results from the administration of more intensive statin treatment to patients with vascular events. Several prospective studies [4,10–13] previously showed that CT-assessed TAC predicted cardiovascular complications beyond coronary heart disease. However, most of these studies did not analyze specifically non-cardiac vascular events, but rather global cardiovascular morbidity or mortality, mixing cardiac and non-cardiac events [4,10]. In addition, a few studies pointed out the potential importance of aortic arch calcium in the association of TAC with non-cardiac vascular events. A prospective study in heavy smokers found that TAC was specifically related to the incidence of non-cardiac events including stroke and peripheral arterial disease, especially when calcium was measured in the aortic arch [12]. Another transversal study found specific associations between aortic arch calcium and cerebrovascular disease [14]. Mechanisms that may explain the associations of TAC and non-cardiac vascular events are different whether one considers cerebrovascular events or peripheral arterial disease. The role of atherosclerotic aortic arch plaque was demonstrated in ischemic stroke [23,24] as well as for predicting recurrent stroke [25]. The association of aorta calcium with peripheral arterial disease may involve the extension of thoracic aorta atherosclerosis to the abdominal aorta and its branches [26,27].

Our second finding was that CAC was not associated with non-cardiac vascular events, and the incorporation of CAC in the multivariable model did not attenuate the correlation of total TAC with non-cardiac events. Such findings may be due to that CAC is perhaps more a measure of localized than generalized atherosclerosis [12]. However, some previous studies in the literature showed that CAC predicted overall cardiovascular morbidity and mortality, better than TAC [4,10]. This is somewhat discrepant with our present findings and one explanation may be that these studies did analyze composite cardiovascular disease endpoints incorporating highly prevalent coronary heart disease that is strongly related to CAC. Also, the inferiority of TAC as regards CAC for predicting cardiovascular events in these studies may imply a field of measurement insufficiently long for detecting aortic arch calcium [4,10].

The exclusion of aortic arch calcium from TAC measurement may annihilate its association with cerebrovascular disease and consequently with non-cardiac vascular events, because plaques in the aortic arch were shown to play a major role in the incidence and prevalence of cerebrovascular disease [23–25]. To explore this possibility, we have analyzed whether incorporation or not of aortic arch calcium in the TAC measurement of our subjects had an impact on the association with non-cardiac events. Despite the potential lack of sensitivity of partial *vs* total TAC for calcium detection (Fig. 2), partial TAC was associated to non-cardiac vascular event with the same strength than total TAC. This finding suggests that measuring total TAC by including aortic arch calcium does not provide incremental information comparatively with partial TAC excluding arch calcium. However, the increased aortic arch calcification burden in patients with non-cardiac vascular events

enhances its potential relevance *per se*.

4.1. Study limitations

First, this study is retrospective and analyzed subjects at risk for cardiovascular disease from whom results cannot be extrapolated to the general population. Second, the radiation dose required by our enlarged field of measurement in order to incorporate aortic arch is greater than the radiation dose when measuring TAC during traditional CAC detection. However, this dose remains weaker than that delivered for a bilateral mammogram.

5. Conclusion

Our study suggests that the assessment of TAC simultaneous with CAC detection may provide complementary information on the extra coronary component of cardiovascular risk, beyond the coronary risk prediction of CAC. However, further studies are required to confirm prospectively this result, as well as to identify the biomarkers involved in the pathogenesis of TAC comparatively to CAC.

Disclosures

None.

Conflict of interest

Any of the authors have actual or potential conflict of interest.

References

[1] S. Parikh, M.J. Budoff, Calcium scoring and cardiac computed tomography in 2014, Cardiol. Clin. 32 (2014) 419–427.
[2] G. Youssef, M.J. Budoff, Coronary artery calcium scoring, what is answered and what questions remain, Cardiovasc Diagn. Ther. 2 (2012) 94–105.
[3] R.L. McClelland, H. Chung, R. Detrano, W. Post, R.A. Kronmal, Distribution of coronary artery calcium by race, gender, and age: results from the Multi-Ethnic Study of Atherosclerosis (MESA), Circulation 113 (2006) 30–37.
[4] J. Yeboah, J.J. Carr, J.G. Terry, J. Ding, I. Zeb, S. Liu, et al., Computed tomography-derived cardiovascular risk markers, incident cardiovascular events, and all-cause mortality in nondiabetics: the Multi-Ethnic Study of Atherosclerosis, Eur. J. Prev. Cardiol. 21 (2014) 1233–1241.
[5] R. Detrano, A.D. Guerci, J.J. Carr, D.E. Bild, G. Burke, A.R. Folsom, et al., Coronary calcium as a predictor of coronary events in four racial or ethnic groups, N. Engl. J. Med. 358 (2008) 1336–1345.
[6] S.E. Elias-Smale, R.V. Proenca, M.T. Koller, M. Kavousi, F.J. van Rooij, M.G. Hunink, et al., Coronary calcium score improves classification of coronary heart disease risk in the elderly: the Rotterdam Study, J. Am. Coll. Cardiol. 56 (2010) 1407–1414.
[7] P. Greenland, L. LaBree, S.P. Azen, T.M. Doherty, R.C. Detrano, Coronary artery calcium score combined with Framingham score for risk prediction in asymptomatic individuals, JAMA 291 (2004) 210–215.
[8] T.S. Polonsky, R.L. McClelland, N.W. Jorgensen, D.E. Bild, G.L. Burke, A.D. Guerci, et al., Coronary artery calcium score and risk classification for coronary heart disease prediction, JAMA 303 (2010) 1610–1616.
[9] P. Madaj, M.J. Budoff, Risk stratification of non-contrast CT beyond the coronary calcium scan, J. Cardiovasc Comput. Tomogr. 6 (2012) 301–307.
[10] N.D. Wong, H. Gransar, L. Shaw, D. Polk, J.H. Moon, R. Miranda-Peats, et al., Thoracic aortic calcium versus coronary artery calcium for the prediction of coronary heart disease and cardiovascular disease events, JACC Cardiovasc. Imaging 2 (2009) 319–326.
[11] M.A. Allison, S. Hsi, C.L. Wassel, C. Morgan, J.H. Ix, C.M. Wright, et al., Calcified atherosclerosis in different vascular beds and the risk of mortality, Arterioscler. Thromb. Vasc. Biol. 32 (2012) 140–146.
[12] P.C. Jacobs, M. Prokop, Y. van der Graaf, M.J. Gondrie, K.J. Janssen, H.J. de Koning, et al., Comparing coronary artery calcium and thoracic aorta calcium for prediction of all-cause mortality and cardiovascular events on low-dose non-gated computed tomography in a high-risk population of heavy smokers, Atherosclerosis 209 (2010) 455–462.
[13] R.D. Santos, J.A. Rumberger, M.J. Budoff, L.J. Shaw, S.H. Orakzai, D. Berman, et al., Thoracic aorta calcification detected by electron beam tomography predicts all-cause mortality, Atherosclerosis 209 (2010) 131–135.
[14] S.E. Elias-Smale, A.E. Odink, R.G. Wieberdink, A. Hofman, M.G. Hunink, G.P. Krestin, et al., Carotid, aortic arch and coronary calcification are related to history of stroke: the Rotterdam Study, Atherosclerosis 212 (2010) 656–660.
[15] M.J. Budoff, K. Nasir, R. Katz, J. Takasu, J.J. Carr, N.D. Wong, et al., Thoracic aortic calcification and coronary heart disease events: the Multi-Ethnic Study of Atherosclerosis (MESA), Atherosclerosis 215 (2011) 196–202.
[16] H. Kalsch, N. Lehmann, S. Mohlenkamp, C. Hammer, A.A. Mahabadi, S. Moebus, et al., Prevalence of thoracic aortic calcification and its relationship to cardiovascular risk factors and coronary calcification in an unselected population-based cohort: the Heinz Nixdorf Recall Study, Int. J. Cardiovasc. Imaging 29 (2013) 207–216.
[17] D. Craiem, G. Chironi, M.E. Casciaro, A. Redheuil, E. Mousseaux, A. Simon, Three-dimensional evaluation of thoracic aorta enlargement and unfolding in hypertensive men using non-contrast computed tomography, J. Hum. Hypertens. 27 (2013) 504–509.
[18] D. Craiem, G. Chironi, A. Redheuil, M. Casciaro, E. Mousseaux, A. Simon, et al., Aging impact on thoracic aorta 3D morphometry in intermediate-risk subjects: looking beyond coronary arteries with non-contrast cardiac CT, Ann. Biomed. Eng. 40 (2012) 1028–1038.
[19] G. Chironi, L. Orobinskaia, J.L. Megnien, M.E. Sirieix, S. Clement-Guinaudeau, M. Bensalah, et al., Early thoracic aorta enlargement in asymptomatic individuals at risk for cardiovascular disease: determinant factors and clinical implication, J. Hypertens. 28 (2010) 2134–2138.
[20] P. Greenland, J.S. Alpert, G.A. Beller, E.J. Benjamin, M.J. Budoff, Z.A. Fayad, et al., 2010 ACCF/AHA guideline for assessment of cardiovascular risk in asymptomatic adults: a report of the American College of Cardiology Foundation/American Heart Association task force on practice guidelines, Circulation 122 (2010) e584–636.
[21] D. Craiem, G. Chironi, M.E. Casciaro, S. Graf, A. Simon, Calcifications of the thoracic aorta on extended non-contrast-enhanced cardiac CT, PLoS One 9 (2014) e109584.
[22] A.S. Agatston, W.R. Janowitz, F.J. Hildner, N.R. Zusmer, M. Viamonte Jr., R. Detrano, Quantification of coronary artery calcium using ultrafast computed tomography, J. Am. Coll. Cardiol. 15 (1990) 827–832.
[23] P. Amarenco, A. Cohen, C. Tzourio, B. Bertrand, M. Hommel, G. Besson, et al., Atherosclerotic disease of the aortic arch and the risk of ischemic stroke, N. Engl. J. Med. 331 (1994) 1474–1479.
[24] R. Deif, M. El-Sayed, F.A. Allah, E. Baligh, N.M. El-Fayomy, L. Ezzat, et al., Atherosclerotic aortic arch plaques in acute ischemic stroke, J. Vasc. Interv. Neurol. 4 (2011) 5–9.
[25] M.R. Di Tullio, C. Russo, Z. Jin, R.L. Sacco, J.P. Mohr, S. Homma, Aortic arch plaques and risk of recurrent stroke and death, Circulation 119 (2009) 2376–2382.
[26] R.W. Jayalath, S.H. Mangan, J. Golledge, Aortic calcification, Eur. J. Vasc. Endovasc. Surg. 30 (2005) 476–488.
[27] D. Tanne, A. Tenenbaum, J. Shemesh, Y. Schwammenthal, E.Z. Fisman, E. Schwammenthal, et al., Calcification of the thoracic aorta by spiral computed tomography among hypertensive patients: associations and risk of ischemic cerebrovascular events, Int. J. Cardiol. 120 (2007) 32–37.

Rev Esp Cardiol. 2016;69(9):827–835

Original article

Association Between Thoracic Aorta Calcium and Thoracic Aorta Geometry in a Cohort of Asymptomatic Participants at Increased Cardiovascular Risk

Damian Craiem,[a,b,c,d,*] Jean-Marc Alsac,[c,d,e] Mariano E. Casciaro,[a] Salma El Batti,[e] Elie Mousseaux,[c,d,f] Marie-Emmanuelle Sirieix,[b,d] and Alain Simon[b,c,d]

[a] *Facultad de Ingeniería Ciencias Exactas y Naturales, Universidad Favaloro, CONICET, Buenos Aires, Argentina*
[b] *Centre de Médecine Préventive Cardiovasculaire, APHP, Hôpital Européen Georges Pompidou, Paris, France*
[c] *INSERM U970, APHP, Hôpital Européen Georges Pompidou, Paris, France*
[d] *Université Paris-Descartes, Paris-Centre de Recherche Cardiovasculaire, Hôpital Européen Georges Pompidou, Paris, France*
[e] *Service de Chirurgie Cardiaque et Vasculaire, APHP, Hôpital Européen Georges Pompidou, Paris, France*
[f] *Service d'Imagerie Cardiovasculaire, APHP, Hôpital Européen Georges Pompidou, Paris, France*

Article #4

Article history:
Received 2 October 2015
Accepted 15 January 2016
Available online 4 May 2016

Keywords:
Aorta
Atherosclerosis
Calcium
Computed tomography

ABSTRACT

Introduction and objectives: Thoracic aorta calcium detection is known to improve cardiovascular risk prediction for cardiac and noncardiac events beyond traditional risk factors. We investigated the influence of thoracic aorta morphometry on the presence and extent of aortic calcifications.
Methods: Nonenhanced computed tomography heart scans were performed in 970 asymptomatic participants at increased cardiovascular risk. An automated algorithm estimated the geometry of the entire thoracic aorta and quantified the aortic calcium Agatston score. A nonparametric model was used to analyze the percentiles of calcium score by age. Logistic regression models were calculated to identify anatomical associations with calcium levels.
Results: Calcifications were concentrated in the aortic arch and descending portions. Higher amounts of calcium were associated with an enlarged, unfolded, less tapered and more tortuous aorta. The size of the ascending aorta was not correlated with aortic calcium score, whereas enlargement of the descending aorta had the strongest association: the risk of having a global calcium score > 90th percentile was 3.62 times higher (confidence interval, 2.30-5.91; $P < .001$) for each 2.5-mm increase in descending aorta diameter. Vessel taper, tortuosity, unfolding and aortic arch and descending volumes were also correlated with higher amounts of calcium.
Conclusions: Thoracic aorta calcium was predominantly found at the arch and descending aorta and was positively associated with the size of the descending aorta and the aortic arch, but not with the size of the ascending aorta. These findings suggest that aortic dilatation may have different mechanisms and may consequently require different preventive strategies according to the considered segments.

Asociación entre el calcio de la aorta torácica y la geometría de esta en una cohorte de sujetos asintomáticos con riesgo cardiovascular aumentado

Palabras clave:
Aorta
Ateroesclerosis
Calcio
Tomografía computarizada

RESUMEN

Introducción y objetivos: La detección del calcio de la aorta torácica mejora la predicción del riesgo cardiovascular, en cuanto a los eventos cardiacos y no cardiacos, respecto a la obtenida solo con los factores de riesgo tradicionales. En este trabajo se ha investigado la influencia de la morfometría de la aorta torácica en la presencia y la magnitud de las calcificaciones aórticas.
Métodos: Se realizaron exploraciones por tomografía computarizada cardiaca sin contraste en 970 participantes asintomáticos con riesgo cardiovascular aumentado. Se utilizó un algoritmo automático para estimar la geometría de toda la aorta torácica y se cuantificó la puntuación de Agatston del calcio aórtico. Se utilizó un modelo no paramétrico para analizar los percentiles de la puntuación de calcio según la edad. Se calcularon modelos de regresión logística para identificar asociaciones anatómicas con las concentraciones de calcio.
Resultados: Las calcificaciones se concentraron en el cayado aórtico y la aorta descendente. Las mayores cantidades de calcio se asociaron con una aorta agrandada, desplegada, con menor estrechamiento y más

SEE RELATED ARTICLE:
http://dx.doi.org/10.1016/j.rec.2016.05.006, Rev Esp Cardiol. 2016;69:813–6.
* Corresponding author: FICEN, Universidad Favaloro, Solis 453, 1078 Ciudad Autónoma de Buenos Aires, Argentina.
E-mail address: damian@craiem.com.ar (D. Craiem).

http://dx.doi.org/10.1016/j.rec.2016.01.031

tortuosa. El tamaño de la aorta ascendente no mostró correlación con la puntuación de calcio de la aorta, mientras que el tamaño de la aorta descendente es el parámetro que mostró mayor asociación: el riesgo de tener una puntuación de calcio global superior al percentil 90 fue 3,62 veces (intervalo de confianza, 2,30-5,91; p < 0,001) mayor por cada 2,5 mm de aumento del diámetro de la aorta descendente. La reducción gradual del diámetro, la tortuosidad, el despliegue y los volúmenes del cayado aórtico y la aorta descendente estaban correlacionados con mayor cantidad de calcio.

Conclusiones: Las calcificaciones se hallaron predominantemente en el cayado aórtico y la aorta descendente y mostraron asociación positiva con el tamaño de la aorta descendente y el cayado aórtico, pero no con el tamaño de la aorta ascendente. Estas observaciones indican que la dilatación aórtica puede tener mecanismos diferentes y, por consiguiente, requiere estrategias preventivas distintas según el segmento considerado.

Abbreviations

MSCT: multislice computed tomography
TA: thoracic aorta
TAC: thoracic aorta calcium

INTRODUCTION

It is important to determine the size of the thoracic aorta (TA) because its early increase may predict future aortic aneurysms whose frequency shows a continuous increase.[1] Estimating aortic size (ie, diameter, volume, tortuosity, tapering) is challenging because the anatomy of the TA is complex, particularly in the aortic arch region, which has several branches and a curvilinear nonplanar path that bends and twists.[2,3] We have recently shown that noncontrast low dose computed tomography for coronary artery calcium scoring allows reconstruction of the global morphology of the TA and simultaneously detection of thoracic aorta calcium (TAC).[4–7]

The Agatston TAC score is an indicator of atherosclerotic disease[8] and the opportunity to assess TA size and TAC simultaneously may allow analysis of the participation of atherosclerotic disease in the early dilatation of the TA according to the considered segment. Moreover, a detailed assessment of the association between aortic calcium and TA geometry could help to elucidate the heterogeneous distribution of calcium deposits along the length of the TA and help to detect vulnerable regions.[9]

In this study, we investigated the association of TA size with TAC in a cohort of 970 asymptomatic participants at increased cardiovascular risk. A detailed 3-dimensional geometric description of the TA and the position and size of TAC were simultaneously analyzed with customized software using nonenhanced extended multislice computed tomography (MSCT) scans. Logistic models adjusted for traditional risk factors were calculated to assess the specific role of the TA geometric variables on the presence of TAC and its extent and spatial distribution.

METHODS

Study Participants

Study participants (n = 970) were recruited over 2 years from September 2009.[4] We included all consecutive patients at risk for cardiovascular disease who underwent a noncontrast MSCT scan as part of a cardiovascular risk stratification program. This scan was performed as part of dual screening: *a)* estimation of calcified coronary atherosclerosis burden, and *b)* detection of early aortic dilatation in all TA sites including the ascending aorta, aortic arch and descending aorta. Informed consent was obtained from all individual participants included in the study. The participants had at least 1 traditional risk factor (hypercholesterolemia in 82%, hypertension in 49%, current smoking in 20% and diabetes in 9%). None of the participants had present or a past history of cardiovascular disease. The Framingham risk score calculated in all participants after recalibration for the French population was less than 20% at 10 years.[10] In accordance with the current guidelines,[11] we stratified the participants' risk of atherosclerotic cardiovascular disease by means of noncontrast low-dose MSCT for coronary artery calcium measurement. An extended scan was used to cover the entire TA for TAC assessment.[4] Brachial blood pressure was determined as the mean of 3 measurements using a sphygmomanometer with the patient in the supine position following a 10-min rest. Hypertension was defined as blood pressure of 140/90 mmHg or above, or use of antihypertensive medication. Total and high-density lipoprotein blood cholesterol and triglyceride concentrations were measured after a 14-hour fast, and low-density lipoprotein concentrations were calculated with the Friedewald formula or, when this formula could not be used, were measured directly. Hypercholesterolemia was determined by fasting low-density lipoprotein cholesterol above 3.3 mmol/L or by the presence of low-density lipoprotein-lowering drug therapy. Blood glucose was measured after an overnight fast and diabetes was determined by fasting blood glucose of 7 mmol/L or above, or by the presence of antidiabetic medication.

The retrospective analysis of personal health data of study participants was authorized by the CNIL *(Commission nationale de l'informatique et des libertés)* and was in accordance with the Declaration of Helsinki.

Image Acquisition

Aortic imaging was obtained with noncontrast cardiac 64-slice MSCT (Light-speed VCT, GE Health care; Milwaukee, Wisconsin, United States) during the acquisition done to quantify coronary artery calcium as reported elsewhere.[4] The measurements were done with 2.5-mm axial slices, 120 kVp, 250-mA tube current, 250-ms exposure time, and a 250-mm field of view. Images were acquired with prospective-electrocardiogram gating at 60% of the R-R interval in the craniocaudal direction from the top of the aortic arch to the level of the diaphragm. The effective radiation dose assessed in a representative subgroup of 200 participants using this extended scan length was 1.23 ± 0.14 mSv.[6] Scans were exported as DICOM (Digital Imaging and Communication in Medicine) files and were analyzed using a customized software designed in our laboratory that estimated the TA geometry in 3 dimensions[6] and calculated the size and position of the TA calcifications.[4] Thoracic aortic size and calcium were measured by the same expert, blinded to clinical parameters. Further details can be found in previous reports.[4–6]

Aortic Size and Shape Measurements

The user started with a manual selection of 2 seed points in the axial slices at the center of the ascending and descending aorta at the pulmonary bifurcation level (see points CA and CD in Figure 1A). Then, an automatic algorithm extracted the central skeleton and estimated the vessel diameter at that point, dynamically expanding and centering circles to inscribe them inside the vessel cross-section area.[6] This circle-fitting algorithm was sequentially applied over the axial computed tomography slices for the descending portion of the aorta and over the oblique planes for the curvilinear part (Figure 1A). These oblique planes were reconstructed in steps of 2° angles following a semitoroidal path. The center point of each circle was used as a seed point for the next estimation. A postprocessing correction was performed to ensure that reconstructed planes remained perpendicular to the true aortic centerline. The result of this process in each patient was a list of ≈150 centerline points with the corresponding diameters that approximated the cross section of the aorta in each position.

The vessel was finally divided into ascending, arch and descending portions delimited by 4 planes at the left main coronary artery, the brachiocephalic and left subclavian arteries and the coronary sinus level (Figure 1).

Twelve geometric variables were chosen to describe the TA morphology in 3 dimensions. These variables were selected because they properly summarized the modifications of TA size and shape due to aging in recent reports.[6,12,13]

The size of the TA was assessed by measuring the mean diameter and the volume of the ascending, arch and descending TA segments. The description of TA shape included another 6 variables: the aortic arch width and height, aortic tortuosity (calculated as the TA curve length divided by the straight line distance between endpoints), aortic tapering (defined as the difference between the mean ascending and mean descending diameters normalized to ascending diameter) and 2 distances (from arch center to centerline points at 45° and 135°) as shown in Figure 1B.

Calcification Assessment

Lesions were quantified with a semi-automatic algorithm using the Agatston score method.[8] For each axial image, the algorithm highlighted all candidate lesions of area > 1 mm^2 and > 130 HU. Subsequently, the user reviewed each axial plane to validate the automated selection. The Agatston score was calculated for each lesion using a weighted value assigned to the highest density of calcification multiplied by the area. Each calcification was assigned to the nearest aortic segment. Finally, the calcium scores were accumulated for each segment. Global and segmental raw and log-transformed scores were reported for each participant.

Statistical Analysis

Normally distributed continuous variables are described as means ± standard deviation (SD) and categorical variables as frequencies (%). Thoracic arch calcium was expressed as raw values and log-transformed values (calculated as log [score + 1]). Participants with and without TAC were compared with chi-square tests for

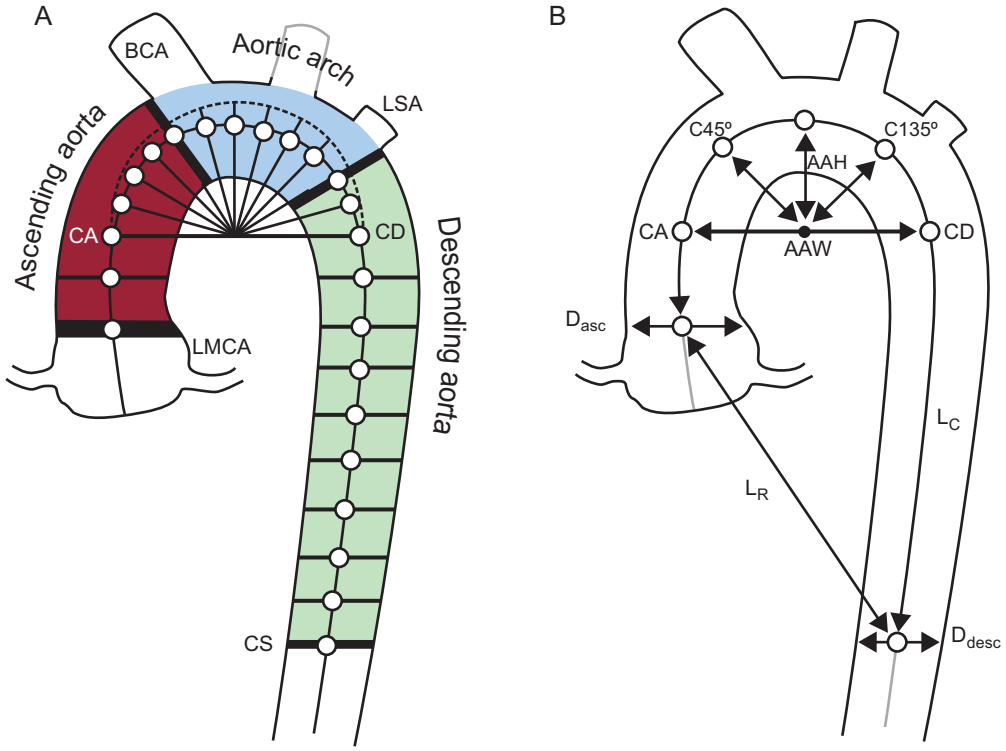

Figure 1. Measurements of aortic size and shape. A: 2 seed points in the ascending and descending thoracic aorta were used for the automated segmentation algorithm that calculated the vessel centerline. The ascending, arch and descending segments were separated by 4 oblique planes at the left main coronary artery, brachiocephalic artery, left subclavian artery, and at the coronary sinus level. B: Right: geometric measurements used to describe the aortic shape. Aortic arch width and height, distances from the arch center to diagonal vectors (C45° and C135°), aortic taper calculated as the percentage of descending to ascending diameter narrowing (D_{desc}/D_{asc}-1) × 100. Aortic tortuosity was defined as the length of the thoracic aorta centerline divided by the linear distance between extreme points. AAH, aortic arch height; AAW, aortic arch width; BCA, brachiocephalic artery; CA, coronary ascending; CD, coronary descending; CS, coronary sinus; D_{asc}, ascending diameter; D_{desc}, descending diameter; LMCA, left main coronary artery; LSA, left subclavian artery; L_C, length of the thoracic aorta centerline; L_R, linear distance between extreme points.

Table 1
Baseline Cohort Characteristics of 970 Participants

	Men			Women			*P* value*
	Without TAC	With TAC	*P* value	Without TAC	With TAC	*P* value	
Number of patients	294	461	–	58	157	–	–
Age, y	51 ± 9	60 ± 8	<.001	54 ± 7	61 ± 7	<.001	.11
Body surface area, m^2	2.02 ± 0.17	2.00 ± 0.17	.12	1.68 ± 0.16	1.71 ± 0.18	.44	<.001
Hypertension, %	42	57	<.001	19	50	<.001	.11
Antihypertensive medication, %	35	52	<.001	17	47	<.001	.23
Hypercholesterolemia, %	75	86	<.001	71	88	<.01	.52
Lipid-lowering medication, %	39	63	<.001	26	55	<.001	.08
Current smoking, %	20	20	.92	28	17	.10	.38
Diabetes mellitus, %	8	10	.41	5	6	.72	.17

TAC, thoracic aorta calcium.
* Men with thoracic aorta calcium vs women with thoracic aorta calcium.

categorical variables and student *t*-tests for variables with normal distribution. The patients were divided by age and TAC percentiles into 4 groups using nonparametric techniques.[14] We followed the article by O'Brien and Dyck[15] when setting normal values in skewed distributions. Accordingly, a model was constructed by using the log-transformed TAC distribution as a function of age and sex. Taking the exponential of the 50th and 90th percentiles (P50 and P90) curves of the TAC as a function of age, participants were separated into 4 groups of TAC level: TAC = 0, TAC > 0 and TAC < P50, TAC > P50 and TAC < P90 and TAC > P90. The trend of the TA geometric characteristic across TAC categories was compared using ANOVA (analysis of variance) adjusted for age, sex, body-size area, and incidence of hypertension and hypercholesterolemia. The association of TAC level with geometric variables taken separately was examined with a logistic regression adjusted for age, sex, body-size area, and incidence of hypertension and hypercholesterolemia. The odds of having increasing levels of TAC with respect to the TAC = 0 group per 1 SD increase in each geometric variable were calculated. The association of the local TAC presence in the ascending, arch and descending segments with the local geometric variables was also determined with separate logistic regressions. Odds ratios per 1 SD increase of each parameter were calculated adjusted for age, sex, body-size area, and incidence of hypertension and hypercholesterolemia. All analyses were performed with JMP 8 software (SAS Institute; Cary, North Carolina, United States).

RESULTS

The clinical characteristics of the study population, separated by the presence and absence of TAC, are shown in Table 1. Images of a representative patient with TAC are shown in Figure 2. Participants with TAC were older than those without ($P < .001$). Hypertension, antihypertensive therapy, hypercholesterolemia and lipid lowering therapy were more frequent in participants with TAC than in those without ($P < .001$ in all cases, except for hypercholesterolemia in women: $P < .01$). Body surface area and the frequency of diabetic and current smoking did not differ with the presence of TAC. Risk factors did not differ between men and women with TAC.

Differences in the presence and extent of TAC by gender are shown in Table 2 and Figure 3. The log-transformed TAC value did not differ between men and women in any segment, even after adjustment for age and body surface area (Table 2). The prevalence and log-transformed TAC score values in the ascending arch and descending segments were globally 21%, 66% and 91% and 3.72 ± 2.08, 4.66 ± 1.80, and 4.57 ± 1.98, respectively. The prevalence of TAC was higher in women than in men ($P < .01$) but this difference disappeared when adjusted for age and body surface area (Figure 3). When analyzed by quartiles of age, we found a higher percentage of younger women with TAC than men, but this difference did not reach statistical significance.

The P90 and P50 curves of the TAC by age and sex are shown in Figure 4. Thoracic aorta calcium exponentially increased with age and P90 curve were similar between men and women while the P50 curve of women was moved upwards compared with the curve of men.

To evaluate the association between TAC and aortic morphology, the cohort was stratified by TAC level and age, and the trend across TAC levels are shown in Table 3. Globally, TA mean diameter and volume increased with TAC level ($P < .001$). The size of the ascending aorta did not change with TAC, whereas both the arch and the descending segments were larger ($P < .001$, except for the

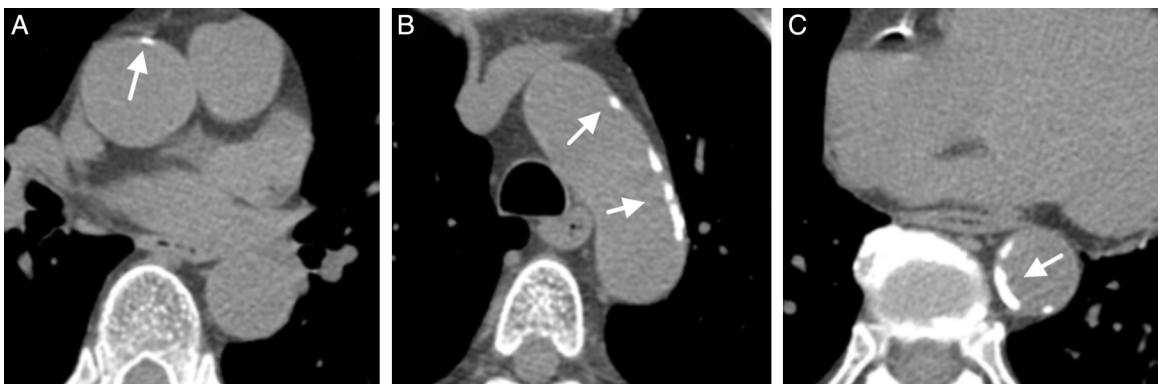

Figure 2. Axial computed tomography images of ascending (A), arch (B) and descending (C) thoracic aorta portions in a representative patient with aortic calcifications (arrows).

Table 2
Extent and Distribution of Calcium in Patients With Thoracic Aorta Calcium

	Men with TAC (n = 461)	Women with TAC (n = 157)	*P value*
Whole TA			
Log-transformed TAC	5.11 ± 1.91	5.24 ± 1.78	.47
Ascending aorta			
$TAC_{Asc} > 0$, %	23	18	.21
Log-transformed TAC_{Asc}	3.72 ± 2.00	3.75 ± 2.37	.31
Aortic arch			
$TAC_{Arch} > 0$, %	67	62	.27
Log-transformed TAC_{Arch}	4.60 ± 1.82	4.87 ± 1.74	.79
Descending aorta			
$TAC_{Desc} > 0$, %	92	93	.56
Log-transformed TAC_{Desc}	4.58 ± 2.01	4.55 ± 1.86	.89

Arch, aortic arch; Asc, ascending; Desc, descending; TA, thoracic aorta; TAC, thoracic aorta calcium.

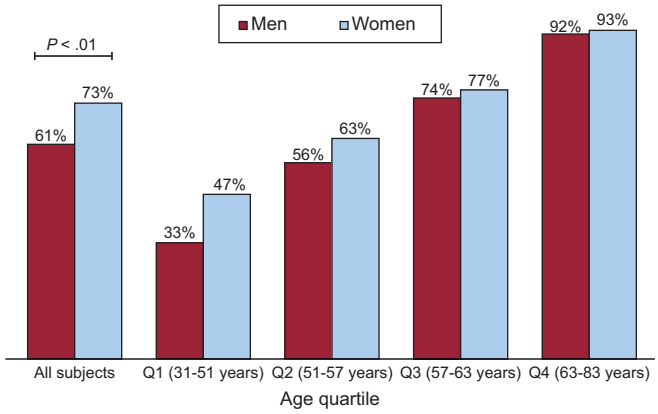

Figure 3. Prevalence of thoracic aorta calcium in men and women by quartiles of age. Q1, quartile 1; Q2, quartile 2; Q3, quartile 3; Q4, quartile 4.

arch diameter: $P < .05$). The aortic shape also differed by TAC level. In participants with more TAC, the arch was wider ($P < .01$), distances to C45° and C135° points were longer ($P < .01$), the whole TA was more tortuous ($P < .001$) and showed less taper (P < .001). Table 4 shows the risk of having a global calcium score < P50, between P50 and P90 and > P90 for 1 SD increase in each geometric variable. Odds ratios were calculated with respect to participants with TAC= 0, independently of traditional risk factors. Geometric variables were sorted by decreasing odds of having TAC and by TAC levels. The only 2 geometric variables associated with greater odds of belonging to the less calcified group (0 < TAC < P50) were descending diameter ($P < .05$) and aortic taper (P < .05). Another 4 variables increased the odds of belonging to the P50 < TAC < P90 group: arch and descending volume ($P < .001$ and $P < .05$, respectively), total TA volume ($P < .05$) and tortuosity ($P < .05$). Finally, 5 additional geometric variables were associated with greater odds of belonging to the most calcified group (TAC > P90): mean diameter, arch diameter, arch width, and distance to C45° and C135° ($P < .01$ in all cases). Descending mean diameter and aortic taper were strongly associated with TAC in the 3 groups, ie, the odds of belonging to the TAC > P90 group increased 3.62-fold for 1 SD increase of the descending diameter, whereas a 1 SD increase of taper reduced the odds by 0.60.

The odds of having TAC for each TA segment is shown in Figure 5. Greater odds of having TAC in all segments was associated with a larger descending TA mean diameter and volume. Additionally, the odds of having TAC in the ascending segment increased with less aortic taper. The TAC in the aortic arch was associated with mean diameter and total volume, arch volume, arch width, and distances to C45° and C135°. Similar associations were found for descending segments, adding arch diameter and tapering but excluding distance to C135°. The ascending TA size, the arch height and TA tortuosity were not associated with the presence of TAC in any segment.

DISCUSSION

To the best of our knowledge, this is the first study that has analyzed the calcifications and the geometry of the TA simultaneously to investigate the association of vessel morphology with

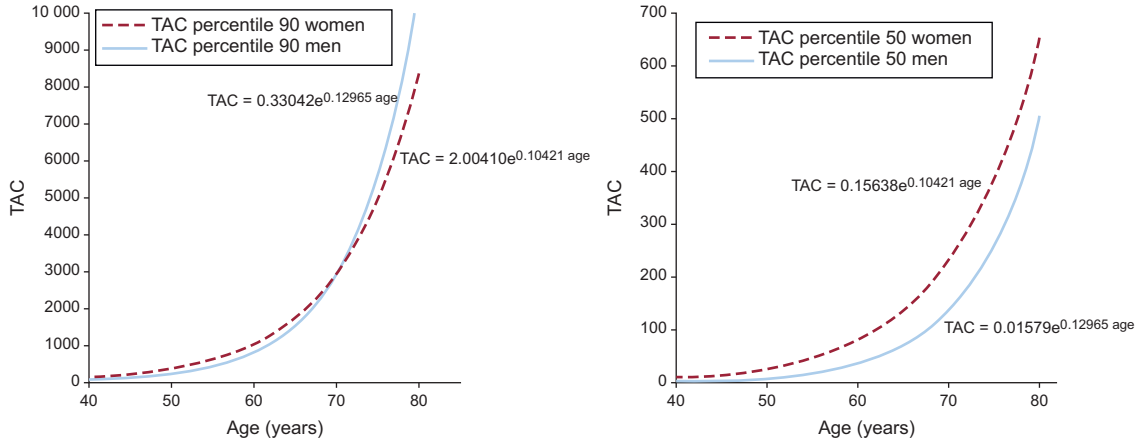

Figure 4. Nonparametric model of thoracic aorta calcium level as a function of age. Curves of the 50th and 90th percentiles are shown for men and women. TAC, thoracic aorta calcium.

Table 3
Comparison of Thoracic Aorta Geometric Characteristics Across Different Levels of Thoracic Aorta Calcium

TA size and shape variables	All (n = 970)	TAC = 0 (n = 352)	0 < TAC ≤ P50 (n = 142)	P50 < TAC ≤ P90 (n = 382)	TAC > P90 (n = 94)	*P* value
Mean diameter, cm	2.92 ± 0.27	2.84 ± 0.25	2.93 ± 0.26	2.98 ± 0.27	3.06 ± 0.28	<.001
Total volume, mL	160 ± 41	145 ± 33	156 ± 41	168 ± 40	183 ± 48	<.001
Ascending diameter, cm	3.32 ± 0.36	3.23 ± 0.34	3.31 ± 0.32	3.38 ± 0.38	3.43 ± 0.36	.61
Ascending volume, mL	53 ± 15	49 ± 14	52 ± 14	55 ± 15	58 ± 16	.34
Arch diameter, cm	2.87 ± 2.27	2.78 ± 0.24	2.90 ± 0.26	2.92 ± 0.27	2.99 ± 0.29	<.05
Arch volume, mL	20 ± 7	18 ± 5	20 ± 7	21 ± 7	23 ± 8	<.001
Descending diameter, cm	2.57 ± 0.25	2.47 ± 0.22	2.57 ± 0.26	2.62 ± 0.23	2.72 ± 0.25	<.001
Descending Volume, mL	87 ± 24	78 ± 19	86 ± 24	92 ± 23	102 ± 29	<.001
Arch width, cm	7.82 ± 1.14	7.43 ± 0.97	7.80 ± 1.06	8.04 ± 1.18	8.36 ± 1.29	<.01
Arch height, cm	5.40 ± 1.14	5.23 ± 1.09	5.27 ± 1.15	5.53 ± 1.17	5.71 ± 1.06	.17
Tortuosity, %	264 ± 30	254 ± 28	266 ± 29	270 ± 28	273 ± 33	<.001
Aortic taper, %	24 ± 7	25 ± 7	24 ± 7	24 ± 7	22 ± 6	<.001
Center to C45°, cm	4.19 ± 0.58	4.03 ± 0.51	4.15 ± 0.58	4.30 ± 0.58	4.42 ± 0.63	<.01
Center to C135°, cm	4.37 ± 0.66	4.17 ± 0.62	4.31 ± 0.63	4.49 ± 0.64	4.69 ± 0.70	<.01

P50, 50th percentil; P90, 90th percentil; TA, thoracic aorta; TAC, thoracic aorta calcium.
Adjusted for age, sex, body surface area, hypertension, and hypercholesterolemia.

Table 4
Probability of Having Increasing Levels of Thoracic Aorta Calcium per 1 Standard Deviation Increase in the Values of Geometric Variables

Geometric variables	0 < TAC ≤ P50 (n = 142) OR (95CI%)	P50 < TAC ≤ P90 (n = 382) OR (95CI%)	TAC > P90 (n = 94) OR (95CI%)
Descending diameter, cm	1.48 (1.06,2.08)[a]	1.68 (1.29,2.20)[b]	3.62 (2.30,5.91)[b]
Aortic taper, %	0.78 (0.61,0.98)[a]	0.73 (0.61,0.87)[b]	0.60 (0.44,0.80)[b]
Arch volume, mL	1.32 (0.99,1.76)	1.35 (1.09,1.68)[c]	1.78 (1.27,2.53)[b]
Descending volume, mL	1.17 (0.84,1.64)	1.38 (1.07,1.80)[a]	2.67 (1.78,4.11)[b]
Total volume, mL	1.12 (0.80,1.56)	1.29 (1.01,1.67)[a]	2.18 (1.47,3.30)[b]
Tortuosity, %	0.98 (0.76,1.26)	1.24 (1.02,1.52)[a]	1.35 (1.01,1.81)[a]
Mean diameter, cm	1.16 (0.84,1.61)	1.18 (0.94,1.49)	1.85 (1.26,2.769)[c]
Arch width, cm	1.12 (0.80,1.58)	1.24 (0.98,1.59)	1.74 (1.20,2.57)[c]
Arch diameter, cm	1.32 (0.99,1.78)	1.12 (0.90,1.39)	1.67 (1.18,2.41)[c]
Center to C45°, cm	1.01 (0.75,1.34)	1.18 (0.95,1.48)	1.62 (1.15,2.29)[c]
Center to C135°, cm	0.85 (0.64,1.12)	1.10 (0.89,1.35)	1.58 (1.16,2.16)[c]
Arch height, cm	0.86 (0.68,1.09)	1.02 (0.86,1.22)	1.23 (0.93,1.62)
Ascending diameter, cm	0.93 (0.70,1.24)	0.99 (0.81,1.21)	1.15 (0.83,1.61)
Ascending volume, mL	0.91 (0.68,1.20)	1.01 (0.83,1.21)	1.14 (0.84,1.54)

95%CI, 95% confidence interval; OR, odds ratio; P50, 50th percentil; P90, 90th percentil; TAC, thoracic aorta calcium.
The logistic regression was adjusted for age, sex, body-size area, and the presence of hypertension and hypercholesterolemia.
[a] $P < .05$.
[b] $P < .001$.
[c] $P <. 01$.

the presence and extent of TAC. Both calcification and geometry were accurately assessed in 3 dimensions and in the entire TA in a cohort of 970 participants at increased cardiovascular risk using MSCT images. Several TA geometric variables were associated with the presence, extent, and location of TA calcifications, independently of age, sex, and traditional risk factors. The main finding of our study with clinical implications is that dilatation of the descending aorta-with a consequent reduction in aortic taper was strongly associated with higher odds of finding TAC, whereas the size of the ascending portion was not related to TAC.

It is difficult to determine if the loss of aortic taper is the cause or the consequence of higher levels of TAC. Generally, calcifications were mostly concentrated in the arch and descending aortic segments[4,16,17] and geometry might help to explain this heterogeneous distribution. While nonoscillatory shear stress is thought to facilitate the formation of fatty infiltrations and cholesterol-rich plaques, calcifications are formed in locations where low shear stress but rapid stress fluctuations are observed.[18,19] Aortic narrowing stabilizes blood flow and delays the attenuation of the helical flow,[3] whereas aortic taper accelerates the flow velocity into the descending region, avoiding flow stagnation and plaque formation.[9] In addition, the influence of the helical flow pattern was suggested to suppress areas of flow stagnation so as to prevent the accumulation of lipids, in particular along the ascending and arch segments.[3] On the other hand, as the atherosclerotic process begins earlier in the descending aorta,[20] the enlargement of the descending TA may be interpreted as a compensatory mechanism to counteract vessel stiffening and progression of lumen stenosis.[21,22] From one perspective, the TA geometry has a direct influence on blood flow velocity profiles, producing predisposed sites for calcification. However, TAC can also be seen as the expression of an arteriosclerotic disorder that actually produces a geometric deformation. Unfortunately, the nonenhanced MSCT technique cannot differentiate between vascular calcification within the intima (in the context of atherosclerotic plaques) and/or within the media (associated with arteriosclerosis[21]),

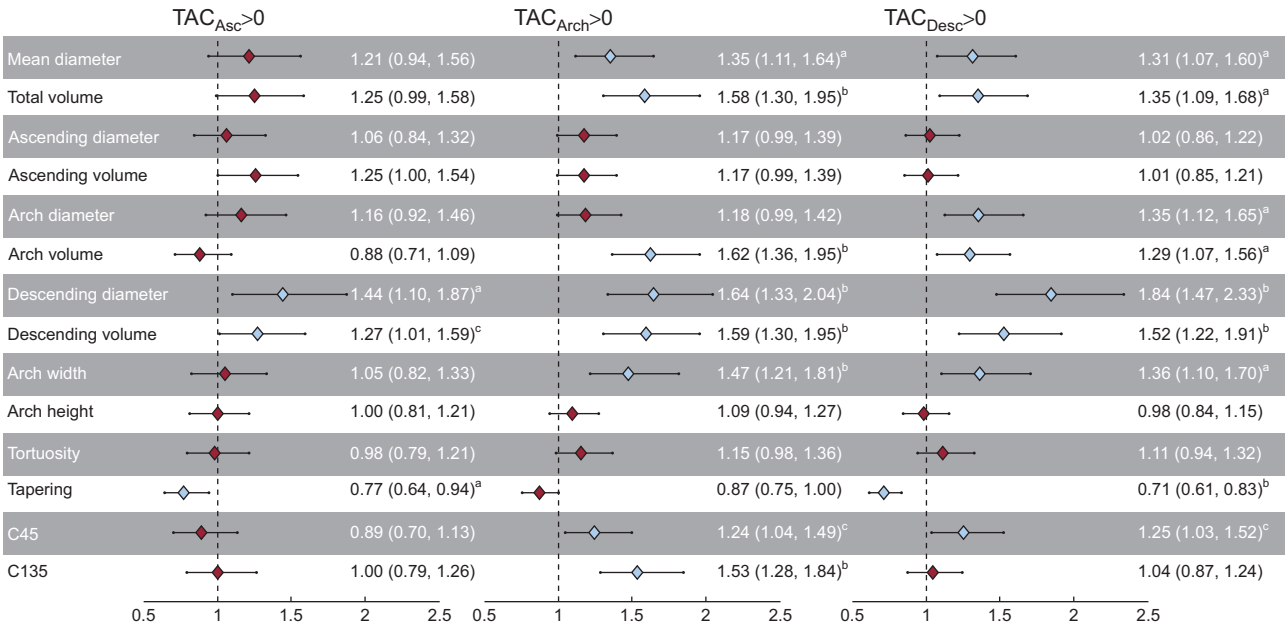

Figure 5. Probability (odds ratio [95% confidence interval]) of having calcifications in the ascending, arch and descending thoracic aorta segments for 1 standard deviation increase in each geometric variable. Arch, aortic arch; Asc, ascending; Arch, aortic arch; Desc, descending; TAC, thoracic aorta calcium. [a]$P < .01$. [b]$P < .001$. [c]$P < .05$.

although both seem involved in TAC detection.[23] Medial calcifications are an indicator of aortic wall disease that may weaken the resistance of the aortic wall to tensile stresses and mechanical forces, promoting a chronic aortic dilatation. As the size increases, a vicious enlargement circle might be triggered. Although it was suggested that atherosclerosis may play a minor role in aortic dilatation with respect to aging and other risk factors,[20] its influence should not be neglected because the effects are concentrated in the distal portion of the TA where: *a)* half of all TA aneurysms occur, and *b)* endovascular stent grafting is quickly becoming the preferred choice of treatment.[24] Briefly, aortic geometry probably influences the location of intimal calcifications whereas medial calcifications could be more associated with aortic stiffening and might be responsible for descending TA dilatation as a compensatory mechanism. The cross-sectional nature of our study does not permit conclusions to be drawn on the cause-effect relationship.

When the TA geometry was analyzed as a function of increasing levels of TAC, several geometric variables were progressively involved in calcium accumulation, independently of age, sex, and traditional risk factors (Table 4). Interestingly, the descending aorta dilatation and loss of tapering were the first anatomic variables that changed in patients with small amounts of calcium, and could indicate the first steps in aortic atherosclerotic disease. Morphological and functional analyses should be complemented to improve the prediction of acute cardiovascular diseases.[25] Vascular calcifications were found to correlate to artery wall forces for different vascular beds[26] and to increased TA stiffness.[27] These encouraging results indicate that the strategy of identifying geometrical and functional risk factors to better understand the mechanisms of atherosclerosis should persist.

Sex differences in the presence and extent of calcification in the aorta are not entirely clear.[28] We did not find significant differences in TAC between men and women when adjusted for age and body-size area, although higher scores were seen in women (Table 2, Figures 3 and 4). Allison et al[29] identified the proximal TA as the only vascular bed where the prevalence of calcification was higher in younger women (< 50 years) compared with men. Other studies found a higher prevalence of TAC in women for all ages[28,30] but contradictory results were also reported.[31] The aortic arch was reported as a vulnerable site for calcification among women[4,32] and might explain the global tendency reported in our study. There is good evidence that the development of osteoporosis in women, as a metabolic bone calcium process, can also help to explain this higher prevalence.[33]

Limitations

Our study had some limitations. First, as previously mentioned, discerning between TAC and TA morphology as the exposure or the outcome could not be elucidated from this cross-sectional study. Second, the participants were at risk for cardiovascular disease and therefore the results cannot be extrapolated to the general population. Third, the radiation dose required by our enlarged field of measurement in order to incorporate the aortic arch was slightly greater than the radiation dose when measuring TAC during traditional coronary artery calcium detection.

Finally, our findings have some clinical implications. At first, the mechanisms of early dilatation of the TA may be different between descending aorta and aortic arch and ascending aorta. Indeed, assuming that TAC is an indicator of atherosclerotic disease, the association of TAC with dilatation of the descending aorta and aortic arch is in favor of mechanisms of atherosclerosis-related aortic dilatation. Our analysis confirms the concept that TA disease is divided into 2 entities: the ascending segment is nonarteriosclerotic in contrast with the descending segment where atherosclerosis is abundant.[1] On the other hand, the absence of an association of TAC with dilatation of the ascending aorta suggests that the latter may be not be mainly linked to atherosclerosis and might depend on other mechanisms. Among them, genetic diseases of the ascending aortic wall with respect to valve malformation play a major role in the development of aneurysms of the ascending TA. Secondly, our findings also have implications about therapeutic interventions to slow or prevent aortic dilatation toward future aneurysms. The atherosclerotic nature of descending aorta dilatation suggests that conventional antiatherosclerotic interventions based on aggressive correction of traditional risk factors are important. The therapeutic prevention of ascending aorta dilatation is unclear due to its lack of direct association with atherosclerotic disease. The

current recommendations suggest the use of beta-blocking medication to prevent progression toward aneurysms, probably because this type of drug may modify the blood flow velocity patterns involved in this aortic segment and attenuate the systolic impact on the aortic wall. All of these clinical implications, however, need to be confirmed by further studies.

CONCLUSIONS

In this study, we showed that TA calcification was associated with TA geometry, independently of age, sex, body surface area, and traditional risk factors. Possible relationships between TA geometry and vascular calcification should be analyzed in terms of blood flow patterns and compensatory biomechanical mechanisms within the artery wall. Thoracic aorta calcium was positively correlated to the size of the descending aorta and of the aortic arch, but not to the size of the ascending aorta. This suggests that TA dilatation may have different mechanisms and consequently different preventive strategies according to the observed segments.

ACKNOWLEDGEMENTS

We thank Sandra Wray for her valuable help in the revision of this manuscript.

CONFLICTS OF INTEREST

None declared.

WHAT IS KNOWN ABOUT THE TOPIC?

- Calcium deposits in arteries are a sign of atherosclerosis and have been associated with a higher risk of mortality and cardiovascular events.
- Calcifications in the coronary arteries and TA can be accurately assessed using cardiac computed tomography scans, but the aortic arch is usually excluded.
- The TAC and measurement has been recognized to improve cardiovascular risk prediction beyond traditional risk factors.
- The TAC has been associated with coronary, cerebral and peripheral vascular disease but the role of geometry on the presence and the extent of calcifications is less well known.

WHAT DOES THIS STUDY ADD?

- The TAC and detailed aortic 3-dimensional geometry were simultaneously assessed using low-dose nonenhanced computed tomography images and including the aortic arch.
- Several aortic geometrical variables were associated with the presence, extent and location of calcifications, independently of age, sex, and traditional risk factors.
- The TAC was positively related to the size of the descending aorta and aortic arch, but not to the size of the ascending aorta.
- The TA dilatation may have different mechanisms and consequently different preventive strategies according to the segments considered.

REFERENCES

1. Elefteriades JA, Farkas EA. Thoracic aortic aneurysm clinically pertinent controversies and uncertainties. J Am Coll Cardiol. 2010;55:841–57.
2. Demertzis S, Hurni S, Stalder M, Gahl B, Herrmann G, Van den Berg J. Aortic arch morphometry in living humans. J Anat. 2010;217:588–96.
3. Liu X, Pu F, Fan Y, Deng X, Li D, Li S. A numerical study on the flow of blood and the transport of LDL in the human aorta: The physiological significance of the helical flow in the aortic arch. Am J Physiol Heart Circ Physiol. 2009;297:H163–70.
4. Craiem D, Chironi G, Casciaro ME, Graf S, Simon A. Calcifications of the thoracic aorta on extended non-contrast-enhanced cardiac CT. PLoS One. 2014;9:e109584.
5. Craiem D, Chironi G, Casciaro ME, Redheuil A, Mousseaux E, Simon A. Three-dimensional evaluation of thoracic aorta enlargement and unfolding in hypertensive men using non-contrast computed tomography. J Hum Hypertens. 2013;27:504–9.
6. Craiem D, Chironi G, Redheuil A, Casciaro M, Mousseaux E, Simon A, et al. Aging impact on thoracic aorta 3D morphometry in intermediate-risk subjects: Looking beyond coronary arteries with non-contrast cardiac CT. Ann Biomed Eng. 2012;40:1028–38.
7. Takasu J, Katz R, Nasir K, Carr JJ, Wong N, Detrano R, et al. Relationships of thoracic aortic wall calcification to cardiovascular risk factors: the Multi-Ethnic Study of Atherosclerosis (MESA). Am Heart J. 2008;155:765–71.
8. Agatston AS, Janowitz WR, Hildner FJ, Zusmer NR, Viamonte Jr M, Detrano R. Quantification of coronary artery calcium using ultrafast computed tomography. J Am Coll Cardiol. 1990;15:827–32.
9. Caballero AD, Laín S. A review on computational fluid dynamics modelling in human thoracic aorta. Cardiovascular Engineering and Technology. 2013;4:103–30.
10. The pcv-metra group, Laurier D, Nguyen PC, Cazelles B, Segond P. Estimation of chd risk in a french working population using a modified framingham model. J Clin Epidemiol. 1994;47:1353–64.
11. Greenland P, Alpert JS, Beller GA, Benjamin EJ, Budoff MJ, Fayad ZA, et al. 2010 ACCF/AHA guideline for assessment of cardiovascular risk in asymptomatic adults: A report of the American College of Cardiology Foundation/American Heart Association Task Force on Practice Guidelines. J Am Coll Cardiol. 2010;56:e50–103.
12. Casciaro ME, Craiem D, Chironi G, Graf S, Macron L, Mousseaux E, et al. Identifying the principal modes of variation in human thoracic aorta morphology. J Thorac Imaging. 2014;29:224–32.
13. Redheuil A, Yu WC, Mousseaux E, Harouni AA, Kachenoura N, Wu CO, et al. Age-related changes in aortic arch geometry: Relationship with proximal aortic function and left ventricular mass and remodeling. J Am Coll Cardiol. 2011;58:1262–70.
14. McClelland RL, Chung H, Detrano R, Post W, Kronmal RA. Distribution of coronary artery calcium by race, gender, and age: Results from the Multi-Ethnic Study of Atherosclerosis (MESA). Circulation. 2006;113:30–7.
15. O'Brien PC, Dyck PJ. Procedures for setting normal values. Neurology. 1995;45:17–23.
16. Itani Y, Watanabe S, Masuda Y. Aortic calcification detected in a mass chest screening program using a mobile helical computed tomography unit relationship to risk factors and coronary artery disease. Circ J. 2004;68:538–41.
17. Agmon Y, Khandheria BK, Meissner I, Schwartz GL, Petterson TM, O'Fallon WM, et al. Independent association of high blood pressure and aortic atherosclerosis: A population-based study. Circulation. 2000;102:2087–93.
18. Wasilewski J, Glowacki J, Polonski L. Not at random location of atherosclerotic lesions in thoracic aorta and their prognostic significance in relation to the risk of cardiovascular events. Pol J Radiol. 2013;78:38–42.
19. Tse KM, Chang R, Lee HP, Lim SP, Venkatesh SK, Ho P. A computational fluid dynamics study on geometrical influence of the aorta on haemodynamics. Eur J Cardiothorac Surg. 2013;43:829–38.
20. Gu X, He Y, Li Z, Kontos MC, Paulsen WH, Arrowood JA, et al. Relation between the incidence, location, and extent of thoracic aortic atherosclerosis detected by transesophageal echocardiography and the extent of coronary artery disease by angiography. Am J Cardiol. 2011;107:175–8.
21. Proudfoot D, Shanahan CM. Biology of calcification in vascular cells: Intima versus media. Herz. 2001;26:245–51.
22. Zarins CK, Xu C, Glagov S. Atherosclerotic enlargement of the human abdominal aorta. Atherosclerosis. 2001;155:157–64.
23. de Jong PA, Hellings WE, Takx RA, Isgum I, Van Herwaarden JA, Mali WP. Computed tomography of aortic wall calcifications in aortic dissection patients. PLoS One. 2014;9:e102036.
24. Brozzi NA, Roselli EE. Endovascular therapy for thoracic aortic aneurysms: State of the art in 2012. Curr Treat Options Cardiovasc Med. 2012;14:149–63.
25. Shirali AS, Bischoff MS, Lin HM, Oyfe I, Lookstein R, Griepp RB, et al. Predicting the risk for acute type b aortic dissection in hypertensive patients using anatomic variables. JACC Cardiovasc Imaging. 2013;6:349–57.
26. Jensky NE, Criqui MH, Wright MC, Wassel CL, Brody SA, Allison MA. Blood pressure and vascular calcification. Hypertension. 2010;55:990–7.
27. Al-Mallah MH, Nasir K, Katz R, Takasu J, Lima JA, Bluemke DA, et al. Thoracic aortic distensibility and thoracic aortic calcium (from the Multi-Ethnic Study of Atherosclerosis [MESA]). Am J Cardiol. 2010;106:575–80.
28. Nasir K, Roguin A, Sarwar A, Rumberger JA, Blumenthal RS. Gender differences in coronary arteries and thoracic aorta calcification. Arterioscler Thromb Vasc Biol. 2007;27:1220–2.

29. Allison MA, Criqui MH, Wright CM. Patterns and risk factors for systemic calcified atherosclerosis. Arterioscler Thromb Vasc Biol. 2004;24:331–6.
30. Kalsch H, Lehmann N, Mohlenkamp S, Hammer C, Mahabadi AA, Moebus S, et al. Prevalence of thoracic aortic calcification and its relationship to cardiovascular risk factors and coronary calcification in an unselected population-based cohort: The heinz nixdorf recall study. Int J Cardiovasc Imaging. 2013;29:207–16.
31. Wong ND, Gransar H, Shaw L, Polk D, Moon JH, Miranda-Peats R, et al. Thoracic aortic calcium versus coronary artery calcium for the prediction of coronary heart disease and cardiovascular disease events. JACC Cardiovasc Imaging. 2009;2:319–26.
32. Odink AE, Van der Lugt A, Hofman A, Hunink MGM, Breteler MMB, Krestin GP, et al. Association between calcification in the coronary arteries, aortic arch and carotid arteries: The rotterdam study. Atherosclerosis. 2007;193:408–13.
33. Iribarren C, Sidney S, Sternfeld B, Browner WS. Calcification of the aortic arch: Risk factors and association with coronary heart disease, stroke, and peripheral vascular disease. JAMA. 2000;283:2810–5.

2.4 Articles #5 et #6

« Deformable surface model for the evaluation of abdominal aortic aneurysms treated with an endovascular sealing system »

« Age-related changes of thoracic aorta geometry used to predict the risk for acute type B dissection »

Le premier travail a été publié dans le journal *Annals of Biomedical Engineering* en 2016 sous la référence :

Casciaro ME, El-Batti S, Chironi G, Simon A, Mousseaux E, Armentano RL, Alsac JM, **Craiem D**. Deformable surface model for the evaluation of abdominal aortic aneurysms treated with an endovascular sealing system. Ann Biomed Eng. 2016 May ;44(5) :1381-91.

Le deuxième travail a été soumis à *International Journal of Cardiology* en Juillet 2016 :

Craiem D, El-Batti S, Casciaro ME, Mousseaux E, Sirieix M-E, Simon A, Alsac JM. Age-related changes of thoracic aorta geometry used to predict the risk for acute type B dissection. (Under review)

2.4.1 Introduction et objectifs

L'une des limites de l'algorithme proposé dans les articles précédents pour segmenter l'aorte thoracique à partir des images non-injectées de TDM, était de partir du principe que l'aorte a une morphologie tubulaire. Cette hypothèse était raisonnable chez les patients de prévention primaire sans pathologie aortique, mais ne tenait plus en présence d'un anévrisme ou d'une dissection. Dans ce cas-là, l'aorte peut devenir tortueuse, changer brusquement de diamètre ou même développer un vrai et un faux chenal au sein de sa lumière. Afin de s'adapter à ces déformations pathologiques, la plateforme informatique a été équipée d'un nouveau module d'analyse des images de scanner injecté utilisées pour le diagnostic et le suivi des anévrismes et des dissections. Un modèle de géométrie de surface déformable innovant a été conçu. Ce modèle se présente initialement sous la forme d'une sphère élastique qui se gonfle et se déforme virtuellement à l'intérieur de la lumière aortique pour adopter sa morphologie 3D. La maille virtuelle est composée de faces triangulaires qui peuvent être utilisées pour faire des estimations volumétriques ainsi que des impressions 3D. Ce nouveau module a été testé dans deux applications cliniques.

Dans un premier temps, il a été utilisé pour quantifier la morphologie des anévrismes de l'aorte abdominale (AAA). Un anévrisme est défini comme une dilatation localisée, permanente et irréversible de l'aorte, généralement associée à une dégradation et à une atteinte de la paroi artérielle (voir chapitre 3, section 1.9, page 23). Les AAA sont pour la plupart asymptomatiques avant leur rupture, provoquant la mort dans 65% des cas, et ils représentent l'une de principales causes de mortalité cardiovasculaire après l'hypertension et l'athérosclérose [66]. La rupture d'un AAA est responsable de 1-3% des décès des hommes entre 65-85 ans dans les pays développés [94]. Son incidence dépend de l'âge, du sexe, de

l'hypertension, du tabagisme et des antécédents familiaux. Cependant, la plupart des AAA sont totalement non-spécifiques [60]. Le traitement des AAA par endoprothèse devient de plus en plus courant, par rapport au traitement par chirurgie ouverte [70]. Les trois événements indésirables survenant à long terme après traitement par endoprothèse sont les endofuites, la dilatation du sac anévrismal et la migration du dispositif. La plupart des endoprothèses sont composées des stents couverts bifurqués, avec une fixation proximale qui prévient la circulation du sang dans l'anévrisme et réalise son étanchéité. Pourtant, de nouveaux dispositifs avec des concepts innovants apparaissent. Récemment, le fabricant d'un nouveau dispositif basé sur un système d'étanchéité par un polymère a présenté ses premiers résultats multicentriques [14]. Cette endoprothèse propose une stratégie originale d'isolation de l'anévrisme de la circulation au moyen d'un sac plastique qui entoure deux stents et qui se remplis avec un polymère, se durcissant in situ (Figure 1 de l'Article #5). Cette technique innovante a pour but de réduire les endofuites, de diminuer la migration du dispositif et d'être efficace même en cas de collet court [67]. La quantité de polymère injecté est déterminée par le monitorage de la pression de remplissage entre 185-220 mmHg dans le sac de polyéthylène. Pourtant, en raison de la fragilité de la paroi dans cette région et de son risque de rupture, le volume prévu à remplir mérite une étude très précise. Une estimation du volume préopératoire (*sizing* en anglais), de la quantité de polymère effectivement injectée et de la taille finale du dispositif n'a jamais été faite auparavant. Les objectifs fixés dans l'Article #5 comprennent la comparaison de ces trois volumes avec une analyse détaillée des régions les plus déformées, au sein de l'anévrisme après la pose de l'endoprothèse chez 8 patients. Le travail inclut également la description de la nouvelle méthodologie de segmentation basée sur le modèle de surface déformable pour estimer la morphologie des AAA avant et après la pose du dispositif.

Une seconde application de l'évaluation volumétrique de la taille de l'aorte, concerne l'étude des dissections de l'aorte thoracique de type B (DATB). Les dissections peuvent se produire à n'importe quel âge, mais elles sont plus fréquentes chez l'homme hypertendu entre 50 et 80 ans. La prévalence des dissections est estimée à ≈5 per 100.000 habitants par an et un tiers implique l'aorte descendante. Malgré les progrès thérapeutiques, la mortalité liée aux dissections aortiques reste élevée. La prédiction de la DATB sur la base du diamètre de l'aorte descendante est très limitée [110]. D'autres variables anatomiques ont été testées pour améliorer cette prédiction [98]. Curieusement, l'influence de l'âge sur ces modèles de risque était systématiquement négligée. Dans l'Article #6 nous avons proposé une étude géométrique de l'aorte thoracique chez des patients avec et sans DATB pour obtenir un modèle de prédiction du risque ajusté à l'âge. Plusieurs variables anatomiques ont été mesurées et testées afin d'ajuster ce modèle. L'application du modèle de surface déformable était adaptée pour évaluer la morphologie de l'aorte thoracique en présence d'une DATB aiguë.

2.4.2 Méthodes

Le modèle déformable a été conçu sur la base des publications réalisées par Park, Miller et Terziopulos [76, 83, 108] afin de contraindre un ballon élastique virtuel à se gonfler à l'intérieur de la lumière aortique et pouvoir ainsi en estimer le volume. La forme initiale du modèle est une sphère composée de nœuds (*vertex* en anglais) connectés élastiquement

et qui forment des faces triangulaires. La position de chaque vertex est calculée de façon dynamique dans l'espace en utilisant les forces intérieures et extérieures qui s'exercent sur la maille déformable. Les forces internes sont les forces d'étirement, de flexion et les dissipatives (Figure 2 de l'Article #5). La seule force extérieure était la force de gonflage qui pousse chaque vertex de la maille perpendiculairement à la surface. Le gonflage simule l'application d'une force sur la face interne de la maille, opposée par les forces externes qui s'exercent sur la paroi artérielle, et les autres structures environnantes qui s'opposent à cette expansion. Pour contrôler la stabilité du modèle, les faces trop grandes se divisent et celles trop petites se résorbent automatiquement (Figure 3 de l'Article #5). Une fois que l'équilibre des forces est atteint et que les mouvements des vertex sont considérés négligeables, l'algorithme s'arrête. La maille 3D du modèle peut donc être utilisée pour décrire la géométrie du vaisseau qui la contient. Les détails mathématiques et numériques de l'algorithme se trouvent dans la méthodologie et l'annexe de l'Article #5. Les paramètres du modèle ont été fixés avec les valeurs montrées dans le Tableau 1 et gardées constantes pour tous les patients.

La sphère déformable virtuelle a été implantée à l'intérieur de 8 anévrismes avant et après la pose d'une endoprothèse Nellix^{TM}pour estimer le volume de la lumière. Les plans axiaux contenant le début et la fin du dispositif ont été utilisés pour limiter l'expansion du modèle. Les stents qui restaient à l'intérieur des AAA sur les images postopératoires ont été effacés avec une méthode de soustraction numérique. Les volumes pré- et post- opératoires ont été comparés avec la quantité de polymère injecté pour chaque patient (Figure 5 de l'Article #5). Le volume qui correspond aux stents (restant à l'intérieur de l'anévrisme) a été estimé à partir des longueurs et des diamètres choisis pour chaque intervention chirurgicale. La méthode automatique de mesure du volume a été validée par les mesures manuelles d'un expert (Figure 6 de l'Article #5). Les modèles déformables avant et après ont également été comparés visuellement en mettant en valeur les régions les plus déformées en couleur avec une échelle métrique de Haussdorff [24] (Figure 4 de l'Article #5).

Pour quantifier la morphologie de l'aorte thoracique en cas de DATB, avec les détails géométriques de chaque chenal à l'intérieur de la lumière, une seule sphère déformable ne suffisait pas. En conséquence, 7 ballons virtuels ont été implantés dans la lumière comme le montre la Figure 1 de l'Article #6. La position initiale de chaque ballon a été déterminée par l'interpolation d'une ligne centrale tracée à partir de 9 points de référence systématiquement marqués par l'utilisateur. Des plans invisibles séparaient les mailles pour les empêcher de se mettre en contact. Les 4 ballons à l'intérieur de l'aorte descendante ont été dupliqués et légèrement déplacés (avec un réglage des paramètres légèrement différents) pour segmenter séparément le vrai et le faux chenal. Pour éviter la prolifération du modèle déformable dans les troncs supra-aortiques (ou autres), des bouchons virtuels étaient disposées par l'utilisateur comme le montre la Figure 2 de l'Article #6. Une fois les modèles arrivés à l'équilibre, la ligne centrale de chaque chenal était calculée ainsi que plusieurs variables anatomiques, incluant le diamètre et la surface de section à chaque point de la ligne centrale, la tortuosité et les volumes des différents segments (Tableau 2 de l'Article #6).

Depuis 2009, l'Hôpital Européen Georges Pompidou (HEGP, Paris, France) a mis en place le programme "SOS Aorte" afin de prendre en charge rapidement toutes les maladies aortiques (`http://hopital-georgespompidou.aphp.fr/sos-aorte-centre-daccueil-24h24-pour-les-urgences-aortiques/`). Nous avons sélectionné tous les patients ayant une DATB aiguë ou une suspicion de DATB jusqu'en Septembre 2015 pour

notre étude rétrospective. Les patients ayant une maladie congénitale du tissu conjonctif, ou chez qui la DATB était associée à un traumatisme ont été exclus. Tous les patients inclus avaient bénéficié d'une TDM avec contraste à l'HEGP pour confirmer ou écarter le diagnostic de DATB. Au final, un groupe *dissection* (n=34) a été comparé à un groupe *contrôle* (n=51).

Les corrélations des variables anatomiques avec l'âge ont permis la construction d'un modèle de régression logistique de risque utilisant une méthode itérative pour la sélection des cofacteurs. La performance du modèle statistique et la sélection des variables ont été validées par une technique *bootstrap* de vérification interne. La méthode itérative de sélection était répétée sur un millier de tirages pour compter le nombre de fois que chaque cofacteur était choisi, et ainsi valider sa pertinence. L'aire sous la courbe de la fonction, plus fréquemment désignée sous le terme de courbe ROC (de l'anglais *receiver operating characteristic*), était calculée pour caractériser la performance du modèle. Finalement, le rapport des cotes de probabilités d'être atteint d'une DATB était calculé pour chaque cofacteur, avec les intervalles de confiance respectifs.

2.4.3 Résultats principaux

Les 8 anévrismes ont été segmentés avec la nouvelle méthode proposée. Une vidéo en ligne illustre le fonctionnement de l'algorithme chez un patient représentatif. Elle est disponible dans l'annexe de l'article (`http://dx.doi.org/10.1007/s10439-015-1446-9`). La Figure 4 de l'Article #5 illustre par des couleurs la déformation provoquée par chaque endoprothèse sur les parois des anévrismes. Les distances maximales entre les mailles avant et après la pose étaient de 9.7±3.6 mm (extrêmes 6 à 16 mm). Les déformations les plus importantes (couleur rouge) étaient détectées au niveau de la région centrale des anévrismes et près des artères iliaques. Le volume du dispositif, avec le polymère à l'intérieur, était en moyenne de 23% supérieur au volume préopératoire de la lumière ($p<0.001$, Figure 5 de l'Article #5). Les valeurs de la quantité de polymère effectivement injectée étaient inférieures au volume postopératoire (-11%, $p<0.01$), mais supérieures au volume préopératoire (+9%, $p<0.05$). Il n'y avait pas de différence significative entre les mesures manuelles et automatiques.

Les résultats de l'application du modèle déformable utilisé pour saisir la morphologie de l'aorte thoracique sont présentés dans l'Article #6. La Figure 2 montre un exemple du modèle 3D ajusté dans le vrai chenal et dans la lumière totale de l'aorte thoracique chez un patient représentatif. Les Tableaux 1, 2 et 3 montrent les caractéristiques cliniques, les mesures anatomiques et la relation de ces variables avec l'âge après ajustement pour les groupes *dissection* et *contrôle*. Il n'y avait pas de différences significatives entre les facteurs de risque traditionnels. Comme le montre la Figure 3 de l'Article #6, la taille de l'aorte disséquée était supérieure à celle de l'aorte non-disséquée dans tous ses segments ($p<0.001$). Le diamètre du vrai chenal représentait en moyenne -20% du diamètre total au niveau de l'artère sous-clavière et jusqu'à -50% au niveau du diaphragme. La plupart des variables anatomiques étaient corrélées à l'âge (Tableau 2 de l'Article #6). Les trois variables qui sont apparues significatives dans le modèle de prédiction de risque de DATB sont : l'âge, le diamètre de la crosse aortique et la longueur de l'aorte thoracique (aire sous la courbe ROC = 0.9764, r=0.85). La validation par la méthode du *bootstrap* a confirmé la sélection de ces trois variables anatomiques dans 99%, 96%, et 88% des cas, respectivement. Finalement, le

volume du vrai chenal était fortement corrélé à l'âge (r=0.72), même après une normalisation par le volume de la lumière totale (Figure 4 de l'Article #6).

2.4.4 Conclusion

Les résultats principaux de notre évaluation sur les anévrismes abdominaux et les dissections de l'aorte descendante concernent l'application d'une nouvelle méthode de segmentation basée sur un modèle de surface déformable. Ce modèle incorporé dans une plateforme informatique nous a permis d'évaluer le volume des anévrismes abdominaux et de quantifier en 3D la géométrie de l'aorte thoracique, notamment en présence d'un vrai et d'un faux chenal. Depuis une décennie, les nouvelles techniques d'imagerie contribuent à la description des anévrismes et à la prédiction de leur rupture. Plusieurs méthodes ont été proposées, dont les contours déformables (*snakes* en anglais) [65], les surfaces déformables [108] et autres algorithmes populaires aux dénominations anglaises multiples : *graph-cuts* [31], *flood-fill* [71] et *water-shed* [13]. Les modèles de surface déformable, comme celui choisi dans notre étude, sont robustes face aux irrégularités environnantes et nécessitent peu d'intervention de la part de l'opérateur [78] . En plus, notre implémentation originale nous a permis de garder des paramètres constants pour tous des patients. D'autres modèles sont très dépendants de la configuration et du nombre de paramètres [10]. L'utilisation de notre algorithme est très intuitive et interactive. L'opérateur observe en temps réel le gonflage de la maille élastique qui se déforme dans une reconstruction 3D de l'aorte, et la courbe du volume atteint son sommet lorsqu'elle a rempli la lumière. Cette visualisation dynamique est rendue possible grâce à la programmation d'algorithmes de traitement d'image en parallèle, qui profitent des multiples processeurs de la carte vidéo. Cette technique de programmation vise à l'implantation des applications en exécution sur les cartes graphiques, au lieu des processeurs centraux, afin d'augmenter significativement la puissance de calcul indispensable aux lourdes images de TDM.

La différence moyenne intra-observateur d'estimation du volume d'un anévrisme de ≈100 ml était inférieur à 0.4 ml. La possibilité d'utiliser plusieurs modèles déformables et de les ajouter l'un après l'autre pour segmenter l'aorte thoracique a été testée et vérifiée avec succès chez plus de 80 patients. Le format du modèle est directement transposable au format des imprimantes 3D, comme illustré par la Figure 2.1 .

En appliquant le modèle déformable pour estimer le volume des anévrismes abdominaux, nous avons trouvé que la taille du dispositif implanté, rempli de polymère, était significativement supérieure au volume de la lumière préopératoire (de l'ordre de 23%). Il est probable que le déplacement et la configuration du thrombus à l'intérieur du sac anévrismal ayant entrainé son écrasement sur la paroi, la présence de bulles d'air immiscées dans le sac de polyéthylène (Figure 4 de l'Article #5) et les restes de sérum physiologique utilisé pour le pré-remplissage, puissent expliquer en partie cette différence. Pourtant, comme le critère de remplissage est fixé par un monitorage de la pression du sac, une expansion réelle de l'anévrisme peut être aussi envisagée. Ce résultat doit alerter les chirurgiens afin de prévenir des ruptures, surtout en cas de parois fragiles comme celles du sac anévrismal. Curieusement, les diamètres pré- et post- opératoires maximales ne présentaient pas de différence significative (4.36±0.79 cm vs 4.05±0.57 cm). Cela confirme l'importance d'une estimation volumique pour évaluer les anévrismes abdominaux et la pertinence de la méthode proposée.

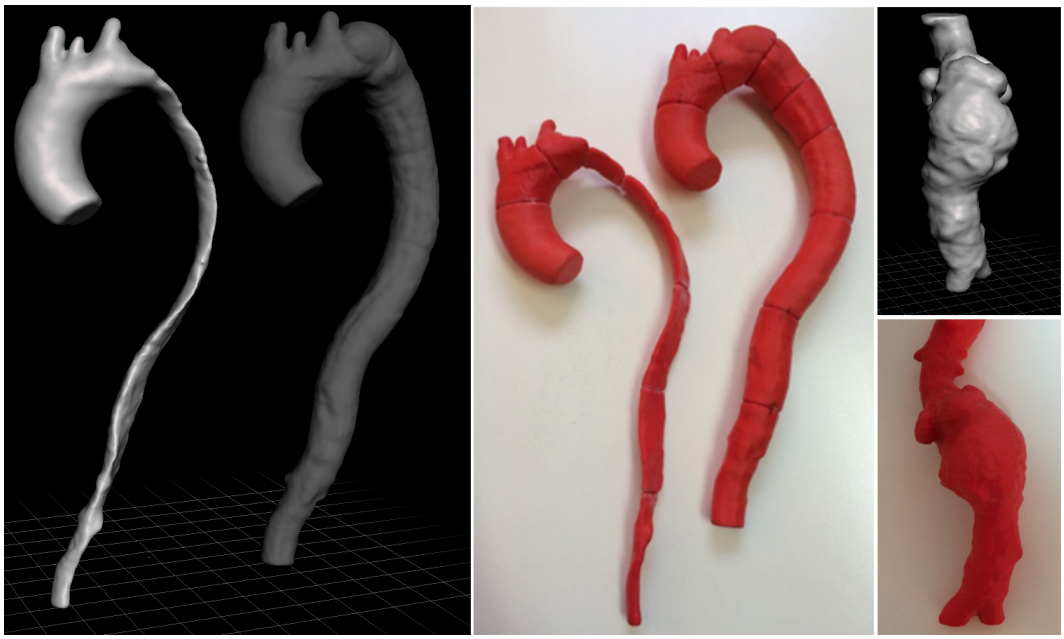

FIGURE 2.1 – Visualisation et impression 3D d'une aorte thoracique disséquée avec le vrai chenal séparé et d'un anévrisme abdominal.

La prédiction d'une DATB se fait généralement en imposant un seuil pour la valeur du diamètre maximale de l'aorte descendante. Pourtant, cette estimation s'est avérée insuffisante [110]. Dans l'application du modèle déformable pour segmenter l'aorte thoracique, nous avons montré que le risque de DATB peut être mieux estimé par les mesures du diamètre de la crosse aortique et de la longueur de l'aorte thoracique, indexés à l'âge du patient. Nous avons soigneusement exclu du modèle logistique initial toutes les variables anatomiques qui pouvaient être directement affectées par la dissection. Le fait d'utiliser un diamètre mesuré dans le segment disséqué de l'aorte descendante après la dissection, comme valeur de référence pour prédire une dissection est contestable de principe. Dans les dissections de l'aorte ascendante (spontanées et rétrogrades), une dilatation significative suit la dissection [92]. Comme dans la plupart des études qui visent à prédire la dissection, les diamètres étaient mesurés justement dans des aortes disséquées, leurs résultats doivent être interprétés avec précaution. Dans notre étude, il faut noter que, même si on a exclu le diamètre et le volume de l'aorte descendante des cofacteurs initiaux, le diamètre de la crosse pouvait ne pas être complètement isolé de l'effet d'une déchirure au niveau de l'artère sous-clavière. Suite à la dissection, une diminution brutale du diamètre de l'ordre de 50% (Figures 3 de l'Article #6) peut forcer le débit dans un vrai chenal écrasé et provoquer une augmentation de la pression en amont, ce qui dilaterait l'aorte ascendante et la crosse. Pour savoir si cette situation s'est produite chez nos patients, le diamètre de l'aorte ascendante a été mesuré avant et après chez les 24 patients qui ont bénéficié d'une pose d'endoprothèse pour restaurer le diamètre de l'aorte descendante. Le diamètre de l'aorte ascendante n'était pas modifié de manière significative (différence moyenne de 0.3 ± 1.9 mm, $p=0.26$), insinuant

que la dilatation de l'aorte ascendante était préexistante.

Les modifications de la morphologie de l'aorte liées au vieillissement sont inévitables et ne peuvent être négligées par aucun modèle de risque géométrique. La Figure 5 de l'Article #6 montre que les courbes qui décrivent les patients à haut risque de DATB, selon notre modèle de risque géométrique, changent avec l'âge. Par exemple, un patient de 50 ans avec une longueur de l'aorte thoracique de 28 cm présente un seuil pour le diamètre de la crosse aortique <30 mm. En même temps, un patient de 70 ans avec la même longueur présente un seuil <35 mm. Cette dépendance à l'âge était également perceptible dans le volume du vrai chenal après la dissection. La taille du vrai et du faux chenal a une influence sur le pronostique du patient [9,109]. Quand le faux chenal se dilate, le vrai chenal s'écrase et limite la perfusion d'autres artères collatérales. En plus, le risque de développer un anévrisme ou d'étendre la dissection augmentent si le faux chenal reste perméable [36]. L'accessibilité par le vrai chenal à un traitement par endoprothèse est aussi un facteur important à évaluer. Nous avons trouvé que le volume du vrai chenal était associé fortement à l'âge, même après une normalisation par le volume de la lumière totale (Figure 5 de l'Article #6). L'explication de ce phénomène peut être liée à une augmentation de la rigidité de la paroi artérielle chez les individus plus âgés, ce qui pourrait éventuellement restreindre l'écrasement du vrai chenal. D'un autre côté, la probabilité d'avoir des anomalies génétiques qui contribuent à une dégradation des éléments élastiques de la paroi, peut être plus importante chez les individus les plus jeunes atteints d'une dissection. D'autres variables anatomiques, comme la taille, la forme et le nombre de portes d'entrée, ainsi que le taux de thrombose du faux chenal, pourraient contribuer à expliquer cette association. Ces mesures n'ont pas été inclues dans notre étude en raison de leur difficile reproductibilité avec les méthodes actuelles de quantification.

L'évaluation du thrombus dans les deux études reste un défi à résoudre pour notre algorithme de segmentation. Le modèle déformable progresse et se dilate sur la base des valeurs de référence à l'intérieur de l'espace initiale de la lumière aortique, dans une région où le contraste circule. L'un des paramètres du modèle permet la modification des niveaux de dispersion (en unités *Hounsfield* et en fonction de la déviation standard des valeurs) afin de contrôler le niveau d'expansion de la maille déformable. Des méthodes d'adaptation qui actualisent ces valeurs au fur et à mesure que la maille gonfle peuvent être envisagées pour segmenter le thrombus séparément. Finalement, dans les 2 études, la technique de scanner se limite à une évaluation structurelle de l'aorte. L'adoption d'autres modalités d'imagerie comme l'IRM, peut ajouter des mesures fonctionnelles pour estimer la rigidité de la paroi aortique [21] ou évaluer des profils de vitesse, afin de nous aider à mieux comprendre et traiter ces maladies aortiques.

Annals of Biomedical Engineering, Vol. 44, No. 5, May 2016 (© 2015) pp. 1381–1391
DOI: 10.1007/s10439-015-1446-9

Deformable Surface Model for the Evaluation of Abdominal Aortic Aneurysms Treated with an Endovascular Sealing System

MARIANO E. CASCIARO,[1,2] SALMA EL-BATTI,[5,6,8] GILLES CHIRONI,[3,4,6] ALAIN SIMON,[3,4,6] ELIE MOUSSEAUX,[4,6,7] RICARDO L. ARMENTANO,[1] JEAN-MARC ALSAC,[4,5,6] and DAMIAN CRAIEM[1,2,3,4,6]

[1]Facultad de Ingeniería Ciencias Exactas y Naturales, Favaloro University, Solís 453, 1078 Ciudad Autónoma de Buenos Aires, Argentina; [2]Consejo Nacional de Investigaciones Científicas y Técnicas (CONICET), Buenos Aires, Argentina; [3]APHP, Centre de Médecine Préventive Cardiovasculaire, Hôpital Européen Georges Pompidou, Paris, France; [4]INSERM U970, Paris, France; [5]Service de Chirurgie Cardiaque et Vasculaire, Paris, France; [6]Université Paris-Descartes, Paris, France; [7]Service d'Imagerie Cardiovasculaire, Paris, France; and [8]Unité de Recherche en Développement, Imagerie et Anatomie, EA 4465, Université Paris 5, Paris, France

(*Received 29 June 2015; accepted 1 September 2015; published online 8 September 2015*)

Associate Editor Estefanía Peña oversaw the review of this article.

Abstract—Rupture of abdominal aortic aneurysms (AAA) is responsible for 1–3% of all deaths among the elderly population in developed countries. A novel endograft proposes an endovascular aneurysm sealing (EVAS) system that isolates the aneurysm wall from blood flow using a polymer-filled endobag that surrounds two balloon-expandable stents. The volume of injected polymer is determined by monitoring the endobag pressure but the final AAA expansion remains unknown. We conceived and developed a fully deformable surface model for the comparison of pre-operative sac lumen size and final endobag size (measured using a follow-up scan) with the volume of injected polymer. Computed tomography images were acquired for eight patients. Aneurysms were manually and automatically segmented twice by the same observer. The injected polymer volume resulted 9% higher than the aneurysm pre-operative lumen size ($p < 0.05$), and 11% lower than the final follow-up endobag volume ($p < 0.01$). The automated method required minimal user interaction; it was fast and used a single set of parameters for all subjects. Intra-observer and manual vs. automated variability of measured volumes were 0.35 ± 2.11 and 0.07 ± 3.04 mL, respectively. Deformable surface models were used to quantify AAA size and showed that EVAS system devices tended to expand the sac lumen size.

Keywords—Nellix device, Endograft, Geometrical deformed model, Endovascular repair, Abdominal aorta.

INTRODUCTION

Abdominal aortic aneurysms (AAA) are defined as a permanent and irreversible localized dilatation of the infrarenal aorta, usually associated with degradation and weakening of the vessel wall. AAA are mostly asymptomatic until they rupture, provoking sudden death in 65% of cases; it has become one of the main causes of cardiovascular mortality after hypertension and atherosclerosis.[20] The rupture of AAA is responsible for 1–3% of all deaths among men aged 65–85 years in developed countries.[29] Its incidence depends on several risk factors including age, male gender, tobacco smoking, hypertension and family history. Nonetheless, most AAA are called non-specific because they are seldom the direct consequence of a specific cause.[14]

The risk of AAA rupture depends on its size and consensus dictates that patients with large aneurysms should undergo surgical treatment.[7] The choice of the aneurysm repair procedure is still under discussion. While open surgical repair has proven to be effective in reducing the risk of rupture, endovascular repair is becoming a promising alternative with significant reduction in early morbidity and mortality.[22] Three of the main long-term adverse events of endovascular aneurysm repair (EVAR) devices are endoleaks, sac enlargement and graft displacement. In general, currently available endografts are bifurcated stents with proximal and distal attachment devices that provide fixation and prevent blood from flowing inside the aneurysm sac. However, novel endograft technologies that

Address correspondence to Damian Craiem, Facultad de Ingeniería Ciencias Exactas y Naturales, Favaloro University, Solís 453, 1078 Ciudad Autónoma de Buenos Aires, Argentina. Electronic mails: dcraiem@favaloro.edu.ar, damian@craiem.com.ar

minimize these complications are constantly emerging. Recently, Endologix (Irvine, Calif) presented the first multicenter report of the Nellix investigational device based on an endovascular aneurysm sealing system (EVAS).[5] This endograft is CE marked since 2013 and proposes a new strategy to isolate the aortic aneurysm wall from blood flow using a polymer-filled endobag that surrounds two balloon-expandable stents, which reach the iliac arteries.[10] Briefly, after a prefill procedure with contrast-enhanced saline solution, the amount of injected polymer is determined by monitoring the endobag pressure which reaches approximately 185–220 mmHg.[5] This innovative technique claims to be less prone to migration (thus avoiding endoleaks) and to be more versatile when dealing with short aneurysm necks and tortuous sac shapes.[17,21] Although commercial software for radiologist and surgeons is able to estimate AAA size,[15] simultaneous information about the pre-operative sizing procedure, the injected polymer volume and the actual post-operative endobag size is still not available. This work sought to investigate the relationship between the pre-operative dimensions of the aneurysm sac lumen and the actual volume of the filling polymer. To the best of our knowledge, this is the first study to simultaneously estimate and invasively assess AAA volumetric size changes before and after EVAS procedure.

Computed tomography (CT) scans are generally employed to evaluate the pre-operative and follow-up patient condition. Multiple segmentation strategies based on CT images were reported to describe the aneurysm geometry in 3D. The most popular choice within deformable models are deformable contours known as snakes[18] and deformable surfaces,[31] although many other are available, some based on graph cuts,[11] flood-fill[23] and water-shed algorithms.[3] Deformable models are known to require little human intervention to generate robust meshes against boundary irregularities, ensuring globally smooth and coherent surfaces between image slices.[25]

In this study, we conceived and developed a deformable surface model that mimics an elastic balloon that inflates inside the lumen of an aneurysm, in order to assess the 3D geometry. The method was inspired by previous reports[24,27] and modified to ensure minimum user interaction using a single set of parameters for the entire set of data. Improvements in mesh adaptation were introduced, and considerable efforts were made in order to minimize the number of parameters. Eight patients that were treated with a 3rd generation Nellix device were retrospectively analyzed, employing pre-operative and follow-up endograft implantation CT images. The pre-operative aneurysm lumen size, the amount of injected polymer and the post-operative endobag volume were measured, compared and discussed.

METHODS

Image Acquisition and Endovascular Repair Procedure

The current study was carried out using 64-slice CT contrast enhanced angiography scan images from the Cardiovascular Surgery Unit of the Hôpital Européen Georges Pompidou (France). The same scanner (Lightspeed VCT; GE Health care, Milwaukee, Wisconsin, USA) was used for pre-operative and follow-up images (within 1–3 months after surgery). Matrix size was 512 × 512 and axial slice distance was 1 mm (or less). Eight patients who had undergone infrarenal AAA repair with Nellix endoprothesis between November 2013 and June 2014 were included in this study. Each patient signed an approved informed consent before the surgery. The retrospective analysis of personal health data of study subjects had the authorization of the CNIL (Commission Nationale de l'Informatique et des Libertés) and was in accordance with the declaration of Helsinki.

Details of the last multicenter clinical trial of this device can be found elsewhere.[5] These endografts consist of dual balloon-expandable stents (diameter = 10 mm), surrounded by an endobag that is later filled with a polymer that occupies the aneurysm sac lumen (Fig. 1). This device is aimed at reducing potential endoleaks by excluding the aneurysm from blood flow while providing a stable anchoring that avoids graft migration. Full detail of the device and clinical procedures are described elsewhere.[10]

Geometrically Deformable Model (GDM)

The deformable model developed in this work is based on the publications of Park, Miller and Terzopoulos *et al.*[24,27,31] and was modified to reduce the number of user-selected parameters. Its main advantage is that the fitting process relies on a unique set of parameters valid for all scans. All of the algorithms were programmed in C++ (Embarcadero Technology, San Francisco, CA). GDM surface fitting can be separated into four steps:

- GDM structure and seeding point
- Internal and external force definition
- Cyclic pressure increase and relaxation
- Finalization criteria

GDM Structure and Seeding Point

The deformable surface initial shape is a closed spheroid balloon with triangular faces positioned by the user inside the lumen of the aneurysm. The amount of faces is determined by the user through the selection of the mean initial edge length, d_{thresh} (see Table 1).

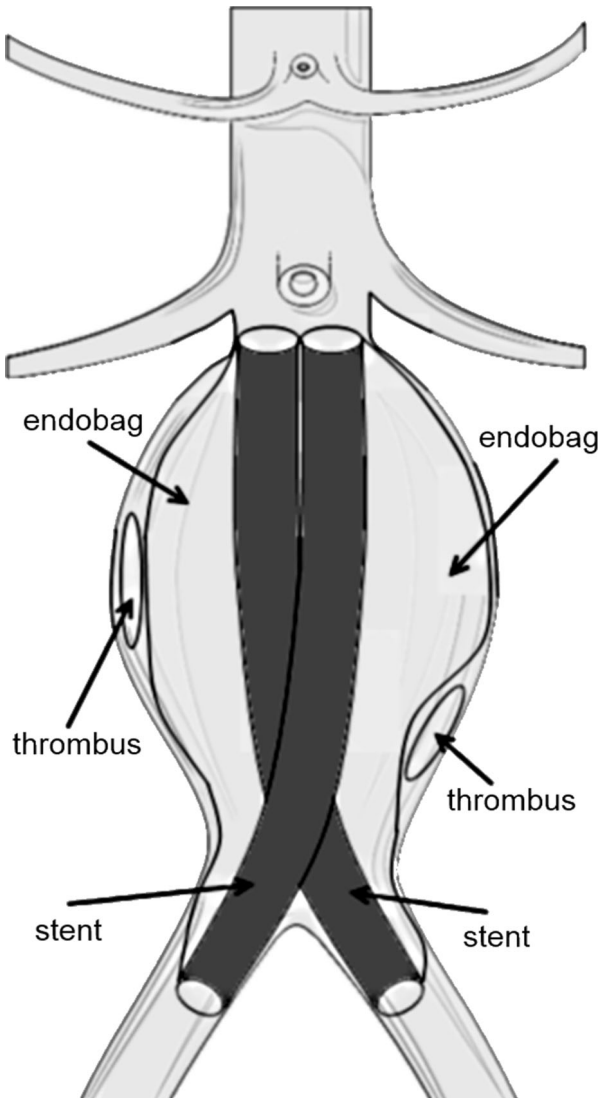

FIGURE 1. The Nellix endograft consists of two balloon-expandable stents surrounded by an endobag that is filled with polymer to stabilize the aneurysm, avoiding endoleaks.

TABLE 1. GDM parameter values.

Coefficient	Symbol	Value
Mass (milligram)	m	3.0
Damping coefficient (mN s/mm)	γ	1.5
Constant inflation force coefficient (N)	α	1.0
Minimum edge value (mm)	d_{thresh}	2.max(dX, dZ)*
Upper HU limit (HU)	$I_{\max}$	$\mu_{\max[95\%CI]} + 6 \cdot \sigma_{\max[95\%CI]}$
Lower HU limit (HU)	$I_{\min}$	$\mu_{\min[95\%CI]} - 3 \cdot \sigma_{\max[95\%CI]}$
Initial GDM radius (px)	r	20 px
Time step (iterations)	dt	1
d_{rest} re-calculation period (iterations)	T_{sizing}	20
Simulated mass injection period (iterations)	T_{adapt}	50

* dX, dZ stand for x and z spatial resolution of the TC images.

Each face consists of vertices connected by elastic edges (Fig. 2(a)). All vertices have a normal vector $\boldsymbol{n}$ that is computed from its N_F neighbor faces. "Appendix" section contains the details about mesh initialization and vertex normal vector computation.

Internal and External Force Definition

Internal forces are due to the interaction between neighboring vertices, and consist of stretching, bending and dissipative forces. The stretching force (**fs**) is the bonding strength between a vertex and its N_v neighbors. It is proportional to the distance between them minus the average edge length in the entire GDM, d_{rest}. Its function is to achieve a constant average distance between vertices, and is calculated as:

$$\boldsymbol{f}_s = \sum_i^{N_v} \frac{(|\Delta \boldsymbol{x}_i| - d_{rest})}{|\Delta \boldsymbol{x}_i|} \Delta \boldsymbol{x}_i, \tag{1}$$

where $\Delta \boldsymbol{x}_i$ is the vector of moduli $|\Delta \boldsymbol{x}_i|$ pointing from the vertex in the $\boldsymbol{x}$ position to its ith neighbor located at $\boldsymbol{x}_i$ (see Fig. 2(a)).

The bending force ($\boldsymbol{f}_b$) is calculated as:

$$\boldsymbol{f}_b = \Delta^C \boldsymbol{x} - \frac{1}{N_v} \sum_i^{N_v} \Delta^C \boldsymbol{x}_i, \tag{2}$$

where $\Delta^C \boldsymbol{x}$ is the average position (center of mass) of the neighbors of $\boldsymbol{x}$. The resulting $\boldsymbol{f}_b$ is a vector that points from the center of mass of $\boldsymbol{x}$ towards the averaged center of mass of all its neighboring vertices, $\Delta^C \boldsymbol{x}_i$, pushing all the centers of masses of nearby vertices towards coplanarity. Figure 2(b) shows an arbitrary configuration of a vertex, its neighbors, their centers of mass and the resulting $\boldsymbol{f}_b$.

Dissipative forces $\boldsymbol{f}_v$ are proportional to the speed of the vertex, $\boldsymbol{v}$, assuming that it is connected with non-ideal springs and/or that it is moving through a viscous fluid. The mathematical expression for this force is:

$$\boldsymbol{f}_v = -\gamma \boldsymbol{v}, \tag{3}$$

where γ is a constant damping coefficient (see Table 1).

The only external force applied to this model is an inflation force $\boldsymbol{f}^p$ that pushes each vertex of the GMD perpendicular to the surface. This force can make the mesh to locally expand or compress, morphing the GDM from a sphere into its final shape. Inflation force simulates the application of an internal pressure p_{int} on the inner surface (expansive force), and an external pressure p_{ext} exerted by the vessel walls or other structures that oppose to the advance of the GDM (compressive force). The pressure difference acting on a face j is responsible for the per-face force:

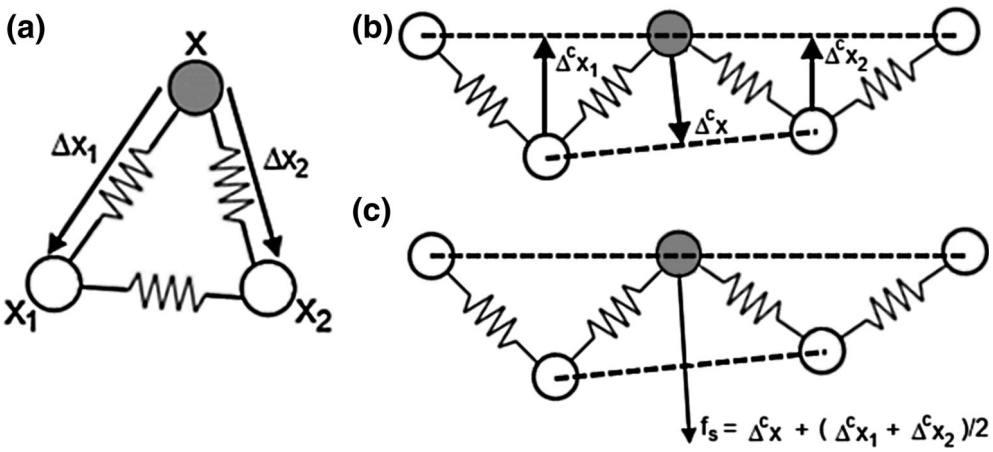

FIGURE 2. (a) GDM face representation: the vertex at position x is connected by elastic edges to its neighbor vertices x_1 and x_2. Vectors Δx_1 and Δx_2 connect x with its neighbors. (b) Shows the vector pointing from each vertex to the center of mass of its two neighbors, namely $\Delta^C x$, $\Delta^C x_1$ and $\Delta^C x_2$. (c) The resulting bending force acting on vertex x is the vector pointing towards the center of mass of its neighbors, $\Delta^C x$, minus the average of the analogous vectors from its neighbors $(\Delta^C x_1 + \Delta^C x_2)/2$.

$$\boldsymbol{f}_j^p = (p_{int} - p_{ext}) a_j \hat{\boldsymbol{n}}_j^F = \Delta p a_j \hat{\boldsymbol{n}}_j^F, \tag{4}$$

where a_j and $\hat{\boldsymbol{n}}_j^F$ are the face's area and normal unitary vector, respectively. The pressure force on the GDM vertices is calculated from the force acting on the neighbor faces (details can be found in "Appendix" section). Rather than assuming a constant internal pressure over time, a non-homogeneous per-vertex pressure is defined as:

$$\Delta p = \frac{\pm\alpha}{2|\boldsymbol{n}|} \tag{5}$$

resulting in a constant per-vertex inflation force given by the expression:

$$\boldsymbol{f}^p = \pm\alpha.\hat{\boldsymbol{n}}. \tag{6}$$

The choice of (+) or (−) signs means that the vertex is traveling through regions where $p_{\text{int}} > p_{\text{ext}}$ or $p_{\text{int}} < p_{\text{ext}}$, respectively. To define these regions, the Hounsfield Unit (HU) in position $\boldsymbol{x}$, namely HU($\boldsymbol{x}$), is evaluated. If HU($\boldsymbol{x}$) lies within the upper/lower intensity limits $I_{\min}$, $I_{\max}$, (+) sign is chosen in Eq. (6), whereas (−) sign is selected otherwise. The values for these intensity limits are calculated from the voxels contained inside the initial spheroid, as explained later in the Model Parameters section. This HU range is expected to include the aneurysm lumen, and to exclude all other tissues (vessel wall, thrombotic regions, *etc.*). Negative sign is also considered if the vertex position is outside user-defined upper and lower limits of the endografts (see Semi-automatic measurements section). The α constant parameter is the magnitude of the resulting expansion or contraction due to the inflation force.

Cyclic Pressure Increase and Relaxation

Our deformable model introduces an original cyclic inflation/relaxation process simulated by the repetition of two iterative steps:

(i) Periodic internal volume injection: it is achieved by increasing the total GDM vertices through the subdivision of all faces having at least one side larger than the mean initial edge length, d_{thresh}. These subdivision stake place every T_{adapt} iterations. The new vertices increase the total model mass and inner pressure without significantly changing GDM surface.

(ii) GDM relaxation: when the new-born vertices begin to spread by the inflation force, inner pressure falls again due to an increase in the GDM surface. This vertex expansion takes place between consecutive T_{adapt} seconds. To simulate an internal force relaxation, every T_{sizing} seconds (with $T_{\text{sizing}} < T_{\text{adapt}}$) the mean average edge distance parameter d_{rest}, is recalculated. This reduces the magnitude of the stretching force allowing the newly injected mass to undergo adaptive size restrictions (Fig. 3).

Finalization Criteria

The net pressure exerted on the GMD inner and outer surface at a given simulation time is estimated as the area-weighted average over all GDM faces:

$$p(t) = \frac{\sum f_i^p}{\sum a_i} = \alpha \frac{N_+ - N_-}{A(t)}, \tag{7}$$

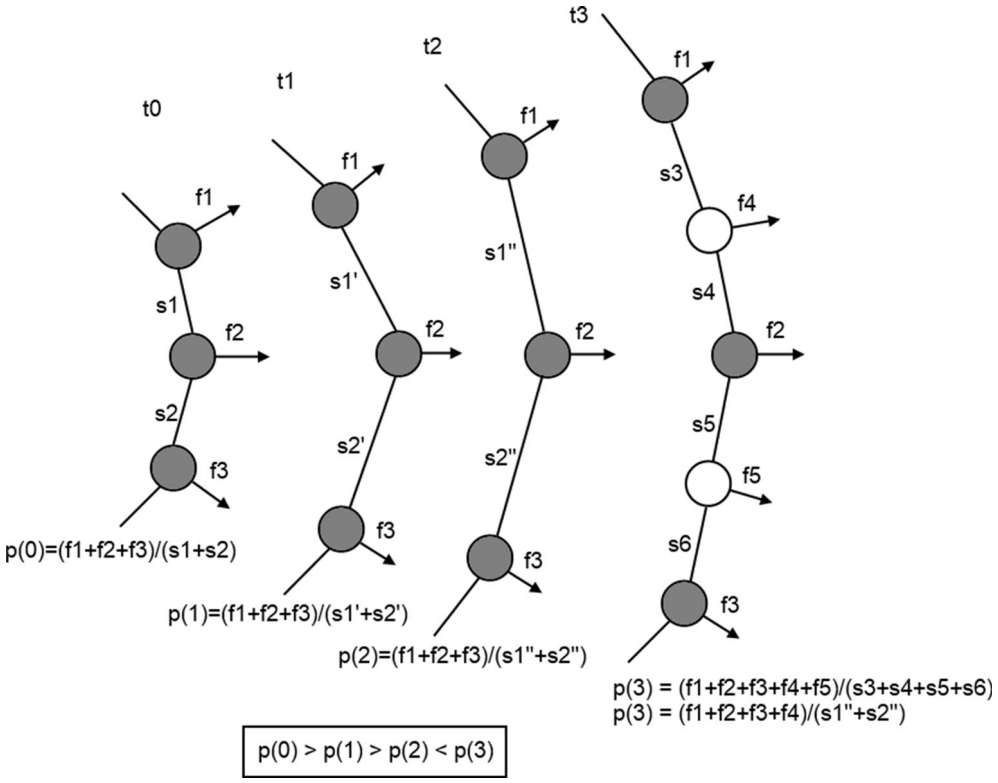

FIGURE3. From instant t_0 to t_2 the gray vertices of the GDM are spreading due to external forces (f_1 to f_3), making surface $s_1 + s_2$ increase to $s_1'' + s_2''$ and generating a pressure drop. At t_3, subdivision results in two new white vertices (and two new force terms) generating a pressure increase.

where N_+ and N_- are the amount of vertices that are in a state of expansion or compression (respectively) and $A(t)$ is the GDM surface. When $N_+ \approx N_-$ internal pressure approaches zero, thus ending the model deformation. A dimensionless pressure curve for a typical inflation sequence (normalized by the parameter α) can be found in the supplementary material.

Model Parameters

The single set of 10 model parameters employed for all patients are shown in Table 1. Seven of these parameters have constant values: mass (m), damping coefficient (γ), inflation force (α), initial sphere radius (r), time step (dt), and the two constant times that regulate the subdivision and relaxation cyclic processes (T_{sizing} and T_{adapt}). Three parameters are calculated when the user initially positions the balloon: minimum edge value (d_{thresh} calculated with the spatial resolution of the scan) and the upper/lower intensity limits ($I_{\max}$ and $I_{\min}$) measured in Hounsfield Units. These intensity limits are calculated using mean and standard deviation of the HU values of the voxels inside the initial spheroid.

Semi-automatic Measurements

All aneurisms were segmented by the same operator. Firstly, the upper and lower limits of the endografts were determined visually in the follow-up scan. This information was then transferred to the pre-operative scan, in order to constrain the growth of the GDM. Distances fixed with respect to anatomical landmarks (e.g., renal and iliac arteries) were used for this purpose. Secondly, the user positioned a virtual balloon inside the AAA and started the inflation process. Intensities inside this initial balloon were used to compute mean and standard deviation values and to set the deformable model parameters. While the sequential expansion and subdivision steps took place, the internal pressure was monitored until it dropped below the configured threshold and the GDM finally conformed to the shape of the aneurysm. The same procedure was repeated in the follow-up scan. In this case, the balloon was positioned inside the polymer-filled endobag of the device after the stents removal. This virtual subtraction was achieved by a standard region growing algorithm, starting in a user-selected pixel belonging to the stent. All connected neighbors intensities were replaced by the mean intensity value

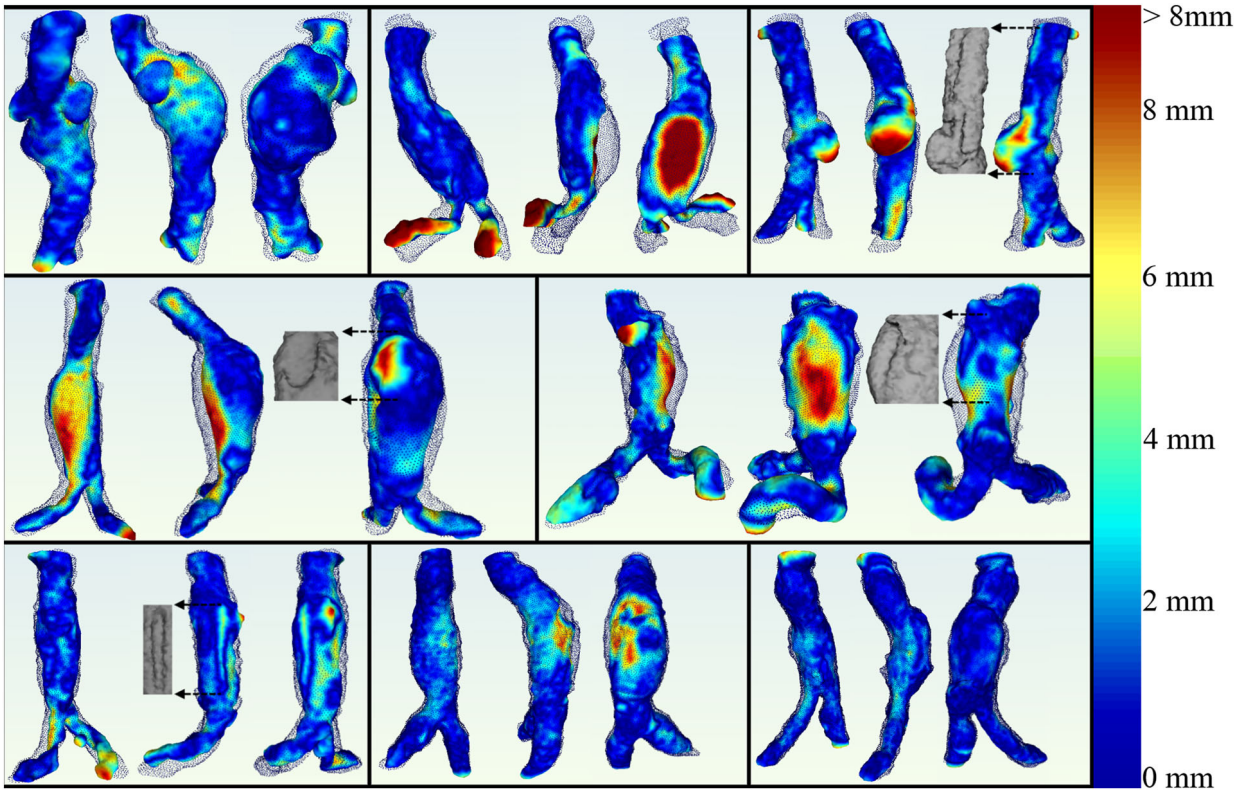

FIGURE 4. Front, side and rear views of the segmentation process in the entire dataset. Pre-operative sac lumen GDM is colored using a Haussdorff metric scale. Superimposed dots are the vertices of the follow-up endobag GDM. Black arrows point at regions of the endobag surface containing large air pockets.

inside the initial balloon. The whole automated measurement was repeated twice by the same expert after a week. Finally, the volumes and maximum axial diameter for the pre-operative sac lumen and the follow-up endobag were calculated for each patient. Pre-operative and follow-up GDMs were automatically aligned trough an Iterative Closest Points algorithm,[6] and surface distances were calculated using Haussdorff metrics.[8]

Manual Validation

A manual validation was carried out for all subjects. The contours of the pre-operative aneurysm sac lumen and of the endobag (after surgery) were manually traced by a single expert every 10 axial slices and integrated to calculate the aneurysm volume.

Statistical Analysis

Two volumes were assessed for each patient: (i) $V_{\text{pre-op}}$: pre-operative aneurysm lumen volume, (ii) $V_{\text{post-op}}$: the follow-up expanded device volume. The volume of the entire deployed device after the polymer injection (V_{deployed}) was calculated by adding the volume of injected polymer to the volume of the device endoframe containing the stents. The latter was calculated assuming an external diameter of 11 mm (10 mm stent + 1 mm polyester sleeve) and the specific stent length used for each patient. Both assessed volumes, expressed as % of change with respect to V_{deployed} were plotted individually. Pre-op and post-op maximum transverse diameters ($D_{\text{pre-op}}$ and $D_{\text{post-op}}$) were automatically calculated through the intersection of axial planes with the GDM surface. Values were expressed as mean ± standard deviation.

Semi-automatic vs. manual and intra-observer repeated measures were compared using the Bland–Altman method.[4] Accordingly, correlation coefficients, means and differences were calculated and residues were plotted.

Matched comparisons of $V_{\text{pre-op}}$ and $V_{\text{post-op}}$ with V_{deployed}, $D_{\text{pre-op}}$ with $D_{\text{post-op}}$, manual vs. automated volumes and intra-observer measurements were made using a Wilcoxon signed-rank test. A significance threshold value of $p < 0.05$ was employed.

RESULTS

All aneurysms were successfully segmented with the automated method. The user-positioned initial balloon

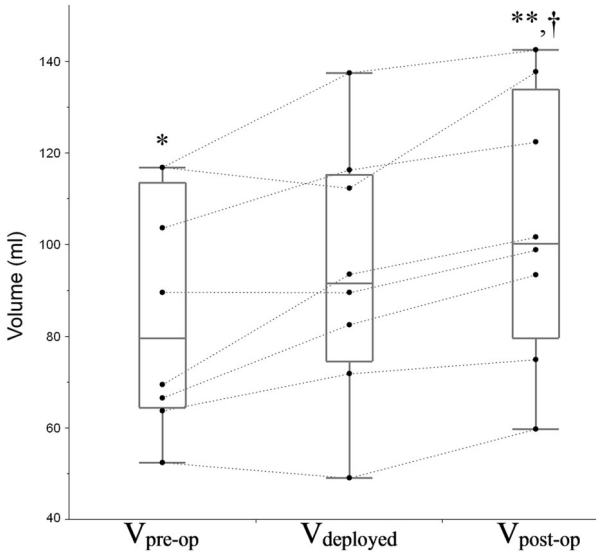

FIGURE 5. Comparison between the aneurysm lumen volume in pre-operative scan ($V_{pre\text{-}op}$), the deployed device volume that includes the injected polymer ($V_{deployed}$) and the final endobag volume during the follow-up scan ($V_{post\text{-}op}$).*$p < 0.05$ with respect to $V_{deployed}$. **$p < 0.01$ with respect to $V_{deployed}$.† $p < 0.001$ with respect to $V_{pre\text{-}op}$.

adopted its final shape in less than 10 s using a standard computer (Intel core i7, 3.4 GHz, 8 GB RAM). A slow-motion video of the GDM growing sequence in a representative patient is available as supplementary material. The length of the implanted stents was 15.8 ± 0.9 cm and the volume of injected polymer was 65.3 ± 25.4 mL.

Figure 4 shows a front, rear and side view of pre-operative and follow-up final GDM surfaces for the entire dataset colored by Haussdorff distances. Maximum and mean distances were 9.7 ± 3.6 mm (range 6.1–16.0 mm) and 1.8 ± 0.5 mm (range 1.1–2.4 mm), respectively. Higher lumen deformations (shown in red) were concentrated in the middle section of the aneurysm sac and around the iliac arteries. Note the arrows that point at visible air pockets found inside some endobags.

The measured volumes $V_{pre\text{-}op}$, $V_{deployed}$ and $V_{post\text{-}op}$ were 84.9 ± 24.5, 94.0 ± 27.8 and 103.9 ± 28.1 mL, respectively (Fig. 5). Accordingly, the deployed device volume (including the injected polymer) resulted 9% higher than $V_{pre\text{-}op}$ ($p < 0.05$), and 11% lower than

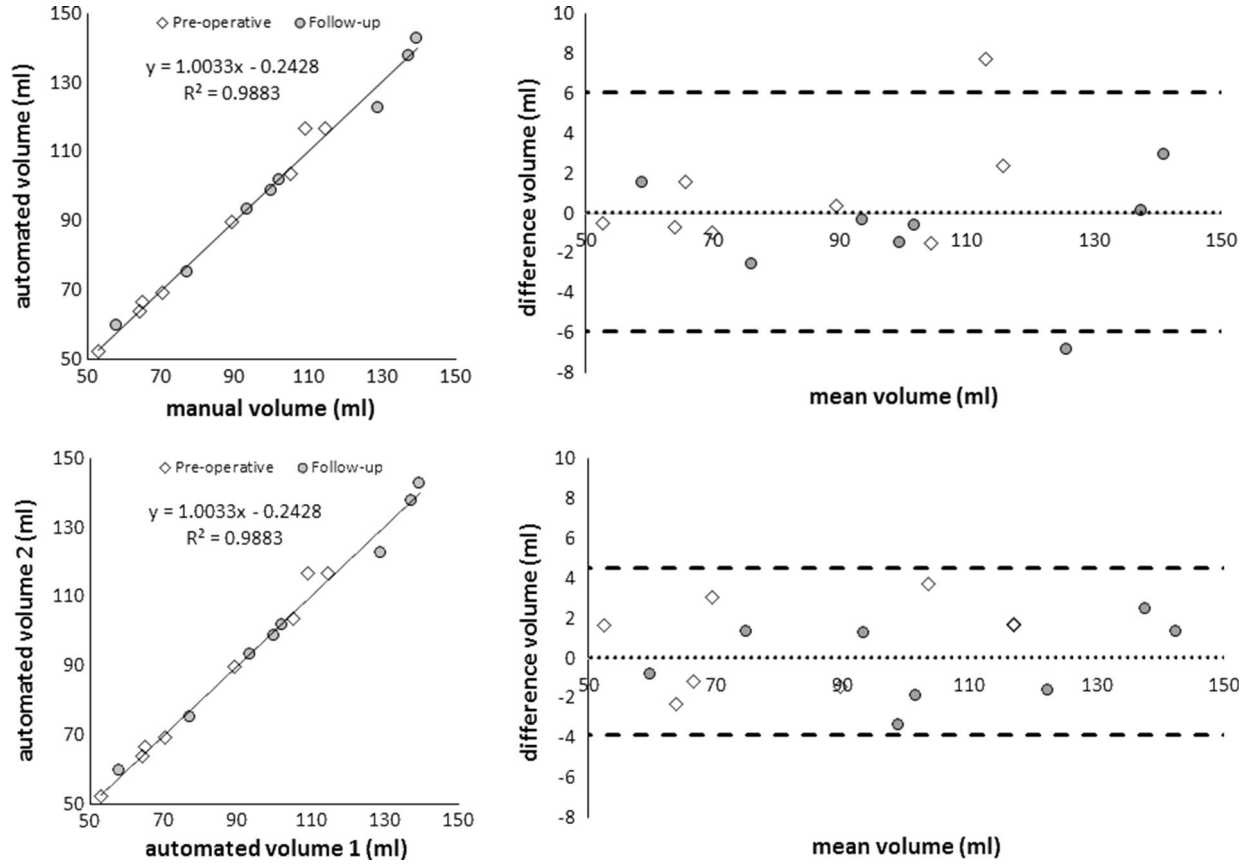

FIGURE 6. Correlations and Bland–Altman residual plots of (top) the automated vs. manual volume and (down) two different automated measurements.

$V_{post\text{-}op}$ ($p < 0.01$). In average, $V_{post\text{-}op}$ was 23% higher than $V_{pre\text{-}op}$ ($p < 0.001$). No significant differences were found between diameters $D_{pre\text{-}op}$ and $D_{post\text{-}op}$, resulting 4.36 ± 0.79 and 4.05 ± 0.57 cm, respectively.

No significant differences were found between Manual vs. Automated measurements and between two repeated measurements performed by the same observer (Fig. 6). For Manual vs. Automatic, correlation coefficient was >0.98 and mean differences were 0.07 ± 3.04 mL. Intra-observer repeatability was also high, with a correlation coefficient >0.99 and a variability of 0.35 ± 2.11 mL. In both cases, no tendencies were observed in the residual plots.

DISCUSSION

In this study, a deformable surface model was employed for the quantification of AAA lumen size before and after the implantation of a novel EVAS endograft device aimed at occupying the aneurysm sac space with a plastic endobag filled with a polymer. The proposed automated approach was fast, and it used a single set of parameters to estimate (i) the aneurysm lumen volume from a pre-operative scan and (ii) the endobag volume from a follow-up scan. We found that the amount of injected polymer was 9% higher than the aneurysm lumen sizing and 11% lower than the final endobag volume, evidencing an enlargement of the aneurysm sac after the device implantation. The use of an automated deformable surface model to reconstruct the AAA geometry helped us to analyze accurately the anatomic and technical complexity involved in the EVAR procedure, comparing virtual sizing with *in vivo* volume corroboration. All of these challenges are eventually involved in the evaluation of innovative endografts technologies as the one used in this study.

One of the major contributions of this work is the disparity found in aneurysm lumen size between pre-operative and follow-up scans with respect to the injected polymer volume. These differences should be analyzed separately. First, the amount of injected polymer was 9% higher than the estimated aneurysm size in the pre-operative scan. This might be explained by the displacement of intra-luminal thrombus during the endobag expansion. Aneurysm wall dilatation and deformation could also take place, since the polymer was injected until the endobag inner pressure reached between 185 and 220 mmHg.[5] This pressure threshold (higher than systolic arterial pressure) guaranteed the complete filling of aneurysm lumen, but systematically exceeded its size, except for two patients where 5-to-7% of the aneurysm lumen remained unoccupied (Fig. 5). Second, the size of the follow-up endobag was 11% larger than the injected polymer volume. This discrepancy is more difficult to explain, since the polymer is supposed to cure almost immediately and no long-term dilatation is expected inside the device endobag. To the best of our knowledge, polymer swellability has not been explicitly informed. Follow-up reports of change in aneurysm size have been limited to aneurysm diameter and cross sectional area but endobag volume was not reported.[21]

We speculate that some foam-like small air bubbles (not visible due to CT resolution and partial volume effect) and remains of saline solution used in the prefill procedure could remain mixed with the polymer. This could partially explain the excessive post-operative volume. Larger air pockets in the surface of the sac, not included in the GDM final volume, were visible inside seven out of eight endografts (see Fig. 4). An average of 5 air pockets (range 1–16) were found per scan, with an average total volume of 0.5 mL (range 0.1–1.5 mL). No references about these visible pockets were found in previous reports, as they may had been neglected due to their small size. Nonetheless, their presence indicates that air remains trapped inside the endobag after procedure.

Globally, if the final endobag volume is compared with the pre-operative sizing, a 23% enlargement of the sac lumen was finally forced inside the aneurysm sac. This difference was almost imperceptible in terms of maximum diameters, highlighting the necessity of volumetric measurements to describe aneurysm shapes. The degree of sac enlargement after the endograft implantation raises concern about the volume of polymer to be injected, since the aneurysm wall is generally fragile and sac expansions should be avoided in order to prevent ruptures. Although the pressure criteria seemed to be effective to almost completely fill the entire lumen, precaution should be taken about possible expansions, in the light of these results. To the best of our knowledge, this is the first study to compare a sizing procedure with its follow-up endobag volume using this EVAS endograft. Even if our measurements show that final volumes tended to be systematically higher that pre-operative sac size, these results should be analyzed with caution and need to be confirmed in a larger population.

The diagnosis of AAA is rapidly evolving by using 3D imaging techniques. *In-vivo* assessment of aneurysm sac size is thought to help predict rupture and evaluate the aneurysm progression. The surgical treatment of non-ruptured AAA is indicated based on the maximal aneurysm diameter (>5.5 cm for men and >5.0 cm for women) and its progressive growth (>1 cm/year growth).[7] This (single) diameter-based decision seems insufficient: smaller aneurysms can also rupture, whereas larger dilatations may remain intact.[33] Accordingly, we showed in this work that

although maximum diameter did not significantly change between pre-operative and follow-up measurements, volumes were significantly different. Furthermore, other approaches such as height, age and gender normalization seem clinically reasonable.[16] New imaging techniques have been contributing for decades to the better description of the aneurysms geometry and rupture prediction. Accordingly, several automated methods have been reported to assess AAA geometry.[1,9,12,19,34] To name a few, three recent examples can be found in this journal. Ayyalasomayajula *et al.*[2] reported a deformable contour model that was used to successfully segment the lumen and intra-luminal thrombus regions using 3D-snakes. Unfortunately, parameter values used to control snakes growth were not user independent, and no particular selection criteria was recommended. Shum *et al.*[30] employed a 2D algorithm based on intensity thresholding and a trained neural network to separate the inner and outer walls of AAA. They found that features such as sac length, sac height, and intra-luminal thrombus volume were more accurate than a single diameter to predict rupture. Finally, Sacks *et al.*[28] assessed the surface geometry of AAA and they found that aneurysms were highly axisymmetric, suggesting an equally complex wall tension distribution. Visibly, the main challenge of AAA segmentation aimed at predicting rupture is the separation of the lumen from thrombotic regions and the arterial wall. Modifications to include these regions into our algorithms should be envisaged in future implementations as discussed hereafter.

This study has some limitations worth mentioning. First, our segmentation method only included the aneurysm lumen and low-contrast thrombotic regions were excluded. Recent reports have revealed three distinct types of thrombus morphology with different mechanical properties.[26] A large inter-patient variation in thrombus structure, as depending on the type of thrombus present, is likely the main factor in volume discrepancies between $V_{\text{pre-op}}$ and V_{deployed}. To overcome this limitation, the modification of some parameters (e.g., the intensity limits) could be tested to include thrombotic regions and the artery wall, or thrombotic regions could be segmented separately using additional GDM. Furthermore, a Finite Element Model could be envisaged assuming the material properties for the arterial wall[32] and the thrombus.[13] Our cohort size was small, as expected from a relatively new EVAS technique. In fact, long-term follow-up data from the ongoing clinical trials is still not available, although recent reports have shown excellent procedure outcomes using this EVAS system, even with challenging aortic neck, aortic bifurcation and iliac artery anatomy.[5] Finally, even if the Nellix endograft gave us the unique opportunity to compare the pre-operative sizing with the injected polymer volume, we did not expect to find the same exact volumes in pre- and post-operative scans. Two main reasons can be mentioned: (i) the deployment of the endograft inside the aneurysm sac could actually modify the shape of the aneurysm and thrombus distribution and (ii) even if the endobag wall is extremely thin, it might fold inside the aneurysm while inflated, leaving some unfilled spaces. Rather than a sizing validation, our deformable model aimed at quantifying these volumetric differences and helping to assess the final aneurysm sac size after the device implantation. We hope this valuable information can help physicians to better anticipate issues and to reduce the risk of rupture during an endograft deployment procedure.

CONCLUSIONS

In this work, we conceived and developed a deformable surface model to compare the pre-operative sizing of AAA with respect to a polymer-filled endobag after the implantation of a novel endograft based on a sealing system (Nellix). The automated method provided fast reliable reconstructions of AAA geometry using a single set of parameters for all patients. We found that follow-up volumes were significantly larger than pre-operative sizes, indicating a possible expansion of the aneurysm sac after the endograft implantation. The use of the Nellix endograft gave us the unique opportunity to corroborate virtual sizing estimations with actual polymer volume injections. Deformable surface models seem a valuable alternative to reconstruct AAA geometry in 3D and to get insight into the evaluation of innovative endografts technologies.

ELECTRONIC SUPPLEMENTARY MATERIAL

The online version of this article (doi: 10.1007/s10439-015-1446-9) contains supplementary material, which is available to authorized users.

APPENDIX

GDM Initialization

The geometrically deformed model (GDM) starts with a regular icosahedron of unit side length. Each of its triangular faces goes through two processes: projection on a sphere of radius r, and subdivision in four new faces. This process is repeated until the average side length is less than a value d_{thresh}, chosen in order to

compromise the amount of model faces, segmentation time, and the spatial resolution of the GDM. The resulting spheroid has approximately $\frac{\pi}{\sqrt{3}}\left(\frac{r}{d_{\text{thresh}}}\right)^2$ initial faces.

Vertex Normal Computation

The vertex normal vector $\boldsymbol{n}$ is the area-weighted sum of the unitary normal vectors to all faces that share the same vertex:

$$\boldsymbol{n} = \frac{\sum_{j=1}^{N_F} a_j \hat{\boldsymbol{n}}_j^F}{\sum_{j=1}^{N_F} a_j}, \tag{A1}$$

where $\hat{\boldsymbol{n}}_j^F$ is the unitary normal vector of the j-th adjacent face, and a_j is the face area. The value of $\hat{\boldsymbol{n}}_j^F$ can be computed by cross-product:

$$\hat{\boldsymbol{n}}_j^F = \frac{\Delta \boldsymbol{x}_{1,j} \times \Delta \boldsymbol{x}_{2,j}}{\left|\left|\Delta \boldsymbol{x}_{1,j}\right| \times \left|\Delta \boldsymbol{x}_{2,j}\right|\right|} = 2\frac{\Delta \boldsymbol{x}_{1,j} \times \Delta \boldsymbol{x}_{2,j}}{a_j}, \tag{A2}$$

where $\boldsymbol{x} = (x, y, z)$ is the vertex position, and $\Delta \boldsymbol{x}_{1,j}$ and $\Delta \boldsymbol{x}_{2,j}$ are the vectors pointing from $\boldsymbol{x}$ to its two neighbor vertices in the jth adjacent face.

Inflation Force over a Vertex

The inflation force $\boldsymbol{f}^p$ on a vertex is approximated by the average force over all of its N_F adjacent faces:

$$\boldsymbol{f}^p = \frac{1}{N_F}\sum_{j=1}^{N_F} \boldsymbol{f}_j^p = \frac{\Delta p}{N_F}\sum_{j=1}^{N_F} a_j \hat{\boldsymbol{n}}_j^F = \frac{2\Delta p}{N_F}\sum_{j=1}^{N_F} \boldsymbol{n} = 2\Delta p \boldsymbol{n}. \tag{A3}$$

Vertex Movement Simulation

Vertex movement is simulated by the kinematic equation of force-accelerated particles (Newton's second law):

$$\boldsymbol{f}(t) = m\boldsymbol{a}(t), \tag{A4}$$

where m is the mass of the vertex, $\boldsymbol{f}(t)$ is the total force acting on it and $\boldsymbol{a}(t)$ is the resulting acceleration. The term $\boldsymbol{f}(t)$ at each instant is calculated as:

$$\boldsymbol{f}(t) = \boldsymbol{f}^p(t) + \boldsymbol{f}_s(t) + 0.5\boldsymbol{f}_b(t) + \boldsymbol{f}_v(t). \tag{A5}$$

The term $\boldsymbol{f}_v(t)$ requires the prior knowledge of the vertex speed $\boldsymbol{v}(t)$ at that moment, which approximated from the known values in a previous instant $t - dt$:

$$\boldsymbol{v}(t) = \boldsymbol{v}(t - dt) + \boldsymbol{a}(t - dt).dt. \tag{A6}$$

The future position of the vertex, $\boldsymbol{x}_f(t)$ is calculated for the next instant $t + dt$:

$$\boldsymbol{x}_f(t + dt) = \boldsymbol{x}(t) + \boldsymbol{v}(t).dt + \frac{1}{2}dt^2\boldsymbol{a}(t) \tag{A7}$$

Future position is calculated for every vertex separately, and then simultaneously updated:

$$\begin{aligned} \boldsymbol{x}(t + dt) &:= \boldsymbol{x}_f(t + dt) \\ t &:= t + dt. \end{aligned} \tag{A8}$$

GDM Parameters and Selection Criteria

Mass and damping coefficient were selected after an initial calibration experiment where the spherical GDM was inflated with a constant normal force plus a random deviation of 1% of this force. After a certain time, inflation force stopped, and the mesh was allowed to relax. The quotient $m/\gamma = 2$ was found to stabilize the GDM in a number of iterations below T_{sizing} with little surface oscillation (i.e., behaving like an overdamped spring system) using a unitary time step. The HU thresholds resulted from a manual seed point selection, where the mean value and standard deviation of HU were computed inside an initial sphere of 20-pixel radius. Assuming Normal and χ^2 distribution, the 95% confidence interval was calculated for mean HU (μ) and standard deviation (σ), respectively. The upper limit was extended $+6$ times σ above the mean and the lower limit 3 times σ below the mean. This upper limit allowed the GDM to adequately expand through some bright structures (e.g., metallic stents or high concentrations of contrast agent). The lower limit was appropriate to constrain the GMD in the presence of dark structures surrounding the aneurysm lumen.

ACKNOWLEDGEMENTS

The authors thank Eng. Sandra Wray for her invaluable help in the writing of this manuscript. This work was partially supported by the project PIP Number 112-200901-00734 (CONICET).

REFERENCES

[1]Auer, M., T. C. Gasser, K. Hållfasthetslära, and T. Skolan. Reconstruction and finite element mesh generation of abdominal aortic aneurysms from computerized tomography angiography data with minimal user interactions. *IEEE Trans. Med. Imaging* 31(4):1022–1028, 2010.

[2]Ayyalasomayajula, A., A. Polk, A. Basudhar, S. Missoum, L. Nissim, and J. P. Vande Geest. Three dimensional active contours for the reconstruction of abdominal aortic aneurysms. *Ann. Biomed. Eng.* 38(1):164–176, 2010.
[3]Bieniek, A., and A. Moga. An efficient watershed algorithm based on connected components. *Pattern Recogn.* 33(6):907–916, 2000.
[4]Bland, J. M., and D. G. Altman. Statistical methods for assessing agreement between two methods of clinical measurement. *Lancet* 1(8476):307, 1986.
[5]Bockler, D., A. Holden, M. Thompson, P. Hayes, D. Krievins, J. P. de Vries, and M. M. Reijnen. Multicenter Nellix endovascular aneurysm sealing system experience in aneurysm sac sealing. *J. Vasc. Surg.* 62(2):290–298, 2015.
[6]Bouaziz, S., A. Tagliasacchi, and M. Pauly. Sparse iterative closest point. *Comput. Graph. Forum* 32(5):113–123, 2013.
[7]Buijs, R. V., T. P. Willems, R. A. Tio, H. H. Boersma, I. F. Tielliu, R. H. Slart, and C. J. Zeebregts. Current state of experimental imaging modalities for risk assessment of abdominal aortic aneurysm. *J. Vasc. Surg.* 57(3):851–859, 2013.
[8]Cignoni, P., C. Rocchini, and R. Scopigno. Metro: measuring error on simplified surfaces. *Comput. Graph. Forum* 17(2):167–174, 1998.
[9]Di Martino, E. S., G. Guadagni, A. Fumero, G. Ballerini, R. Spirito, P. Biglioli, and A. Redaelli. Fluid-structure interaction within realistic three-dimensional models of the aneurysmatic aorta as a guidance to assess the risk of rupture of the aneurysm. *Med. Eng. Phys.* 23(9):647–655, 2001.
[10]Donayre, C. E., C. K. Zarins, D. K. Krievins, A. Holden, A. Hill, C. Calderas, J. Velez, and R. A. White. Initial clinical experience with a sac-anchoring endoprosthesis for aortic aneurysm repair. *J. Vasc. Surg.* 53(3):574–582, 2011.
[11]Duquette, A. A., P.-M. Jodoin, O. Bouchot, and A. Lalande. 3D segmentation of abdominal aorta from CT-scan and MR images. *Comput. Med. Imaging Graph.* 36(4):294, 2012.
[12]Gao, L., D. G. Heath, and E. K. Fishman. Abdominal image segmentation using three-dimensional deformable models. *Invest. Radiol.* 33(6):348–355, 1998.
[13]Gasser, T. C., G. Gorgulu, M. Folkesson, and J. Swedenborg. Failure properties of intraluminal thrombus in abdominal aortic aneurysm under static and pulsating mechanical loads. *J. Vasc. Surg.* 48(1):179–188, 2008.
[14]Johnston, K. W., R. B. Rutherford, M. D. Tilson, D. M. Shah, L. Hollier, and J. C. Stanley. Suggested standards for reporting on arterial aneurysms. Subcommittee on reporting standards for arterial aneurysms, Ad Hoc Committee on Reporting Standards, Society for Vascular Surgery and North American Chapter, International Society for Cardiovascular Surgery. *J. Vasc. Surg.* 13(3):452, 1991.
[15]Kaladji, A., A. Lucas, G. Kervio, P. Haigron, and A. Cardon. Sizing for endovascular aneurysm repair: clinical evaluation of a new automated three-dimensional software. *Ann. Vasc. Surg.* 24(7):912–920, 2010.
[16]Kanaoka, Y., S. Ohgi, and T. Mori. Quantitative evaluation of abdominal aortic aneurysm. *Vasc. Endovasc. Surg.* 33(1):59–65, 1999.
[17]Karthikesalingam, A., R. J. Cobb, A. Khoury, E. C. Choke, R. D. Sayers, P. J. Holt, and M. M. Thompson. The morphological applicability of a novel endovascular aneurysm sealing (EVAS) system (Nellix) in patients with abdominal aortic aneurysms. *Eur. J. Vasc. Endovasc. Surg.* 46(4):440–445, 2013.
[18]Kass, M., A. Witkin, and D. Terzopoulos. Snakes: active contour models. *Int. J. Comput. Vision* 1(4):321–331, 1988.
[19]Kim, H. C., Y. H. Seol, S. Y. Choi, J. S. Oh, M. G. Kim, and K. Sun. A study of AAA image segmentation technique using geometric active contour model with morphological gradient edge function. *Conf. Proc. IEEE Eng. Med. Biol. Soc.* 4437–4440:2007, 2007.
[20]Kniemeyer, H. W., T. Kessler, P. U. Reber, H. B. Ris, H. Hakki, and M. K. Widmer. Treatment of ruptured abdominal aortic aneurysm, a permanent challenge or a waste of resources? Prediction of outcome using a multi-organ-dysfunction score. *Eur. J. Vasc. Endovasc. Surg.* 19(2):190–196, 2000.
[21]Krievins, D. K., A. Holden, J. Savlovskis, C. Calderas, C. E. Donayre, F. L. Moll, B. Katzen, and C. K. Zarins. EVAR using the Nellix sac-anchoring endoprosthesis: treatment of favourable and adverse anatomy. *Eur. J. Vasc. Endovasc. Surg.* 42(1):38–46, 2011.
[22]Lederle, F. A., J. A. Freischlag, T. C. Kyriakides, F. T. Padberg, Jr., J. S. Matsumura, T. R. Kohler, P. H. Lin, J. M. Jean-Claude, D. F. Cikrit, K. M. Swanson, *et al.* Outcomes following endovascular vs. open repair of abdominal aortic aneurysm: a randomized trial. *JAMA* 302:1535–1542, 2009.
[23]Lee, E. Region Filling Using Two Dimensional Grammars. *Proc. 1987 IEEE Int. Conf. Robot Autom.* pp. 147–1478, 1987.
[24]Miller, J., D. Breen, W. Lorensen, R. O'Bara, and M. Wozny. Geometrically deformed models: a method for extracting closed geometric models form volume data. *ACM* 25:217–226, 1991.
[25]Montagnat, J., H. Delingette, and N. Ayache. A review of deformable surfaces: topology, geometry and deformation. *Image Vis. Comput.* 19(14):1023–1040, 2001.
[26]O'Leary, S. A., E. G. Kavanagh, P. A. Grace, T. M. McGloughlin, and B. J. Doyle. The biaxial mechanical behaviour of abdominal aortic aneurysm intraluminal thrombus: classification of morphology and the determination of layer and region specific properties. *J. Biomech.* 47(6):1430–1437, 2014.
[27]Park, J.-Y., T. McInerney, D. Terzopoulos, and M.-H. Kim. A non-self-intersecting adaptive deformable surface for complex boundary extraction from volumetric images. *Comput. Graph.* 25(3):421–440, 2001.
[28]Sacks, M. S., D. A. Vorp, M. L. Raghavan, M. P. Federle, and M. W. Webster. In vivo three-dimensional surface geometry of abdominal aortic aneurysms. *Ann. Biomed. Eng.* 27(4):469–479, 1999.
[29]Sakalihasan, N., R. Limet, and O. D. Defawe. Abdominal aortic aneurysm. *Lancet* 365(9470):1577–1589, 2005.
[30]Shum, J., G. Martufi, E. Di Martino, C. B. Washington, J. Grisafi, S. C. Muluk, and E. A. Finol. Quantitative assessment of abdominal aortic aneurysm geometry. *Ann. Biomed. Eng.* 39(1):277–286, 2011.
[31]Terzopoulos, D., A. Witkin, and M. Kass. Constraints on deformable models: recovering 3D shape and nonrigid motion. *Artif. Intell.* 36(1):91–123, 1988.
[32]Vande Geest, J. P., M. S. Sacks, and D. A. Vorp. The effects of aneurysm on the biaxial mechanical behavior of human abdominal aorta. *J. Biomech.* 39:1324–1334, 2006.
[33]Wever, J. J., J. D. Blankensteijn, W. P. T. M. Mali, and B. C. Eikelboom. Maximal aneurysm diameter follow-up is inadequate after endovascular abdominal aortic aneurysm repair. *Eur. J. Vasc. Endovasc. Surg.* 20(2):177–182, 2000.
[34]Subasic M., Loncaric S, Fau-Sorantin E., and Sorantin E. 3-D image analysis of abdominal aortic aneurysm. (0926-9630 (Print)).

Age-related changes of thoracic aorta geometry used to predict the risk for acute type B dissection

Damian Craiem[a,b,c,d], Salma El Batti[e], Mariano E. Casciaro[a], Elie Mousseaux[c,d,f], Marie-Emmanuelle Sirieix[b,d], Alain Simon[b,c,d], Jean-Marc Alsac[c,d,e]

[a]Facultad de Ingeniería Ciencias Exactas y Naturales, Favaloro University, CONICET, Argentine

[b]Centre de Médecine Préventive Cardiovasculaire, APHP, Hôpital Européen Georges Pompidou, Paris, France

[c]INSERM U970, APHP, Hôpital Européen Georges Pompidou, Paris, France

[d]Université Paris-Descartes, Paris-Centre de Recherche Cardiovasculaire, Hôpital Européen Georges Pompidou, Paris, France

[e]Service de Chirurgie Cardiaque et Vasculaire, APHP, Hôpital Européen Georges Pompidou, Paris, France

[f]Service d'Imagerie Cardiovasculaire, APHP, Hôpital Européen Georges Pompidou, Paris, France

Address of correspondence:

Dr Damian CRAIEM.

Favaloro University, FICEN,

Solis 453, CP 1078. Ciudad Autónoma de Buenos Aires. Argentina

email: damian@craiem.com.ar

Tel: (+54 11) 4378-1132.

Abstract

Aims- Risk models that use a single aortic diameter threshold have failed to successfully predict acute type B aortic dissection (TBAD). We thought to identify meaningful age-indexed anatomical variables to predict TBAD risk.

Methods and Results- A geometric deformable model, consisting of virtual elastic balloons that inflate inside a vessel lumen, was developed to quantify thoracic aorta geometry. In the presence of TBAD, true and total artery lumen morphology were assessed. A stepwise logistic model was built to predict TBAD risk. Initial covariates included age, gender, body mass index and all anatomic variables not directly related to the dissected segment. Patients with acute TBAD (n=34, 62±12 years old, 57% male gender) were compared with subjects with symptoms of dissection, but with a subsequent negative diagnosis (n=51, 62±12 years old, 76% male gender). Patient risk factors did not differ between groups. Most aortic anatomical variables were age-dependent. Aortic size was larger in every segment of the dissected with respect to non-dissected aortas ($p<0.001$). Variables entering the TBAD risk prediction model were aortic arch diameter, thoracic aorta length and age (predictability=0.9764, $r=0.85$), confirmed by a bootstrap internal validation. In dissected aortas, the true lumen volume was correlated to age ($r=0.72$).

Conclusions- TBAD probability increases with a larger aortic arch diameter and a longer thoracic aorta, whereas threshold values increase with age. The aortic morphology was age-dependent. After dissection, true lumen volume correlated to age. The use of threshold values indexed to age should be encouraged to better prevent and eventually treat TBAD.

1. Introduction

Acute aortic dissection is currently an increasingly common cause of surgical aortic emergencies with an estimated incidence rate of 3 to 6 per 100.000 persons per year (1). Dissection can occur at any age, mostly in adults aged between 50 and 80 years, and is more frequent in hypertensive males (2). One third of all aortic dissections are classified as type B (i.e., concerning only the descending aorta) (3). Despite advances in medical and surgical treatments, the mortality of aortic dissection remains high (4). Since a relatively small percentage of hypertensive patients develop aortic dissections, novel characteristics other than the traditional risk factors are required to detect and prevent them. Previous attempts to predict type B aortic dissection (TBAD) risk based on descending aorta dilatation have not been accurate enough (5). Although anatomical variables other than diameter have been proposed to improve TBAD prediction (6), the influence of aging on aortic morphometry was systematically neglected from the risk models. This is particularly odd, since the thoracic aorta tends to dilate, lengthen and unfold throughout life (7-9) and setting threshold values for anatomical variables not indexed by age seems illogical. Furthermore, after dissection occurs, aging could also impact true lumen size, conditioning perfusion towards other vessels and the eventual endograft access if thoracic endovascular aortic repair (TEVAR) is required (3).

In this study we sought to identify meaningful anatomical variables associated with higher risk of TBAD and to build a risk model indexed by age. Patients with acute TBAD were compared with control subjects with symptoms evoking aortic dissection, which was discarded after scan images. Automated geometric deformable models were used to accurately assess several anatomic variables, including vessel cross-sectional area, length, tortuosity and volume estimated through the ascending, the arch and descending segments of the thoracic aorta. Correlations of anatomic variables to age were calculated for these three segments. The volume of the true lumen with respect to age was also analyzed.

2. Methods

2.1. Study subjects and image acquisition

Since 2009, the Hôpital Européen Georges Pompidou (Paris, France) runs a program called “SOS Aorte”, which gathers information about all patients with aortic emergencies treated in the hospital and stores it into a database. For this study, patients with an acute TBAD were retrospectively reviewed until September 2015. The institutional review committee approved this study and waived the need for individual patient consent. Subjects were excluded if i) the dissection was due to a traumatic event or ii) it was a type A aortic dissection (i.e. concerning the ascending aorta), or iii) evidences of congenital or connective tissue disease were found. A total of 34 patients were included in this study and hereafter called the “dissection group”. These patients were compared with a “control group” of 51 subjects with a suspected dissection, but whose scans examination and outcomes

revealed their aortas were not dissected. Symptoms included sharp chest, abdominal or back pain. Patients with cancer or any other aortic disease were excluded from this study. All patients were studied on the same 64-slice scanner (Light-speed VCT; GE Health care, Milwaukee, Wisconsin, USA) using an ECG-gated computed tomography angiography (CTA) procedure. The thoracic aorta was visualized using an injection of 100 to 120 ml of contrast and the following configuration: 80 HU threshold within the aorta before starting the volumetric acquisition; 330ms rotation speed; 64x0.6 mm collimation; pitch of 0.2; voltage of 140kV and current between 500 and 850 mAs.

2.2. Thoracic aorta segmentation

2.2.1. Geometric deformable model (GDM)

A novel algorithm based on deformable surface models was used in this study to fully describe the three-dimensional (3D) morphometry of the thoracic aorta. Accurate measurements of aortic dimensions and shape, including true and total (i.e., true plus false) artery lumen centerline and volume, were automated to reduce user intervention. The proposed algorithm was developed by our group to assess the geometry of abdominal aortic aneurysms before and after endograft implantation (10) and was adapted for the thoracic aorta geometry in this study. A geometric deformable model (GDM) was developed based on the publications by Park, Miller and Terzopoulos et al. [11-13] to mimic a virtual elastic balloon that inflates inside the aortic lumen to measure its volume. The GDM initial shape is a closed spheroidal balloon composed by vertexes connected with elastic edges that form triangular faces. The position of each vertex is dynamically calculated using internal and external forces. Internal forces consist of stretching, bending and dissipative forces. The only external force applied to this model is an inflation pressure that pushes each vertex of the mesh perpendicularly to the surface. The inflation process simulates the application of an internal pressure on the inner surface (i.e. an expansive force), and an external pressure exerted by the vessel walls or other structures in the scan images that oppose to the advance of the GMD (i.e. a compressive force). When equilibrium between forces is reached and no significant changes in the GDM volume are detected, the 3D mesh can be used to describe geometrically the vessel that contains it.

2.2.2. Semi-automatic measurement

In order to quantify the thoracic aorta geometry, seven virtual spherical balloons were “implanted” inside the thoracic aorta lumen as shown in Fig. 1.

Nine points inside the aortic lumen were set manually: two in the axial section at the level of the pulmonary artery (CA and CD), three at oblique planes 45º, 90º and 135º, another two at the sinotubular junction (SJ) level and one at the diaphragm (DIA) level. Finally, a last point at mid distance between SJ and DIA. Virtual balloons of 10mm diameter were then implanted in the seven intermediate points

linking SJ to DIA. A preliminary centerline was calculated interpolating a spline. Nine invisible orthogonal planes were placed between the seed points in order to constrain the growth of the adjacent meshes and avoid mesh superposition.

In the presence of a TBAD, the user was asked to always position the seed points inside the true lumen (TL). Instead of separately segmenting the false lumen, the five points positioned by the user between the LSA and DIA were duplicated and manually placed on the dissection flap. When these balloons were inflated, their expansion covered the entire lumen (i.e. both the true and false lumens), called hereafter total artery lumen (TAL). In order to avoid the undesired growth of the GMD through the lumen of supra aortic arteries nor through flap tears, a “patch tool” was implemented as shown in Fig. 2. Before inflating the balloons, the user was able to place these patches to block the mesh expansion. Once all of the meshes were inflated until equilibrium, two independent centerlines were calculated: one for the TL and another for the TAL as shown in Fig. 2.

A slow motion video showing the balloons growing inside the true aortic lumen in a representative patient with TBAD is provided in the supplemental material.

2.2.3. Geometrical variables

All voxels inside the meshes were painted as to calculate a volume and refine the centerlines estimations. The user was finally asked to indicate the positions of the brachiocephalic and the left subclavian arteries (BSA and LSA, respectively) in order to separate ascending, arch and descending segments. The following geometrical variables were then automatically calculated for patients in both groups:

- Mean diameter, length and volume of each segment;
- Aortic arch width as the distance between CA and CD, and the distances from the aortic arch midpoint to C45º, C90º (arch height) and C135º;
- The tortuosity of the ascending portion, which includes the aortic arch (from SJ to LSA) and of the entire thoracic aorta (from SJ to DIA). Tortuosity was defined as the curvilinear length of a centerline divided by the linear distance between its ends.

In patients with TBAD, separate measurements were made for TL and TAL centerlines.

Geometric modifications of the dissected and non-dissected segments of the thoracic aorta can be suspected after dissection occurs (14). Accordingly, a contraction of the descending aorta lumen due to TBAD could impact the morphology of the ascending aorta. To further investigate this issue, manual measurements of the ascending aorta diameter were taken from all patients in the dissection group that benefited from TEVAR within a week after surgery when the descending aorta flow was restored.

2.3. Statistical analysis

Groups were compared using unpaired t-student tests for continuous variables and chi-square tests for categorical variables. Geometrical comparisons were restricted to the ascending aorta and aortic arch proximal to LSA because the presence of a TBAD could interfere in certain measurements of the descending aorta. Within the dissection group, paired t-tests were used to compare true and total artery lumen variables.

The effect of aging on aortic geometry was analyzed calculating linear correlations of anatomic variables to age, after adjusting for body mass index (BMI) and gender. Correlations were restricted, once again, to anatomical variables not affected by the dissection. For patients in the dissection group, correlations between descending aorta TL volume and age before and after normalization to TAL volume were calculated and plotted separately.

In order to identify significant predictors of TBAD, stepwise logistic regression analysis was used. All of the significant anatomical variables in the group comparisons, together with age, gender and BMI, were considered as covariates in the initial model. Odds ratios and 95% confidence intervals (95% C.I.) were reported for unit increment of each identified covariate. The area under the receiver-operating curve (ROC) was adopted as the apparent performance of the fitted risk model for TBAD prediction. A bootstrap method was used for the internal validation of the selection of model variables and performance (15). One-thousand samples were bootstrapped with replacement repeating the same stepwise procedure. Finally, we counted the number of times each variable entered the model to evaluate its consistency. The optimism in the apparent performance was calculated as the averaged difference between the performance in each bootstrap sample and the performance of using the model as estimated for each sample in the original sample (15). Ascending aorta diameters before and after TEVAR were compared using a paired t-test. All statistical analysis was performed using JMP (SAS, NC, USA) and Matlab (Mathworks, MA, USA) for bootstrap validation.

3. Results

The control and dissection groups are described in Table 1. No significant differences were observed in age, gender, BMI or traditional risk factors between groups.

The aortic anatomical variables of both groups are shown in Table 2, and an equivalent lumen diameter at different positions of the thoracic aorta is shown in Figure 3. The average diameter, lumen volume and centerline length of ascending aorta and arch segments were larger in the dissection group with respect to the control group ($p<0.001$). Ascending aortic tortuosity (including the aortic arch) did not differ between groups, whereas vectors C90º (aortic height) and C45º were longer in patients with TBAD ($p<0.001$). In the last two columns of Table 2, a comparison between TL and TAL of patients with TBAD is shown. The average

diameter of the TL in the descending aorta was halved with respect to TAL (p<0.001), lumen volume was reduced by 71% (p<0.001), centerline length shortened by 8% (p<0.001) and tortuosity decreased 3% (p<0.001). The length of the entire thoracic aorta centerline path was 6% shorter in the TL with respect to TAL (p<0.001) and 2% less tortuous (p<0.05), respectively. The TL centerline path was closer to the aortic arch center, as evidenced by a shorter aortic arch width (-8%, p<0.001) and C135º vector length (-10%,p<0.001) with respect to TAL.

Changes of anatomical variables per decades of life after adjustment for gender and BMI are shown in Table 3. Anatomical variables were positively associated with age both in subjects with and without TBAD. In the control group, correlations to age were stronger for ascending and aortic arch size (p<0.001 and p<0.01 respectively), entire thoracic aorta tortuosity (p<0.01) and C45º vector length (p<0.01). In the dissection group, variables that showed stronger correlations to age were ascending aorta volume (p<0.01), ascending + aortic arch length (p<0.01), total thoracic aorta length (p<0.001), aortic arch height (p<0.001) and C45º vector length (p<0.01. When patients in the dissection group were analyzed separately, the descending TL volume was strongly correlated to age (p<0.001, r=0.72), even after normalization for TAL volume (Fig. 4).

After a stepwise logistic regression process, only three variables appeared in the risk model to predict TBAD. The linear equation into the logistic regression resulted: y = 7.5311 x arch diameter + 0.7793 x aortic length – 0.1851 x age – 34.2420 (r = 0.85). Accordingly, the probability of TBAD can be calculated using this linear equation as $1/1 + e^{-y}$, where e is the natural exponential function. For example, a 60 year-old patient with an aortic arch diameter of 3.2 cm and aortic length of 28 cm yields y = 0.57092 and the probability of TBAD results 64%. The odds ratio and 95% C.I. for 1 mm increase in aortic arch diameter was 2.12 [1.43-3.76] and for 1 cm increase in aortic length was 2.18 [1.45-4.17]. Assuming a fixed 90% probability of TBAD, the interplay between aortic arch diameter and aortic length values adjusted for age, is shown in Fig. 5. Subjects with anatomical variables above their corresponding age curves are at high risk (probability > 90%) of TBAD. Finally, the consistency in the covariates selection for the model was tested with a bootstrap method and internal validations. Aortic arch diameter, length and age entered in 99%, 96% and 88% of the 1000 bootstrapped repetitions, respectively. The other anatomic variables entered less than 50% of the time. The predictability of the model (evaluated with the area under the ROC) was 0.9764 and the optimism of this apparent performance resulted 0.0162.

A subgroup of 24 patients from the 34 in the dissection group benefited from TEVAR for TBAD. The ascending diameter did not change before and after surgery (mean differences 0.3±1.9 mm, p=0.26) when the descending aorta flow was restored.

4. Discussion

Current image modalities allow for a better understanding of the thoracic aorta development throughout life (7-9). Age-associated changes of aortic geometry are now unquestionable and should not be excluded from any risk model developed to prevent aortic diseases. Accordingly, in this study we show that the risk of TBAD can be successfully predicted using aortic arch diameter and thoracic aorta length, indexed to age. Aging was associated with most of the three-dimensional anatomical variables assessed in patients with and without TBAD. Additionally, after dissection occurs, the true lumen volume was positively correlated to age. These findings, which encourage the calculation of threshold values indexed to age, should help to better prevent and eventually treat TBAD.

In the International Registry of Aortic Dissection (IRAD), where 12 international referral centers and more than 4400 patients participate, the mean age was 63 years, 65% were men and 77% had a history of hypertension (2), comparable to demographics in our patients. Using the IRAD database, the attempt to set a threshold value for descending aorta diameter to early recognize TBAD patients had major limitations. For instance, the IRAD reported that 80% of their patients would skip detection using the proposed 5.5 cm threshold for descending aorta diameter (5, 16). The IRAD does not have a control group and thus, aortic dissection prediction was not possible. In the current study, the three variables that were kept by the stepwise logistic process to predict TBAD were aortic arch diameter, total aortic length and age. The internal validation using a bootstrap method confirmed the final variable selection. The logistic model explained 72% of all the variability. It reached a high predictability value of 0.9764 with an internal optimism estimation of 0.0162. In a recent report, aortic arch diameter and aortic length also appeared as significant anatomic variables to predict TBAD risk, together with the brachiocephalic angle and the entire aorta tortuosity (6). The angulations of the supra-aortic arteries were not measured in our study because these vessels were excluded from the expansion region of the automated deformable model. Whereas in this previous study tortuosity included the abdominal aorta, our study was limited to the thoracic aorta; this is probably the reason why tortuosity was not yielded as an explanatory variable. On the other hand, age was consistently selected into our model, accounting for 88% of the samples in a 1000 times bootstrap validation. Age-associated changes of anatomic variables in the thoracic aorta have been widely reported (7-9, 17, 18), with a significant acceleration of aortic enlargement and unfolding in hypertensive patients (19). In accordance with the literature (9, 17, 18, 20), we found that the diameter and length of the ascending and aortic arch segments increased 1 mm and 3 mm per decade of life, respectively (Table 3). Our model suggests that, in order to predict the risk of TBAD, threshold values for anatomical variables should be indexed to age. This is clear in Fig. 5, where the 90% probability of TBAD curves show that elderly patients have longer and larger threshold values for the anatomical predictors. For instance, a 50 year-old patient with a 28cm thoracic aorta length has an aortic arch diameter threshold of <3 cm, whereas in a 70 year-old patient with the same aortic length, the upper threshold is 3.5 cm. This seems

logical, since the fact that the aorta enlarges throughout life is undeniable, and expecting a single threshold value for aortic diameter to predict TBAD for all subjects would be inaccurate.

The attempt to use a diameter measured within the aortic damaged segment after aortic dissection has occurred seems initially questionable. Rylski et al. have recently compared the ascending aorta size before and after type A aortic dissection onset (14). They reported a significant expansion of the ascending aorta (without significant length modifications), both in retrograde and spontaneous cases, showing that aortic size is clearly affected by dissection. Since aortic diameters in most studies have been measured in dissected aortas, published data on aortic dissection prediction should be carefully interpreted. In our study, the adoption of the ascending or aortic arch dimensions as covariates could raise some concerns because these regions could not be completely isolated from the dissection effect. One can imagine that an abrupt reduction of the descending aorta lumen, which forces blood to flow through a small true lumen, could eventually rise blood pressure and induce an ascending aorta expansion. To further investigate this issue, the ascending aorta diameter of patients from dissection group that benefit from TEVAR was assessed. After a successful recovery of the descending aorta lumen, ascending aorta diameter did not significantly change, suggesting that aortic dilatation was probably present before the TBAD onset (Fig. 3). Nevertheless, the hypothesis of a proximal aorta expansion due to a distal dissection cannot be completely rejected and should be further explored.

When dissection occurs, the assessment of the TL size could be of interest because it influences the prognosis of TBAD patients (21, 22). As the false lumen dilates, the TL is contracted, leading to critical limitation of vessel perfusion through the TL (3). Moreover, the risk of developing an aneurysm or further dissection increases if the false lumen remains patent (23). Actually, since the expanded use of endovascular interventions has a growing effect on management of TBADs (2), the assessment of TL morphology might anticipate the accessibility of the endograft into the vasculature. We found that the TL volume was correlated to age, even after normalization to total artery lumen (Figure 5). At this moment we do not have a proper explanation for this observation. It was shown that the aortic growth rate decreases with age in non-complicated TBAD medically treated patients (22). The structure of the aortic wall, which degenerates over time, may become stiffer due to the increased occurrence of atherosclerosis. A comparable effect could help explain the less collapsed TL in elderly patients observed in our study. Additionally, younger subjects with aortic dissection may have higher chances of genetic abnormalities that contribute to the degradation of aortic elastic elements and a consequent contraction of the TL. We are aware that additional variables, such as size, location and number of entry tears, or the thrombotic level of the false lumen could also influence TL volume. These measurements were not taken into account in our study because they could not be assessed with a reasonable reproducibility.

Some limitations of this study need to be addressed. Our results should be interpreted with caution since our groups are small in order to draw definitive conclusions from. Only the thoracic aorta was measured. Some scans covered the abdominal aorta, but they were more prone to contrast artifacts. The automated algorithm still needs manual interventions. We are currently exploring to gradually incorporate new tools to automatically describe the morphology of entry tears and the false lumen patency. Nevertheless, it seems potentially useful even for other applications like TEVAR planning for dissection patients. The fact that volumes were not helpful contributors into the final risk prediction model does not mean their assessment was redundant because all diameter and length measurements were ultimately based on the volume technique. Finally, the analysis made in this study was essentially structural and not functional. The interaction of aortic dilatation and elasticity with aging would certainly improve TBAD prediction (24), suggesting that structural and functional measurements should be visualized as a future strategy to better understand aortic diseases.

Conclusions

In this study we show that the probability of TBAD increases with a larger aortic arch diameter and a longer thoracic aorta, whereas threshold values increase with age. In fact, age was not only associated with most of the three-dimensional anatomical variables assessed in patients with and without TBAD, but also with the true lumen volume after dissection occurs. These findings, which encourage the calculation of threshold values indexed to age to predict TBAD risk, should help to identify vulnerable patients, better prevent and eventually treat TBAD.

Acknowledgements

The authors thank Eng. Sandra Wray for her invaluable help in the correction of this manuscript.

References

1. Erbel R, Aboyans V, Boileau C, Bossone E, Bartolomeo RD, Eggebrecht H et al. 2014 ESC Guidelines on the diagnosis and treatment of aortic diseases: Document covering acute and chronic aortic diseases of the thoracic and abdominal aorta of the adult. The Task Force for the Diagnosis and Treatment of Aortic Diseases of the European Society of Cardiology (ESC). *Eur Heart J* 2014; 35(41):2873-2926.
2. Pape LA, Awais M, Woznicki EM, Suzuki T, Trimarchi S, Evangelista A et al. Presentation, Diagnosis, and Outcomes of Acute Aortic Dissection: 17-Year Trends From the International Registry of Acute Aortic Dissection. *J Am Coll Cardiol* 2015; 66(4):350-358.
3. Karmy-Jones R, Simeone A, Meissner M, Granvall B, Nicholls S. Descending thoracic aortic dissections. *Surg Clin North Am* 2007; 87(5):1047-1086, viii-ix.
4. Hagan PG, Nienaber CA, Isselbacher EM, Bruckman D, Karavite DJ, Russman PL et al. The International Registry of Acute Aortic Dissection (IRAD): new insights into an old disease. *JAMA* 2000; 283(7):897-903.
5. Trimarchi S, Jonker FH, Froehlich JB, Upchurch GR, Moll FL, Muhs BE et al. Acute type B aortic dissection in the absence of aortic dilatation. *J Vasc Surg* 2012; 56(2):311-316.
6. Shirali AS, Bischoff MS, Lin HM, Oyfe I, Lookstein R, Griepp RB et al. Predicting the risk for acute type B aortic dissection in hypertensive patients using anatomic variables. *JACC Cardiovasc Imaging* 2013; 6(3):349-357.
7. Craiem D, Chironi G, Redheuil A, Casciaro M, Mousseaux E, Simon A et al. Aging impact on thoracic aorta 3D morphometry in intermediate-risk subjects: looking beyond coronary arteries with non-contrast cardiac CT. *Ann Biomed Eng* 2012; 40(5):1028-1038.
8. Redheuil A, Yu WC, Mousseaux E, Harouni AA, Kachenoura N, Wu CO et al. Age-related changes in aortic arch geometry: Relationship with proximal aortic function and left ventricular mass and remodeling. *Journal of the American College of Cardiology* 2011; 58(12):1262-1270.
9. Sugawara J, Hayashi K, Yokoi T, Tanaka H. Age-Associated Elongation of the Ascending Aorta in Adults. *J Am Coll Cardiol Img* 2008; 1(6):739-748.
10. Casciaro ME, El-Batti S, Chironi G, Simon A, Mousseaux E, Armentano RL et al. Deformable Surface Model for the Evaluation of Abdominal Aortic Aneurysms Treated with an Endovascular Sealing System. *Ann Biomed Eng* 2015.
11. Miller JV, Breen DE, Lorensen WE, O'Bara RM, Wozny MJ. Geometrically deformed models: a method for extracting closed geometric models form volume data. *SIGGRAPH Comput Graph* 1991; 25(4):217-226.
12. Park J-Y, McInerney T, Terzopoulos D, Kim M-H. A non-self-intersecting adaptive deformable surface for complex boundary extraction from volumetric images. *Computers & Graphics* 2001; 25(3):421-440.
13. Terzopoulos D, Witkin A, Kass M. Constraints on deformable models:Recovering 3D shape and nonrigid motion. *Artificial Intelligence* 1988; 36(1):91-123.
14. Rylski B, Blanke P, Beyersdorf F, Desai ND, Milewski RK, Siepe M et al. How does the ascending aorta geometry change when it dissects? *J Am Coll Cardiol* 2014; 63(13):1311-1319.
15. Steyerberg EW, Harrell FE, Jr., Borsboom GJ, Eijkemans MJ, Vergouwe Y, Habbema JD. Internal validation of predictive models: efficiency of some procedures for logistic regression analysis. *J Clin Epidemiol* 2001; 54(8):774-781.

16. Trimarchi S, Jonker FH, Hutchison S, Isselbacher EM, Pape LA, Patel HJ et al. Descending aortic diameter of 5.5 cm or greater is not an accurate predictor of acute type B aortic dissection. *J Thorac Cardiovasc Surg* 2011; 142(3):e101-107.
17. Rylski B, Desjardins B, Moser W, Bavaria JE, Milewski RK. Gender-related changes in aortic geometry throughout life. *Eur J Cardiothorac Surg* 2014; 45(5):805-811.
18. Wolak A, Gransar H, Thomson LEJ, Friedman JD, Hachamovitch R, Gutstein A et al. Aortic Size Assessment by Noncontrast Cardiac Computed Tomography: Normal Limits by Age, Gender, and Body Surface Area. *JACC: Cardiovascular Imaging* 2008; 1(2):200-209.
19. Craiem D, Chironi G, Casciaro ME, Redheuil A, Mousseaux E, Simon A. Three-dimensional evaluation of thoracic aorta enlargement and unfolding in hypertensive men using non-contrast computed tomography. *J Hum Hypertens* 2013; 27(8):504-509.
20. Turkbey EB, Jain A, Johnson C, Redheuil A, Arai AE, Gomes AS et al. Determinants and normal values of ascending aortic diameter by age, gender, and race/ethnicity in the Multi-Ethnic Study of Atherosclerosis (MESA). *Journal of magnetic resonance imaging : JMRI* 2014; 39(2):360-368.
21. Andacheh ID, Donayre C, Othman F, Walot I, Kopchok G, White R. Patient outcomes and thoracic aortic volume and morphologic changes following thoracic endovascular aortic repair in patients with complicated chronic type B aortic dissection. *J Vasc Surg* 2012; 56(3):644-650; discussion 650.
22. Tolenaar JL, van Keulen JW, Jonker FH, van Herwaarden JA, Verhagen HJ, Moll FL et al. Morphologic predictors of aortic dilatation in type B aortic dissection. *J Vasc Surg* 2013; 58(5):1220-1225.
23. Evangelista A, Salas A, Ribera A, Ferreira-Gonzalez I, Cuellar H, Pineda V et al. Long-term outcome of aortic dissection with patent false lumen: predictive role of entry tear size and location. *Circulation* 2012; 125(25):3133-3141.
24. Cavalcante JL, Lima JA, Redheuil A, Al-Mallah MH. Aortic stiffness: current understanding and future directions. *J Am Coll Cardiol* 2011; 57(14):1511-1522.

Table 1. Demographics in patients with and without acute type B aortic dissection.

	control group	dissection group	p value
Number of patients	51	34	
Age, yrs (range)	62±14 (34-88)	62±12 (40-88)	0.95
Male gender, n (%)	29 (57)	26 (76)	0.06
Body mass index, kg/m^2 (range)	27.9±6.1 (17-46)	27.6±5.8 (18-43)	0.83
Hypertension, n (%)	28 (55)	24 (71)	0.14
Treatment hypertension, n (%)	26 (51)	14 (41)	0.37
Current or past smoker, n (%)	13 (26)	15 (44)	0.09
Diabetes, n (%)	6 (12)	2 (6)	0.35

Values expressed as mean ± standard deviation or percentages.

Table 2. Anatomical variables.

	Control group	Dissection group		
Aortic measurements		Ascending + aortic arch	Descending TAL	Descending TL
Average diameter, cm				
Ascending	2.98±0.37	3.47±0.46 (+16%)*		
Arch	2.61±0.29	3.30±0.42 (+26%)*		
Descending	2.27±0.28		3.45±0.46*	1.81±0.48 (-48%)‡
Lumen volume, cm^3				
Ascending	43±15	71±29 (+65%)*		
Arch	22±8	39±14 (+77%)*		
Descending	69±23		198±71*	58±31 (-71%)‡
Length, cm				
Ascending + aortic arch	9.79±1.37	11.42±1.58 (+17%)*		
Descending	16.95±2.53		21.69±3.10*	19.93±3.61 (-8%)‡
Thoracic aorta	26.73±3.21		33.11±3.72*	31.10±4.38 (-6%)‡
Tortuosity				
Ascending + aortic arch	1.29±0.08	1.26±0.07		
Descending	1.18±0.09		1.32±0.15*	1.28±0.15 (-3%)‡
Thoracic aorta	2.75±0.44		3.30±0.31*	3.22±0.70 (-2%)†
Aortic arch shape, cm				
Height	4.2±0.9	5.2±0.7 (+24%)*		
C45° vector	4.1±0.6	4.9±0.7 (+20%)*		
Width	8.3±1.3		10.3±1.9*	9.5±1.9 (-8%)‡
C135° vector	4.3±0.8		5.2±0.9*	4.7±0.9 (-10%)‡

TL=true lumen. TAL=total arterial lumen.

*p<0.001 with respect to control group values (unpaired t-test)

†p<0.05, ‡p<0.001; with respect to TAL (paired t-test).

Table 3. Correlation of anatomical variables with age after adjustment for BMI and gender.

	Control group		Dissection group	
Geometrical variable	β_{age}	model r	β_{age}	model r
Average diameter, cm/10-yrs				
Ascending	0.14‡	0.69	0.14*	0.50
Arch	0.08†	0.69	0.04	0.27
Lumen volume, cm^3/10-yrs				
Ascending	5.7‡	0.66	10.7†	0.51
Arch	1.8†	0.70	2.6	0.40
Length, cm/10-yrs				
Ascending + aortic arch	0.29*	0.57	0.67†	0.55
Entire thoracic aorta	0.91*	0.50	2.50‡	0.73
Tortuosity, 1/10-yrs				
Ascending + aortic arch	0.02	0.51	0.00	0.26
Entire thoracic aorta	0.16†	0.59	0.25†	0.66
Aortic arch shape, cm/10-yrs				
Height	0.22*	0.50	0.32‡	0.60
C45° vector	0.18†	0.55	0.31†	0.61

*p<0.05, †p<0.01, ‡p<0.001.

TL=true lumen. TAL=total arterial lumen.

Figure legends

Figure 1. Illustration of the 9 points required by the user to start the automated segmentation method of the thoracic aorta. Seven deformable spheroids were inflated inside the thoracic aorta lumen. BCA=brachiocephalic artery, CS=coronary sinus, DIA= diaphragm, LSA=left subclavian artery, SJ= sinotubular junction.

Figure 2. Top: three virtual patches positioned at the brachiocephalic artery, left subclavian artery and at the main entry tear to restrain the deformable surfaces expansion. Bottom: the true lumen segmentation with arrows pointing the patches (left) together with true and total artery lumens centerlines (right).

Figure 3. Equivalent aortic diameter at different levels of the thoracic aorta derived from cross-sectional area measurements. BCA=brachiocephalic artery, CS=coronary sinus, DIA=diaphragm, LSA=left-subclavian artery, SJ=sinotubular junction, TL=true lumen, TAL=total artery lumen.

Figure 4. Correlation between descending aorta TL volume with age before and after normalization by the TAL volume (n=34). TL=true lumen. TAL=total aortic lumen.

Figure 5. Risk model of aortic dissection using thoracic aorta length and mean aortic arch diameter as anatomic variables indexed to age (r^2=0.72, AUC=0.9764). The 90% probability of AAD curves adjusted for age are shown.

FIGURE 1

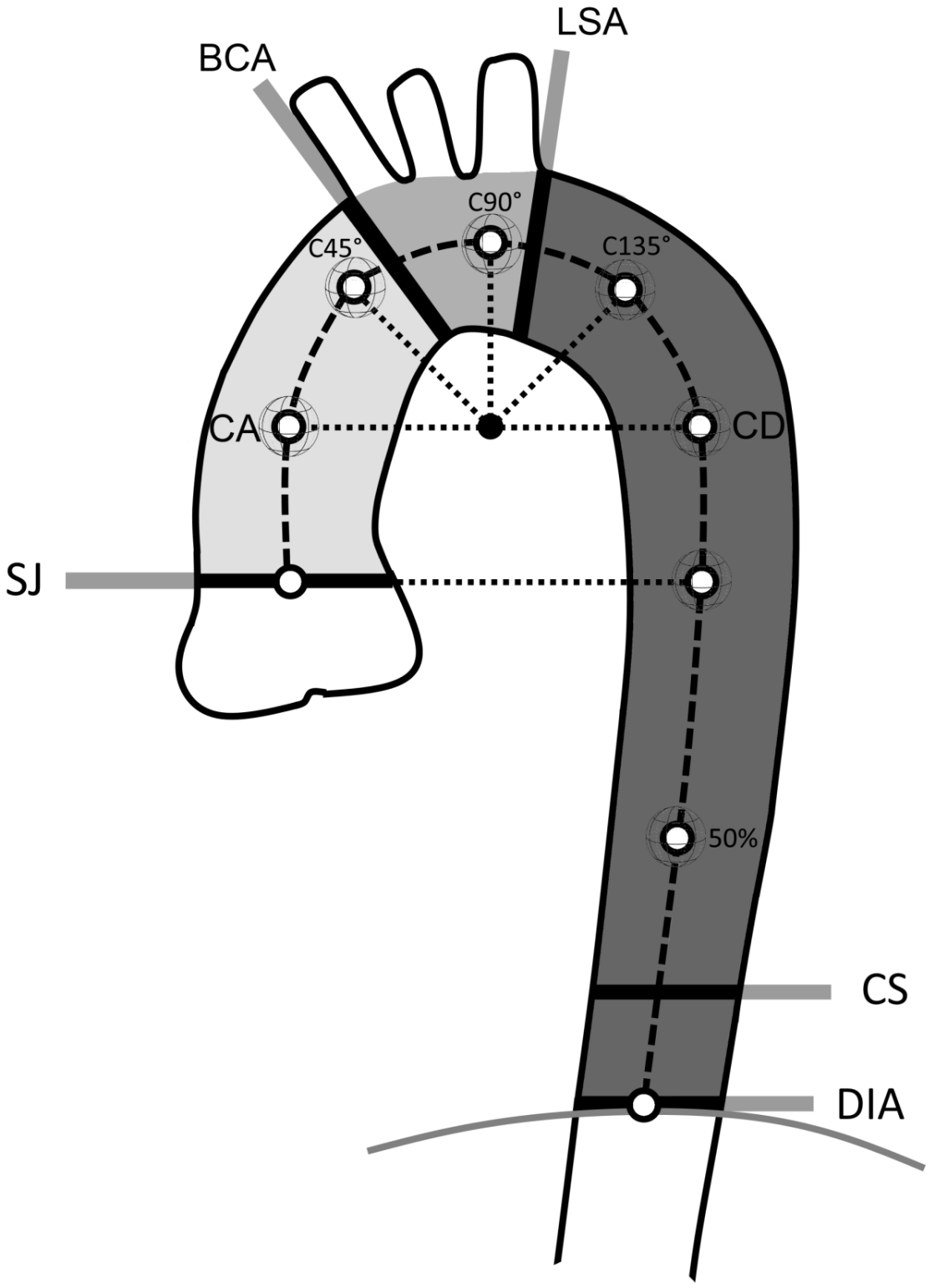

FIGURE 2

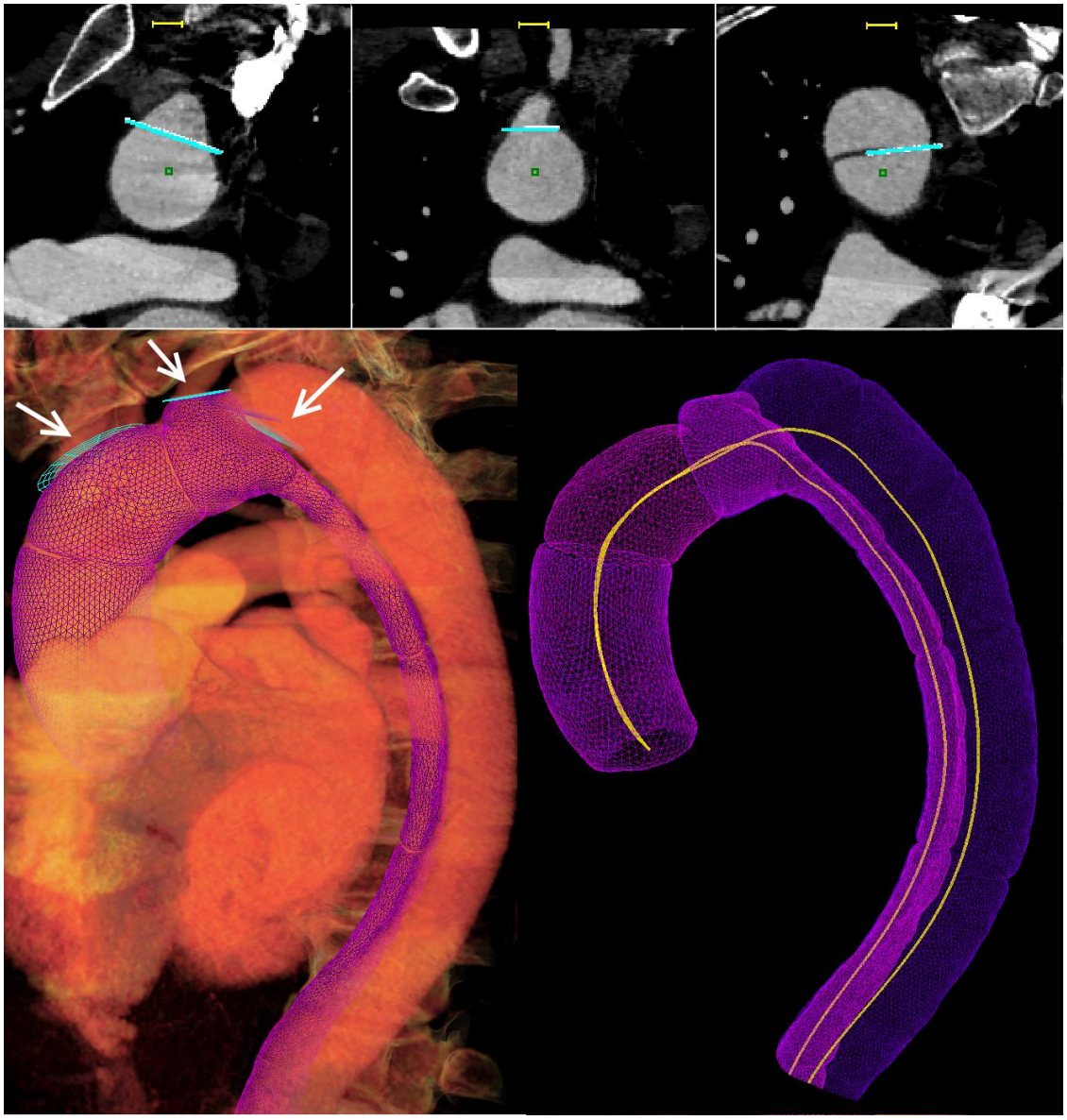

FIGURE 3

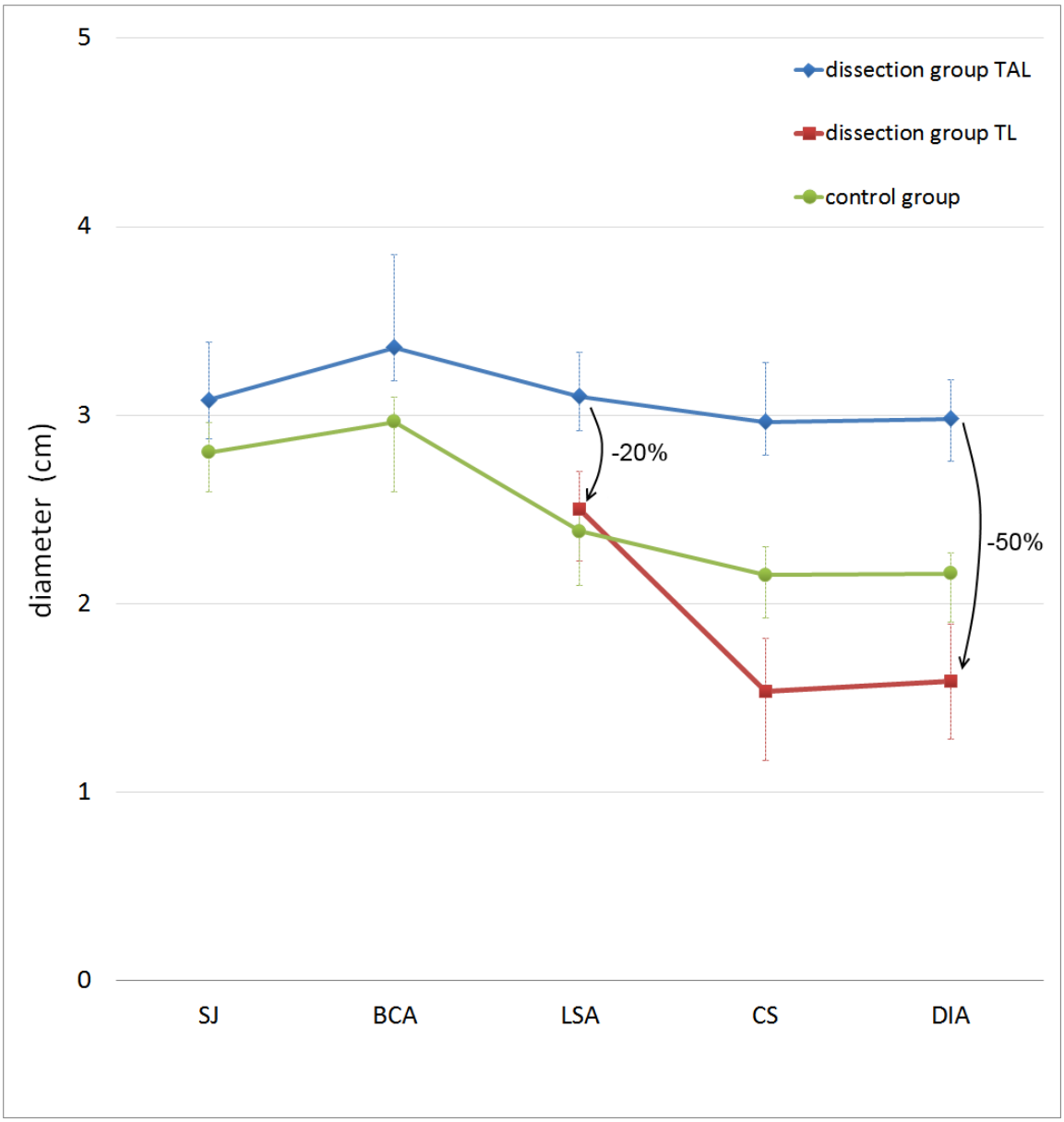
5
4
3
2
1
0
diameter (cm)
dissection group TAL
dissection group TL
control group
-20%
-50%
SJ
BCA
LSA
CS
DIA

FIGURE 4

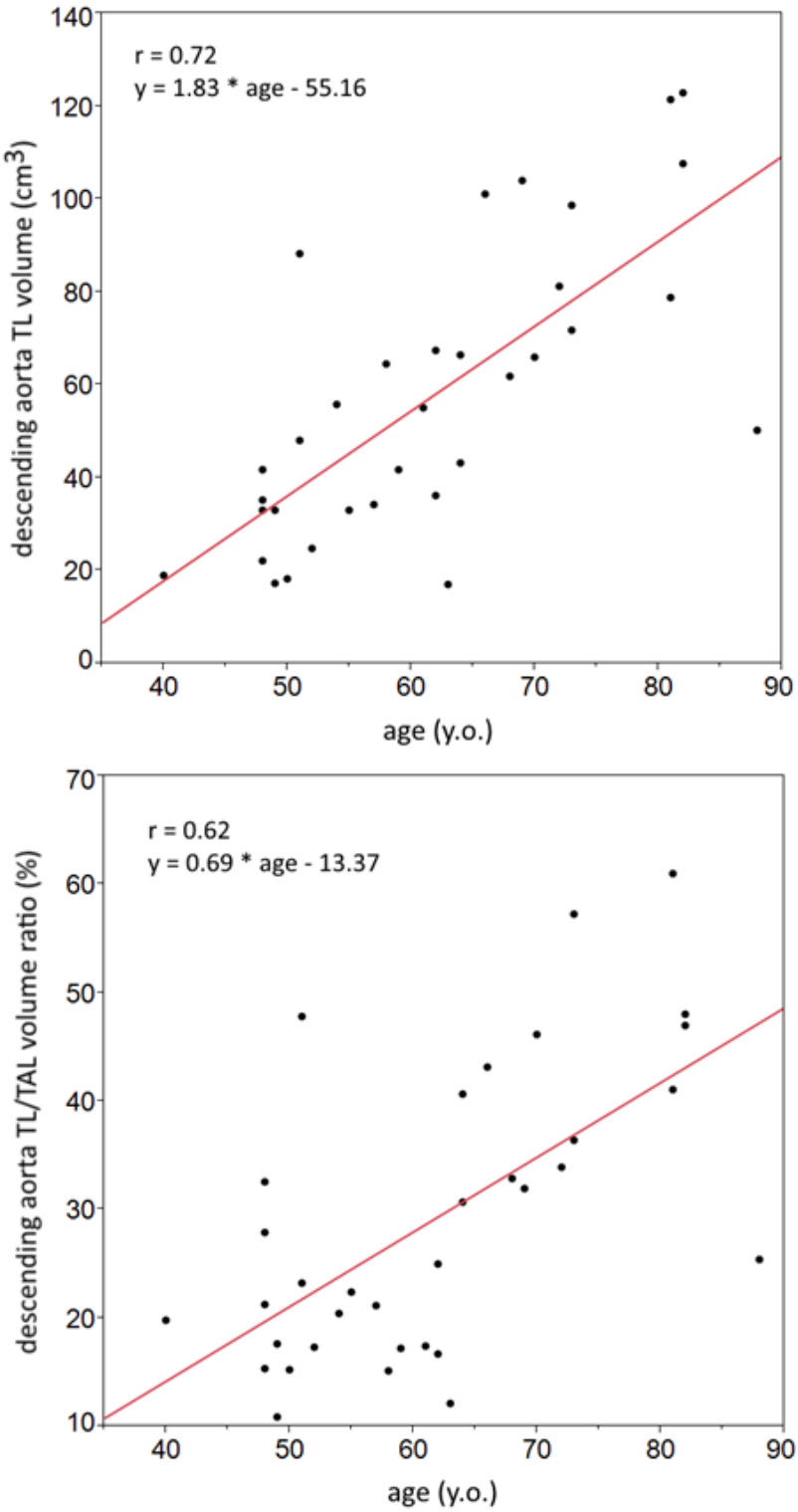
r = 0.72
y = 1.83 * age - 55.16
descending aorta TL volume (cm3)
age (y.o.)
r = 0.62
y = 0.69 * age - 13.37
descending aorta TL/TAL volume ratio (%)
age (y.o.)

FIGURE 5

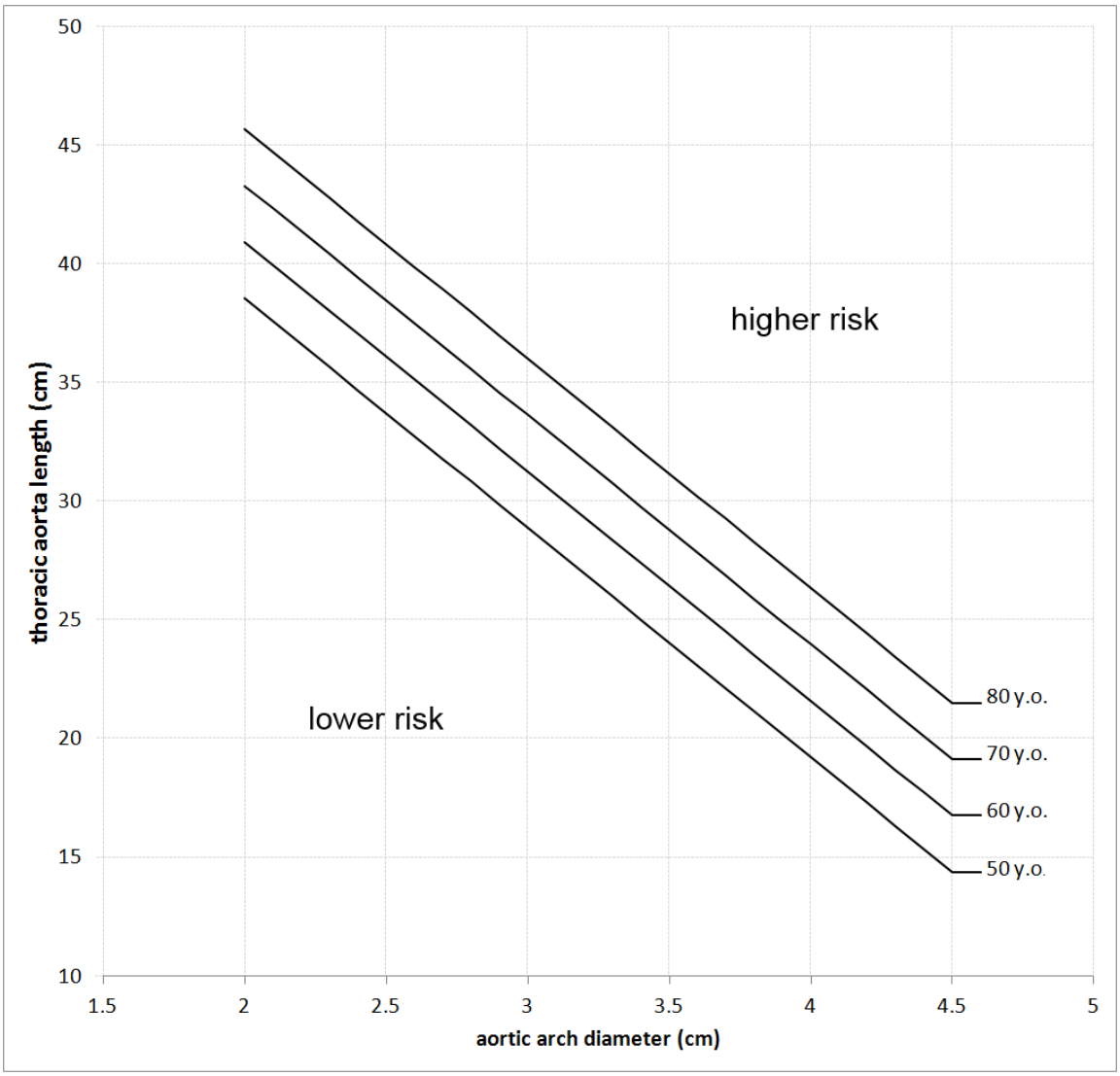
50
45
40
35
30
25
20
15
10
thoracic aorta length (cm)
higher risk
lower risk
80 y.o.
70 y.o.
60 y.o.
50 y.o.
1.5
2
2.5
3
3.5
4
4.5
5
aortic arch diameter (cm)

Chapitre 3

Discussion générale et perspectives

3.1 Résultats principaux

Les principaux résultats de nos travaux sont les suivants :

— La variabilité morphologique de l'aorte thoracique chez les patients asymptomatiques à risque intermédiaire peut se résumer en 3 facteurs : la taille globale du vaisseau, le déroulement et l'asymétrie de la crosse aortique. Ces 3 facteurs synthétisent 80% de la variance totale, avec une contribution cumulée de 46%, 22% et 12%, respectivement. Globalement, la dispersion des variables anatomiques qui décrivent la morphologie de l'aorte reste modérée, de l'ordre de 10%. Un atlas anatomique, qui inclut un catalogue en 3D d'aortes standardisées et leurs principales variantes, a été construit et mis en ligne.

— L'analyse systématique des calcifications dans l'aorte thoracique chez nos patients montre que les régions les plus touchées sont la crosse aortique, suivi par l'aorte thoracique descendante proximale et distale. L'aorte ascendante est la région la moins touchée. Le score calcique est fortement corrélé à l'âge, avec une prévalence de 89% chez les individus de plus de 64 ans. Nos résultats sont originaux dans le sens où la crosse aortique et l'aorte thoracique descendante proximale concentraient 60% des calcifications repérées, mais ces deux régions sont généralement *invisibles* par une TDM de routine sans contraste. En élargissant le champ de façon à inclure la crosse aortique dans notre étude, la prévalence des calcifications a doublé, passant de 31% à 64%. Cela veut dire que 52% des patients auraient échappé à la détection des calcifications avec une imagerie TDM standard.

— Le score de CAT calculé dans la totalité de l'aorte thoracique était associé à la survenue d'événements vasculaires non-cardiaques, indépendamment de l'âge, du sexe et des facteurs de risque cardiovasculaires coexistants. Cette association reste significative quand le score de CAC était rajouté au modèle multivarié. Nos résultats suggèrent que la quantification du score de CAT, peut fournir des informations complémentaires au score de CAC, notamment sur les composantes extra-coronaires du risque cardiovasculaire.

— La géométrie de l'aorte thoracique conditionne la présence, la distribution et l'extension (en volume et en densité) des calcifications aortiques. Les aortes les plus calcifiées étaient les plus grandes, les plus déroulées, les plus tortueuses et les moins sténosées. En particulier, nous avons trouvé que la dilatation de l'aorte thoracique descendante était associée positivement avec le score de CAT, tandis que la taille de l'aorte ascendante ne jouait pas de rôle significatif. Ces différences régionales dans les mécanismes de dilatation et de formation des calcifications suggèrent que les stratégies thérapeutiques de prévention doivent être adaptées aux segments touchés.

— Dans une évaluation volumétrique de l'endoprothèse Nellix^{TM}, basée sur un système d'étanchéité par un polymère, nous avons trouvé que le volume du dispositif implanté rempli de polymère était 23% supérieur au volume de la lumière préopératoire. Les diamètres maximaux ne présentaient pas de différences significatives entre eux. L'expansion du sac anévrismal suite à la pose et au remplissage du dispositif était visualisée et calculée avec une méthode quantitative.

— La probabilité d'avoir une dissection aortique du type B (DATB) augmente en cas de crosse aortique élargie et d'aorte thoracique allongée. Les valeurs seuils de diamètre et de longueur dans le modèle de prédiction de risque augmentent avec l'âge du patient. En fait, le vieillissement était un facteur déterminant de l'anatomie de l'aorte thoracique chez les patients avec et sans DATB. En particulier, suite à la dissection, nous avons trouvé une corrélation positive entre le volume du vrai chenal et l'âge. Ce modèle de prédiction chiffré, et la caractérisation de la morphologie des chenaux sont sensés permettre l'identification des patients vulnérables, et de mieux prévenir ou même traiter les DATB.

3.2 Discussion et perspectives

L'objectif de notre travail était la détermination de l'influence de la géométrie de l'aorte sur les principales maladies qui l'affectent. Pour cela, des outils informatiques originaux ont été développés pour obtenir des mesures tridimensionnelles de la morphologie de l'aorte saine et pathologique à partir des images de TDM. Trois maladies principales atteignant l'aorte ont été abordées : l'athérosclérose calcifiée, l'anévrisme de l'aorte abdominale (AAA) et la DATB. Pour chacune d'entre elles, un module informatique a été conçu et mis au point sur une plateforme informatique pour aider les médecins à réaliser des quantifications géométriques précises et fiables. Ainsi, la morphologie de l'aorte thoracique non-pathologique et la distribution des calcifications ont pu être évaluées chez plus d'un millier de patients sur des images de TDM sans contraste. L'algorithme a été conçu sur le principe d'une forme tubulaire de ces aortes. Les déformations majeures provoquées par les AAA et les DATB nous ont obligé à la conception d'algorithmes plus robustes pour segmenter l'aorte. Par ailleurs, nous avons incorporé des modèles de surfaces déformables et d'algorithmes de visualisation plus performants en traitement d'images pour faire face à ces défis. Avoir la possibilité de se fixer comme objectif une étude morphologique de l'aorte, et pouvoir ensuite développer les outils informatiques spécifiques à cette fin, constituent l'un des avantages de

notre équipe de travail.

L'hypothèse de notre recherche était que la géométrie spécifique des artères de chaque individu joue un rôle additionnel à celui des facteurs de risque traditionnels dans la survenue et le traitement des maladies aortiques. L'hypothèse de l'existence de ces *facteurs de risque géométriques* a été vérifiée par l'étude des calcifications de l'aorte thoracique, par l'analyse du volume du sac anévrismal suite à la pose d'une endoprothèse, et par l'identification des variables anatomiques qui pourraient prédire le risque de dissection. Nous avons trouvé des éléments de preuve essentiels à la répartition hétérogène des calcifications dans l'aorte thoracique, avec une accumulation associée à sa taille et à sa forme. En particulier, une dilatation de l'aorte descendante et un rétrécissement décimé par rapport au diamètre de l'ascendante ont été trouvés chez les patients plus calcifiés, indépendamment d'autres facteurs de risque. Le volume global et la tortuosité ont été aussi détectés comme des facteurs additionnels. De plus, la présence de calcium dans l'aorte thoracique présentait une association plus spécifique avec la survenue d'événements non-cardiaques par rapport aux événements coronaires. Ce lien entre la géométrie aortique et l'événement a été l'objet de plusieurs discussions dans nos articles. Comment savoir, par exemple, si la dilatation de l'aorte descendante ou la progression de la tortuosité associées au score de CAT sont une conséquence du taux de calcium pariétal ou sa cause ? En principe, les images de TDM sans contraste ne permettent pas la discrimination entre des calcifications dans l'intima ou dans la media, et donc la séparation des comportements athéroscléreux de ceux liés à une augmentation de la rigidité. Pourtant, quelques pistes peuvent être explorées pour répondre à cette question à partir des simulations numériques disponibles dans la littérature.

La concentration des lésions observées dans certaines régions de la crosse aortique et de l'aorte descendante (alors que l'aorte ascendante restait épargnée par les calcifications) suggère leur association aux conditions biomécaniques et hémodynamiques liées à la géométrie. Il existe des explications possibles à cette prédilection des lésions sur certains sites. Les notions qu'un débit perturbé et que les tensions sur la paroi artérielle pourraient conditionner l'apparition de plaques d'athérome sont généralement acceptées dans les simulations numériques [54, 97]. Alors que les tensions de cisaillement non-oscillatoires facilitent la formation de plaques et d'infiltrations lipidiques, les calcifications sont plutôt formées dans les régions ou les tensions de cisaillement sont faibles mais avec des fluctuations rapides [116]. Il se trouve justement que la courbure interne de la crosse aortique et la paroi postérieure de l'aorte descendante sont les régions où se produit une inversion de flux en diastole dont résulte une tension de cisaillement oscillatoire. Ce phénomène a été aussi observé au niveau de vaisseaux irréguliers ou très tortueux. Par exemple, des simulations de flux chez des lapins ont montré que les régions à proximité du canal artériel et des branches intercostales produisent des ondulations géométriques de la tension de cisaillement, ce qui les rendent plus vulnérables à la formation de plaques [114]. Toutes ces régions vulnérables étaient particulièrement touchées par des calcifications chez nos patients. En revanche, quand les vitesses du flux s'accélèrent, d'autres hypothèses qui reposent sur la concentration de LDL aident à comprendre ses effets [43]. Des simulations récentes, qui comprenaient des modèles de transport de LDL, ont montré que les profils de vitesse hélicoïdales présents dans l'aorte ascendante empêchaient la formation de dépôt lésionnel [72]. Avec un raisonnement similaire, un rétrécissement du calibre de l'aorte (nommé *tapering* en anglais) qui accélère les vitesses dans les segments distaux, pourrait empêcher la stagnation du flux et éviter la

formation de plaques. Toutes ces simulations numériques sont cohérentes avec nos résultats et nous aident à expliquer comment la géométrie de l'aorte conditionne les profils de vitesse du flux, qui ensuite impactent le développement d'athérosclérose.

Par ailleurs, nos travaux montrent que la morphologie aortique a une influence non seulement sur la localisation des calcifications mais également sur leur quantité et leur densité. La méthode d'Agatston quantifie le nombre, la taille et la densité des calcifications. Elle peut être appliquée sur les calcifications coronaires (score de CAC) et aortiques (score de CAT) repérées par une TDM cardiaque sans injection. La méthode standard qui explore les artères coronaires est utilisée pour visualiser en partie l'aorte, mais exclut la partie supérieure de la crosse. Nous avons décidé de rajouter cette région dans nos explorations et ainsi d'étudier pour la première fois le score de CAT global et sa valeur prédictive dans une population à risque intermédiaire. Notre travail a permis de montrer que cette région curvilinéaire inexplorée concentrait la plupart des calcifications. Plusieurs variables anatomiques étaient associées au score de CAT, dont l'influence de la taille de l'aorte thoracique descendante, et l'absence de calcification au niveau de l'aorte ascendante. De plus, nos résultats suggèrent que le score de CAT peut être un meilleur prédicteur des événements non-cardiaques que le score de CAC, qui est plutôt associé aux événements cardiovasculaires. Cela s'explique probablement par la possibilité que le score de CAT représente en partie les effets liés à l'athérosclérose mais aussi à l'artérosclérose, comme nous avons discuté dans les Articles #3 et #4. Quelques aspects limitant nos résultats doivent être mentionnés, ainsi que les perspectives envisageables à court terme pour les surmonter. L'exploration de l'aorte abdominale peut être reproduite facilement avec les méthodes déjà disponibles dans la plateforme et qui sont d'ailleurs en ce moment même en train d'être évaluées. De plus, de nouveaux appareils permettant une acquisition à faible dose de meilleure qualité (avec et sans contraste) seront bientôt disponibles à l'hôpital. Avec cette nouvelle technologie, les dépistages des calcifications dans toute l'aorte (incluant l'aorte abdominale) seront envisageables avec une quantification anatomique simultanée. Une systématisation de cette exploration globale de l'aorte et la mis en œuvre d'une étude longitudinale, nous donneront la possibilité de mieux détecter et suivre les patients les plus vulnérables sur la base de leur morphologie aortique et de leur score calcique, au delà des facteurs de risque traditionnels.

Dans l'évaluation volumétrique de l'aorte pathologique, les méthodes de surface déformable ont fait la preuve de leur performance appropriée, flexibles et intuitives pour l'opérateur. Elles ont d'abord servi à segmenter le sac anévrismal avant et après la pose d'une endoprothèse Nellix^{TM}(basée sur un système d'étanchéité par un polymère). Nos mesures ont montré que la pose de cette endoprothèse, qui se fait selon un critère de monitorage de la pression, dilatait les anévrismes de l'ordre de 23% en moyenne. Cette expansion correspond à des déformations de la paroi anévrismale d'entre 6 et 16 mm. Ce type de quantifications volumétriques spécifiques pour chaque patient, permet aussi d'observer graphiquement le déplacement de la paroi exercé par le dispositif (Figure 4 de l'Article #5). Elles donnent un intérêt supplémentaire que les mesures classiques du diamètre maximal ne permettent pas de mettre significativement en valeur. La complexité morphologique des AAA oblige probablement à une étude individuelle pré- et post- opératoire comme celle proposée dans notre travail. Les perspectives sur ce sujet sont nombreuses. Initialement, tous les patients opérés (et même ceux avec traitement médicamenteux) doivent être suivi pour évaluer la progression de l'AAA. Un suivi volumétrique permettra de mieux évaluer la progression

de l'AAA, et les différents types de traitements et modèles d'endoprothèse à envisager. Ce suivi longitudinal est envisagé actuellement avec les méthodes développées. Nous sommes conscients que les outils peuvent être perfectionnés, notamment en terme d'évaluation du volume et de la distribution du thrombus dans le sac anévrismal, qui semblent capitales pour le pronostique de la maladie [42, 81]. Ces résultats sont attendus, particulièrement dans le contexte actuel où les essais cliniques randomisés [27, 102] démontrent que les bénéfices à court terme du traitement par endoprothèse diminue au cours du suivi à long terme, comparés à la chirurgie conventionnelle. Le choix du meilleur dispositif pour chaque individu n'est pas évident. Nous sommes en train d'analyser avec des méthodes de simulation numérique de fluides, quel est l'impact de la pose d'une endoprothèse Nellix^{TM}sur l'hémodynamique autour des artères rénales. La Figure 3.1 montre des résultats préliminaires de ce sujet. La montée de la pression dans cette région rénale en rouge, due probablement au déplacement de la bifurcation aortique imposé par le dispositif, pourrait ainsi être déterminée et comparée avec d'autres modèles de prothèses.

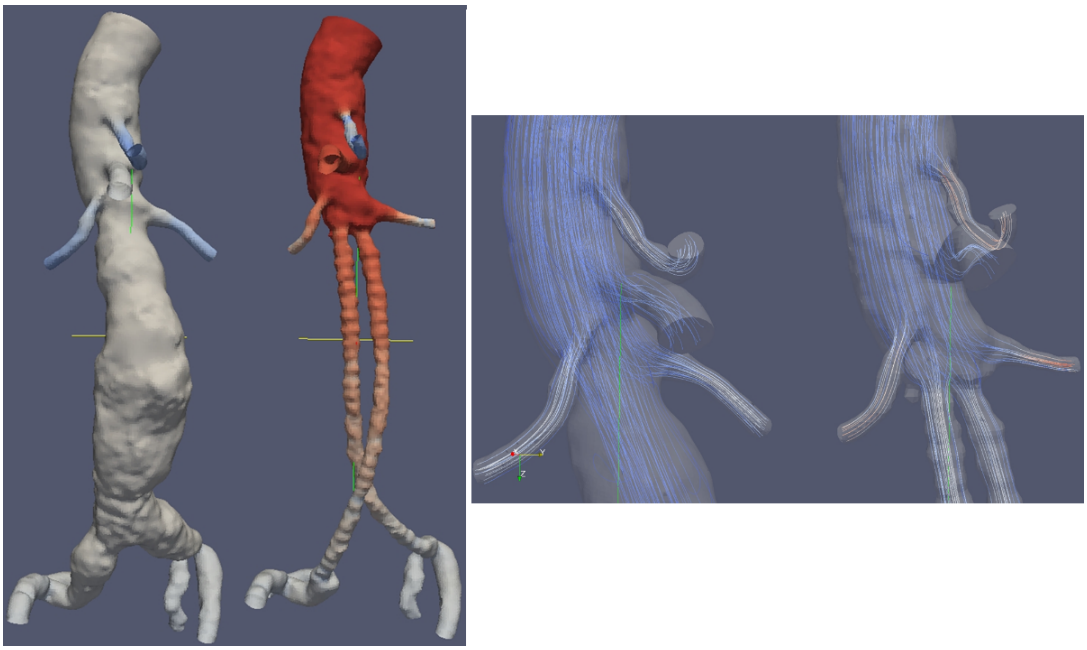

FIGURE 3.1 – Estimation de la pression avec des méthodes de simulation numérique de fluides avant et après la pose d'une endoprothèse Nellix^{TM}.

Dans notre dernier travail, le modèle de surface déformable a été adapté pour être appliqué aux caractéristiques géométriques de l'aorte thoracique en présence d'une dissection de type B. La comparaison avec des patients ayant eu une suspicion de DATB, écartée par les images de TDM, nous a permis de construire un modèle de risque avec des variables anatomiques. Ces variables ont été soigneusement choisies par des méthodes statistiques parmi celles qui n'étaient pas directement contaminées par la dissection. Ni l'hypertension seule, ni l'utilisation d'un diamètre maximal de l'aorte descendante, ne sont suffisantes pour prédire le risque de DATB [110]. La tendance actuelle consiste justement à ajouter des me-

sures tridimensionnelles qui pourraient être faites à partir d'imageries non-invasives [98]. Le diamètre de la crosse aortique et la longueur de l'aorte thoracique étaient automatiquement sélectionnés dans notre modèle de prédiction du risque ajusté à l'âge. Pourtant, le caractère transversal de notre analyse limite son application. Actuellement, une étude prospective est envisagée à l'Hôpital Européen Georges Pompidou dans le cadre du programme *SOS Aorte*, où les patients sont suivis régulièrement pour évaluer la progression de leur dissection. Comme dans le cas des AAA, ce suivi mérite une attention particulière. Le choix entre le traitement médical et la pose d'une endoprothèse chez les patients présentant une DATB non-compliquée reste un sujet d'actualité [96]. Les preuves des bénéfices du traitement par endoprothèse se manifestent à 5 ans, avec une diminution de la mortalité liée à la maladie aortique et à sa progression [79]. Des simulations numériques de flux sont également envisagées, en particulier, par la mise à disposition de nouvelles techniques d'imagerie.

Pour notre travail sur la structure de l'aorte, les images de TDM sont irréfutables, en termes de qualité et de résolution. Pourtant, des analyses fonctionnelles complémentaires sont envisagées à partir de nouvelles séquences d'IRM qui permettent une quantification simultanée de la structure en 3D et de la vitesse des flux en chaque point d'analyse [100]. Même si la résolution spatiale est inférieure, la possibilité d'étudier la déformation de l'aorte au cours du cycle cardiaque permet d'estimer la rigidité artérielle. Avec les calculs de lignes de flux (*streamlines* en anglais), les alternatives pour étudier les portes d'entrée et même les tensions de cisaillements individualisés se multiplient. La fusion des images et des mesures fait partie des défis qui s'imposent à notre équipe de travail à l'avenir.

Enfin, le caractère interdisciplinaire de notre recherche doit être remarqué. Les algorithmes de détections, mesures, visualisations et stockages d'images synthétisées dans la plateforme informatique ont été conçu avec l'aide d'une équipe de collaboration international entre cardiologues, radiologues, chirurgiens et ingénieurs biomédicaux. Les algorithmes spécifiques pour traiter les images sans et avec contraste ont été programmés spécialement pour cette thèse. Quelques impressions 3D ont été testées, comme celles montrées dans la Figure 2.1 de la page 79. De plus, une application pour téléphones portables ou tablettes montrant les reconstructions 3D des anévrismes a été prototypée pour améliorer l'interaction avec les spécialistes en maladies aortiques. Nous sommes convaincus que c'est dans la collaboration multidisciplinaire, dont nos travaux sont le reflet, que se trouve le potentiel nécessaire à l'amélioration de la prédiction précoce des maladies aortiques et de l'évaluation de leurs traitements.

Annexe A

Annexe (Travaux préliminaires)

Annals of Biomedical Engineering, Vol. 40, No. 5, May 2012 (© 2011) pp. 1028–1038
DOI: 10.1007/s10439-011-0487-y

Aging Impact on Thoracic Aorta 3D Morphometry in Intermediate-Risk Subjects: Looking Beyond Coronary Arteries with Non-Contrast Cardiac CT

DAMIAN CRAIEM,[1,2] GILLES CHIRONI,[3,4,5] ALBAN REDHEUIL,[4,6,7] MARIANO CASCIARO,[1,2] ELIE MOUSSEAUX,[4,6,7] ALAIN SIMON,[3,4,5] and RICARDO L. ARMENTANO[1]

[1]Favaloro University, Av. Belgrano 1723, CP 1093 Buenos Aires, Argentina; [2]CONICET, Buenos Aires, Argentina; [3]Centre de Médecine Préventive Cardiovasculaire, Hôpital Européen Georges Pompidou, APHP, Paris, France; [4]Faculté de Médecine, Université Paris Descartes, Sorbonne Paris Cité, Paris, France; [5]Centre de Recherche Cardiovasculaire de l'HEGP (INSERM U970), Paris, France; [6]Département de Radiologie Cardiovasculaire, Hôpital Européen Georges Pompidou, APHP, Paris, France; and [7]Unité INSERM 678, Paris, France

(*Received 2 September 2011; accepted 5 December 2011; published online 16 December 2011*)

Associate Editor Joan Greve oversaw the review of this article.

Abstract—An increasing number of intermediate risk asymptomatic subjects benefit from measures of atherosclerosis burden like coronary artery calcification studies with non-contrast heart computed tomography (CT). However, additional information can be derived from these studies, looking beyond the coronary arteries and without exposing the patients to further radiation. We report a semi-automatic method that objectively assesses ascending, arch and descending aorta dimension and shape from non-contrast CT datasets to investigate the effect of aging on thoracic aorta geometry. First, the segmentation process identifies the vessel centerline coordinates following a toroidal path for the curvilinear portion and axial planes for descending aorta. Then, reconstructing oblique planes orthogonal to the centerline direction, it iteratively fits circles inside the vessel cross-section. Finally, regional thoracic aorta dimensions (diameter, volume and length) and shape (vessel curvature and tortuosity) are calculated. A population of 200 normotensive men was recruited. Length, mean diameter and volume differed by 1.2 cm, 0.13 cm and 21 cm^3 per decade of life, respectively. Aortic shape uncoiled with aging, reducing its tortuosity and increasing its radius of curvature. The arch was the most affected segment. In conclusion, non-contrast cardiac CT imaging can be successfully employed to assess thoracic aorta 3D morphometry.

Keywords—Aging, Aortic arch uncoiling, Aorta 3D reconstruction, Aorta volume, Aorta tortuosity.

INTRODUCTION

Cardiovascular disease is the most costly disease in developed countries and is even more costly than all cancer-related morbidity and mortality combined.[23] Since unexpected death is the most common manifestation of the disease, primary prevention should be potentiated to early and efficiently detect its genesis. Once the disease is diagnosed, a complete set of pharmacological therapies are available for its treatment.[6] In clinical practice, asymptomatic individuals are usually classified in low, medium or high risk groups, with respect to traditional risk factor scoring, predicting future coronary events at 10 years.[15] However, most of the asymptomatic patients are not aware of their subclinical disease and might skip detection by the risk profile algorithms.[16] In fact, most heart attacks and strokes occur in people at average risk scores who are misclassified.[20] On the basis of these observations, new screening tools are needed to early detect the silent development of the disease.[27]

Some measures of disease burden in clinical practice, as coronary artery calcification (CAC) with non-contrast heart computed tomography (CT), intima-media thickness and plaques assessment with ultrasound or the ankle-brachial index, have been included in recent guidelines.[14] The aim of these subclinical measures is to take into account the individual actual burden of atherosclerotic disease. Specifically, CAC scores quantify the calcified plaque in the epicardial coronary arteries that has confirmed its incremental value above conventional measures of predicting cardiovascular events in patients at medium risk.[3,25] Current state of the art employ multislice computed tomography techniques to assess CAC from a non-contrast triggered heartscan using a relatively low radiation dose. However, further information could be derived from these heartscans, looking beyond the coronary arteries. The idea is that the patient might

Address correspondence to Damian Craiem, Favaloro University, Av. Belgrano 1723, CP 1093 Buenos Aires, Argentina. Electronic mail: dcraiem@favaloro.edu.ar

benefit from additional anatomic information that can be provided by the same non-contrast CT scan without any further radiation exposure.

In this context, we propose to estimate the size and the shape of the thoracic aorta exploiting non-contrast CT images from CAC studies. An advanced 3D description of the aortic geometry can be potentially used to better understand the impact of cardiovascular risk factors (i.e., hypertension, smoking status or diabetes) on aortic regional size and shape and to evaluate early aortic aneurysms and endovascular grafts.[9,33] Aortic size is typically assessed with manual measurements of ascending and descending aortic diameter.[4] Nevertheless, the human aorta has a complex geometry that cannot be properly evaluated with these limited planar estimations focused on two sites.[9] In addition, there is no reason to limit aortic geometry assessment to 2D measurements when volumetric information is available. Several aortic segmentation methods were developed in 3D, including deformable and adapting shape models,[7,10,24] dynamic programing,[18] the Hough transform [2] and active surface approaches.[26] A detailed list of reports, including aortic segmentation for aneurysms detection, can be found elsewhere.[33] Recently, also a 4D aortic tracking algorithm was reported using magnetic resonance images.[34] Nevertheless, as far as we know, 3D segmentation algorithms that extract the thoracic aorta geometry from non-contrast cardiac CT scans used in CAC studies have not been reported at the moment in a large cohort of patients.

In this work we developed a new potential diagnostic tool to examine the thoracic aorta morphometry using non-contrast CT images. We proposed a semi-automatic algorithm that minimized user intervention. The thoracic aorta centerline was extracted and its cross-sectional area (CSA) was estimated in the ascending, arch and descending portions. Several descriptors of the aortic size and shape were calculated. In this first protocol, the algorithm was evaluated in 200 normotensive subjects at intermediate 10-year Framingham risk score [15] to investigate the association of aging on thoracic aorta morphometry. A reproducibility analysis and a phantom validation were included in this study.

METHODS

The reported method consists of three main stages: centerline extraction, CSA estimation and morphometric calculations. The algorithm is based on the observation that the aortic cross-section is approximately circular and the curvilinear part of the vessel forms a torus. The coordinates of the thoracic aorta centerline are first extracted. Then, orthogonal planes to the centerline curve direction are calculated at each centerline coordinate and circles are fitted to estimate the vessel CSA. In a third and last stage, the thoracic aorta size and shape descriptors are calculated using the centerline coordinates and their associated CSA values. All the algorithms were programed in C++.

Centerline Extraction

The user selects the starting axial slice at the center of the pulmonary artery level and places 2 initial seed points inside the ascending and descending aorta cross-sections (Fig. 1a). This starting plane is the one usually employed to manually measure the ascending and descending aortic diameter.[4] Using these 2 seed points, the automated process extracts the thoracic aorta centerline and estimates the vessel CSA at each centerline coordinate as explained next.

We propose an adaptive circle-fitting algorithm that finds the largest circle inscribed into the vessel cross-section using planes orthogonal to the vessel centerline. This circle-fitting algorithm starts automatically setting a 10 × 10 cm ROI, centered in a seed point inside the vessel cross-section. Then it performs four steps:

Step 1. A median filter that eliminates spurious pixels

Step 2. A morphological gray-scale opening transformation (erosion followed by dilation) with a circle ($r = 1$ cm) as the structuring element that isolates the vessel from surrounding tissues. The aim of this filter was to separate the vessel from surrounding tissues with circular/elliptical shapes of radius below 1 cm

Step 3. A k-means algorithm with two clusters (binarization)

Step 4. A growing circle iterative algorithm is performed. A circle ($r = 5$ pixels) is placed on the seed point and then the algorithm iteratively expands the circle pixel by pixel and corrects its center when it touches a border, ensuring that all circle points rest inside the vessel outer borders. A similar algorithm can be found in Funka-Lea *et al.*,[11] where the growing algorithm was employed to determine the ellipsoid of maximum volume contained within the heart

Once the iterative process in Step 4 ends, the (x, y, z) coordinate of the circle center is considered as a valid point of the aortic centerline and its surface the corresponding CSA value.

The circle-fitting algorithm is initially applied on the ascending and descending seed points placed by the user in the starting axial plane, to find the centerline points C_A and C_D, respectively (white circles in Fig. 1a).

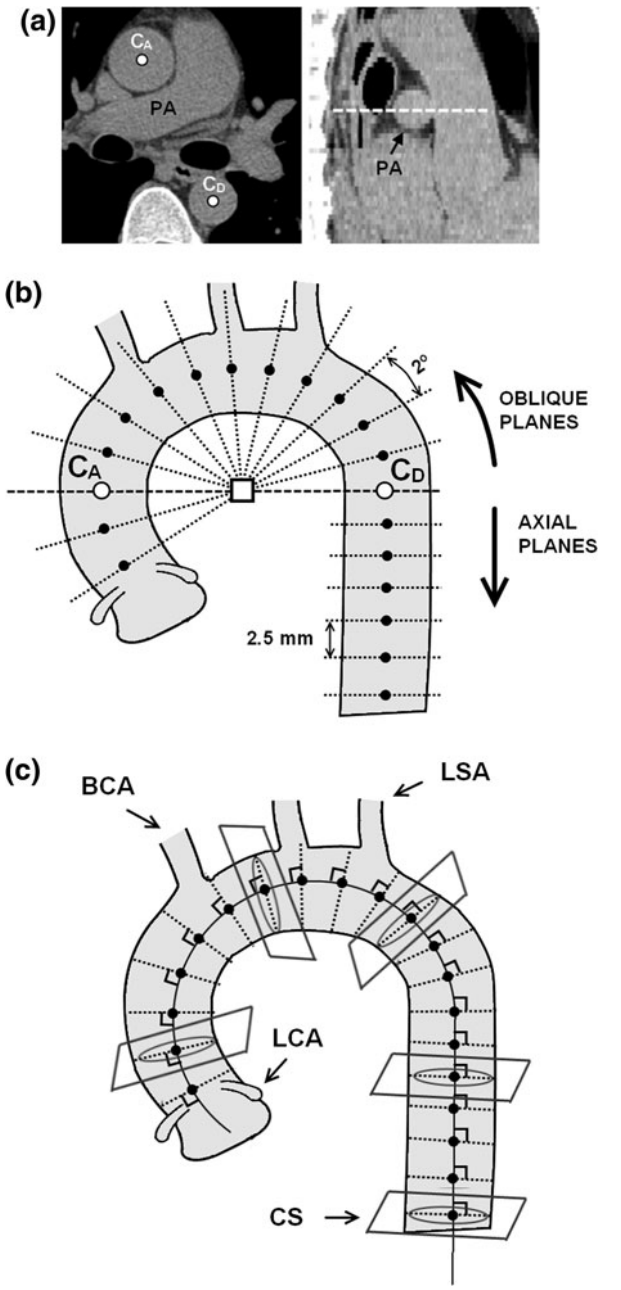

FIGURE 1. Thoracic aorta morphology extraction. (a) Image of the axial initial plane corresponding to the center (dashed line) of the pulmonary artery (PA). The user placed seed points C_A and C_D (white circles) inside the ascending and descending aorta, respectively. (b) Axial and oblique planes are reconstructed to extract the aortic centerline coordinates. (c) Aortic cross-sectional area is measured in each centerline coordinate following an orthogonal direction to the centerline curve. LCA: left coronary artery; BCA: brachiocephalic artery; LSA: left subclavian artery; CS: coronary sinus.

The aortic centerline is estimated separating the vessel into 2 portions. First, axial images are analyzed below the descending aorta seed point C_D (toward diaphragm). Accordingly, the circle-fitting algorithm determines the centerline points C_i of the descending aorta portion (black circles in Fig. 1b under C_D). For each successive plane i, the preceding C_{i-1} circle center is used as the current seed point. Second, and above the descending aorta seed point C_D (toward the annulus), images reformatted from oblique planes following a torus sector are employed (Fig. 1b). This curvilinear portion of the vessel corresponds to the rest of the aortic descending, arch and ascending parts. Instead of using axial slices, oblique planes are reconstructed pivoting in 2° steps around the mid-point between C_A and C_D (open square in Fig. 1b). A detailed description of the reconstruction can be found in Appendix. Images of the oblique planes were calculated using a trilinear interpolation to obtain a resolution of ≈0.5 mm (similar to axial resolution). Again, for each successive oblique plane i, the previous C_{i-1} circle center is used as the current seed point for the new estimation. The planes turn from angle 0° (seed point C_D), passes through the top of the arch at 90°, then by the ascending seed point C_A at 180°, until angle 240° at the annulus. It is worth noting that, even if in some oblique planes the aortic CSA results in an ellipsoidal shape, the algorithm always inscribes the largest achievable circle within vessel outer borders and adds the inscribed circle center as a new valid centerline coordinate. The circles dimensions are not employed in this stage because (so far) the planes are not strictly orthogonal to the centerline. At this stage, assuming planes perpendicular to the axis of rotation for the descending portion of the aorta and oblique planes perpendicular to a 240°-toroid for its curvilinear path, the 3D coordinates of the thoracic aorta midline are estimated. The discrete centerline coordinates are finally interpolated and smoothed to construct an approximated aortic centerline curve.

CSA Estimation

In this stage, orthogonal planes to the direction of the centerline curve extracted in the last section are calculated for each centerline point (Fig. 1c). Within these oblique plane images, circles are inscribed for a second time inside the vessel outer borders. Again, for each plane, current seed points are adopted from the precedent estimation. The aortic cross-sectional shape results roughly circular because planes are now closely perpendicular to the centerline path. Each aortic centerline coordinate is now associated to its corresponding CSA value.

Thoracic Aorta Dimensions

The aortic external surface was approximated in 3D as a pile of cylinders perpendicular to the aortic centerline curve (Fig. 2a). Using a custom plane reconstruction tool, that allowed to virtually travel perpendicularly through the aortic centerline, the user

was asked to identify 4 particular anatomical planes: coronary sinus (CS), left subclavian artery (LSA), brachiocephalic artery (BCA) and left coronary artery (LCA). These 4 planes divided the aorta into the ascending (from LCA to BCA), arch (from BCA to LSA) and descending (from LSA to CS) portions (Fig. 2a). The measured CSA values were represented with respect to the centerline coordinates distance to the coronary sinus (Fig. 2b). The area under the curve represents the thoracic aorta volume. Ascending, arch and descending aorta volume, length, mean CSA and mean diameter values were calculated for each patient.

Thoracic Aorta Shape

Average aortic curvature and tortuosity were calculated for the portion starting at the coronary sinus up to the descending seed point C_D using the definitions in Wood *et al.*[32] Average curvature (AC) was defined as

$$\mathrm{AC} = \frac{\sum_i |k_i|}{N}$$

where k is the curvature at a point (x, y, z) of the centerline curve defined as the derivative with respect to the arc length s of the tangent direction:

$$k = \sqrt{\left(\frac{d^2x}{ds^2}\right)^2 + \left(\frac{d^2y}{ds^2}\right)^2 + \left(\frac{d^2z}{ds^2}\right)^2}$$

The arch radius of curvature was defined as the inverse of AC. Aortic tortuosity is defined as the incremental curve length L_C to the straight line distance d between its end points (coronary sinus and C_D):

$$\mathrm{AT} = \frac{L_C - d}{d}$$

The aortic arch height was defined as the distance from the center of the aortic arch (mid-point between C_A and C_D) to the aortic centerline coordinate corresponding to 90°. The aortic arch width (AAW) was calculated as the distance between C_A and C_D. The aortic arch radius was defined as AAW/2.

EXPERIMENTAL METHODS

Population

The study population comprised 200 men addressed for 1-day hospitalization between September 2009 and October 2010 in the framework of an ongoing cardiovascular risk screening program based on cardiovascular risk stratification including subclinical atherosclerosis imaging.[4] Subjects were asymptomatic and randomly selected from the hospital database. Hypertensive patients were not included in this study, hypertension being defined by resting brachial blood pressure of 140 and/or 90 mmHg or above, and/or by presence of antihypertensive medication. All subjects were free of any overt cardiovascular disease and symptom. They had undergone non-contrast cardiac CT for coronary calcium scoring in view of cardiovascular risk reclassification because they were at intermediate Framingham score, i.e., they had 6–20% probability of coronary event in the next 10 years.[14] The retrospective analysis of personal health data of study subjects had the authorization of the CNIL

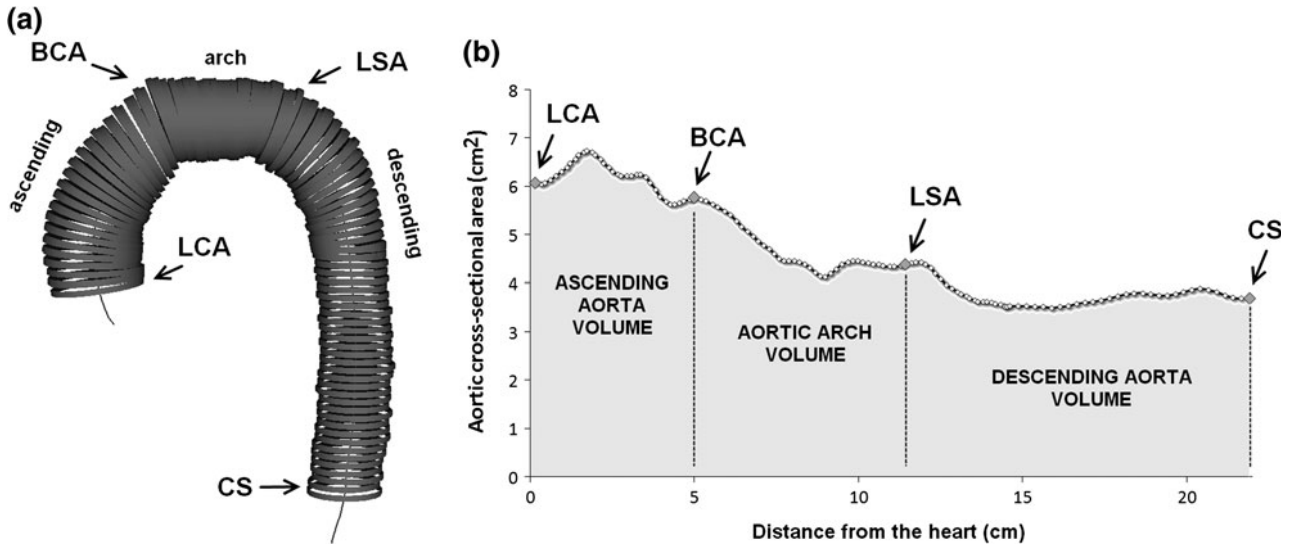

FIGURE 2. (a) Three-dimensional reconstruction of the thoracic aorta. Ascending aorta goes from left coronary artery (LCA) to brachiocephalic artery (BCA), aortic arch from BCA to left subclavian artery (LSA) and descending aorta from LSA to coronary sinus (CS). (b) Aortic cross-sectional area evolution from LCA to CS for a representative subject. Aortic volumes for each portion were calculated from the area under this curve.

(Commission nationale de l'informatique et des libertés) and was in accordance with the declaration of Helsinki.

Image Data Acquisition

Images were obtained with a 64-slice MSCT scanner (Light-speed VCT; GE Health care, Milwaukee, WI, USA) using 2.5 mm slice thickness, 120 kV, 250-mA tube current, 250-ms exposure time, a 2350-mm field of view and ECG triggering at the heart rate-dependent 60% percentage of the *R–R* interval (middle of diastole). Images were acquired in the craniocaudal direction from the top of the aortic arch to the level of the diaphragm in a single breath-hold for all examinations. They were transferred to a dedicated workstation (Advantage window, GE Healthcare; NetraMD; ScImage, Los Altos, CA, USA) and exported as DICOM files. The same reader imported these files and measured all the patients using the designed software.

Reproducibility Analysis, Phantom Validation and Manual Comparison

Duplicate readings of the same scan in 30 randomly selected subjects (aged 58 ± 9 y.o., $p = 0.33$ with respect to whole population) allowed determining coefficients of variation (CV) of thoracic aorta size measurements. A second observer read the same 30 scans for an inter-observer comparison. The algorithm was also tested on an aortic arch phantom consisting in a 70 cm flexible tube with a constant external diameter of 3.85 cm.

At the starting axial plane, the semi-automatic method was also compared against manual measurements of the ascending aorta diameter. Mean differences, CV and Pearson correlation coefficients were calculated.

Associations of Aging with Thoracic Aorta Geometry

Associations of aortic dimensions with age were tested by linear regression models after adjusting for body surface area (BSA). Statistical significance was set at $p < 0.05$. All statistical analyses were performed with JMP (SAS NC USA) software. The association of aging with thoracic aorta dimension and shape was also analyzed by separating the patients according to age tertiles and averaging aortic diameter differences and 3D centerline curves between each group. In the latter, all vessels were centered on the mid-point C_A–C_D and coordinates of aortic centerlines were averaged.

RESULTS

The clinical characteristics of the study population are summarized in Table 1. Most of the patients were hypercholesterolemic (78%), 6% were diabetics and 26% smokers. The algorithm successfully assessed the dimensions and shape of all the 200 thoracic aortas. The dimensions of the vessel were described using length, mean diameter and volume. Results are shown in Table 2. For a total length of ≈25 cm, ascending and descending aorta portions represented 25 and 64% of total aortic length, whereas these proportions were 33 and 54% of total aortic volume, respectively. Thoracic aortic diameter regularly decreased from 3.2 cm in ascending to 2.5 cm (−22%) in descending aorta portion. The shape of the curvilinear part of the vessel from 0° to 180°, including parts of the ascending and descending aorta and the entire aortic arch, were described using the aortic arch width (AAW) and height, its curvature and tortuosity. The arch height was 21% larger than its radius (AAW/2). The aortic arch radius of curvature (calculated as the inverse of an average

TABLE 1. Clinical characteristics of the study population.

	Value	Range
Number	200	
Male gender, *n* (%)	200 (100)	
Age (years)	54 ± 8	31–73
BSA (m^2)	1.98 ± 0.16	1.56–2.50
Blood pressure (mmHg)		
Systolic	119 ± 10	95–139
Diastolic	72 ± 7	51–89
Hypercholesterolemia, *n* (%)	155 (78)	
Diabetes, *n* (%)	12 (6)	
Current smoking, *n* (%)	51 (26)	

Data are means ± SD or number of subjects (%).

TABLE 2. Morphometric measurements of the thoracic aorta in 200 normotensive men.

Thoracic aorta dimension and shape	Mean ± SD
Length (cm)	
Total	24.9 ± 2.2
Ascending	6.1 ± 0.7
Arch	2.8 ± 0.6
Descending	16.0 ± 1.8
Mean diameter (cm)	
Total	2.9 ± 0.2
Ascending	3.2 ± 0.3
Arch	2.8 ± 0.2
Descending	2.5 ± 0.2
Volume (cm^3)	
Total	148 ± 30
Ascending	49 ± 12
Arch	17 ± 5
Descending	81 ± 17
Arch width (cm)	7.6 ± 1.0
Arch height (cm)	4.6 ± 0.6
Arch radius of curvature (cm)	3.1 ± 0.4
Arch tortuosity	0.9 ± 0.2

Data are means ± SD.

curvature) resulted 18% smaller with respect to the arch radius, suggesting an uncoiled shape with respect to a perfect 180°-toroid. Tortuosity values were ≈0.9, meaning that the curve length was almost twice the distance from extreme points (C_A and C_D). For comparison, the tortuosity of a perfect 180°-toroid is ≈0.6.

Table 3 presents the relationship of aging (per decade of life) with morphometric measurements, adjusted to BSA. To visualize the effects, patients were also separated in groups of young (30–49 y.o., $n = 60$), middle-age (50–58 y.o., $n = 78$) and older (59–73 y.o., $n = 62$) according to age tertiles and averaged aortic dimension and shape were sketched in Figs. 3 and 4, respectively. Globally, thoracic aorta size significantly increased with each decade of life: length increased at a rate of 1.2 cm ($p < 0.001$), mean diameter 0.13 cm ($p < 0.001$) and aortic volume 21 cm^3 ($p < 0.001$). The aortic arch was the segment with the most important change in length and volume. Mean aortic diameter increase was homogeneous between segments as can be corroborated from Fig. 3. The effect of this global enlargement with aging on the thoracic aorta shape is shown in Fig. 4, where young and older patients were compared. Aging was associated with an uncoiling effect on the curvilinear portion of thoracic aorta, evidenced by the shape descriptors listed at the end of Table 3. The aortic arch width and height increased 9% ($p < 0.0001$) and 6% ($p < 0.001$) per decade, respectively. Accordingly, the aortic arch radius of curvature increased 7% ($p < 0.001$) and the aortic arch tortuosity decreased 4% ($p < 0.0001$). From the front view of Fig. 4, it is clear that the aortic portion that goes from the top of the arch (90°) toward the descending aorta (0°) evidenced more deformation than the ascending aorta segment. In the lateral view, a vertical unfolding was also observed in older with respect to young subjects.

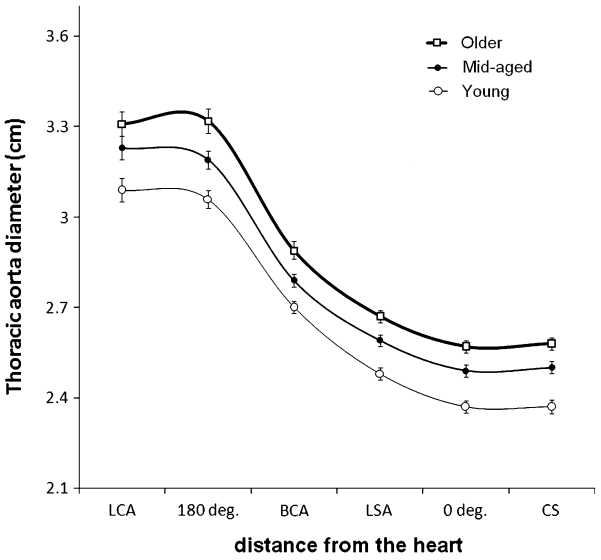

FIGURE 3. Aging impact on thoracic aorta diameter from left coronary artery (LCA) to coronary sinus (CS). Patients were separated by age tertiles in groups of young (30–49 y.o., $n = 60$), mid-aged (50–58 y.o., $n = 78$) and older subjects (59–73 y.o., $n = 62$). BCA: brachiocephalic artery. LSA: left subclavian artery.

TABLE 3. Associations of aging with morphometric measurements after adjustment by body surface area.

Thoracic aorta dimension and shape	β	% change	Model R
Length (cm)/10 years			
Total	1.2 [0.8, 1.6]‡	5	0.43
Ascending	0.2 [0.1, 0.3]†	3	0.26
Arch	0.2 [0.1, 0.3]†	7	0.26
Descending	0.8 [0.5, 1.1]‡	5	0.37
Mean diameter (cm)/10 years			
Total	0.13 [0.10, 0.16]‡	4	0.58
Ascending	0.15 [0.10, 0.20]‡	5	0.51
Arch	0.12 [0.09, 0.15]‡	4	0.53
Descending	0.12 [0.10, 0.15]‡	5	0.60
Volume (cm^3)/10 years			
Total	21 [17, 25]‡	14	0.62
Ascending	6 [5, 8]‡	12	0.51
Arch	3 [2, 3]‡	18	0.49
Descending	12 [10, 15]‡	15	0.60
Arch width (cm)/10 years	0.70 [0.57, 0.82]‡	9	0.65
Arch height (cm)/10 years	0.26 [0.15, 0.36]†	6	0.33
Arch radius of curvature (cm)/10 years	0.21 [0.15, 0.28]†	7	0.30
Arch tortuosity, 1/10 years	−0.04 [−0.07, −0.01]‡	−4	0.49

Data are mean per 10 year change [95% confidence intervals]. $N = 200$ men.
†$p < 0.001$; ‡$p < 0.0001$.

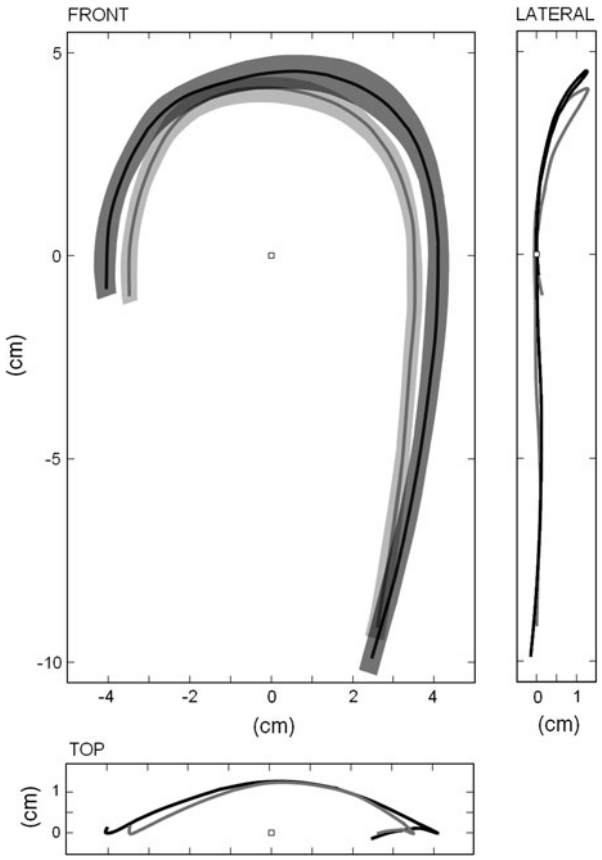

FIGURE 4. Aging impact on thoracic aorta shape. Front, lateral and top view of the averaged 3D thoracic aorta centerline reconstruction for young (gray line, 30–49 y.o., *n* = 60) and older (black line, 59–73 y.o., *n* = 62) subjects. In the front view, standard deviations were also painted. Note the uncoiling effect of aging on thoracic aorta shape.

Duplicate readings of the same scan of 30 subjects of the ascending, arch and descending aorta portions resulted in coefficients of variations (CV) below 4%: CV was 0.2%, 0.3%, and 0.1%, respectively for diameters, 2.1%, 3.5%, and 1.3%, respectively for lengths, and 2.2%, 4.0%, and 1.3%, respectively for volumes. In the inter-observer analysis, coefficients of variations were below 6%: CV was 0.2%, 0.4%, and 0.2%, respectively for diameters, 2.6%, 4.1%, and 2.0%, respectively for lengths, and 2.7%, 4.4%, and 2.0%, respectively for volumes.

In the aortic phantom of 70 cm length, 3.85 cm constant diameter and corresponding volume of 814.88 cm^3 we found (using the semi-automatic algorithm) a measured mean diameter of 3.848 cm (variability of 0.05%) and a total volume of 814.04 cm^3 without significant measurement bias through the tube length.

Manual measurements of the ascending aorta diameter at the starting axial plane resulted 3.3 ± 0.4 cm. Mean differences (±SD) with respect to the semi-automatic measurements were 0.04 ± 0.01 cm. Measurements were highly correlated ($R = 0.93$) with CV = 2.0%.

DISCUSSION

In this cross-sectional study, we proposed a semi-automatic method for a regional 3D description of the thoracic aorta using non-contrast cardiac CT images. We tested our method in a cohort of 200 normotensive men and we report detailed thoracic aorta volumetric information and the associations of aging with the vessel morphometry. The most important findings were that aortic size (diameter, length and volume) and shape (curvature and tortuosity) were significantly and positively associated with age and, whereas the vessel dimensions increased, its shape evidenced a significant uncoiling. As the methodology exploits images from non-contrast cardiac CT studies that are increasingly employed in coronary calcium assessment, new potential clinical applications can be proposed. The discussion is organized in 3 parts and aims to: i) analyze the relationships of aging with aortic morphometry found in our cohort of patients, ii) evaluate the aortic segmentation algorithm and to propose potential applications for it and iii) analyze the limitations of the current study.

Relationships of Aging with Aortic Morphometry

The values found for ascending and descending aortic diameters in our population rested within normal limits. Mean ascending and descending aortic diameters were 3.2 and 2.5 cm, respectively. Wolak *et al.* reported similar values, adjusted to age and BSA in more than 4000 patients, of 3.3 ± 0.3 and 2.5 ± 0.2 cm, respectively.[31] We report a positive age-associated enlargement of thoracic aorta volume that was similar in the ascending, arch and descending aorta portions. We found increments of 14% in volume, 5% in length and 4% in mean diameter per decade of life. The aortic arch being the portion with most important deformation: volume increment was 18% and lengthening 7% per decade. For a first estimation, if the thoracic aorta is considered a deformable cylinder, a 5% increase in length and 4% in diameter, would result in $(1.04)^2 \times 1.05 \approx 14\%$ increase in volume, which is coherent with our findings. The positive association between aging and aortic diameter was widely documented.[4,19,31] Typical aortic diameter enlargement of 0.08–0.12 cm/10 years are in agreement with ≈0.13 cm/10 years found in our study.[1,30] We also found that thoracic aorta lengthened with age at a rate of 1.2 cm/10 years (5%/10 years),

mostly associated to absolute changes in the descending portion. It should be noted that this association persisted after BSA adjustment. Our values agree with thoracic aorta lengthening predicted from Dotter *et al.*[8] model, that used 2D angiocardiographic images. Accordingly, and for an age range of 30–70 y.o., these authors predict values of ≈1.4 cm/10 years (4%/10 years). Recently, Sugawara *et al.*[28] reported lengthening values in healthy adults of ≈0.9 cm/10 years (12%/10 years) related to ascending aorta elongation, with no associations with the descending aorta path. We report an elongation of 3%/10 years for the ascending and 5%/10 years for descending aorta. Some methodological differences could explain these discrepancies. First, our patients were not healthy, accounting 80% of hypercholesterolemic, 30% of smoking and 6% of diabetic patients. Second, Sugawara *et al.*[28] measured with MRI the whole descending portion, from the top of the aortic arch to the level of the common iliac bifurcation (≈40 cm), whereas we stopped at the coronary sinus level (≈16 cm). We decided to analyze the thoracic aorta until that level because that axial plane was easily identified by the user. In fact, beyond the coronary sinus level, the quality of the images suffers a progressive degradation due to CT scan technical limitations. In that sense, Sugawara *et al.*[28] analyzed a longer portion of the aorta and the tethering conditions to surrounding structures could have conditioned the lengthening values. Moreover, the thoracic and the abdominal aorta undergo unequal deformations.[12] While the abdominal aorta shortens with an increase of intravascular pressure, these longitudinal contractions were related to elongations of the thoracic segment.[22] Thus, our estimations of descending aorta lengthening with age cannot be directly compared with other studies performed on thoracic and abdominal aorta segments. Further studies should be performed to clarify this particular issue.

We also report additional 3D information about the shape of the thoracic aorta. The average arch radius of curvature, calculated as the inverse of the aortic centerline curvature, was 3.1 cm. Arch radius (arch width/2) was 3.8 cm and arch height was 4.6 cm. The aging process significantly increased the aortic arch width and, in a lesser proportion, its height and radius of curvature. Aging also produced a significant tortuosity decrease. Based on these observations, while aging induced an important volume increase in all the vessel segments (Fig. 3), the curvilinear portion of the thoracic aorta showed a consequent uncoiling effect. After adjustment for BSA, aortic arch width was the strongest descriptor independently associated with age, accounting for 65% of the model variability (Table 3). This aortic unfolding process is familiar for practicing physicians in chest radiographs reports and can be visualized in Fig. 4, where young and older patients were compared. In the front view, it is clear that the segment that goes from the top of the arch toward the descending aorta is the one that suffers most deformation with aging. It should be noted that this segment includes the aortic isthmus, where around 70% of the post-traumatic lesions are observed.[13] Also, aortic deformations with aging might be associated to "material fatigue" due to the progressive changes in elastic fibers.[21] For that reason, not only aortic volume, length and diameters, but also aortic shape should be evaluated to better understand the influence of cardiovascular risk factors on the vessel geometry.

Aortic Segmentation Algorithm: Potential Applications

Contrast multislice cardiac CT offers excellent time–space resolution for *in vivo* anatomical quantifications but the non-contrast alternative is progressively leading to atherosclerosis burden diagnosis through the coronary artery calcium test (CAC). This test has proved to be reproducible, safe and convenient to quantify atherosclerosis and was recently included in the clinical recommendations to be applied in intermediate risk asymptomatic patients in order to reclassify them at higher risk.[14] Accordingly, the increasing number of patients who undergo CAC tests could directly benefit from the proposed morphometric thoracic aorta estimation with no additional radiation exposure. Contrast CT and MRI techniques provide higher contrast and greater resolution (particularly in the axial direction) with respect to non-contrast CT. In this context, previous works, using robust and objective techniques, were developed to successfully characterize the 3D geometry of arteries.[5,29] However, these methods are not compatible with non-contrast CT image quality where simplified calculations should be proposed. Using non-contrast CT images, traditional methods restrict the aortic size measurement to the ascending and descending diameters. Our main innovation is the estimation of the aortic diameter in ≈150 points all along its length. A vessel is a tridimensional body and volume rather than diameter (or CSA) should be employed to accurately describe its size. The ascending and descending parts of the aorta may roughly follow vertical directions that could be reconstructed with axial planes, but the aortic arch is curvilinear and its 3D description requires custom algorithms. A key advantage of our algorithm is that aorta is segmented from within its lumen. Accordingly, while centerline is extracted and CSA estimated, the vessel is at the same time isolated from different surrounding structures, avoiding unwanted elements to interfere with the segmentation process. The algorithm assumes a circular cross-section and an initial

axial-toroidal path that proved to be efficient for extracting the vessel midline.[17] The application designed to assess thoracic aorta morphometry was fast and straightforward. The user was required in one opportunity to click on the ascending and descending cross-section and then the algorithm took less than 1 min to extract the centerline and reconstruct the aortic shape in 3D with a standard 2.4 GHz computer. The selection of the starting plane was easy for the user because it is the one usually employed to manually measure the ascending and descending aortic diameters.[4] An additional minute was required for the user to identify the 4 anatomical landmarks and to read the morphometric parameters of each aortic portion. The coefficient of variation in duplicate readings of thoracic aorta volume and length were below 4%, in agreement with diameter estimations.[19] Also, the validation of the diameter estimation in the aortic curvilinear phantom showed a small variability of 0.05% along its ≈40 cm length.

Some potential applications of our method can be proposed. The early detection of aortic aneurysms can be envisaged. Even if our algorithm was not specifically designed for that (see limitations), it may further be tested to early detect aneurysms or at least quantify the regional deformation of the thoracic aorta in a large cohort of patients. An increasing number of aortic arch pathologies and endovascular graft designs are now evaluated with imaging techniques that are becoming essential to minimize morbidity and mortality.[33] Finally, a long term objective would be to prospectively study aortic morphometry together with cardiovascular risk factors, where many questions regarding the effects of hypertension or diabetes on thoracic aortic geometry remain to be answered.[4]

Study Limitations

This study has some limitations that must be addressed. First, the study cohort only included men due to a bias in subjects recruitment referred by general practitioners to hospital that reflects lesser attention to cardiovascular preventive intervention in women.[14] Second, we did not include subjects with thoracic aorta aneurysm, because our objective was to assess the feasibility and reproducibility of our algorithm to measure thoracic aorta dimensions, rather than to diagnose aneurysm. Third, as we already mentioned, the subjects examined in this study were not representative of the general population. Patients referred to our cardiovascular prevention unit and undergo CAC detection are generally above-average risk of coronary disease and carry at least one traditional risk factor. However, we decided to only recruit normotensive patients for this study to better isolate other effects as hypertension on thoracic aorta geometry. Even if 80% of the patients were hypercholesterolemic, this condition did not show a particular influence on thoracic aorta dimensions in previous reports.[4,31] In addition, our study was cross-sectional without longitudinal follow-up, and did not allow assessing the actual effects of aging on aortic dimensions and geometry.

Regarding the detection algorithm, 3 limitations should be mentioned. First, the proposed semi-automatic method requires user intervention to set the 2 initial seed points and then to identify 4 landmarks to separate the thoracic aorta into 3 portions. Additional techniques as the Hough transform can be implemented to automatically set the initial seed points and to reduce interobserver variability.[17] Second, the aortic volume was estimated in one instant of the cardiac cycle, assuming a circular cross-section and including the vessel wall. It is clear that the circular cross-section assumption might not be valid in cases of advanced aortic aneurysm. A revised algorithm should be proposed to detect important asymmetrical expansions. The assumption that aortic diameter could be estimated including the vessel wall is generally accepted in non-contrast CT.[9] Third, only the tubular portion of the thoracic aorta was measured, excluding the aortic annulus, due to space resolution limitations inherent to the non-contrast CT technique that did not allow a proper segmentation. Further efforts should be made to improve the aortic segmentation, reducing user intervention and revising the circular vessel cross-section constraint, as well as including the aortic annulus.

APPENDIX

The curvilinear portion of the thoracic aorta was analyzed reconstructing oblique planes that turned around the mid-point between centerline coordinates C_A and C_D as shown in Fig. 1b. Starting from an axial plane P_0, that contain C_A and C_D, the algorithm makes a fixed translation-rotation and a subsequent dynamic rotation pivoting around the center of the aortic arch.

The plane P_0 was defined as:

$$P_0 = \lambda \cdot \hat{x} + \varepsilon \cdot \hat{y} + z_{C_A,C_D} \cdot \hat{z}$$

where $\hat{x}, \hat{y}$ and $\hat{z}$ are the unit vectors of the 3D euclidean space along the coronal, sagital and axial directions of the CT volume, z_{C_A,C_D} is the z-coordinate of the slice containing C_A and C_D and parameters λ, ε are such that:

$$\lambda, \varepsilon \in N^0 / \{\lambda < 512 \wedge \varepsilon < 512\}$$

P_0 was first translated and rotated with the following transformation

$$rtP_0 = R_{\alpha,\hat{z}}(P_0 - \langle P_0 \rangle)$$

where $\langle P_0 \rangle$ is the center-point of the plane P_0 and $R_{\alpha,\hat{z}}$ is the rotation matrix

$$R_{\alpha,\hat{z}} = \begin{bmatrix} \cos\alpha & -\sin\alpha & 0 \\ \sin\alpha & \cos\alpha & 0 \\ 0 & 0 & 1 \end{bmatrix}$$

that aligns P_0 with the vector connecting C_A and C_D. Accordingly, angle α was calculated as:

$$\alpha = a\cos\left(\frac{\hat{x} \cdot (C_A - C_D)}{\|C_A - C_D\|}\right)$$

Finally, the resulting plane was sequentially rotated in 2° steps, using the transformation

$$P_i = R_{\theta_i,u} \cdot rtP_0$$

where $R_{\theta_i,u}$ is the rotation matrix:

$$R_{\theta,u} = \begin{bmatrix} \cos\theta + u_x^2(1-\cos\theta) & u_x u_y(1-\cos\theta) - u_z\sin\theta & u_x u_z(1-\cos\theta) + u_y\sin\theta \\ u_y u_x(1-\cos\theta) + u_z\sin\theta & \cos\theta + u_y^2(1-\cos\theta) & u_y u_z(1-\cos\theta) - u_x\sin\theta \\ u_z u_x(1-\cos\theta) - u_y\sin\theta & u_z u_y(1-\cos\theta) + u_x\sin\theta & \cos\theta + u_z^2(1-\cos\theta) \end{bmatrix}$$

which performs a rotation of θ degrees around the axis u, orthogonal to the segment $\overline{C_A - C_D}$ and the unit vector $\hat{z}$, calculated from the following a vector product:

$$u = \frac{(C_A - C_D) \otimes \hat{z}}{\|C_A - C_D\|}$$

The curvilinear path of the thoracic aorta was covered assigning values of θ_i angle from 0° to 240°.

ACKNOWLEDGMENTS

This work was supported by the project PIP number 112-200901-00734 (CONICET) and the Houssay post-doctoral program (CONICET).

REFERENCES

[1]Agmon, Y., B. K. Khandheria, I. Meissner, G. L. Schwartz, J. D. Sicks, A. J. Fought, W. M. O'Fallon, D. O. Wiebers, and A. J. Tajik. Is aortic dilatation an atherosclerosis-related process? Clinical, laboratory, and transesophageal echocardiographic correlates of thoracic aortic dimensions in the population with implications for thoracic aortic aneurysm formation. *J. Am. Coll. Cardiol.* 42(6):1076–1083, 2003.

[2]Behrens, T., K. Rohr, and H. S. Stiehl. Robust segmentation of tubular structures in 3-D medical images by parametric object detection and tracking. *IEEE Trans. Syst. Man Cybern. B Cybern.* 33(4):554–561, 2003.

[3]Budoff, M. J., and K. M. Gul. Expert review on coronary calcium. *Vasc. Health Risk Manag.* 4(2):315–324, 2008.

[4]Chironi, G., L. Orobinskaia, J. L. Megnien, M. E. Sirieix, S. Clement-Guinaudeau, M. Bensalah, A. Azarine, E. Mousseaux, and A. Simon. Early thoracic aorta enlargement in asymptomatic individuals at risk for cardiovascular disease: determinant factors and clinical implication. *J. Hypertens.* 28(10):2134–2138, 2010.

[5]Choi, G., C. Cheng, N. Wilson, and C. Taylor. Methods for quantifying three-dimensional deformation of arteries due to pulsatile and nonpulsatile forces: implications for the design of stents and stent grafts. *Ann. Biomed. Eng.* 37(1):14–33, 2009.

[6]Chyu, K. Y., and P. K. Shah. Emerging therapies for atherosclerosis prevention and management. *Cardiol. Clin.* 29(1):123–135, 2011.

[7]de Bruijne, M., B. van Ginneken, M. A. Viergever, and W. J. Niessen. Adapting active shape models for 3D segmentation of tubular structures in medical images. *Inf. Process. Med. Imaging* 18:136–147, 2003.

[8]Dotter, C. T., D. J. Roberts, and I. Steinberg. Aortic length: angiocardiographic measurements. *Circulation* 2(6):915–920, 1950.

[9]Elefteriades, J. A., and E. A. Farkas. Thoracic aortic aneurysm clinically pertinent controversies and uncertainties. *J. Am. Coll. Cardiol.* 55(9):841–857, 2010.

[10]Frangi, A. F., W. J. Niessen, R. M. Hoogeveen, T. van Walsum, and M. A. Viergever. Model-based quantitation of 3-D magnetic resonance angiographic images. *IEEE Trans. Med. Imaging* 18(10):946–956, 1999.

[11]Funka-Lea, G., Y. Boykov, C. Florin, M. P. Jolly, R. Moreau-Gobard, R. Ramaraj, and D. Rinck. Automatic heart isolation for CT coronary visualization using graph-cuts. In: Biomedical Imaging: Nano to Macro, 2006. 3rd IEEE International Symposium on, 2006, pp. 614–617.

[12]Gentile, B. J., D. R. Gross, C. J. Chuong, and N. H. Hwang. Segmental volume distensibility of the canine thoracic aorta in vivo. *Cardiovasc. Res.* 22(6):385–389, 1988.

[13]Giulini, S. M., and S. Bonardelli. Post-traumatic lesions of the aortic isthmus. *Ann. Ital. Chir.* 80(2):89–100, 2009.

[14]Greenland, P., J. S. Alpert, G. A. Beller, E. J. Benjamin, M. J. Budoff, Z. A. Fayad, E. Foster, M. A. Hlatky, J. M. Hodgson, F. G. Kushner, *et al.* ACCF/AHA guideline for assessment of cardiovascular risk in asymptomatic adults: a report of the American College of Cardiology Foundation/American Heart Association Task Force on Practice Guidelines. *J. Am. Coll. Cardiol.* 56(25):e50–e103, 2010.

[15]Greenland, P., S. C. Smith, Jr., and S. M. Grundy. Improving coronary heart disease risk assessment in asymptomatic people: role of traditional risk factors and noninvasive cardiovascular tests. *Circulation* 104(15):1863–1867, 2001.

[16]Kannel, W. B., R. B. D'Agostino, L. Sullivan, and P. W. Wilson. Concept and usefulness of cardiovascular risk profiles. *Am. Heart J.* 148(1):16–26, 2004.
[17]Kovács, T. Automatic segmentation of the vessel lumen from 3D CTA images of aortic dissection. In: Selected Readings in Vision and Graphics, edited by L. Van Gool, G. Székely, M. Gross, and B. Schiele. Konstanz: Hartung-Gorre Verlag, 2010.
[18]Kurkure, U., O. C. Avila-Montes, and I. A. Kakadiaris. Automated segmentation of thoracic aorta in non-contrast CT images. In: Biomedical Imaging: From Nano to Macro, 2008. ISBI 2008. 5th IEEE International Symposium on, 2008, pp. 29–32.
[19]Mao, S. S., N. Ahmadi, B. Shah, D. Beckmann, A. Chen, L. Ngo, F. R. Flores, Y. L. Gao, and M. J. Budoff. Normal thoracic aorta diameter on cardiac computed tomography in healthy asymptomatic adults: impact of age and gender. *Acad. Radiol.* 15(7):827–834, 2008.
[20]Muntendam, P., C. McCall, J. Sanz, E. Falk, and V. Fuster. The BioImage Study: novel approaches to risk assessment in the primary prevention of atherosclerotic cardiovascular disease—study design and objectives. *Am. Heart J.* 160(1): 49–57e41, 2010.
[21]O'Rourke, M., A. Farnsworth, and J. O'Rourke. Aortic dimensions and stiffness in normal adults. *JACC Cardiovasc. Imaging* 1(6):749–751, 2008.
[22]Patel, D. J., A. J. Mallos, and D. L. Fry. Aortic mechanics in the living dog. *J. Appl. Physiol.* 16:293–299, 1961.
[23]Roger, V. L., A. S. Go, D. M. Lloyd-Jones, R. J. Adams, J. D. Berry, T. M. Brown, M. R. Carnethon, S. Dai, G. de Simone, E. S. Ford, *et al.* Heart disease and stroke statistics–2011 update: a report from the American Heart Association. *Circulation* 123(4):e18–e209, 2011.
[24]Rueckert, D., P. Burger, S. M. Forbat, R. D. Mohiaddin, and G. Z. Yang. Automatic tracking of the aorta in cardiovascular MR images using deformable models. *IEEE Trans. Med. Imaging* 16(5):581–590, 1997.
[25]Rumberger, J. A. Using noncontrast cardiac CT and coronary artery calcification measurements for cardiovascular risk assessment and management in asymptomatic adults. *Vasc. Health Risk Manag.* 6:579–591, 2010.
[26]Schwartz, E., R. Gottardi, J. Holfeld, C. Loewe, M. Czerny, and G. Langs. Evaluating deformation patterns of the thoracic aorta in gated CTA sequences. In: Biomedical Imaging: From Nano to Macro, 2010 IEEE International Symposium on, 2010, pp. 21–24.
[27]Shah, P. K. Screening asymptomatic subjects for subclinical atherosclerosis: can we, does it matter, and should we? *J. Am. Coll. Cardiol.* 56(2):98–105, 2010.
[28]Sugawara, J., K. Hayashi, T. Yokoi, and H. Tanaka. Age-associated elongation of the ascending aorta in adults. *J. Am. Coll. Cardiol. Imaging* 1(6):739–748, 2008.
[29]Thomas, J. B., L. Antiga, S. L. Che, J. S. Milner, D. A. Steinman, J. D. Spence, and B. K. Rutt. Variation in the carotid bifurcation geometry of young versus older adults: implications for geometric risk of atherosclerosis. *Stroke* 36(11):2450–2456, 2005.
[30]Vasan, R. S., M. G. Larson, and D. Levy. Determinants of echocardiographic aortic root size. The Framingham Heart Study. *Circulation* 91(3):734–740, 1995.
[31]Wolak, A., H. Gransar, L. E. J. Thomson, J. D. Friedman, R. Hachamovitch, A. Gutstein, L. J. Shaw, D. Polk, N. D. Wong, R. Saouaf, *et al.* Aortic size assessment by noncontrast cardiac computed tomography: normal limits by age, gender, and body surface area. *JACC Cardiovasc. Imaging* 1(2):200–209, 2008.
[32]Wood, N. B., S. Z. Zhao, A. Zambanini, M. Jackson, W. Gedroyc, S. A. Thom, A. D. Hughes, and X. Y. Xu. Curvature and tortuosity of the superficial femoral artery: a possible risk factor for peripheral arterial disease. *J. Appl. Physiol.* 101(5):1412–1418, 2006.
[33]Worz, S., H. von Tengg-Kobligk, V. Henninger, F. Rengier, H. Schumacher, D. Bockler, H. U. Kauczor, and K. Rohr. 3-D quantification of the aortic arch morphology in 3-D CTA data for endovascular aortic repair. *IEEE Trans. Biomed. Eng.* 57(10):2359–2368, 2010.
[34]Zhao, F., H. Zhang, A. Wahle, M. T. Thomas, A. H. Stolpen, T. D. Scholz, and M. Sonka. Congenital aortic disease: 4D magnetic resonance segmentation and quantitative analysis. *Med. Image Anal.* 13(3):483–493, 2009.

Journal of Human Hypertension (2013), 1–6

www.nature.com/jhh

ORIGINAL ARTICLE

Three-dimensional evaluation of thoracic aorta enlargement and unfolding in hypertensive men using non-contrast computed tomography

D Craiem[1,2], G Chironi[1,3,4], ME Casciaro[2], A Redheuil[3,5,6], E Mousseaux[3,5,6] and A Simon[1,3,4]

Aging produces a simultaneous thoracic aorta (TA) enlargement and unfolding. We sought to analyze the impact of hypertension on these geometric changes. Non-contrast computed tomography images were obtained from coronary artery calcium scans, including the entire aortic arch, in 200 normotensive and 200 hypertensive asymptomatic men. An automated algorithm reconstructed the vessel in three-dimensions, estimating orthogonal aortic sections along the whole TA pathway, and calculated several geometric descriptors to assess TA morphology. Hypertensive patients were older with respect to normotensive ($P<0.001$). Diameter and volume of TA ascending, arch and descending segments were higher in hypertensive patients with respect to normotensive ($P<0.001$) and differences persisted after adjustment for age. Hypertension produced an accelerated unfolding effect on TA shape. We found increments in aortic arch width ($P<0.001$), radius of curvature ($P<0.001$) and area under the arch curve ($P<0.01$) with a concomitant tortuosity decrease ($P<0.05$) and no significant change in aortic arch height. Overall, hypertension produced an equivalent effect of $2-7$-years of aging. In multivariate analysis adjusted for age and hypertension treatment, diastolic pressure was more associated to TA size and shape changes than systolic pressure. These data suggest that hypertension accelerates TA enlargement and unfolding deformation with respect to the aging effect.

Journal of Human Hypertension advance online publication, 24 January 2013; doi:10.1038/jhh.2012.69

Keywords: thoracic aorta 3D reconstruction; non-contrast MSCT; aortic arch uncoiling; aging; tridimensional image segmentation

INTRODUCTION

The thoracic aorta (TA) is subject to progressive size increase and a concomitant unfolding process.[1–3] The noninvasive assessment of TA geometry was employed to better predict aneurisms, preventing complications as dissection or rupture[4] and also to provide basic information for development of endovascular devices for the aortic arch.[5,6] TA size assessment is traditionally based on the measurement of aortic diameter.[3,7] However, diameter estimation may be a source of error[3,7,8] because TA shape is complex with a curvilinear pathway that produces oblong contours using axial planes.[4] Also, TA size is not reflected solely by diameter because the TA length is another determinant of the vessel size.[4,9,10] Taking into account these considerations, we have recently validated a new automated tool, based on the computerized reconstruction and analysis of orthogonal sections and lengths of ascending, arch and descending TA segments.[11] Briefly, this tool allows for a virtual three-dimensional reconstruction and assessment of the vessel size and shape. This methodology was specifically designed to evaluate patients referred to our department for non-contrast multislice computed tomography assessment of coronary artery calcium (CAC) in view of cardiovascular risk refinement.[8,12,13] Measurements can be done on routine scans, extending the field of view to cover the top of the aortic arch.

Hypertension was identified as a major determinant of aortic size[8,14,15] but its simultaneous influence on the aortic size and shape was less investigated. The aim of the present study was to assess the impact of hypertension on TA geometry, expressed in terms of an equivalent aging factor. Several descriptors were proposed to accurately describe the deformation of the TA curvilinear portion, focusing on its three-dimensional shape.

SUBJECTS AND METHODS

Study subjects

Individuals were initially screened by occupational health physicians or general internists. Those with the presence of at least one established risk factor for coronary heart disease, such as advanced age, hypertension, hypercholesterolemia, diabetes mellitus or current smoking, were referred to hospital for atherosclerosis imaging-based risk management. In the present study, we included 200 normotensive and 200 hypertensive men that fulfilled the two following criteria: they had no symptom of known history of cardiovascular disease, including coronary heart disease, stroke and peripheral vascular disease; and they had undergone noncontrast cardiac computed tomography (CT) for CAC screening during their hospitalization between September 2009 and October 2010. The retrospective analysis of personal health data of study subjects had the authorization of the *Commission nationale de l'informatique et des libertés* and was in accordance with the declaration of Helsinki.

Risk factors

All risk factors were measured at the same time as aortic imaging. Weight and height were measured for calculation of body surface area. Brachial

[1]Centre de Médecine Préventive Cardiovasculaire, Hôpital Européen Georges Pompidou, APHP, Paris, France; [2]Universidad Favaloro, CONICET, Buenos Aires, Argentina; [3]Université Paris Descartes, Sorbonne Paris Cité, Faculté de Médecine, Paris, France; [4]Centre de Recherche Cardiovasculaire de l'HEGP (INSERM U970), Paris, France; [5]Département de Radiologie Cardiovasculaire, Hôpital Européen Georges Pompidou, APHP, Paris, France and [6]Unité INSERM 678, Paris, France. Correspondence: Dr D Craiem, Universidad Favaloro (FICEN). Av. Belgrano 1723, C.P. 1093, Buenos Aires, Argentina.
E-mail: dcraiem@favaloro.edu.ar
Received 29 August 2012; revised 11 December 2012; accepted 17 December 2012

blood pressure (BP) was determined as the mean of three measurements by sphygmomanometer procedure in the supine position after 10 min rest. Hypertension was defined by BP of 140 or 90 mm Hg or above, or presence of hypertensive medication. Total and high-density lipoprotein blood cholesterol and triglyceride were measured in the supine position after 14-h fasting and low-density lipoprotein was calculated with the Friedewald formula or, if not applicable, directly measured. Hypercholesterolemia was defined by fasting low-density lipoprotein cholesterol above 3.3 mmol l^{-1} or by presence of low-density lipoprotein-lowering drug treatment. Blood glucose was measured after overnight fast and diabetes was defined by fasting blood glucose of 7 mmol l^{-1} or above, or by presence of antidiabetic medication. Past or current smokers were defined as subjects who smoke or had smoked at least on cigarette per day, every day or some day. Clinical characteristics are shown in Table 1. Comparing hypertensive with respect to normotensive subjects, only age and BP were significantly higher, whereas body surface area and the proportion of patients that had hypercholesterolemia (≈80%), diabetes (≈10%) or smokers (≈60%) resulted similar.

Image acquisition

Aortic imaging was obtained with non-contrast cardiac 64-slice multislice computed tomography (Light-speed VCT; GE Health care, Milwaukee, WI, USA) during the acquisition done to quantify CAC. Measures were done with 2.5-mm axial slices, 120 kVp, 250-mA tube current, 250-ms exposure time and a 250-mm field of view. Images were acquired with prospective-electrocardiography gating at 60% of R-R interval in the cranio-caudal direction from the top of the aortic arch to the level of the diaphragm. Scans were exported as DICOM files and analyzed by a custom-designed software that estimated the three-dimensional TA geometry.[11]

Aortic size and shape measurements

Details of the automated tool can be found elsewhere.[11] In a first step, the technician identifies the CT axial slice corresponding to the level of the pulmonary artery bifurcation, in which sections of ascending and descending aorta are approximately circular (Figure 1). Then, two seed points inside the aortic cross-sections are manually set and an automated process begins. First, a circle fitting algorithm finds the largest circle inscribed into the cross-sectional area. The centers of the circles, C_A and C_D, are adopted as aortic centerline points (Figure 1). In a second step, the rectilinear portion of the TA (downstream to C_D) is analyzed, applying the circle fitting algorithm to the aortic sections to estimate centerline points of the descending aorta (Figure 2a). In a third step, the curvilinear portion of the TA (upstream to C_A) is measured reconstructing oblique planes that follow the aortic curvature. The planes were calculated using a trilinear interpolation and pivoting by incremental two-degree angle around the arch center (midpoint between C_A and C_D) as shown in Figure 2b. Aortic sections in the corresponding planes are approximately circular and then centerline points are accurately assessed. The distance between two centerline points in the curvilinear portion was determined by the two-degree angle step, that is, 2.8 ± 0.3 mm (Figure 2b). Once all centerline points were obtained for the whole TA (black points in Figure 2b), the aortic centerline is automatically reconstructed with a cubic spline. For each centerline point, orthogonal planes to the centerline curve are calculated (Figure 2c) and definitive aortic circular sections are estimated with the circle fitting algorithm, assigning a diameter value to each centerline point and allowing the reconstruction of the aortic volume in a three-dimensional space.[11,16]

The vessel was divided into three anatomical segments by appropriate orthogonal planes (Figure 2c): (i) the ascending aorta, beginning at the plane corresponding to the left main coronary artery and extending to the plane corresponding to the origin of the brachiocephalic artery; (ii) the aortic arch, beginning at the brachiocephalic artery plane and extending to the plane corresponding to the origin of the left subclavian artery; (iii) the descending aorta beginning at the left subclavian artery plane and extending to the coronary sinus. In each TA segment, diameter, volume and length are automatically measured.

For the curvilinear portion that goes from C_A at 0° to C_D at 180°, several shape descriptors were assessed as shown in Figure 3: the aortic arch width and height, the radius of curvature defined in,[17] the aortic tortuosity calculated as one minus the ratio of curve length to the straight line distance between endpoints,[11] the aortic tapering defined as the difference between descending and ascending diameters over the curvilinear length, the distance from arch center to $C_{45°}$ and $C_{135°}$ coordinates and the area under the curve (AUC).

Duplicate readings of the same scans showed maximum coefficient of variation valuesof 0.3% for TA diameter and 4% for TA volume. Maximum interobserver variability was 0.4% and 4.4% for TA diameter and volume, respectively.[11]

Statistical analysis

Baseline characteristics of normotensive and hypertensive subjects were compared by use of a χ^2 statistic for dichotomous variables and analysis of variance for continuous variables. Size and shape measurements were informed as mean ± s.d. for each group and were analyzed in terms of hypertension presence in a multivariate model adjusted for age. The parameter estimates of the linear regression analysis indicate the change per 10 years age (β_{AGE} ± s.e.) and the presence (*vs* absence) of hypertension (β_{HTA} ± s.e.). The quotient $\beta_{HTA}x10/\beta_{AGE}$ was proposed to quantify an equivalent of aging (in years) for the presence of hypertension. The percentage change of geometrical measurements was calculated with respect to normotensive values, adopted as a reference. Additional multivariate models, adjusted for age and hypertension treatment, were calculated by entering geometrical measurements as dependent variables and diastolic or systolic BP as independent variables. Statistical analysis were performed with JMP (SAS NC USA) software and significance was set at $P < 0.05$.

Table 1. Clinical characteristics of the study population

	Normotensive	*Hypertensive*	P
Number of men	200	200	—
Age, years	54 ± 8	59 ± 8	< 0.001
Body surface area, m^2	1.98 ± 0.14	2.00 ± 0.15	NS
Hypertension treatment, *n*(%)	0	179 (90)	—
Blood pressure, mm Hg			
Systolic	120 ± 9	128 ± 14	< 0.001
Diastolic	73 ± 7	76 ± 10	< 0.001
Pulse	47 ± 7	52 ± 9	< 0.001
Hypercholesterolemia, *n* (%)	154 (80)	169 (84)	NS
Diabetes, *n* (%)	13 (7)	26 (13)	< 0.05
Past or current smoking, *n* (%)	125 (64)	108 (56)	NS

Abbreviation: NS, non significant. Data are mean ± s.d. or number of patients n (%).

Figure 1. Initial seed points for the automated algorithm. Circular sections of ascending and descending aorta in the CT slice at the pulmonary artery (PA) bifurcation level. C_A and C_D show the ascending and descending aorta centers.

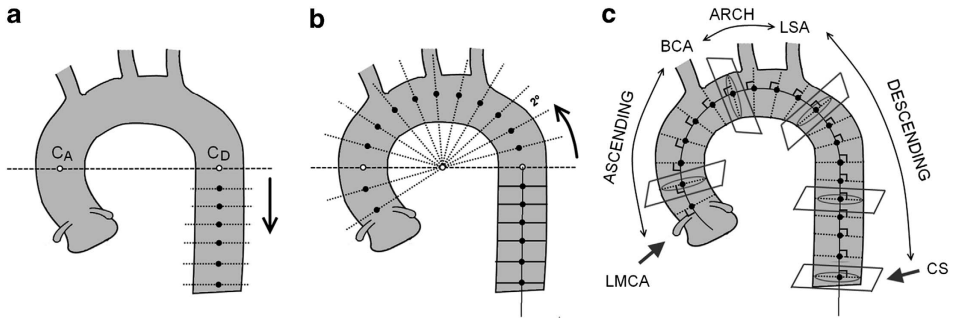

Figure 2. Schematic representation of the process to measure TA dimensions. (**a**), rectilinear descending aorta centerline points downstream C_D (see Figure1) in CT axial slices spaced out 2.5 mm apart. (**b**), curvilinear aorta portion centerline points upstream C_D in orthogonal planes pivoting by 2° angle increment around the midpoint between C_D and C_A (see Figure 1) and spaced out 2.8 ± 0.3 mm apart. (**c**), aortic circular sections in planes orthogonal to total TA centerline. BCA: brachiocephalic artery; CS: coronary sinus; LMCA: left main coronary artery; LSA: left subclavian artery. C_A and C_D design centers of ascending and descending TA.

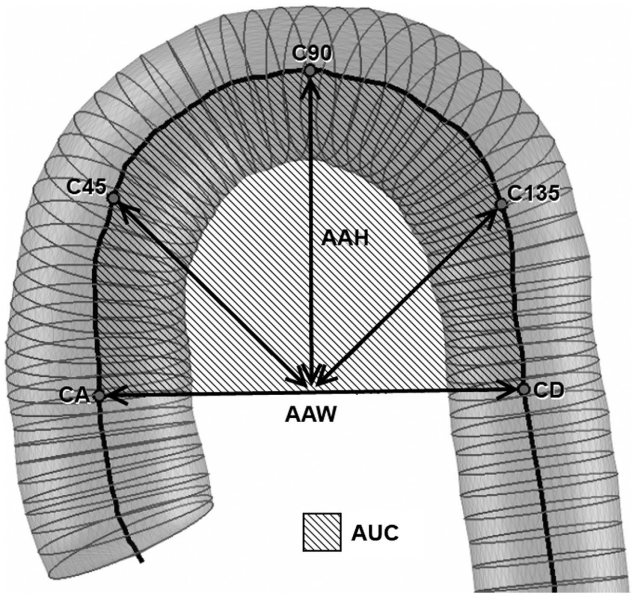

Figure 3. Morphologic descriptors for the TA curvilinear portion. AAW: aortic arch width; AAH: aortic arch height; AUC: area under the curve; C_A and C_D design centers of ascending and descending TA.

RESULTS

Table 2 shows absolute geometric values for normotensive and hypertensive patients. In hypertensive subjects, ascending, arch and descending TA segments were larger with respect to normotensive ($P<0.001$). Diameters were 5–7% and volumes 16–22% higher ($P<0.001$). In the aortic curvilinear portion (semi-arc from 0°–180°), an unfolding effect was evidenced with hypertension. The arch was 9% wider ($P<0.001$), the radius of curvature increased 8% ($P<0.001$), tortuosity decreased 6% ($P<0.01$) and the AUC grew 14% ($P<0.001$). The vectors from the arch center to the posterior ($C_{135°}$) and anterior ($C_{45°}$) sections increased 8% and 6%, respectively ($P<0.001$). Aortic tapering was more pronounced during hypertension (+6%) although it did not attaint significance ($P=0.06$). When variables were adjusted for age, all changes remained significant between normotensive and hypertensive subjects ($P<0.001$ for diameters, volumes arch width, radius of curvature and distance from center to $C_{135°}$, $P<0.01$ for the curvilinear length, distance from center to $C_{45°}$ and AUC, $P<0.05$ for tortuosity) except for aortic arch height and tapering (Table 2, right). The presence of hypertension resulted equivalent to an aging of 5-years in ascending, 5 − 6-years in arch and 2 − 4-years in descending TA segments. In the curvilinear portion, the presence of hypertension was equivalent to an aging of 8-years for radius of curvature, 7-years for tortuosity and 4-years for the arch width. The equivalence for distance from arch center to $C_{135°}$ and AUC was 3-years of aging.

Table 3 shows the associations of TA size and shape measures with systolic and diastolic BP after adjusting for age and current drug treatments. Diastolic BP was positively associated with TA size ($P<0.001$ for diameters and volumes for the 3 segments). Also, a positive association was found with the arch width ($P<0.001$), radius of curvature ($P<0.01$), arch center to $C_{45°}$ and $C_{135°}$ distances ($P<0.001$) and AUC ($P<0.001$). Systolic BP was positively associated with TA size in the arch ($P<0.01$) and the descending segment ($P<0.001$) but only marginally with the ascending portion ($P<0.05$ for diameter). Also, a positive association was found between systolic BP and the arch width ($P<0.001$), radius of curvature ($P<0.01$) and arch center to $C_{135°}$ distance ($P<0.05$) whereas a negative relation was found with tortuosity ($P<0.05$). The most sensitive variable was the arch width, that widened 12% with a 10 mm Hg increase in systolic BP ($P<0.001$). The aortic arch height and tapering were not associated to BP components.

DISCUSSION

This study provides an exhaustive description of the TA geometry assessed non-invasively by non-contrast multislice computed tomography in asymptomatic adults in relation with hypertension. The main result is that the presence of hypertension accelerates the TA enlargement in its three portions and significantly widens the aortic arch. If the TA size is evaluated in terms of the vessel volume, including the radial expansion (diameter) and lengthening, the enlargement due to hypertension represented an equivalent aging of 5-, 6- and 2-years for the ascending, arch and descending segments, respectively. Similarly, the unfolding process was mostly evidenced with an increase of the aortic arch width (+4 years), radius of curvature (+8 years) and a reduction of tortuosity (+7 years). Analyzing BP components, whereas diastolic BP was associated with distention and unfolding of the whole vessel, systolic BP mostly affected TA arch and descending portions. Systolic BP dominated the arch widening, attaining 12% for a 10 mm Hg increase. This study shows that non-contrast multislice computed tomography scans, initially designated to assess calcifications, can provide extra-coronary geometric information to reconstruct the TA in three-dimensions.

Table 2. Thoracic aorta geometric measurements: Absolute values for normotensive *vs* hypertensive patients and a multivariate regression model adjusted for age

	Normotensive	*Hypertensive*			*Multivariable model adjusted for age*				
Size and shape measures	*n = 200 men Mean ± s.d.*	*n = 200 men Mean ± s.d.*	*(%) change*	*P*	$\beta_{AGE} \pm$ *s.e. (10 years aging)*	$\beta_{HTA} \pm$ *s.e. (hypertension)*	β_{HTA} *(%) change*	$\beta_{HTA}x10/\beta_{AGE}$ *(aging effect of HTA (years))*	*R*
Ascending aorta									
Mean diameter, cm	3.23 ± 0.33	3.45 ± 0.34	7	<0.001	0.14 ± 0.02‡	0.07 ± 0.02‡	2	+5	0.45‡
Volume, cm^3	51 ± 14	60 ± 16	17	<0.001	6.2 ± 0.9‡	3.1 ± 0.7‡	6	+5	0.45‡
Aortic arch									
Mean diameter, cm	2.81 ± 0.23	2.97 ± 0.23	6	<0.001	0.11 ± 0.01‡	0.05 ± 0.01‡	2	+5	0.51‡
Volume, cm^3	18 ± 6	22 ± 7	22	<0.001	2.0 ± 0.4‡	1.2 ± 0.3‡	7	+6	0.36‡
Descending aorta									
Mean diameter, cm	2.55 ± 0.20	2.68 ± 0.20	5	<0.001	0.11 ± 0.01‡	0.04 ± 0.01‡	2	+4	0.55‡
Volume, cm^3	83 ± 20	96 ± 23	16	<0.001	13.1 ± 1.1‡	3.0 ± 1.0‡	4	+2	0.57‡
Aortic curvilinear portion (0°–180°)									
Arch width, cm	7.67 ± 0.98	8.38 ± 1.02	9	<0.001	0.56 ± 0.05‡	0.21 ± 0.05‡	3	+4	0.56‡
Radius of curvature, cm	3.17 ± 0.44	3.43 ± 0.45	8	<0.001	0.13 ± 0.03‡	0.10 ± 0.02‡	3	+8	0.37‡
Tortuosity	0.85 ± 0.18	0.80 ± 0.17	−6	<0.01	−0.03 ± 0.01*	0.02 ± 0.01*	2	+7	0.17†
Arch height, cm	4.67 ± 0.65	4.86 ± 0.70	4	<0.01	0.23 ± 0.04	NS		—	0.31‡
Tapering, cm/10 cm length	−0.48 ± 0.15	−0.51 ± 0.19	6	0.06	NS	0.02 ± 0.01*	−4	—	NS
Center to 45° distance, cm	4.21 ± 0.50	4.47 ± 0.50	6	<0.001	0.26 ± 0.03‡	0.06 ± 0.02†	1	+2	0.49‡
Center to 135° distance, cm	4.39 ± 0.62	4.76 ± 0.66	8	<0.001	0.32 ± 0.04‡	0.10 ± 0.03‡	2	+3	0.49‡
Area under the arch curve, cm^2	28.3 ± 6.3	32.2 ± 7.1	14	<0.001	3.60 ± 0.36‡	1.00 ± 0.31†	4	+3	0.51‡

Percentage changes are calculated with respect to mean normotensive values adopted as a reference. ‡$P<0.001$,†$P<0.01$. *$P<0.05$.

Segmentation algorithm

At first, we have to emphasize that the automated tool was able to isolate the TA and to estimate the three-dimensional geometry with a high reproducibility rate and accuracy in less than 1 min. True orthogonal aortic sections are assessed in ≈180 sites all along the TA centerline, overcoming the traditional limitation of measuring only ascending and descending diameters (Figure 2). Furthermore, the coordinates of the centerline points are determined during this process, allowing to calculate volume and deformation descriptors that are significantly involved in the aortic structural alterations.[9,10]

Hypertension role on TA size and shape

Associations of age with TA size are consistent with those previously discussed with TA diameter[3,7,8,14] and justify to assess the potential role of hypertension in terms of aging. Hypertension was found a strong independent determinant factor for size increase in the three TA segments, confirming its major influence on TA enlargement.[9,14,18] In a multivariate model adjusted for age, the impact of hypertension on TA geometry was evaluated calculating an equivalent factor in years of aging (Table 2). Overall, the presence of hypertension increased 2% TA diameters and 4 − 7% TA volumes, equivalent to an aging of ≈5-years. The less affected segment was the descending portion. In terms of curvilinear deformation, hypertension produced an equivalent aging of 8-years for the radius of curvature and 7-years for tortuosity. The rest of the parameters, except the arch height and tapering, accounted for an aging of 3 − 4-years. These results show that the TA unfolding process that progresses with aging is accelerated in the presence of hypertension.

We also analyzed the relation between TA geometry and BP variables in a multivariate model adjusted for age and hypertensive treatment (Table 3). We observed that TA size evenly increased along its length with diastolic BP. Also, diastolic BP was positively associated with the radius of curvature, the aortic arch width, the 45° and 135° vectors and the AUC. Probably, the relative constant diastolic BP value along the arterial tree reflects the minimum tension that is permanently stimulating the vessel wall and might have a key role in aortic geometric evolution. Systolic BP values were stronger associated with changes in TA size, mostly in the arch and descending portions. Regarding the vessel shape, the aortic arch width and radius of curvature were also sensitive to systolic BP. The role of systolic BP on the proximal aortic size is controversial. Certain studies have reported negative[1,14,15,18] while others have showed positive associations.[19,20] The classic notion that associates aging with systolic BP increase is based on a wave propagation argument and suggests a sequence of elastic fragmentation, aortic stretching, wall stiffening and pressure wave acceleration that amplifies systolic BP.[2,21] On the contrary, several studies reported aortic enlargement with increasing diastolic BP and reduction with increasing systolic BP.[14,15,22,23] This associations were confirmed in a recent report that studied a community-based data of more than 4500 individuals followed for 16 years.[1] In this longitudinal study, a dynamic remodeling that expands the aortic size is proposed as a compensatory mechanism to limit the systolic BP increase. In fact, a vessel expansion would induce a striking drop of the characteristic impedance to weaken pulsatile components.[24]

Table 3. Associations of geometric measurements with BP components after adjustment for age and hypertension treatment

Size and shape measures (units per 10 mm Hg increase in BP)	*Diastolic BP*			*Systolic BP*		
	β ± s.e.	*(%) change*	*R*	*β ± s.e.*	*(%) change*	*R*
Ascending aorta						
Mean diameter, cm	0.08 ± 0.02‡	2	0.48‡	0.03 ± 0.01*	1	0.44‡
Volume, cm^3	2.9 ± 0.8‡	6	0.47‡	NS	—	0.44‡
Aortic arch						
Mean diameter, cm	0.06 ± 0.01‡	2	0.56‡	0.03 ± 0.01†	1	0.57‡
Volume, cm^3	1.5 ± 0.3‡	8	0.40‡	0.7 ± 0.2†	4	0.37‡
Descending aorta						
Mean diameter, cm	0.05 ± 0.01‡	2	0.59‡	0.03 ± 0.01‡	1	0.57‡
Volume, cm^3	5.1 ± 1.0‡	6	0.61‡	2.5 ± 0.7‡	3	0.59‡
Aortic curvilinear portion (0°–180°)						
Arch width, cm	0.21 ± 0.05‡	3	0.57‡	0.91 ± 0.04‡	12	0.56‡
Radius of curvature, cm	0.08 ± 0.02†	3	0.39‡	0.05 ± 0.01†	2	0.37‡
Tortuosity,	NS	-	0.17†	− 0.01 ± 0.00*	− 1	0.20†
Arch height, cm	NS	-	0.32‡	NS	—	0.32‡
Tapering, cm/10 cm length	NS	-	NS	NS	—	NS
Center to 45° distance, cm	0.09 ± 0.03‡	2	0.51‡	NS	—	0.50‡
Center to 135° distance, cm	0.13 ± 0.03‡	3	0.51‡	0.05 ± 0.02*	1	0.49‡
Area under the arch curve, cm^2	1.03 ± 0.34‡	4	0.52‡	NS	—	0.51‡

Abbreviations: BP, blood pressure; NS, non significant. Data are mean ± s.e. values per 10 mm Hg increase in BP and % change with respect to normotensive population mean values in Table 2. ‡$P<0.001$,†$P<0.01$. *$P<0.05$.

Therefore, an aortic root dilatation could be part of an adaptation mechanism to reduce the characteristic impedance and the systolic BP. In addition, it was reported that the increase in systolic BP within hypertensive subjects could be attributed to aortic stiffening and a mitigated aortic size expansion rather than to wave propagation causes.[18] It is to note that the inverse relation between systolic BP and aortic size can be also predicted from elastic modulus or characteristic impedance estimations.[15,24] In our opinion, there is a propensity to directly associate systolic BP with aortic size, which is contaminated by the aging effect. In the present study, we find that TA size has a strong dependence on diastolic BP in all its segments but we observed that systolic BP was mostly associated to a descending TA expansion. All these effects could be thought in the mentioned context of a remodeling process that expands the proximal TA portion, limiting the systolic BP. Further studies are needed to confirm these observations.

Study limitations

The measurement of BP in the brachial artery, and not centrally, may induce some distortions that need to be discussed. In particular, we found that brachial systolic BP was not strongly associated to the size of the ascending TA (Table 3). We consider that TA size associations with central pressure components would remain unaffected with respect to brachial measurements, as shown in other studies.[9,24] Chen *et al.* proposed a general transfer function to estimate central aortic pressure waveform from a radial tonometry.[25] Using their regression models to convert brachial to central systolic and diastolic values, we verified that results in Table 3 remained unchanged. Furthermore, assuming an amplification effect, central systolic BP values would result lower, reducing even more the weak association we found with ascending TA size. As tonometry was not available in our study, further measurements are required to elucidate the specific role of systolic BP. Additionally, and due to the absence of contrast imaging, TA cross-sectional measures represent the sum of the vessel wall and the lumen, impeding to discriminate whether an increase in aortic volume is due to true luminal enlargement or to compensatory remodeling in response to wall plaque. We are also aware that the exact definition of the TA segments in our work may not match with other reports and then comparisons should be made with caution for the segments length and volume.[9,10] In the TA exploration, primarily intended for CAC measurement, the field of view was extended to cover the aortic arch. The total scan length in our protocol was 10–15% higher with respect to routinely CAC scans. Such extended scan length has an additional radiation dose cost for the patient but offers the benefit of extra-coronary measures like the ones proposed in our study or even further complete TA calcification assessments that contain the aortic arch. Aortic valve disease is known to be associated with an aortopathy but it was not systematically evaluated in our study except by echocardiography in those patients with heart murmur at auscultation or those with electrocardiography abnormalities, which represented a very small proportion in our sample. Screening patients with aortic valve disease such as bicuspid valve or aortic stenosis may be performed in future studies. Lastly, the cross-sectional design of our study does not allow assessing the time-dependent and causal relationships between parameters.

In conclusion, in this work we showed that hypertension accelerates the aortic enlargement and collaborates with the aortic arch widening process. Globally, the presence of hypertension was equivalent to a 5-years-old aging. Measures were assessed using an original non-invasive method capable of measuring accurately and rapidly TA geometry from non-contrast CT scans. Whereas diastolic BP was associated to TA enlargement in its three segments, systolic BP was mostly related with changes in the aortic arch and descending portions. Using this new methodology, further studies could be proposed to accurately assess the differential impact of other determinant risk factors on TA size and shape.

What is known about this topic

- Aging and hypertension are determinant risk factors that are involved in changes of the thoracic aorta geometry.
- Non-contrast CT is employed as a noninvasive method to estimate aortic enlargement by measuring two single diameters in the ascending and descending portions.
- Several studies report aortic size progression whereas less is known about aortic regional and three-dimensional shape evolution.

What this study adds

- Hypertension accelerates thoracic aorta enlargement and the aortic arch widening process, independently of aging.
- The presence of hypertension was found to produce an equivalent 5-years-old aging on aortic deformation, mostly evidenced in the ascending and aortic arch portions.
- Diastolic BP was associated to size and shape changes in the entire thoracic aorta whereas systolic BP had an effect mostly on aortic arch and descending portions.

CONFLICT OF INTEREST

The authors declare no conflict of interest.

ACKNOWLEDGEMENTS

This work was partially supported by post-doctoral scholarship cooperation program between France and Argentina 'Bernardo Houssay'. We thank Mrs Latifa Boudali for her invaluable assistance in database management.

REFERENCES

1 Lam CS, Xanthakis V, Sullivan LM, Lieb W, Aragam J, Redfield MM *et al.* Aortic root remodeling over the adult life course: longitudinal data from the Framingham Heart Study. *Circulation* 2010; **122**: 884–890.
2 O'Rourke M, Farnsworth A, O'Rourke J. Aortic dimensions and stiffness in normal adults. *JACC Cardiovasc Imaging* 2008; **1**: 749–751.
3 Wolak A, Gransar H, Thomson LEJ, Friedman JD, Hachamovitch R, Gutstein A *et al.* Aortic size assessment by noncontrast cardiac computed tomography: normal limits by age, gender, and body surface area. *JACC: Cardiovascular Imaging* 2008; **1**: 200–209.
4 Elefteriades JA, Farkas EA. Thoracic aortic aneurysm clinically pertinent controversies and uncertainties. *J Am Coll Cardiol* 2010; **55**: 841–857.
5 Hinchliffe RJ, Krasznai A, Schultzekool L, Blankensteijn JD, Falkenberg M, Lonn L *et al.* Observations on the failure of stent-grafts in the aortic arch. *Eur J Vasc Endovasc Surg* 2007; **34**: 451–456.
6 Melissano G, Civilini E, Bertoglio L, Calliari F, Setacci F, Calori G *et al.* Results of endografting of the aortic arch in different landing zones. *Eur J Vasc Endovasc Surg* 2007; **33**: 561–566.
7 Mao SS, Ahmadi N, Shah B, Beckmann D, Chen A, Ngo L *et al.* Normal thoracic aorta diameter on cardiac computed tomography in healthy asymptomatic adults: impact of age and gender. *Acad Radiol* 2008; **15**: 827–834.
8 Chironi G, Orobinskaia L, Megnien JL, Sirieix ME, Clement-Guinaudeau S, Bensalah M *et al.* Early thoracic aorta enlargement in asymptomatic individuals at risk for cardiovascular disease: determinant factors and clinical implication. *J Hypertens* 2010; **28**: 2134–2138.
9 Redheuil A, Yu WC, Mousseaux E, Harouni AA, Kachenoura N, Wu CO *et al.* Age-related changes in aortic arch geometry: relationship with proximal aortic function and left ventricular mass and remodeling. *J Am Coll Cardiol* 2011; **58**: 1262–1270.
10 Sugawara J, Hayashi K, Yokoi T, Tanaka H. Age-associated elongation of the ascending aorta in adults. *J Am Coll Cardiol Img* 2008; **1**: 739–748.
11 Craiem D, Chironi G, Redheuil A, Casciaro M, Mousseaux E, Simon A *et al.* Aging impact on thoracic aorta 3D morphometry in intermediate-risk subjects: looking beyond coronary arteries with non-contrast cardiac CT. *Ann Biomed Eng* 2012; **40**: 1028–1038.
12 Greenland P, Alpert JS, Beller GA, Benjamin EJ, Budoff MJ, Fayad ZA *et al.* 2010ACCF/AHA guideline for assessment of cardiovascular risk in asymptomatic adults: a report of the American College of Cardiology Foundation/American Heart Association Task Force on Practice Guidelines. *J Am Coll Cardiol 2010* **56**: e50–103.
13 Chironi G, Simon A, Megnien JL, Sirieix ME, Mousseaux E, Pessana F *et al.* Impact of coronary artery calcium on cardiovascular risk categorization and lipid-lowering drug eligibility in asymptomatic hypercholesterolemic men. *Int J Cardiol* 2011; **151**: 200–204.
14 Agmon Y, Khandheria BK, Meissner I, Schwartz GL, Sicks JD, Fought AJ *et al.* Is aortic dilatation an atherosclerosis-related process? Clinical, laboratory, and transesophageal echocardiographic correlates of thoracic aortic dimensions in the population with implications for thoracic aortic aneurysm formation. *J Am Coll Cardiol* 2003; **42**: 1076–1083.
15 Vasan RS, Larson MG, Levy D. Determinants of echocardiographic aortic root size. The Framingham Heart Study. *Circulation* 1995; **91**: 734–740.
16 Zhao F, Zhang H, Wahle A, Thomas MT, Stolpen AH, Scholz TD *et al.* Congenital aortic disease: 4D magnetic resonance segmentation and quantitative analysis. *Med Image Anal* 2009; **13**: 483–493.
17 Wood NB, Zhao SZ, Zambanini A, Jackson M, Gedroyc W, Thom SA *et al.* Curvature and tortuosity of the superficial femoral artery: a possible risk factor for peripheral arterial disease. *J Appl Physiol* 2006; **101**: 1412–1418.
18 Mitchell GF, Conlin PR, Dunlap ME, Lacourciere Y, Arnold JM, Ogilvie RI *et al.* Aortic diameter, wall stiffness, and wave reflection in systolic hypertension. *Hypertension* 2008; **51**: 105–111.
19 Ingelsson E, Pencina MJ, Levy D, Aragam J, Mitchell GF, Benjamin EJ *et al.* Aortic root diameter and longitudinal blood pressure tracking. *Hypertension* 2008; **52**: 473–477.
20 Jondeau G, Boutouyrie P, Lacolley P, Laloux B, Dubourg O, Bourdarias JP *et al.* Central pulse pressure is a major determinant of ascending aorta dilation in Marfan syndrome. *Circulation* 1999; **99**: 2677–2681.
21 O'Rourke MF, Nichols WW. Aortic diameter, aortic stiffness, and wave reflection increase with age and isolated systolic hypertension. *Hypertension* 2005; **45**: 652–658.
22 Bella JN, Wachtell K, Boman K, Palmieri V, Papademetriou V, Gerdts E *et al.* Relation of left ventricular geometry and function to aortic root dilatation in patients with systemic hypertension and left ventricular hypertrophy (the LIFE study). *Am J Cardiol* 2002; **89**: 337–341.
23 Cuspidi C, Meani S, Fusi V, Valerio C, Sala C, Zanchetti A. Prevalence and correlates of aortic root dilatation in patients with essential hypertension: relationship with cardiac and extracardiac target organ damage. *J Hypertens* 2006; **24**: 573–580.
24 Mitchell GF, Lacourciere Y, Ouellet JP, Izzo Jr. JL, Neutel J, Kerwin LJ *et al.* Determinants of elevated pulse pressure in middle-aged and older subjects with uncomplicated systolic hypertension: the role of proximal aortic diameter and the aortic pressure-flow relationship. *Circulation* 2003; **108**: 1592–1598.
25 Chen CH, Nevo E, Fetics B, Pak PH, Yin FC, Maughan WL *et al.* Estimation of central aortic pressure waveform by mathematical transformation of radial tonometry pressure. Validation of generalized transfer function. *Circulation* 1997; **95**: 1827–1836.

Bibliographie

[1] Transesophageal echocardiographic correlates of thromboembolism in high-risk patients with nonvalvular atrial fibrillation. the stroke prevention in atrial fibrillation investigators committee on echocardiography. *Ann Intern Med*, 128(8) :639–47, 1998.

[2] Endoprothèses pour anévrisme aortique. *Le moniteur Hospitalier*, 260, 2013.

[3] V. Aboyans, V. Bataille, P. Bliscaux, S. Ederhy, D. Filliol, B. Honton, B. Kurtz, E. Messas, D. Mohty, E. Brochet, and S. Kownator. Effectiveness of screening for abdominal aortic aneurysm during echocardiography. *Am J Cardiol*, 114(7) :1100–4, 2014.

[4] A. S. Agatston, W. R. Janowitz, F. J. Hildner, N. R. Zusmer, J. Viamonte, M., and R. Detrano. Quantification of coronary artery calcium using ultrafast computed tomography. *J Am Coll Cardiol*, 15(4) :827–32, 1990.

[5] Y. Agmon, B. K. Khandheria, I. Meissner, G. L. Schwartz, J. D. Sicks, A. J. Fought, W. M. O'Fallon, D. O. Wiebers, and A. J. Tajik. Is aortic dilatation an atherosclerosis-related process ? clinical, laboratory, and transesophageal echocardiographic correlates of thoracic aortic dimensions in the population with implications for thoracic aortic aneurysm formation. *J Am Coll Cardiol*, 42(6) :1076–83, 2003.

[6] M. H. Al-Mallah, K. Nasir, R. Katz, J. Takasu, J. A. Lima, D. A. Bluemke, G. Hundley, R. S. Blumenthal, and M. J. Budoff. Thoracic aortic distensibility and thoracic aortic calcium (from the multi-ethnic study of atherosclerosis [MESA]). *Am J Cardiol*, 106(4) :575–80, 2010.

[7] M. A. Allison, S. Hsi, C. L. Wassel, C. Morgan, J. H. Ix, C. M. Wright, and M. H. Criqui. Calcified atherosclerosis in different vascular beds and the risk of mortality. *Arterioscler Thromb Vasc Biol*, 32(1) :140–146, 2012.

[8] P. Amarenco, A. Cohen, C. Tzourio, B. Bertrand, M. Hommel, G. Besson, C. Chauvel, P. J. Touboul, and M. G. Bousser. Atherosclerotic disease of the aortic arch and the risk of ischemic stroke. *N Engl J Med*, 331(22) :1474–9, 1994.

[9] I. D. Andacheh, C. Donayre, F. Othman, I. Walot, G. Kopchok, and R. White. Patient outcomes and thoracic aortic volume and morphologic changes following thoracic endovascular aortic repair in patients with complicated chronic type B aortic dissection. *J Vasc Surg*, 56(3) :644–50 ; discussion 650, 2012.

[10] A. Ayyalasomayajula, A. Polk, A. Basudhar, S. Missoum, L. Nissim, and J. P. Vande Geest. Three dimensional active contours for the reconstruction of abdominal aortic aneurysms. *Ann Biomed Eng*, 38(1) :164–76, 2010.

[11] D. J. Ballard, G. Filardo, G. Fowkes, and J. T. Powell. Surgery for small asymptomatic abdominal aortic aneurysms. *Cochrane Database Syst Rev*, (4) :CD001835, 2008.

[12] D. T. Baril, T. S. Jacobs, and M. L. Marin. Surgery insight : advances in endovascular repair of abdominal aortic aneurysms. *Nat Clin Pract Cardiovasc Med*, 4(4) :206–213, 2007.

[13] A. Bieniek and A. Moga. An efficient watershed algorithm based on connected components. *Pattern Recognit*, 33(6) :907–916, 2000.

[14] D. Bockler, A. Holden, M. Thompson, P. Hayes, D. Krievins, J. P. de Vries, and M. M. Reijnen. Multicenter Nellix endovascular aneurysm sealing system experience in aneurysm sac sealing. *J Vasc Surg*, 2015.

[15] M. J. Bown, M. J. Sweeting, L. C. Brown, J. T. Powell, and S. G. Thompson. Surveillance intervals for small abdominal aortic aneurysms : a meta-analysis. *JAMA*, 309(8) :806–13, 2013.

[16] A. R. Brady, S. G. Thompson, F. G. Fowkes, R. M. Greenhalgh, and J. T. Powell. Abdominal aortic aneurysm expansion : risk factors and time intervals for surveillance. *Circulation*, 110(1) :16–21, 2004.

[17] N. A. Brozzi and E. E. Roselli. Endovascular therapy for thoracic aortic aneurysms : state of the art in 2012. *Curr Treat Options Cardiovasc Med*, 14(2) :149–63, 2012.

[18] M. J. Budoff and K. M. Gul. Expert review on coronary calcium. *Vasc Health Risk Manag*, 4(2) :315–24, 2008.

[19] M. J. Budoff, K. Nasir, R. Katz, J. Takasu, J. J. Carr, N. D. Wong, M. Allison, J. A. Lima, R. Detrano, R. S. Blumenthal, and R. Kronmal. Thoracic aortic calcification and coronary heart disease events : the multi-ethnic study of atherosclerosis (MESA). *Atherosclerosis*, 215(1) :196–202, 2011.

[20] P. Cao, P. De Rango, F. Verzini, G. Parlani, L. Romano, and E. Cieri. Comparison of surveillance versus aortic endografting for small aneurysm repair (CAESAR) : results from a randomised trial. *Eur J Vasc Endovasc Surg*, 41(1) :13–25, 2011.

[21] J. L. Cavalcante, J. A. Lima, A. Redheuil, and M. H. Al-Mallah. Aortic stiffness : current understanding and future directions. *J Am Coll Cardiol*, 57(14) :1511–22, 2011.

[22] R. A. Chaer, R. Vasoncelos, L. K. Marone, G. Al-Khoury, R. Y. Rhee, J. S. Cho, and M. S. Makaroun. Synchronous and metachronous thoracic aneurysms in patients with abdominal aortic aneurysms. *J Vasc Surg*, 56(5) :1261–5, 2012.

[23] G. Chironi, L. Orobinskaia, J. L. Megnien, M. E. Sirieix, S. Clement-Guinaudeau, M. Bensalah, A. Azarine, E. Mousseaux, and A. Simon. Early thoracic aorta enlargement in asymptomatic individuals at risk for cardiovascular disease : determinant factors and clinical implication. *J Hypertens*, 28(10) :2134–8, 2010.

[24] P. Cignoni, C. Rocchini, and R. Scopigno. Metro : Measuring error on simplified surfaces. *Comput Graphics Forum*, 17(2) :167–174, 1998.

[25] D. Craiem, G. Chironi, M. E. Casciaro, A. Redheuil, E. Mousseaux, and A. Simon. Three-dimensional evaluation of thoracic aorta enlargement and unfolding in hypertensive men using non-contrast computed tomography. *J Hum Hypertens*, 27(8) :504–509, 2013.

[26] D. Craiem, G. Chironi, A. Redheuil, M. Casciaro, E. Mousseaux, A. Simon, and R. L. Armentano. Aging impact on thoracic aorta 3D morphometry in intermediate-risk subjects : Looking beyond coronary arteries with non-contrast cardiac CT. *Ann Biomed Eng*, 40(5) :1028–1038, 2012.

[27] G. Dangas, D. O'Connor, B. Firwana, S. Brar, S. Ellozy, A. Vouyouka, M. Arnold, C. E. Kosmas, P. Krishnan, J. Wiley, J. Suleman, J. Olin, M. Marin, and P. Faries. Open versus endovascular stent graft repair of abdominal aortic aneurysms : a meta-analysis of randomized trials. *JACC Cardiovasc Interv*, 5(10) :1071–80, 2012.

[28] P. A. de Jong, W. E. Hellings, R. A. Takx, I. Isgum, J. A. van Herwaarden, and W. P. Mali. Computed tomography of aortic wall calcifications in aortic dissection patients. *PLoS One*, 9(7) :e102036, 2014.

[29] A. Diwan, R. Sarkar, J. C. Stanley, G. B. Zelenock, and T. W. Wakefield. Incidence of femoral and popliteal artery aneurysms in patients with abdominal aortic aneurysms. *J Vasc Surg*, 31(5) :863–9, 2000.

[30] C. T. Dotter, D. J. Roberts, and I. Steinberg. Aortic length : angiocardiographic measurements. *Circulation*, 2(6) :915–20, 1950.

[31] A. A. Duquette, P.-M. Jodoin, O. Bouchot, and A. Lalande. 3d segmentation of abdominal aorta from CT-scan and MR images. *Computerized medical imaging and graphics : the official journal of the Computerized Medical Imaging Society*, 36(4) :294, 2012.

[32] H. Eggebrecht, M. Thompson, H. Rousseau, M. Czerny, L. Lonn, R. H. Mehta, and R. Erbel. Retrograde ascending aortic dissection during or after thoracic aortic stent graft placement : insight from the european registry on endovascular aortic repair complications. *Circulation*, 120(11 Suppl) :S276–81, 2009.

[33] J. A. Elefteriades and E. A. Farkas. Thoracic aortic aneurysm clinically pertinent controversies and uncertainties. *J Am Coll Cardiol*, 55(9) :841–57, 2010.

[34] R. Erbel, V. Aboyans, C. Boileau, E. Bossone, R. D. Bartolomeo, H. Eggebrecht, A. Evangelista, V. Falk, H. Frank, O. Gaemperli, M. Grabenwoger, A. Haverich, B. Iung, A. J. Manolis, F. Meijboom, C. A. Nienaber, M. Roffi, H. Rousseau, U. Sechtem, P. A. Sirnes, R. S. Allmen, and C. J. Vrints. 2014 ESC guidelines on the diagnosis and treatment of aortic diseases : Document covering acute and chronic aortic diseases of the thoracic and abdominal aorta of the adult. the task force for the diagnosis and treatment of aortic diseases of the european society of cardiology (ESC). *Eur Heart J*, 35(41) :2873–926, 2014.

[35] R. Erbel, F. Alfonso, C. Boileau, O. Dirsch, B. Eber, A. Haverich, H. Rakowski, J. Struyven, K. Radegran, U. Sechtem, J. Taylor, C. Zollikofer, W. W. Klein, B. Mulder, and L. A. Providencia. Diagnosis and management of aortic dissection. *Eur Heart J*, 22(18) :1642–81, 2001.

[36] A. Evangelista, A. Salas, A. Ribera, I. Ferreira-Gonzalez, H. Cuellar, V. Pineda, T. Gonzalez-Alujas, B. Bijnens, G. Permanyer-Miralda, and D. Garcia-Dorado. Long-term outcome of aortic dissection with patent false lumen : predictive role of entry tear size and location. *Circulation*, 125(25) :3133–41, 2012.

[37] R. Fattori, P. Cao, P. De Rango, M. Czerny, A. Evangelista, C. Nienaber, H. Rousseau, and M. Schepens. Interdisciplinary expert consensus document on management of type B aortic dissection. *J Am Coll Cardiol*, 61(16) :1661–78, 2013.

[38] R. Fattori, D. Montgomery, L. Lovato, S. Kische, M. Di Eusanio, H. Ince, K. A. Eagle, E. M. Isselbacher, and C. A. Nienaber. Survival after endovascular therapy in patients with type B aortic dissection : a report from the international registry of acute aortic dissection (IRAD). *JACC Cardiovasc Interv*, 6(8) :876–82, 2013.

[39] M. S. Freiberg, A. M. Arnold, A. B. Newman, M. S. Edwards, K. L. Kraemer, and L. H. Kuller. Abdominal aortic aneurysms, increasing infrarenal aortic diameter, and risk of total mortality and incident cardiovascular disease events : 10-year follow-up data from the cardiovascular health study. *Circulation*, 117(8) :1010–7, 2008.

[40] A. Frydrychowicz, A. Berger, A. Munoz Del Rio, M. F. Russe, J. Bock, A. Harloff, and M. Markl. Interdependencies of aortic arch secondary flow patterns, geometry, and age analysed by 4-dimensional phase contrast magnetic resonance imaging at 3 tesla. *Eur Radiol*, 22(5) :1122–30, 2012.

[41] Y. C. Fung. *Biomechanics : circulation*. Springer, USA, second edition edition, 1984.

[42] T. C. Gasser, G. Gorgulu, M. Folkesson, and J. Swedenborg. Failure properties of intraluminal thrombus in abdominal aortic aneurysm under static and pulsating mechanical loads. *J Vasc Surg*, 48(1) :179–88, 2008.

[43] D. P. Giddens, C. K. Zarins, and S. Glagov. The role of fluid mechanics in the localization and detection of atherosclerosis. *J Biomech Eng*, 115(4B) :588–94, 1993.

[44] M. C. Godoy, N. S. Cayne, and J. P. Ko. Endovascular repair of the thoracic aorta : preoperative and postoperative evaluation with multidetector computed tomography. *J Thorac Imaging*, 26(1) :63–73, 2011.

[45] M. Grabenwoger, F. Alfonso, J. Bachet, R. Bonser, M. Czerny, H. Eggebrecht, A. Evangelista, R. Fattori, H. Jakob, L. Lonn, C. A. Nienaber, G. Rocchi, H. Rousseau, M. Thompson, E. Weigang, and R. Erbel. Thoracic endovascular aortic repair (TEVAR) for the treatment of aortic diseases : a position statement from the european association for cardio-thoracic surgery (EACTS) and the european society of cardiology (ESC), in collaboration with the European Association of Percutaneous Cardiovascular Interventions (EAPCI). *Eur J Cardiothorac Surg*, 42(1) :17–24, 2012.

[46] P. Greenland, J. S. Alpert, G. A. Beller, E. J. Benjamin, M. J. Budoff, Z. A. Fayad, E. Foster, M. A. Hlatky, J. M. Hodgson, F. G. Kushner, M. S. Lauer, L. J. Shaw, J. Smith, S. C., A. J. Taylor, W. S. Weintraub, N. K. Wenger, A. K. Jacobs, J. L. Anderson, N. Albert, C. E. Buller, M. A. Creager, S. M. Ettinger, R. A. Guyton, J. L. Halperin, J. S. Hochman, R. Nishimura, E. M. Ohman, R. L. Page, W. G. Stevenson, L. G. Tarkington, and C. W. Yancy. 2010 ACCF/AHA guideline for assessment of cardiovascular risk in asymptomatic adults : a report of the american college of cardiology foundation/american heart association task force on practice guidelines. *J Am Coll Cardiol*, 56(25) :e50–103, 2010.

[47] X. Gu, Y. He, Z. Li, M. C. Kontos, W. H. J. Paulsen, J. A. Arrowood, G. W. Vetrovec, and J. V. Nixon. Relation between the incidence, location, and extent of thoracic aortic atherosclerosis detected by transesophageal echocardiography and the extent

of coronary artery disease by angiography. *The American Journal of Cardiology*, 107(2) :175–178, 2011.

[48] P. G. Hagan, C. A. Nienaber, E. M. Isselbacher, D. Bruckman, D. J. Karavite, P. L. Russman, A. Evangelista, R. Fattori, T. Suzuki, J. K. Oh, A. G. Moore, J. F. Malouf, L. A. Pape, C. Gaca, U. Sechtem, S. Lenferink, H. J. Deutsch, H. Diedrichs, J. Marcos y Robles, A. Llovet, D. Gilon, S. K. Das, W. F. Armstrong, G. M. Deeb, and K. A. Eagle. The international registry of acute aortic dissection (IRAD) : new insights into an old disease. *JAMA*, 283(7) :897–903, 2000.

[49] D. M. Hermann, N. Lehmann, J. Gronewold, M. Bauer, A. A. Mahabadi, C. Weimar, K. Berger, S. Moebus, K. H. Jockel, R. Erbel, and H. Kalsch. Thoracic aortic calcification is associated with incident stroke in the general population in addition to established risk factors. *Eur Heart J Cardiovasc Imaging*, 16(6) :684–90, 2015.

[50] L. F. Hiratzka, G. L. Bakris, J. A. Beckman, R. M. Bersin, V. F. Carr, J. Casey, D. E., K. A. Eagle, L. K. Hermann, E. M. Isselbacher, E. A. Kazerooni, N. T. Kouchoukos, B. W. Lytle, D. M. Milewicz, D. L. Reich, S. Sen, J. A. Shinn, L. G. Svensson, and D. M. Williams. 2010 ACCF/AHA/AATS/ACR/ASA/SCA/SCAI/SIR/STS/SVM Guidelines for the diagnosis and management of patients with thoracic aortic disease. A Report of the American College of Cardiology Foundation/American Heart Association Task Force on Practice Guidelines, American Association for Thoracic Surgery, American College of Radiology,American Stroke Association, Society of Cardiovascular Anesthesiologists, Society for Cardiovascular Angiography and Interventions, Society of Interventional Radiology, Society of Thoracic Surgeons,and Society for Vascular Medicine. *J Am Coll Cardiol*, 55(14) :e27–e129, 2010.

[51] K. Hoshina, M. Nemoto, T. Hashimoto, S. Miura, G. Urabe, T. Nakazawa, A. Hosaka, M. Kato, N. Ohkubo, T. Miyairi, H. Okamoto, K. Shigematsu, and T. Miyata. Study design of PROCEDURE study. a randomized comparison of the dose-dependent effects of pitavastatin in patients with abdominal aortic aneurysm with massive aortic atheroma : Prevention of cholesterol embolization during endovascular and Open Aneurysm Repair with Pitavastatin (PROCEDURE) study. *Ann Vasc Dis*, 6(1) :62–6, 2013.

[52] D. P. Howard, A. Banerjee, J. F. Fairhead, J. Perkins, L. E. Silver, and P. M. Rothwell. Population-based study of incidence and outcome of acute aortic dissection and premorbid risk factor control : 10-year results from the Oxford Vascular Study. *Circulation*, 127(20) :2031–7, 2013.

[53] R. Hultgren, E. Larsson, C. M. Wahlgren, and J. Swedenborg. Female and elderly abdominal aortic aneurysm patients more commonly have concurrent thoracic aortic aneurysm. *Ann Vasc Surg*, 26(7) :918–23, 2012.

[54] Y. Huo, X. Guo, and G. S. Kassab. The flow field along the entire length of mouse aorta and primary branches. *Ann Biomed Eng*, 36(5) :685–99, 2008.

[55] T. Ihara, K. Komori, K. Yamamoto, M. Kobayashi, H. Banno, and A. Kodama. Three-dimensional workstation is useful for measuring the correct size of abdominal aortic aneurysm diameters. *Ann Vasc Surg*, 27(2) :154–61, 2013.

[56] E. Ingelsson, M. J. Pencina, D. Levy, J. Aragam, G. F. Mitchell, E. J. Benjamin, and R. S. Vasan. Aortic root diameter and longitudinal blood pressure tracking. *Hypertension*, 52(3) :473–7, 2008.

[57] P. C. Jacobs, M. Prokop, Y. van der Graaf, M. J. Gondrie, K. J. Janssen, H. J. de Koning, I. Isgum, R. J. van Klaveren, M. Oudkerk, B. van Ginneken, and W. P. Mali. Comparing coronary artery calcium and thoracic aorta calcium for prediction of all-cause mortality and cardiovascular events on low-dose non-gated computed tomography in a high-risk population of heavy smokers. *Atherosclerosis*, 209(2) :455–62, 2010.

[58] R. W. Jayalath, S. H. Mangan, and J. Golledge. Aortic calcification. *Eur J Vasc Endovasc Surg*, 30(5) :476–88, 2005.

[59] N. E. Jensky, M. H. Criqui, M. C. Wright, C. L. Wassel, S. A. Brody, and M. A. Allison. Blood pressure and vascular calcification. *Hypertension*, 55(4) :990–7, 2010.

[60] K. W. Johnston, R. B. Rutherford, M. D. Tilson, D. M. Shah, L. Hollier, and J. C. Stanley. Suggested standards for reporting on arterial aneurysms. subcommittee on reporting standards for arterial aneurysms, ad hoc committee on reporting standards, Society for Vascular Surgery and North American Chapter, International Society for Cardiovascular Surgery. *J Vasc Surg*, 13(3) :452–458, Mar 1991.

[61] G. Jondeau, P. Boutouyrie, P. Lacolley, B. Laloux, O. Dubourg, J. P. Bourdarias, and S. Laurent. Central pulse pressure is a major determinant of ascending aorta dilation in Marfan syndrome. *Circulation*, 99(20) :2677–81, 1999.

[62] H. Kalsch, N. Lehmann, S. Mohlenkamp, A. Becker, S. Moebus, A. Schmermund, A. Stang, A. A. Mahabadi, K. Mann, K. H. Jockel, R. Erbel, and H. Eggebrecht. Body-surface adjusted aortic reference diameters for improved identification of patients with thoracic aortic aneurysms : results from the population-based Heinz Nixdorf Recall study. *Int J Cardiol*, 163(1) :72–8, 2013.

[63] H. Kalsch, N. Lehmann, S. Mohlenkamp, C. Hammer, A. A. Mahabadi, S. Moebus, A. Schmermund, A. Stang, M. Bauer, K. H. Jockel, and R. Erbel. Prevalence of thoracic aortic calcification and its relationship to cardiovascular risk factors and coronary calcification in an unselected population-based cohort : the Heinz Nixdorf Recall study. *Int J Cardiovasc Imaging*, 29(1) :207–16, 2013.

[64] R. Karmy-Jones, A. Simeone, M. Meissner, B. Granvall, and S. Nicholls. Descending thoracic aortic dissections. *Surg Clin North Am*, 87(5) :1047–86, viii–ix, 2007.

[65] M. Kass, A. Witkin, and D. Terzopoulos. Snakes : Active contour models. *Int J Comput Vision*, 1(4) :321–331, 1988.

[66] H. W. Kniemeyer, T. Kessler, P. U. Reber, H. B. Ris, H. Hakki, and M. K. Widmer. Treatment of ruptured abdominal aortic aneurysm, a permanent challenge or a waste of resources ? prediction of outcome using a multi-organ-dysfunction score. *Eur J Vasc Endovasc Surg*, 19(2) :190–6, 2000.

[67] D. K. Krievins, A. Holden, J. Savlovskis, C. Calderas, C. E. Donayre, F. L. Moll, B. Katzen, and C. K. Zarins. EVAR using the Nellix sac-anchoring endoprosthesis : treatment of favourable and adverse anatomy. *Eur J Vasc Endovasc Surg*, 42(1) :38–46, 2011.

[68] C. S. Lam, V. Xanthakis, L. M. Sullivan, W. Lieb, J. Aragam, M. M. Redfield, G. F. Mitchell, E. J. Benjamin, and R. S. Vasan. Aortic root remodeling over the adult life course : longitudinal data from the Framingham Heart Study. *Circulation*, 122(9) :884–90, 2010.

[69] S. L. Lansman, C. Hagl, D. Fink, J. D. Galla, D. Spielvogel, M. A. Ergin, and R. B. Griep. Acute type B aortic dissection : surgical therapy. *Ann Thorac Surg*, 74(5) :S1833–5 ; discussion S1857–63, 2002.

[70] F. A. Lederle, J. A. Freischlag, T. C. Kyriakides, J. Padberg, F. T., J. S. Matsumura, T. R. Kohler, P. H. Lin, J. M. Jean-Claude, D. F. Cikrit, K. M. Swanson, and P. N. Peduzzi. Outcomes following endovascular vs open repair of abdominal aortic aneurysm : a randomized trial. *JAMA*, 302(14) :1535–42, 2009.

[71] E. T. Lee, Y. J. Pan, and P. Chu. An algorithm for region filling using two-dimensional grammars. *Int J Intell Syst*, 2(3) :255–263, 1987.

[72] X. Liu, F. Pu, Y. Fan, X. Deng, D. Li, and S. Li. A numerical study on the flow of blood and the transport of ldl in the human aorta : the physiological significance of the helical flow in the aortic arch. *Am J Physiol Heart Circ Physiol*, 297(1) :H163–70, 2009.

[73] A. M. Malek, S. L. Alper, and S. Izumo. Hemodynamic shear stress and its role in atherosclerosis. *JAMA*, 282(21) :2035–42, 1999.

[74] G. Mancia. 2013 ESH/ESC guidelines for the management of arterial hypertension : the task force for the management of arterial hypertension of the european society of hypertension (esh) and of the european society of cardiology (ESC). *Eur Heart J*, 34(28) :2159–219, 2013.

[75] S. S. Mao, N. Ahmadi, B. Shah, D. Beckmann, A. Chen, L. Ngo, F. R. Flores, Y. l. Gao, and M. J. Budoff. Normal thoracic aorta diameter on cardiac computed tomography in healthy asymptomatic adults : Impact of age and gender. *Acad Radiol*, 15(7) :827–834, 2008.

[76] J. Miller, D. Breen, W. Lorensen, R. O'Bara, and M. Wozny. Geometrically deformed models : a method for extracting closed geometric models form volume data. In *SIGGRAPH 91 Proceedings of the 18th annual conference on Computer graphics and interactive techniques*, pages 217–226. ACM, 1991.

[77] G. F. Mitchell, P. R. Conlin, M. E. Dunlap, Y. Lacourciere, J. M. Arnold, R. I. Ogilvie, J. Neutel, J. Izzo, J. L., and M. A. Pfeffer. Aortic diameter, wall stiffness, and wave reflection in systolic hypertension. *Hypertension*, 51(1) :105–11, 2008.

[78] J. Montagnat, H. Delingette, and N. Ayache. A review of deformable surfaces : topology, geometry and deformation. *Image Vision Comput*, 19(14) :1023–1040, 2001.

[79] C. A. Nienaber, S. Kische, H. Rousseau, H. Eggebrecht, T. C. Rehders, G. Kundt, A. Glass, D. Scheinert, M. Czerny, T. Kleinfeldt, B. Zipfel, L. Labrousse, R. Fattori, and H. Ince. Endovascular repair of type b aortic dissection : long-term results of the randomized investigation of stent grafts in aortic dissection trial. *Circ Cardiovasc Interv*, 6(4) :407–16, 2013.

[80] C. A. Nienaber, H. Rousseau, H. Eggebrecht, S. Kische, R. Fattori, T. C. Rehders, G. Kundt, D. Scheinert, M. Czerny, T. Kleinfeldt, B. Zipfel, L. Labrousse, and H. Ince. Randomized comparison of strategies for type b aortic dissection : the investigation of stent grafts in aortic dissection (INSTEAD) trial. *Circulation*, 120(25) :2519–28, 2009.

[81] S. A. O'Leary, E. G. Kavanagh, P. A. Grace, T. M. McGloughlin, and B. J. Doyle. The biaxial mechanical behaviour of abdominal aortic aneurysm intraluminal thrombus : classification of morphology and the determination of layer and region specific properties. *J Biomech*, 47(6) :1430–7, 2014.

[82] M. O'Rourke, A. Farnsworth, and J. O'Rourke. Aortic dimensions and stiffness in normal adults. *JACC Cardiovasc Imaging*, 1(6) :749–51, 2008.

[83] J.-Y. Park, T. McInerney, D. Terzopoulos, and M.-H. Kim. A non-self-intersecting adaptive deformable surface for complex boundary extraction from volumetric images. *Computers and Graphics*, 25(3) :421–440, 2001.

[84] M. J. Perko, M. Norgaard, T. M. Herzog, P. S. Olsen, T. V. Schroeder, and G. Pettersson. Unoperated aortic aneurysm : a survey of 170 patients. *Ann Thorac Surg*, 59(5) :1204–9, 1995.

[85] D. Proudfoot and C. M. Shanahan. Biology of calcification in vascular cells : intima versus media. *Herz*, 26(4) :245–51, 2001.

[86] A. Redheuil, W. C. Yu, E. Mousseaux, A. A. Harouni, N. Kachenoura, C. O. Wu, D. Bluemke, and J. A. C. Lima. Age-related changes in aortic arch geometry : Relationship with proximal aortic function and left ventricular mass and remodeling. *J Am Coll Cardiol*, 58(12) :1262–1270, 2011.

[87] A. Redheuil, W. C. Yu, C. O. Wu, E. Mousseaux, A. de Cesare, R. Yan, N. Kachenoura, D. Bluemke, and J. A. Lima. Reduced ascending aortic strain and distensibility : earliest manifestations of vascular aging in humans. *Hypertension*, 55(2) :319–26, 2010.

[88] J. B. Ricco, J. Cau, C. Marchand, M. Marty, M. H. Rodde-Dunet, P. Fender, H. Allemand, and A. Corsini. Stent-graft repair for thoracic aortic disease : results of an independent nationwide study in France from 1999 to 2001. *J Thorac Cardiovasc Surg*, 131(1) :131–7, 2006.

[89] A. M. Rogers, L. K. Hermann, A. M. Booher, C. A. Nienaber, D. M. Williams, E. A. Kazerooni, J. B. Froehlich, P. T. O'Gara, D. G. Montgomery, J. V. Cooper, K. M. Harris, S. Hutchison, A. Evangelista, E. M. Isselbacher, and K. A. Eagle. Sensitivity of the aortic dissection detection risk score, a novel guideline-based tool for identification of acute aortic dissection at initial presentation : results from the International Registry of acute Aortic Dissection. *Circulation*, 123(20) :2213–8, 2011.

[90] I. S. Rogers, J. M. Massaro, Q. A. Truong, A. A. Mahabadi, M. F. Kriegel, C. S. Fox, G. Thanassoulis, E. M. Isselbacher, U. Hoffmann, and C. J. O'Donnell. Distribution, determinants, and normal reference values of thoracic and abdominal aortic diameters by computed tomography (from the Framingham Heart Study). *Am J Cardiol*, 111(10) :1510–6, 2013.

[91] H. Rousseau, V. Chabbert, M. A. Maracher, O. El Aassar, J. Auriol, P. Massabuau, and R. Moreno. The importance of imaging assessment before endovascular repair of thoracic aorta. *Eur J Vasc Endovasc Surg*, 38(4) :408–421, 2009.

[92] B. Rylski, P. Blanke, F. Beyersdorf, N. D. Desai, R. K. Milewski, M. Siepe, F. A. Kari, M. Czerny, T. Carrel, C. Schlensak, T. Kruger, M. J. Mack, W. T. Brinkman, F. W. Mohr, C. D. Etz, M. Luehr, and J. E. Bavaria. How does the ascending aorta geometry change when it dissects ? *J Am Coll Cardiol*, 63(13) :1311–9, 2014.

[93] B. Rylski, M. Suedkamp, F. Beyersdorf, B. Nitsch, I. Hoffmann, M. Blettner, and E. Weigang. Outcome after surgery for acute aortic dissection type a in patients over 70 years : data analysis from the german registry for acute aortic dissection type a (GERAADA). *Eur J Cardiothorac Surg*, 40(2) :435–40, 2011.

[94] N. Sakalihasan, R. Limet, and O. D. Defawe. Abdominal aortic aneurysm. *Lancet*, 365(9470) :1577–89, 2005.

[95] U. K. Sampson, P. E. Norman, F. G. Fowkes, V. Aboyans, Y. Song, J. Harrell, F. E., M. H. Forouzanfar, M. Naghavi, J. O. Denenberg, M. M. McDermott, M. H. Criqui, G. A. Mensah, M. Ezzati, and C. Murray. Estimation of global and regional incidence and prevalence of abdominal aortic aneurysms 1990 to 2010. *Glob Heart*, 9(1) :159–70, 2014.

[96] A. J. Scott and C. D. Bicknell. Contemporary management of acute type B dissection. *Eur J Vasc Endovasc Surg*, 51(3) :452–9, 2016.

[97] N. Shahcheraghi, H. A. Dwyer, A. Y. Cheer, A. I. Barakat, and T. Rutaganira. Unsteady and three-dimensional simulation of blood flow in the human aortic arch. *J Biomech Eng*, 124(4) :378–87, 2002.

[98] A. S. Shirali, M. S. Bischoff, H. M. Lin, I. Oyfe, R. Lookstein, R. B. Griepp, and G. Di Luozzo. Predicting the risk for acute type b aortic dissection in hypertensive patients using anatomic variables. *JACC Cardiovasc Imaging*, 6(3) :349–57, 2013.

[99] T. Sommer, W. Fehske, N. Holzknecht, A. V. Smekal, E. Keller, G. Lutterbey, B. Kreft, C. Kuhl, J. Gieseke, D. Abu-Ramadan, and H. Schild. Aortic dissection : a comparative study of diagnosis with spiral CT, multiplanar transesophageal echocardiography, and MR imaging. *Radiology*, 199(2) :347–52, 1996.

[100] Z. Stankovic, B. D. Allen, J. Garcia, K. B. Jarvis, and M. Markl. 4d flow imaging with mri. *Cardiovasc Diagn Ther*, 4(2) :173–192, Apr 2014.

[101] P. W. Stather, N. Dattani, M. J. Bown, J. J. Earnshaw, and T. A. Lees. International variations in AAA screening. *Eur J Vasc Endovasc Surg*, 45(3) :231–4, 2013.

[102] P. W. Stather, D. Sidloff, N. Dattani, E. Choke, M. J. Bown, and R. D. Sayers. Systematic review and meta-analysis of the early and late outcomes of open and endovascular repair of abdominal aortic aneurysm. *Br J Surg*, 100(7) :863–72, 2013.

[103] J. Sugawara, K. Hayashi, T. Yokoi, and H. Tanaka. Age-associated elongation of the ascending aorta in adults. *J Am Coll Cardiol Img*, 1(6) :739–748, 2008.

[104] T. Suzuki, A. Distante, A. Zizza, S. Trimarchi, M. Villani, J. A. Salerno Uriarte, L. de Luca Tupputi Schinosa, A. Renzulli, F. Sabino, R. Nowak, R. Birkhahn, J. E. Hollander, F. Counselman, E. Bossone, and K. Eagle. Preliminary experience with the

smooth muscle troponin-like protein, calponin, as a novel biomarker for diagnosing acute aortic dissection. *Eur Heart J*, 29(11) :1439–45, 2008.

[105] S. Svensjo, M. Bjorck, M. Gurtelschmid, K. Djavani Gidlund, A. Hellberg, and A. Wanhainen. Low prevalence of abdominal aortic aneurysm among 65-year-old swedish men indicates a change in the epidemiology of the disease. *Circulation*, 124(10) :1118–23, 2011.

[106] L. G. Svensson, N. T. Kouchoukos, D. C. Miller, J. E. Bavaria, J. S. Coselli, M. A. Curi, H. Eggebrecht, J. A. Elefteriades, R. Erbel, T. G. Gleason, B. W. Lytle, R. S. Mitchell, C. A. Nienaber, E. E. Roselli, H. J. Safi, R. J. Shemin, G. A. Sicard, r. Sundt, T. M., W. Y. Szeto, and r. Wheatley, G. H. Expert consensus document on the treatment of descending thoracic aortic disease using endovascular stent-grafts. *Ann Thorac Surg*, 85(1 Suppl) :S1–41, 2008.

[107] J. Takasu, R. Katz, K. Nasir, J. J. Carr, N. Wong, R. Detrano, and M. J. Budoff. Relationships of thoracic aortic wall calcification to cardiovascular risk factors : the Multi-Ethnic Study of Atherosclerosis (MESA). *Am Heart J*, 155(4) :765–71, 2008.

[108] D. Terzopoulos, A. Witkin, and M. Kass. Constraints on deformable models :recovering 3d shape and nonrigid motion. *Artif Intell*, 36(1) :91–123, 1988.

[109] J. L. Tolenaar, J. W. van Keulen, F. H. Jonker, J. A. van Herwaarden, H. J. Verhagen, F. L. Moll, B. E. Muhs, and S. Trimarchi. Morphologic predictors of aortic dilatation in type b aortic dissection. *J Vasc Surg*, 58(5) :1220–5, 2013.

[110] S. Trimarchi, F. H. Jonker, J. B. Froehlich, G. R. Upchurch, F. L. Moll, B. E. Muhs, V. Rampoldi, H. J. Patel, and K. A. Eagle. Acute type B aortic dissection in the absence of aortic dilatation. *J Vasc Surg*, 56(2) :311–6, 2012.

[111] S. Trimarchi, C. A. Nienaber, V. Rampoldi, T. Myrmel, T. Suzuki, R. H. Mehta, E. Bossone, J. V. Cooper, D. E. Smith, L. Menicanti, A. Frigiola, J. K. Oh, M. G. Deeb, E. M. Isselbacher, and K. A. Eagle. Contemporary results of surgery in acute type A aortic dissection : The International Registry of Acute Aortic Dissection experience. *J Thorac Cardiovasc Surg*, 129(1) :112–22, 2005.

[112] J. van der Linden, L. Hadjinikolaou, P. Bergman, and D. Lindblom. Postoperative stroke in cardiac surgery is related to the location and extent of atherosclerotic disease in the ascending aorta. *J Am Coll Cardiol*, 38(1) :131–5, 2001.

[113] R. S. Vasan, M. G. Larson, and D. Levy. Determinants of echocardiographic aortic root size. The Framingham Heart Study. *Circulation*, 91(3) :734–40, 1995.

[114] P. E. Vincent, A. M. Plata, A. A. Hunt, P. D. Weinberg, and S. J. Sherwin. Blood flow in the rabbit aortic arch and descending thoracic aorta. *J R Soc Interface*, 8(65) :1708–19, 2011.

[115] O. Vriz, C. Driussi, M. Bettio, F. Ferrara, A. D'Andrea, and E. Bossone. Aortic root dimensions and stiffness in healthy subjects. *Am J Cardiol*, 112(8) :1224–9, 2013.

[116] J. Wasilewski, J. Glowacki, and L. Polonski. Not at random location of atherosclerotic lesions in thoracic aorta and their prognostic significance in relation to the risk of cardiovascular events. *Pol J Radiol*, 78(2) :38–42, 2013.

[117] A. Wolak, H. Gransar, L. E. J. Thomson, J. D. Friedman, R. Hachamovitch, A. Gutstein, L. J. Shaw, D. Polk, N. D. Wong, R. Saouaf, S. W. Hayes, A. Rozanski, P. J. Slomka, G. Germano, and D. S. Berman. Aortic size assessment by noncontrast cardiac computed tomography : Normal limits by age, gender, and body surface area. *JACC : Cardiovascular Imaging*, 1(2) :200–209, 2008.

[118] N. D. Wong, H. Gransar, L. Shaw, D. Polk, J. H. Moon, R. Miranda-Peats, S. W. Hayes, L. E. Thomson, A. Rozanski, J. D. Friedman, and D. S. Berman. Thoracic aortic calcium versus coronary artery calcium for the prediction of coronary heart disease and cardiovascular disease events. *JACC Cardiovasc Imaging*, 2(3) :319–26, 2009.

[119] J. Yeboah, J. J. Carr, J. G. Terry, J. Ding, I. Zeb, S. Liu, K. Nasir, W. Post, R. S. Blumenthal, and M. J. Budoff. Computed tomography-derived cardiovascular risk markers, incident cardiovascular events, and all-cause mortality in nondiabetics : the Multi-Ethnic Study of Atherosclerosis. *Eur J Prev Cardiol*, 2013.

[120] D. Zhu, N. C. Mackenzie, C. Farquharson, and V. E. Macrae. Mechanisms and clinical consequences of vascular calcification. *Front Endocrinol (Lausanne)*, 3 :95, 2012.

Résumé

Les nouvelles technologies d'imagerie basées sur la tomodensitométrie en coupe permettent l'évaluation de très haute qualité de la structure 3D de l'aorte thoracique. La reconstruction virtuelle et les modèles géométriques de l'aorte sont indispensables à l'exploitation des images dont le temps de traitement manuel reste cependant considérable et les outils numériques insuffisants ou inadaptés pour mesurer correctement sa morphologie.

L'aorte n'est pas un simple tube de conduction du sang mais un organe de régulation de la pulsatilité des ondes de pression provoquées par l'éjection cardiaque. Ses désordres biomécaniques peuvent accélérer la formation de calcifications dans sa paroi et entrainer des risques de graves complications, comme les anévrismes et les dissections. La réparation aortique basée sur l'implantation d'endoprothèses est en pleine évolution et requiert des renseignements morphologiques précis pour en améliorer le taux de succès.

Notre objectif a été d'étudier la géométrie tridimensionnelle de l'aorte en développant des algorithmes appropriés. Une plateforme informatique a été conçue et testée pour étudier trois pathologies de l'aorte : l'athérosclérose calcifiée, l'anévrisme et la dissection. L'hypothèse du travail a été que la géométrie spécifique des artères de chaque individu joue un rôle complémentaire à celui des facteurs de risque traditionnels dans le développement de ces pathologies. Notre premier travail a montré que trois facteurs résument 80% de la variabilité géométrique de l'aorte thoracique : le volume aortique, le déroulement et la symétrie de l'arche aortique, avec des taux de variabilité respectifs de 46%, 22% et 12%.

Dans deux travaux suivants, nous avons montré que les calcifications de l'aorte thoracique se concentrent principalement dans la crosse et dans le segment descendant proximal, et que cette distribution était associée à la morphologie de l'aorte indépendamment de l'âge, du sexe, de la surface corporelle et des facteurs de risque traditionnels. Le quatrième travail a montré que le score de dépôt calcique dans toute l'aorte thoracique incluant la crosse était plus étroitement associé aux complications non-cardiaques, vasculaires périphériques et cérébrales, que le score traditionnel de calcium coronaire. Il faut noter que la crosse aortique n'est pas visualisée dans les études de routine de calcium coronaire sans injection.

Le cinquième travail décrit un modèle déformable capable de segmenter la lumière aortique dans un contexte pathologique. Il a été appliqué pour étudier de façon automatisée la taille d'un anévrisme abdominal avant et après la pose d'une endoprothèse. Dans le dernier travail, la méthode précédente a été adaptée pour étudier la géométrie aortique des patients atteints de dissection comparativement à un groupe témoin de patients qui en étaient indemnes. Trois variables géométriques ont été identifiées dans le modèle de prédiction du risque de dissection : le diamètre de la crosse, la longueur de l'aorte thoracique et l'âge.

En conclusion, nos résultats montrent que les maladies aortiques sont étroitement associées à la géométrie de l'aorte indépendamment des facteurs de risque traditionnels. Les algorithmes que nous avons développés ouvrent la voie à l'automatisation et à une réduction de la variabilité des mesures.

Mots clefs : Aorte, tomodensitométrie, traitement numérique d'images, calcification artérielle, anévrisme aortique, dissection aortique.

Abstract

Title : Development and evaluation of new 3D geometric analysis tools to prevent and treat aortic diseases.

New imaging technologies, including those associated with multislice computed tomography, allow to evaluate the structure of the thoracic aorta in 3D with an impressive resolution. Aortic virtual reconstruction and geometric modeling are essential for imaging evaluation because manual measurements are time-consuming, and the available tools still need to be adapted to complex aortic morphologies.

The aorta is more than a simple tubular conduit vessel for blood. It also regulates the pulsatile pressure waves that are injected into the arterial system by the left ventricle. The biomechanical disorders produced by these waves can accelerate the formation of calcium deposits within the arterial wall. Furthermore, they are thought to be responsible for severe aortic complications, including aneurysms and dissections. Endovascular aortic repair is a modern technique based on the implantation of an endograft to restore the normal blood flow. Precise morphological measurements are required to improve this technique, for both surgery planning and patient follow up.

Our objective was to develop original algorithms to study the aortic geometry in 3D. A computing platform was designed and tested to analyze three main aortic pathologies : calcified atherosclerosis, aneurysms and dissections. The hypothesis of our study was that the individual arterial geometry of a subject plays a complementary role in the development of vascular pathologies beyond traditional risk factors.

Our first work revealed that 80% of the total geometric variability in the thoracic aorta might be explained using 3 factors : the aortic volume, the aortic arc unfolding and its asymmetry. Variability percentages accounted for 46%, 22% and 12%, respectively.

The next 2 works, showed that calcifications in the thoracic aorta were concentrated in the aortic arch and in the proximal descending segment. This spatial distribution was associated with aortic morphology, independently of age, sex, body surface area and traditional risk factors. Our fourth article revealed that calcium deposits in the entire thoracic aorta (including the aortic arch) was associated with non-cardiac events, beyond the standard coronary artery calcium score. It is noteworthy that the aortic arch region is systematically excluded from standard scans.

Our fifth manuscript described a novel deformable model applied to the aortic segmentation under pathological contexts. It was used to estimate the size and shape of abdominal aneurysms before and after endograft implantation. In the last work, this method was adapted to study the geometry of the thoracic aorta of patients with an aortic dissection with respect to a control group. Three anatomic variables were identified for the risk prediction model : the aortic arch diameter, the thoracic aortic length and the age of the patient.

In conclusion, our results show that aortic diseases are closely associated with aortic geometry, independently from traditional risk factors. The developed algorithms improved the automation of measurements and reduced the variability of the estimations.

Keywords : Aorta, computed tomography, digital image processing, arterial calcification, aortic aneurysm, aortic dissection